# ROLE OF MODULATION OF THE MITOCHONDRIAL QUALITY CONTROL IN HYPERTENSION-INDUCED HEART FAILURE

**Ph.D. Thesis**

**Author: Orsolya Horváth**

**Program leader: Prof. Kálmán Tóth, M.D., D.Sc.**
**Project Leaders: Prof. Róbert Halmosi M.D., D.Sc.**
**László Deres Ph.D.**

**1st Department of Medicine**
**University of Pécs, Medical School**
**Hungary**

**2021**

# Table of contents

# ABBREVIATIONS

| | |
|---|---|
| **A** | mitral peak velocity of late diastolic filling |
| **A'** | late diastolic mitral annular velocity |
| **ADP** | adenosine diphosphate |
| **Akt** | protein kinase B |
| **AMPK** | AMP-activated protein kinase |
| **ANOVA** | analysis of variance |
| **ATP** | adenosine triphosphate |
| **BGP-15** | O-[3-piperidino-2-hydroxy-1-propyl]-nicotinic acid amidoxime dihydrochloride |
| **BNP** | brain-derived natriuretic peptide |
| **CD** | diameter of cardiomyocytes |
| **CDK** | cyclin dependent kinase |
| **COX1** | cytochrome c oxidase subunit 1 |
| **COX3** | cytochrome c oxidase subunit 3 |
| **CREB** | cAMP response element-binding protein |
| **DAB** | 3,3'-diaminobenzidine |
| **DMEM** | Dulbecco's modified Eagle Medium |
| **DRP1** | dynamin-related protein 1 |
| **DUSPs** | dual-specificity phosphatases |
| **E** | mitral peak velocity of early diastolic filling |
| **E'** | early diastolic mitral annular velocity |
| **ECM** | extracellular matrix |
| **EF** | ejection fraction |
| **eNOS** | endothelial nitric oxide synthase |
| **ERK1/2** | extracellular signal-regulated kinase 1/2 |
| **ETC** | electron transport chain, mitochondrial |
| **FBS** | fetal bovine serum |
| **Fis1** | mitochondrial fission 1 protein |
| **GAPDH** | glyceraldehyde 3-phosphate dehydrogenase |

| | |
|---|---|
| **GED** | GTPase effector domain |
| **GPCR** | G-protein-coupled receptor |
| **GPx** | glutathione peroxidase |
| **GRx** | glutathione reductase |
| **GSH** | reduced glutathione |
| **GSK-3β** | glycogen synthase kinase 3 beta |
| **GSSG** | oxidized glutathione |
| **$H_2O_2$** | hydrogen peroxide |
| **HF** | heart failure |
| **HFmrEF** | HF with mid-range ejection fraction |
| **HFpEF** | HF with preserved ejection fraction |
| **HFrEF** | HF with reduced ejection fraction |
| **IFM** | interfibrillar mitochondria |
| **IHD** | ischemic heart disease |
| **IMM** | inner mitochondrial membrane |
| **JNK** | c-jun N-terminal kinase |
| **LV** | left ventricle |
| **LVEDV** | left ventricular end-diastolic volume |
| **LVEF** | left ventricular ejection fraction |
| **LVESV** | left ventricular end-systolic volume |
| **LVIDd** | left ventricular end-diastolic inner diameter |
| **LVIDs** | left ventricular end-systolic inner diameter |
| **MAO** | monoamine oxidase |
| **MAPKs** | mitogen-activated protein kinases |
| **Mff** | mitochondria fission factor |
| **Mfn1/2** | mitofusins 1 and 2 |
| **MID49** | mitochondrial dynamics protein of 49 kDa |
| **MID51** | mitochondrial dynamics protein of 51 kDa |
| **MKP-1** | MAPK phosphatase-1 |
| **MMPs** | matrix metalloproteinases |

| | |
|---|---|
| **mPTP** | mitochondrial permeability transition pore |
| **NADH** | nicotinamide adenine dinucleotide |
| **NCX** | Na+/Ca2+ exchanger |
| **NO** | nitrogen monoxide |
| **NOXs** | nicotinamide -adenine dinucleotide phosphate oxidases |
| **NRCM** | neonatal rat cardiomyocytes |
| **NRF-1/2** | nuclear respiratory factor 1 and 2 |
| **OMM** | outer mitochondrial membrane |
| **OPA1** | optic atrophy 1 |
| **PARP-1** | poly(ADP-ribose) polymerase-1 |
| **PBS** | phosphate-buffered saline |
| **PDC** | pyruvate dehydrogenase complex |
| **PGC-1α** | peroxisome proliferator-activated receptor) - γ coactivator-1α |
| **PI3K** | phosphatidylinositol 3-kinase |
| **PKA** | protein kinase A |
| **PKC** | protein kinase C |
| **PW** | posterior wall of the left ventricle |
| **ROS** | reactive oxygen species |
| **RyR2** | ryanodine receptor 2 |
| **SDS** | sodium dodecyl sulfate |
| **SERCA2** | sarcoplasmic reticulum Ca2+-adenosine triphosphatase 2 |
| **SHR** | Spontaneously hypertensive rat |
| **SODs** | superoxide dismutases |
| **SSM** | subsarcolemmal mitochondria |
| **Tfam** | mitochondrial transcription factor A |
| **TGF-β** | transforming growth factor-beta |
| **TNF-α** | tumor necrosis factor-alpha |
| **VDAC** | voltage-dependent anion channel |
| **WKY** | Wistar-Kyoto rats |
| **XO** | xanthine oxidase |

# 1. INTRODUCTION

## 1.1 Heart Failure

Heart failure (HF) is a complex clinical syndrome where the functionally or structurally damaged heart is unable to maintain the proper cardiac output [1]. Heart failure affects nearly 64 million people worldwide [2]. In developed countries, 2% of the adult population suffers from heart failure, and this proportion rises to 10-15% for those who are over 70 years of age [3]. It is characterized by poor clinical outcome despite the growing number of therapeutic approaches, moreover the number of hospitalizations for HF as well as the HF associated mortality is increasing, thereby placing a heavy burden on health services and economy [3].

The etiological factors of heart failure can be divided into three groups including the diseased myocardium, the abnormal loading conditions and arrhythmias (tachy-, bradyarrhythmias) [4]. Considering the diseased myocardium, the most important risk factor of heart failure is the ischemic heart disease (IHD) especially in the case of a previous myocardial infarction. IHD can cause myocardial scarring, abnormal coronary microcirculation as well as endothelial dysfunction [5]. Some of the toxic agents for example recreational substance abuse (alcohol, drugs) and different medications (cytostatic, immunomodulating drugs) might also lead to the damage of the myocardium [6].

Hypertension is the most important risk factor resulting in abnormal loading conditions. The treatment of hypertension is a challenging task, since a high proportion of patients cannot reach the goal blood pressure level, what contributes to the development of heart failure [7]. Sustained elevation of blood pressure induces myocardial remodelling, which is characterized by interstitial fibrosis and cardiomyocyte hypertrophy [8, 9]. These cellular alterations are promoted by oxidative stress [10] and by the activation of various intracellular signal transduction pathways [11, 12] . Numerous studies have demonstrated that mitochondria, which are responsible for the cellular energy supply, are also damaged in hypertension-induced cardiac remodelling and heart failure [13, 14]. Reactive oxygen species (ROS) induced mitochondrial DNA damage can be found in the background of these injuries and mitochondria themselves become the main sources of endogenous ROS

production [15]. The long-term presence of these pathophysiological factors can finally lead to heart failure [16].

In order to prevent the poor outcome of HF, it is crucial to identify and eliminate the causes and precipitating factors.

The main terminology determines three types of HF based on the left ventricular ejection fraction (LVEF), which can be calculated by dividing the volume of blood pumped from the left ventricle per beat by the volume of blood collected in the left ventricle at the end of diastolic filling (end-diastolic volume) [4]. In HF with reduced EF (HFrEF), the contraction of the heart muscle and systolic function are affected (systolic HF; LVEF < 40%). In patients where LVEF is> 50%, we can speak about a so-called preserved ejection function, however, the filling during diastole is impaired (diastolic HF, HFpEF). There is a "grey zone" in the range of 40-49%, which is defined as HF with mid-range ejection fraction (HFmrEF) [4].

Treating heart failure, despite the numerous therapeutic possibilities, appears to be a challenging task nowadays. The major goal during the treatment is to improve the quality of life and functional capacity as well as to prevent hospital admissions and to try to reduce mortality. Beta blockers, angiotensin-converting enzyme inhibitors and mineralocorticoid receptor antagonist represent the main groups of therapeutic possibilities [4, 17]. In spite of these approaches, the prognosis of the HF is still poor, and we do not have a proven beneficial option for the treatment of diastolic HF yet. Therefore, finding novel therapeutic targets and developing new compounds are extremely important to improve the outcome of HF in the future.

## 1.2 The Spontaneously Hypertensive Rat as an animal model for chronic heart failure

The Spontaneously Hypertensive Rat (SHR) strain was developed by Professor Kyuzo Aoki and colleagues in the 1960's [18]. This strain is the result of selective inbreeding of Wistar-Kyoto (WKY) rats with consistently elevated blood pressure. The SHR has become one of the most intensively studied murine strain of cardiovascular diseases because the progression of hypertrophy and impaired cardiac function in the SHR is similar to the clinical course of patients with hypertension [19–21].

SHRs are normotensive at birth with systolic blood pressure around 100-120 Hgmm. The persistent hypertension (160-180 Hgmm) develops by the age of approximately 8-10 weeks [22]. Following a relatively long period of stable hypertension and compensated cardiac hypertrophy, at approximately 18 months of age, it begins to develop evidences of impaired cardiac function in animals [19, 23, 24]. The development of hypertension in animals is similar to humans; it evolves more rapidly and becomes more severe in male SHRs than in female rats. Phenotypic trait of this strain is characterized by cardiac hypertrophy and fibrotic remodelling during aging [25, 26]. Therefore, we decided to use this strain as an animal model so as to study the hypertension-induced heart failure.

### 1.3 Oxidative stress and heart failure

During oxidative stress, the production of the free radicals is increased while the endogenous antioxidant system is not able to protect against them adequately. Many types of free radicals can be distinguished, however, those derived from oxygen are the ones with the most significant effects on biological systems, commonly known as reactive oxygen species. ROS are oxygen-based chemical molecules, containing unpaired electrons in their outer orbit, resulting in high reactivity and instability [27]. ROS try to create a new electron pair, thereby exerting damaging effects as they remove the desired electron from other biomolecules in the body. ROS includes peroxides, superoxide anions and hydroxyl radicals.

ROS can be produced by either endogenous or exogenous sources [28]. The endogenous sources of ROS include different cellular organs such as mitochondria, peroxisomes and endoplasmic reticulum, where the rate of oxygen consumption is high. It should be noted that white blood cells are also capable of endogenous ROS production as a part of the immune response, for example in various inflammatory and cardiovascular diseases. Endogenous ROS production can even be observed under physiological circumstances during aerobic metabolism of nutrients. Mitochondria produce adenosine triphosphate (ATP) during the process of respiration, which is called oxidative phosphorylation [29]. In the electron transport chain, electrons migrate through a series of proteins via oxidation-reduction reactions, with each acceptor protein along the chain having a greater reduction potential than the previous one. The last destination for an electron along this chain is an oxygen molecule. The superoxide radicals are produced at two major sites in

the electron transport chain, namely complex I (NADH dehydrogenase) and complex III (ubiquinone cytochrome c reductase) [30].

Other sources of ROS production are NADPH oxidases (NOXs), nitric oxide synthase (NOS), lipo- and cyclooxygenases, xanthine oxidase, cytochrome P450 enzyme system and monoamine oxidases (MAO) [31].

In addition to endogenous free radicals, we can also talk about exogenous free radicals. This type of ROS production can be stimulated by various external influences including smoking, xenobiotics, drugs, heavy metals or radiation [28].

A complex antioxidant system provides protection against increased ROS production [29]. Antioxidant molecules donate an electron to a rampaging free radical and neutralize ROS molecules, thus reducing its capacity to damage. The antioxidant system might be divided into two groups, the enzymatic and non-enzymatic antioxidants.

Superoxide dismutases (SODs) are responsible for catalysing the breakdown of superoxide anions into oxygen and hydrogen peroxide [29]. Depending on the metal cofactor, three different groups can be distinguished, the Fe-SOD, the Mn-SOD and the CuZn-SOD. In humans, three forms of SOD are present. SOD1 is located in the cytosol and contains CuZn ions which is fundamental in the protection against ischaemic heart disease [32]. SOD2 (mitochondrial SOD/mnSOD) is localised in the mitochondria and is in charge of the elimination of ROS production during terminal oxidation and therefore it maintains the proper mitochondrial function [33]. Finally, SOD3 (extracellular SOD/ecSOD) is presented in extracellular space and its activity in the vessels is 10-fold higher than in other tissues [34]. As a result of its location, the ecSOD is critical in the prevention of endothelium-derived ROS and DNA damage.

Being enzymatic antioxidants, the catalase and the glutathione systems are in charge of the decomposition of hydrogen peroxide to oxygen and water [35]. Hydrogen peroxide formed as a by-product of normal metabolism proves to be extremely noxious, therefore it is crucial to be eliminated into less dangerous substances.

Glutathione, glutathione peroxidases (GPx), glutathione reductase (GRx) and glutathione S-transferases are the parts of the glutathione system. Glutathione peroxidase catalyses the breakdown of hydrogen peroxide and organic lipid hydroperoxides by oxidizing reduced glutathione (GSH) into oxidized glutathione (GSSG). Glutathione reductase is responsible for the reverse transformation by regenerating GSH from GSSG[36].

Non-enzymatic antioxidants such as vitamin A,E,C, flavonoids, glutathione and carotenoids are also able to terminate free radical-induced chain reactions [37, 38].

Antioxidants play vital role in the defense system at different levels such as prevention, free radical scavenging and repair. The preventive antioxidants representing the first line responsible for the suppression of free radical formation. The antioxidants that have scavenger effect against the active radicals are the second line. These scavenging antioxidants could be hydrophilic or lipophilic for example vitamin C, bilirubin and albumin are hydrophilic while vitamin E and ubiquinol are lipophilic [39]. The third line consists of the repair and de novo antioxidants which can recognise and remove the damaged and modified proteins and are able to repair the oxidative stress-induced DNA damage [38]. These peptidases, proteinases, nucleases and proteolytic enzymes are present both in the cytosol and in the mitochondria.

The damaging impacts of free radicals affect all organs in the human body and therefore play an extremely important role in the pathomechanism of many diseases including various cardiac diseases, but its significance cannot be neglected even in the processes of ageing [27].

Numerous experimental and clinical studies have already confirmed the role of oxidative stress in the development of heart failure [27, 40, 41] (Fig. 1). ROS have a major role in the activation of signalling pathways and transcription factors participating in maladaptive cardiac hypertrophy. In addition, it is important to mention that they significantly increase fibroblast proliferation and activate matrix metalloproteinases, which ultimately lead to maladaptive myocardial remodelling and heart failure [42]. Increased ROS production also has a direct effect on cardiomyocyte electrophysiology since - due to ROS production - the function of $Na^+/Ca^{2+}$ exchanger (NCX) is reversed resulting in $Ca^{2+}$ influx and $Na^+$ efflux. Moreover, ROS influence the contractile function of cardiomyocytes via increasing ryanodine receptor 2 (RyR2) activity and inhibiting sarcoplasmic reticulum $Ca^{2+}$-adenosine triphosphatase 2 (SERCA2) activity, therefore the calcium sensitivity of myofilaments is decreased, which leads to contractile dysfunction. ROS production has a negative effect on mitochondria as well, causing dysfunction in the energy metabolism [42].

ROS are produced by mitochondria, NOX, uncoupled nitric oxide synthases and xanthine oxidase (XO) within the cardiomyocytes, among them mitochondria are considered to be the main source of ROS. Under physiological conditions in mitochondria, ATP is synthesized from approximately 98% of the electrons transported in the respiratory chain and only insignificant amounts of ROS are formed (approximately 2%). The endogenous antioxidant system is able to protect adequately against this ROS production [27].

However, in the failing heart the mitochondrial electron transport could be the predominant source of ROS production via decreased activity of Complex I and III.

Therefore, a very strong pathophysiological connection can be observed between mitochondrial dysfunction and oxidative stress [43]. NADPH oxidase complex produces negligible amount of superoxide anion ($O_2^-$) via transferring an electron to molecular oxygen from NADPH [44].

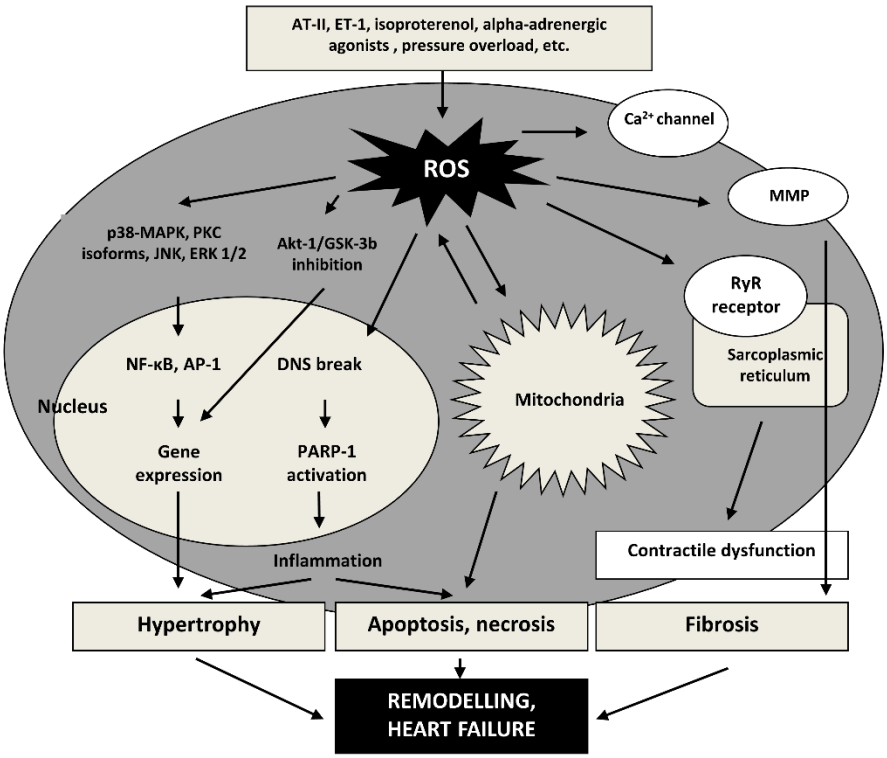


**Figure 1. The role of oxidative stress in myocardial remodelling at heart failure** [45]

In the human heart, NOX1, NOX2 and NOX4 isoforms play an important role and are expressed abundantly in endothelial cells, cardiac myocytes and fibroblasts [46, 47]. Several factors - involved in the pathomechanism of heart failure - including tumor necrosis factor-alpha (TNF-1), endothelin-1, angiotensin II and mechanical stretch are able to enhance the activity of NOX [27].

The uncoupled nitric oxide synthases can contribute to more ROS production. Under oxidative stress, NOS becomes uncoupled and structurally unstable leading to an increased generation of ROS instead of NO [48].

The structural and functional cell-damaging effect of ROS is partly exerted via the modulation of various signalling pathways as well as intracellular molecules [49]. Endogenous ROS production can promote apoptosis via ROS-mediated DNA and mitochondrial damage. Moreover, ROS seem to play a decisive role in the progression of pathological cardiac hypertrophy to heart failure via activating different transcriptions factors and signalling pathways. Cardiomyocyte hypertrophy can be triggered via ROS generation by G-protein-coupled receptor (GPCR) agonists, including angiotensin II, endothelin-1, and α-adrenoreceptor agonists. Angiotensin II plays a crucial role in the progression of cardiac hypertrophy via activating Nox2 [50]. Another important negative effect of oxidative stress is the DNA damage and the DNA damage-induced overactivation of nuclear enzyme poly(ADP-ribose) polymerase-1 (PARP-1). PARP-1 enzyme is responsible for the initiation of DNA repair and is activated by single-strand and double-strand DNA breaks. Cleavage of NAD results in the formation of ADP-ribose subunits upon its activation, which in a polymer form binds to the damaged DNA segment in order to aid the DNA repair process [51, 52]. However, in the case of PARP-1 enzyme over-activation, the amount of high-energy phosphates is significantly reduced within the cells, causing programmed or necrotic cell death [51].

In addition, matrix metalloproteinases (MMPs) activation can be observed during oxidative stress. MMPs are important in the remodelling, in cell migration, proliferation and apoptosis under normal circumstances. Nevertheless, in the failing heart an elevated activation of MMPs can be noticed, which finally leads to LV dilatation, systolic dysfunction and further progression of heart failure [53].

## 1.4 The role of signal transduction factors in the process of oxidative cell damage and in cardiovascular remodelling

Heart failure can be seen as a final common state of various cardiac diseases, for example, hypertension, cardiomyopathies and valvular heart diseases [54].

Cardiac remodelling is referred to as a group of molecular, cellular and interstitial changes that manifest clinically as changes in size, mass (hypertrophy and atrophy), geometry (heart wall thickness), fibrosis and function of the heart after injury [55]. Cardiac remodelling can be divided into two major groups, the physiologic and the pathologic remodelling. Physiologic remodelling - typical of athletes and pregnant women - can be characterized by adaptive hypertrophy and is not accompanied by cardiac fibrosis [56,

57]. During adaptive hypertrophy, the activation of phosphatidylinositol 3-kinase (PI3K) and protein kinase B (Akt) can be seen. Akt-1 belongs to prosurvival signalling factors and can promote the physiological hypertrophy, however it inhibits the pathological hypertrophy that is mainly characterized by cardiac collagen accumulation [58–60]. Glycogen synthase kinase 3 beta (GSK-3β) is a downstream target of Akt-1 and Akt-1 can trigger the survival of chronically stressed cardiomyocytes in heart failure via the phosphorylation of GSK-3β. Due to increased phosphorylation of Akt-1 and GSK-3β, the cytoprotective impact is mediated via their protective effect on the structure and function of mitochondria [61]. Moreover, the extracellular signal-regulated kinase 1/2 (ERK1/2) is also activated, which is responsible for hypertrophic growth [57, 59, 62]. Based on the fact that ERK1/2 is a member of prosurvival signalling factors, its activation is beneficial in the failed myocardium [23, 63]. Myocardial hypertrophy is an adaptive process that occurs in response to both various physiological and pathological stimuli including angiotensin II, endothelin-1, and catecholamines as well as mechanical stress, which stimulates ERK1/2 activation in cardiomyocytes [64].

Hypertension results in abnormal loading conditions and therefore can lead to the development of left ventricular hypertrophy and finally to heart failure, and it is associated with increased production of tumor necrosis factor-α (TNF-α) and angiotensin II [65, 66]. Protein kinase C (PKC) and the members of mitogen-activated protein kinase cascades (MAPKs) family, such as ERK1/2, C-jun N-terminal kinase (JNK) and p38 MAPK are all involved in cardiac remodelling [11]. The PKC family contains ten isoforms, one of them, i.e. PKCε, has an important role in ischaemic preconditioning and may protect against myocardial cell death[64]. It is well known that MAPK signalling pathway plays an important role in the pathogenesis of hypertension-induced cardiac remodelling and heart failure [11, 67, 68]. MAP kinases, predominantly p38 MAPK and JNK are also regulators of myocardial fibrosis [24, 69, 70] . The activity of MAP kinases is regulated by dual-specificity phosphatases (DUSPs) or MAPK phosphatases (MKPs) that can dephosphorylate MAPKs and in this way can inhibit their activity [67, 71]. Instead of myocardial hypertrophy, increased cell death and interstitial collagen accumulation become more and more dominant. Heart failure is characterized by an increased collagen type I deposition. Collagen type I is one of the major components of the interstitium in human cardiac tissue while collagen type III is one other important component [72]. Ventricular remodelling is defined by cardiomyocyte hypertrophy and an extensive myocardial collagen deposition [73]. Transforming growth factor-β

(TGFβ)/Smad signalling route seems to be also important in the regulation of cardiac fibrosis [74, 75]. Activation of TGF-β/Smad signalling promotes myofibroblast formation and extracellular matrix (ECM) production, which lead to cardiac fibrosis [76].
In the failing heart it is crucial to ensure adequate blood supply that follows the growth of the left ventricular hypertrophy. If the rate of angiogenesis is inadequate, the transition to heart failure can occur because of the imbalance between the supply and demand of nutrients and oxygen in the heart [77].

## 1.5 Mitochondrial structure, function and quality control

Mitochondria are double-membrane-bound organelles and they are often referred to as the powerhouses of the cell. The outer membrane separates the mitochondria from the cytosol, and the inner membrane forming cristae by deep invagination encircles matrix space.
The primary task of mitochondria is the generation of adenosine triphosphate (ATP) from adenosine diphosphate (ADP) by oxidative phosphorylation, but they also have important roles in ion homeostasis, in several metabolic pathways, in programmed cell death and in ROS production. [78]. Not surprisingly, mitochondria are most abundant in cardiac muscle cells, comprising approximately 25% of cell volume in the human myocardium. Oxidative phosphorylation takes place in the inner mitochondrial membrane, where the mitochondrial electron transport chain (ETC) is localised. ETC consists of 4 complexes: nicotinamide-adenine dinuculeotide dehydrogenase (complex I; CI), succinate dehydrogenase (CII), cytochrome bc1 complex (CIII), and cytochrome c oxidase (CIV) [79]. ATP synthase (CV) is responsible for the synthesis of ATP from ADP and inorganic phosphate. These complexes are in charge of mitochondrial respiration and ATP generation, therefore they are indispensable for proper mitochondrial and cellular function [80]. Complex I-III of the respiratory chain are critical for ROS production and therefore mitochondria can become the main source of endogenous ROS production [81]. Mitochondria can generate significant amounts of ROS under several pathologic conditions including hypoxia, mitochondrial hyperpolarization and inhibition of respiratory complexes. Cardiolipin, which is a phospholipid component of the inner mitochondrial membrane, is crucial for ETC activity and is also responsible for the attachment of soluble cytochrome c to the inner membrane [82].

Mitochondria are also playing a part in the calcium homeostasis. They can transiently store calcium, which is an important second messenger and is related to contractile function and mitochondrial metabolism [14].

Mitochondria contain their own genome, the mitochondrial DNA (mtDNA), which is a double-stranded circular molecule located in the mitochondrial matrix. Mitochondrial DNA encodes 13 protein subunits and all of them are involved in the oxidative phosphorylation system [83, 84]. During oxidative stress, among others, mitochondrial DNA is damaged, which leads to insufficient ATP generation, deterioration of mitochondrial function and finally to cell death [85].

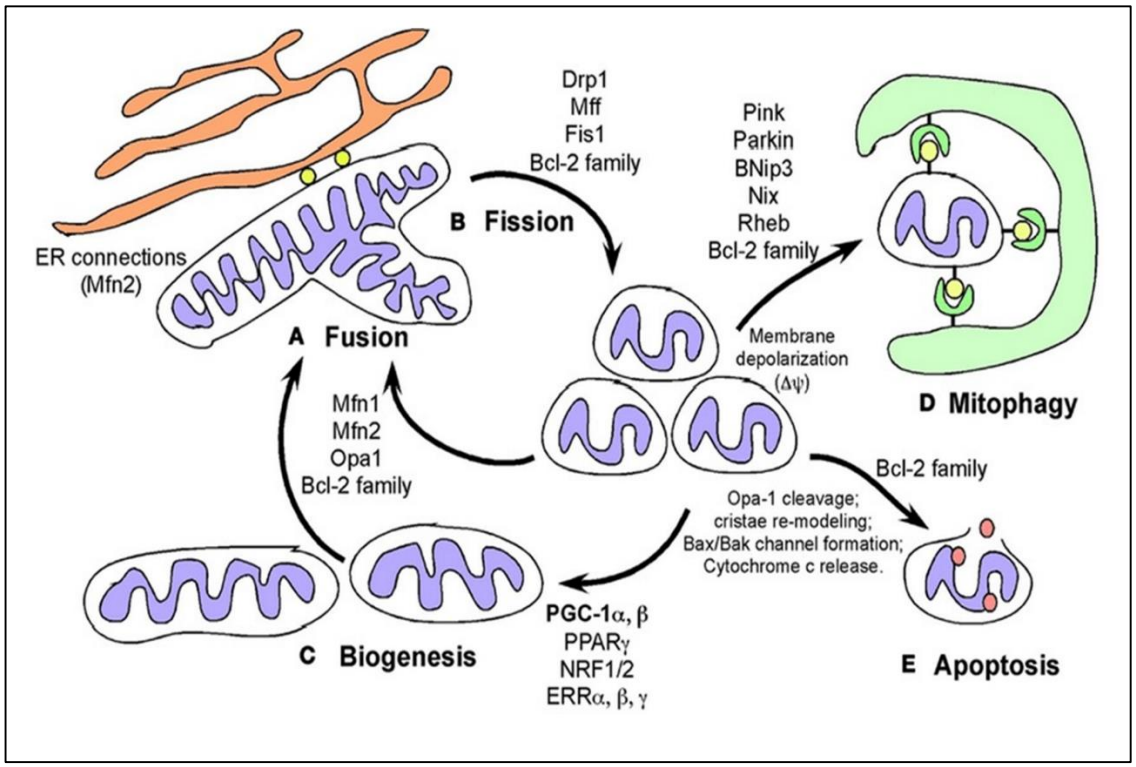


**Figure 2. Life cycle of mitochondria** [86] Mitochondria are undergoing coordinated cycles of fusion and fission, referred as 'mitochondrial dynamics', in order to maintain their shape, distribution and size. OPA-1 at the IMM and Mfn1 and Mfn2 at the OMM are promoting the fusion of membranes of juxtaposed mitochondria. Mitochondrial fission is promoted by the dynamin-related protein (DRP1) that is recruited to mitochondria in response to stress. Mitochondrial biogenesis is accompanied by an increased variation in mitochondria number, size and mass as well. The damaged mitochondria are degraded during mitophagy.

Mitochondria are dynamically changing organelles constantly undergoing fusion and fission processes – called as mitochondrial dynamics - that regulate the length, shape, size and number of mitochondria (Fig. 2). Mitochondrial fusion is referred to as a process by which the fusion of two mitochondria results in a mitochondrion, in contrast the division

of one mitochondrion into two daughter mitochondria is called as mitochondrial fission. Mitochondrial fusion is mediated by GTPases homologues, mitofusins 1 and 2 (MFN1 and MFN2) as well as optic atrophy 1 (OPA1). They regulate the fusion of outer (OMM) and inner mitochondrial membrane (IMM).

The dynamin-like GTPase OPA1 plays a key role in the mediation of inner mitochondrial membrane fusion in mammals. OPA1 contains three conserved regions, the GTP-binding domain, the middle domain and the GTP-effector domain, and two sites for proteolytic cleavage. These cleavages are mediated by two intermembrane enzymes: the ATP-dependent zinc metalloprotease YME1L and the mitochondrial metalloendopeptidase OMA1. As a result of these cleavages, short, soluble forms of OPA1 (S-OPA1) are generated from the long isoforms (L-OPA1). OMA1-dependent cleavage of OPA1 occurs only in response to cellular insults, such as mitochondrial membrane depolarization and results in mitochondrial fragmentation.

Mitochondrial fission is regulated by dynamin-related protein 1 (DRP1), which is a member of the dynamin superfamily GTPases and contains the following regions: the GTPase effector domain (GED) in C-terminal, the N-terminal GTPase domain, the middle and the variable domains. DRP1 is usually localized in the cytosol and translocates to OMM where it is harboured via receptors. The following proteins are involved in the recruitment of DRP1 to the outer mitochondrial membrane: mitochondria fission factor (Mff), mitochondrial dynamics protein of 49 kDa (MID49), 51 kDa (MID51), and fission 1 (Fis1) protein. DRP1 forms a ring-like structure around the mitochondria what results in the narrowing of the membrane [87]. After that, the hydrolysis of GTP enhances the constriction of membrane and therefore determines the potential future site of mitochondrial fission [87–89]. DRP1 is controlled by numerous post-translational modifications including phosphorylation, ubiquitinylation, SUMOylation and nitrosylation [87, 90]. Two main phosphorylation sites in DRP1 have been identified which lead to the modulation of its function. DRP1$^{Ser616}$ phosphorylation modulated by cyclin dependent kinase (CDK)1/ cyclinB/CDK5 or protein kinase C (PKC) activates the translocation of DRP1 to OMM and therefore induces subsequent mitochondrial fragmentation[91]. DRP1$^{Ser637}$ phosphorylation regulated by protein kinase A (PKA) suppresses its translocation to mitochondria and thus inhibits its activity. Calcineurin on the other hand dephosphorylates DRP1$^{Ser637}$ and activates it [89, 92].

In addition to mitochondrial dynamics, another very important part of the mitochondrial quality control is the mitochondrial biogenesis as well. Mitochondrial biogenesis can be

determined as the growth and division of pre-existing mitochondria, it is accompanied by an increased variation in mitochondria number, size and mass as well. Mitochondrial biogenesis is influenced by environmental stress such as low temperature, caloric restriction, exercise, oxidative stress and cell division [93].

The most important regulatory factor playing a part in the mitochondrial biogenesis is peroxisome proliferator-activated receptor-γ coactivator-1α (PGC-1α), which is a co-transcriptional regulatory factor [94]. PGC-1α enhances mitochondrial biogenesis via activating transcription factors e.g. nuclear respiratory factor 1 (NRF-1) and NRF-2 and therefore promotes the expression of mitochondrial transcription factor A (Tfam). Tfam is involved in the replication and transcription of mitochondrial DNA [93, 95]. The regulation of PGC-1α can be mediated in several ways. cAMP response element-binding protein (CREB) seems to be able to regulate the expression level of PGC-1α directly. AMP-activated protein kinase (AMPK) is another important regulator of mitochondrial biogenesis which is a decisive sensor of the cell energy status and becomes activated due to increased AMP/ATP ratio [93].

## 1.6 The role of mitochondria in cardiac remodelling and heart failure

The mitochondrial network plays a fundamental role in energy metabolism and therefore in maintaining the proper cardiac function. It is well known that mitochondrial energy production is damaged in the failing heart and the driving force behind these processes is the mitochondrial dysfunction. The rate of ATP production is decreased due to the defect of mitochondrial electron transport chain complexes. Moreover, the ROS production enhances during cardiac remodelling especially on the Complex I-III , therefore mitochondria become the main source of ROS generation as well as the major target of the ROS induced damage. The abnormalities of mitochondrial ultrastructure, dynamics and function altogether lead to a disruption of energy supply and ultimately to the development of heart failure (Fig.3).

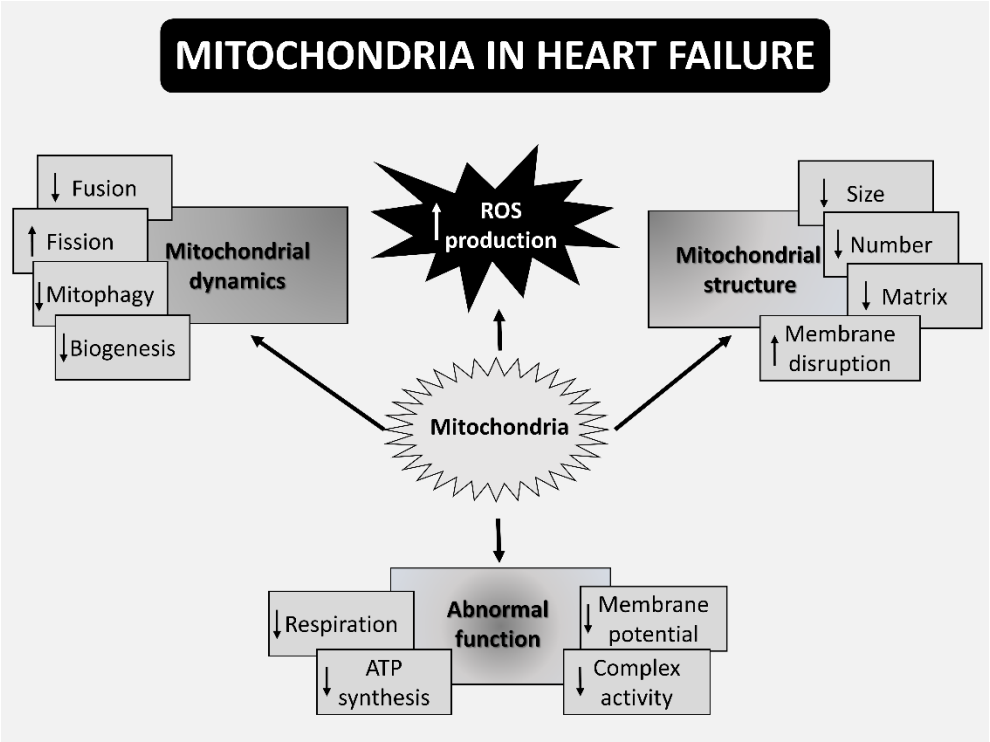


**Figure 3. The role of mitochondria in the progression of heart failure** ([78] Modified by the author)

In the human heart, there are different subpopulations of mitochondria [96]. The subsarcolemmal (SSM) subpopulation shows a heterogenic morphology and is primarily responsible for the membrane transport and further nuclear processes. Interfibrillar mitochondria (IFM) are more pleomorphic, packed between the contractile elements and play an important role in $Ca^{2+}$ buffering as well as in ATP production during the process of contraction and relaxation. Abnormal mitochondrial morphologies including reduced organelle size, fragmentation, hyperplasia, disruption of inner and outer membranes have already been observed in animal models of heart failure as well as in humans with heart failure. These morphological changes are also associated with functional abnormalities, what contributes to energy depletion.

The disruption of mitochondrial dynamics has also been described in several cardiac diseases including hypertension and heart failure. The imbalance between fusion and fission processes leads to impaired mitochondrial function. The reduction of fusion process is associated with abnormal cristae morphology, mitochondrial fragmentation and increased apoptosis, while increased fission results in fragmentation of mitochondrial network. Significant decrease has been detected in the case of OPA1 and MFN2 while

DRP1 expression level has been increased markedly in heart failure patients. It is also known that MFN1 or OPA1 ablation induces LV hypertrophy in mice [97]. In addition to ultrastructural and dynamic changes, functional changes such as reduced ATP production and elevated ROS production are also accompanied by the progression of heart failure. There is a strong connection between mitochondrial membrane potential and mitochondrial ROS production in cardiomyocytes. The opening of mitochondrial permeability transition pore (mPTP) is triggered by oxidative stress and elevated calcium concentration, which leads to the reduction of membrane potential and therefore to decreased ATP production leading finally to cell death. Excessive ROS production damages the mitochondrial ETC, causes DNA strand breaks, oxidises proteins and triggers lipid peroxidation thereby leading to mitochondrial functional impairment [85, 98]. These alterations - mtDNA damage, decreased enzymatic activity of CI, CIII, enhanced ROS production - have been reported in animal models of heart failure [40, 99]. In heart failure, fission processes predominate, resulting in a fragmented mitochondrial network that is unable to perform its function of providing energy to the cell, thereby inducing cell death. One of the associated phenomena of fission processes is the increased ROS production. These results raised the possibility that mitochondria could be new therapeutic targets in the treatment of heart failure [100]. Several studies have been performed on the inhibition of the DRP1 fission protein using the Mdivi-1 DRP1 inhibitor, but these are only effective in the short term. Mitophagy is a process by which damaged, fragmented mitochondria are eliminated. DRP1 protein plays an essential role in the fragmentation of mitochondria, so its long-term inhibition cannot be used as a therapeutic option [101, 102].

Therefore, pharmacological modulation and the promotion of mitochondrial fusion activity could have a beneficial effect on mitochondrial quality control processes under cellular stress and in this way could be a novel therapeutic approach in various cardiac diseases characterized by mitochondrial damage induced by oxidative stress. As a result, BGP-15 molecule has become the focus of our attention, which, in addition to its various cytoprotective effects, also promotes mitochondrial fusion [103].

## 1.7 BGP-15

BGP-15 ($C_{14}H_{22}N_4O_2 \cdot 2HCl$; O-[3-piperidino-2-hydroxy-1-propyl]-nicotinic acid amidoxime dihydrochloride) is a nicotinic amidoxime derivate (Fig. 4). It was originally developed as an insulin-sensitizer molecule by the N-Gene Research Laboratories Inc (Peter Literati-Nagy and Balazs Sümegi) in the late 90's. However, in the last few years, its protective effects have been proved in a wide range of experimental models. Despite these promising results, its specific intracellular target is still unknown and the exact mechanism of action has not been elucidated.

BGP-15 molecule is able to increase insulin sensitivity in an insulin resistant state by supressing JNK's inhibitory effect on the insulin receptor [104, 105].

BGP-15 also protects against oxidative stress during ischemia-reperfusion in a Langendorff heart perfusion system [106, 107]. Szabados et al. demonstrated that BGP-15 is able to reduce the mitochondrial ROS production and to inhibit the PARP-1 enzyme and thus protects against oxidative stress-induced cell death.

BGP-15 also prevents against atrial fibrillation in a transgenic mouse model of heart failure via increased phosphorylation of the insulin-like growth factor 1 receptor (IGF1RB) [108]. Furthermore, it has beneficial effects on diastolic dysfunction in a diabetic cardiomyopathy model using Goto–Kakizaki rats [109]. BGP-15 also prevented against the imatinib-induced cardiotoxic effects via decreased oxidative damage [110]. Sarszegi et al. showed that BGP-15 decreased the activity of p38 MAP kinase and JNK, and increased the phosphorylation of Akt and GSK-3β. BGP-15 protects against the ROS-induced mitochondrial ROS production and preserved the mitochondrial membrane potential in WRL-68 cell line [111]. Nagy G. et al. demonstrated that BGP-15 protects against the acetaminophen-provoked hepatocellular injury [112]. Moreover, Szabo et al. demonstrated that BGP-15 protects the lung structure in a model of pulmonary arterial hypertension [103]. More importantly it was the first article to describe that BGP-15 promotes mitochondrial fusion via activating Opa1 protein.

Fibrotic remodelling increased ROS production, activation of MAPK signalling pathways and mitochondrial damage - play a significant role in the above-mentioned diseases as well as in the pathomechanism of heart failure. Furthermore, it appears that very little information or nothing at all is available on the effect of BGP-15 regarding the development of hypertensive cardiomyopathy. Therefore, the aim of our study was to investigate the role of BGP-15 in hypertension-induced heart failure. We focused

predominantly on factors that regulate the remodelling processes, myocardial fibrosis and the pattern of related signalling pathways.

In addition, our goal was to further characterize the mitochondrial effects of BGP-15 in a chronic hypertension induced heart failure animal model and “in vitro” using primer neonatal rat cardiomyocytes (NRCM). We studied the impact of BGP-15 on the processes of mitochondrial quality control, particularly on fusion-fission processes, on mitochondrial biogenesis as well as on mitochondrial function.

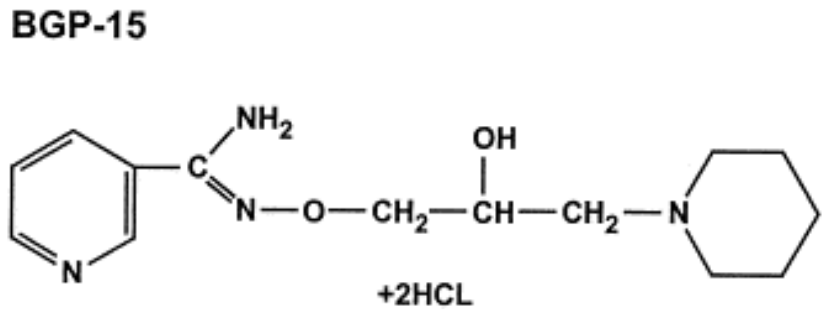


**Figure 4.** ***Chemical structure of BGP-15 (O-[3-piperidino-2-hydroxy-1-propyl]-nicotinic acid amidoxime dihydrochloride)***[107]

# 2. AIMS OF THE WORK

The aim of our work was to examine the effects of BGP-15 in a chronic hypertension-induced heart failure model and “in vitro” using primer neonatal rat cardiomyocytes (NRCM).

1. Our goal was to study the effect of BGP-15 on structure and function of heart.

2. We aimed to investigate the effects of BGP-15 on signal transduction pathways taking part in the development of cardiac remodelling and heart failure.

3. We aimed to determine its effect on the myocardial fibrotic processes.

4. We examined the effects of BGP-15 on mitochondrial fusion and fission processes as well as on mitochondrial biogenesis.

5. We tried to clarify the role of BGP-15 on mitochondrial function under stress situations.

# 3. MATERIALS AND METHODS

## 3.1 Ethics Statement

Animals received care according to the Guide for the Care and Use of Laboratory Animals published by the US National Institute of Health (NIH Publication No. 85–23, revised 1996) and the experiment was approved by the Animal Welfare Committee of the University of Pecs, Medical School (Permit number: BA02/2000-54/2017).

## 3.2 Animal model

15-month-old male Wistar Kyoto (WKY) and spontaneously hypertensive rats (Charles River Laboratories, Budapest, Hungary) were used in the experiments. One or two animals were housed per cage under standardized conditions throughout the experiment, with 12h dark-light cycle in solid-bottomed polypropylene cages and received commercial rat chew and water ad libitum. 7 SHRs were sacrificed at the beginning of the experiment as a baseline group (SHR-Baseline). SHRs were randomly divided into two groups: SHR-B and SHR-C. SHR-B group was treated with BGP-15, a water-soluble compound (25 mg/b.w. in kg/day, n=7), while SHR-C group received only placebo (n=7, SHR-C) per os for 18 weeks. BGP-15 was a gift from N-Gene Inc. (New York, NY, USA). Dosage of BGP-15 administered in the drinking water was based on our preliminary data regarding the volume of daily fluid consumption. WKY rats were used as age-matched normotensive controls (n=7). Non-invasive blood pressure measurements were performed on each animal on three occasions at Weeks 0, 9, and 18 of the treatment period. Blood pressure measurements were performed by the non-invasive tail-cuff method as described earlier [24, 113]. Blood pressure was measured by Non-Invasive Blood Pressure System with rat species platform (Panlab, Harvard Apparatus; LE5002;). At the beginning and at the end of the 18-week-long period, echocardiographic measurements were performed. At the end of the 18 weeks, animals were sacrificed, blood was collected to determine the concentration of plasma brain-derived natriuretic peptide (BNP), then hearts were removed. Atria and great vessels were trimmed from the ventricles and the weight of the ventricles was measured. Hearts were fixed in 10% formalin for histology or freeze-clamped for Western blot analysis. In order to detect the extent of fibrotic areas, histologic samples were stained with Picrosirius red and Collagen

type I immunohistochemistry was also made. The phosphorylation state of TGFβ, Smad2 and 3, Akt-1, GSK-3β and MAPK signalling molecules was monitored by Western blotting. In our research, the following group notations were used according to the applied treatment: WKY: age-matched normotensive Wistar-Kyoto rats, SHR-Baseline: 15-month-old spontaneously hypertensive rats before the treatment period, SHR-C: 19-month-old spontaneously hypertensive rats after the 18-week-long placebo treatment, SHR-B: 19-month-old spontaneously hypertensive rats after the 18-week-long treatment period with BGP-15.

### 3.3 Neonatal rat cardiomyocyte (NRCM) cell culture

Cardiomyocytes were isolated using the Pierce™ Primary Cardiomyocyte Isolation Kit (Life Technologies, Carlsbad, CA, USA #88281) from 1-3-day-old neonatal Wistar rats. The animals were sacrificed and then their hearts were removed and minced into 1-3 $mm^3$ pieces. The pieces were digested with an enzyme complex (Cardiomyocyte Isolation Enzyme 1 (with papain) and Cardiomyocyte Isolation Enzyme 2 (with thermolysin)). After the tissue became primarily a single-cell suspension, the cells were plated in 6-well plates with a density of $2.5 \times 10^6$ cell/well with specific Dulbecco's modified Eagle Medium (DMEM) for Primary Cell Isolation containing 10% fetal bovine serum (FBS), 100 IU/mL penicillin and 100μg/mL streptomycin. The medium was replaced 24 hours later with fresh Complete DMEM for Primary Cell Isolation containing Cardiomyocyte Growth Supplement, which inhibited the division of fibroblasts and therefore could maintain the cardiomyocyte suspension in high purity during the culture period. NRCMs were cultivated in normal culture conditions, 37°C, saturated humidity atmosphere of 95% air and 5% $CO_2$. Fresh medium was added every 2-3 days.

### 3.4 Treatments of neonatal rat cardiomyocytes

On the day of the experiments, cells were washed once in PBS and added fresh medium, then treated with 150 μM $H_2O_2$ with or without 50 μM BGP-15 for 0.5 hour. The following groups were created according to the applied treatment: Control group: cells without any treatment, BGP-15 group: cells with only 50 μM BGP-15 for 0.5 hour, $H_2O_2$

group: cells with 150 μM $H_2O_2$ for 0.5 hour, $H_2O_2$+BGP-15 group: cells with 150 μM $H_2O_2$ and 50 μM BGP-15 for 0.5 hour.

### 3.5 Echocardiographic measurements

Transthoracic echocardiography was performed under inhalation anaesthesia at the beginning of the experiment and on the day of sacrifice. The rats were lightly anesthetized with a mixture of 1.5% isoflurane and 98.5% of oxygen. The chest of animals was shaved and acoustic coupling gel was applied. The animals were imaged in the left lateral position, and a warming pad was used to maintain normothermia. Heart rate did not differ considerably during anaesthesia among the groups. Ventricular dimensions, wall thicknesses and systolic functions were measured from parasternal short and long axis views just above the papillary level. Parameters that are required for the evaluation of diastolic function (E, A, as well as E') were measured from the apical 4 chamber view. For the imaging of rats, a VEVO 770 high-resolution ultrasound imaging system (VisualSonics, Toronto, Canada) was used, which was equipped with a 25-MHz transducer. The investigators were blinded to the treatment protocol. LV inner dimensions (LVIDd and LVIDs), thickness of septum and posterior wall (PW), LV end-diastolic volume (LVEDV), LV end-systolic volume (LVESV), E/A as well as E/E' ratio were determined. EF (percentage) was calculated by 100×[(LVEDV−LVESV)/LVEDV].

### 3.6 Determination of Plasma B-Type Natriuretic Peptide Level

Blood samples were collected by cardiac puncture into Vacutainer tubes containing EDTA and aprotinin (0.6 IU/ml) and centrifuged at 1600 g for 15 minutes at 4°C to separate plasma, which was collected and kept at −70°C. Plasma B-type natriuretic peptide-32 levels (BNP-32) were determined by Enzyme-Linked Immunosorbent Assay method (BNP-32, Rat BNP 32 ELISA Kit, Abcam, ab108815CA, USA) as the datasheet recommends.

### 3.7 Histology

For histological examination hearts were removed at the end of the study after euthanasia performed by overdosing of isoflurane. Ventricles were fixed in 6% formalin and sliced

and embedded in paraffin. 5 μm thick sections were cut serially from the base to apex by a microtome. 7 animals from each group and 3 sections from each animal were used to determine the degree of cardiac fibrosis. Three images (magnification 10 ×) were randomly taken from the middle region of the LV wall on each section. The fibrotic area was determined on each image, and the mean value of nine images represents each animal. LV sections were stained with Picrosirius red to detect interstitial fibrosis. Slices were also processed for type I collagen (Bios rabbit polyclonal 1:500) immunohistochemistry. Binding was visualized with biotinylated/HRP conjugated secondary antibody followed by the avidin-biotin-peroxidase detection system (PK-6200 Universal Vectastain ABC Elite Kit, Vector Laboratories, Burlingame, CA) using 3,3'-diaminobenzidine (DAB) as chromogen. Progress of the immunoreaction was monitored using light microscope and the reaction was stopped by the removal of excess DAB with a gentle buffer wash. The degree of fibrosis was quantified by the NIH ImageJ image processing program via its colour deconvolution plug-in.

Picrosirius red staining was performed to measure cardiomyocyte diameter (CD) as a cellular marker of myocardial hypertrophy. 7 animals from each group and 3 sections from each animal were used to determine the cell diameter. Three images (magnification 10 ×) were randomly taken from the free LV wall on each section. Fitted polygon technique was used to determine the area of the cells. Then, the calculated diameter was used for statistical analysis. In order to evaluate the cardiomyocyte diameter, 250 cardiomyocytes were measured from each animal. The mean value of cell diameter of an animal derived from 250 measurements and each group contained 7 animals.

### 3.8 Transmission electron microscopy

For electron microscopy analysis, hearts were perfused retrogradely through the aortic root with ice-cold PBS to wash out the blood and then with modified Kranovsky fixative (2% paraformaldehyde, 2.5 % glutaraldehyde, 0.1 M Na-cacodylate buffer, pH 7.4 and 3 mM $CaCl_2$). 1 mm thick sections were cut from the free wall of the left ventricle. Dehydrated blocks were embedded in Durcupan resin. From the embedded blocks, semithin sections of 500 nm and ultrathin sections of 50 nm were cut with a Leica ultramicrotome, and mounted either on mesh, or on Collodion-coated (Parlodion, Electron Microscopy Sciences, Fort Washington, PA) single-slot, copper grids. Additional contrast was provided to these sections with uranyl acetate and lead citrate

solutions and the preparations were examined with a JEOL 1200EX-II electron microscope. 4 animals from each group, 3–5 blocks from each animal were used. The area of the interfibrillar mitochondria (IFM) were measured by freehand polygon selection (n~500/group) using the ImageJ software.

## 3.9 Western-blot analysis

### 3.9.1. Total western blot sample preparation from cardiac tissue

50 milligrams of heart samples were homogenized in ice-cold Tris buffer (50 mmol/l, pH 8.0) containing protease inhibitor (1:100; Sigma-Aldrich Co., #P8340), phosphatase inhibitor (1:100; Sigma-Aldrich Co., #P5726) and 50 mM sodium vanadate. The supernatants were harvested in 2x concentrated sodium dodecyl sulfate (SDS)-polyacrilamide gel electrophoresis sample buffer.

### 3.9.2. Fractionated western blot sample preparation from cardiac tissue

100 milligrams of heart tissues were minced in ice-cold isolation solution (150 mM NaCl, 50 mM TRIS, 1 mM EDTA, protease inhibitor (1:100; Sigma-Aldrich Co., #P8340) and phosphatase inhibitor (1:100; Sigma-Aldrich Co., #P5726)). Samples were gently disrupted on ice with Turrax, then processed in a Potter-Elvehjem tissue homogenizer. Samples were centrifuged for 12 minutes at 750 g. Supernatants containing the cytosolic and mitochondrial fractions were aspirated and the precipitated nuclear fractions were harvested in 2× SDS–polyacrylamide gel electrophoresis sample buffer and denatured at 95°C for 5 minutes. Supernatants were then centrifuged for 12 minutes at 11.000 g to gain cytosolic fraction in the supernatant and mitochondrial fraction in the precipitate. Samples were harvested separately in 2× SDS–polyacrylamide gel electrophoresis sample buffer and denatured at 95°C for 5 minutes.

### 3.9.3. Total western-blot sample preparation from NRCM cells

After the appropriate treatment cells were harvested. The cell pellet was suspended in ice-cold PBS buffer, then centrifuged for 5 min at 1,200 rpm at room temperature. The pellets were suspended in 300 μL NP-40 lysis buffer (Amresco, J619) containing protease inhibitor (1:100; Sigma-Aldrich Co., #P8340) and phosphatase inhibitor (1:100; Sigma-Aldrich Co., #P5726). The samples were shaken for 30 min at 4 °C, then they were centrifuged for 20 min (4 °C 12,000 rpm). 4x concentrated SDS-polyacrylamide gel electrophoresis sample buffer was added to each sample.

### 3.9.4. Fractionated western blot sample preparation from NRCM cells

The cell pellet was suspended in an ice-cold isolation solution (0.5mM TRIS, 1M EGTA, 0.4M sucrose) containing 0.5 mM sodium metavanadate, 0.05M EDTA and protease inhibitor (1:100; Sigma-Aldrich Co., #P8340). Samples were disrupted on ice by Turrax, then processed by a Potter-Elvehjem tissue homogenizer. Centrifugation was carried out for 15 minutes at 750 g. The nuclear fraction in the precipitate was harvested in 72% trichloroacetic acid. Subsequently, supernatants were aspirated and centrifuged for 15 minutes at 10.000 g to gain cytosolic fraction in the supernatant and mitochondrial in the precipitate. Samples were harvested separately in 72% trichloroacetic acid. The precipitated fractions were centrifuged for 10 minutes at 15.000 g. Each precipitate was harvested separately in a 50 mM TRIS and SDS-polyacrilamide gel electrophoresis sample buffer. The samples were shaken for overnight at 4°C and denatured at 95°C for 5 minutes. After that they were centrifuged for 10 minutes at 15.000 g and the supernatants were collected as the mitochondrial fraction.

### 3.9.5. Electrophoresis and transfer of proteins

After the preparation, the tissue and cell culture samples were processed in the same manner. Protein levels were measured with Nanodrop. Glyceraldehyde 3-phosphate dehydrogenase (GAPDH; 1:1000; Cell Signaling #2118) and pyruvate dehydrogenase (PDC; 1:1000; Cell Signaling #3205) were used as a representative loading control. Proteins were separated on 12% SDS-polyacrylamide gel and transferred to nitrocellulose membranes. After blocking (2h with 5% BSA in Tris-buffered saline contained with 1% Tween-20), membranes were probed overnight at 4°C with primary antibodies recognizing the following antigens: transforming growth factor-β (TGF-β; 1:1000; Cell Signaling #3711), Smad2 (1:1000; Invitrogen, 436500), phospho-specific Smad2 Ser465/467 (1:1000; Invitrogen, MA5-15122), Smad3 (1:1000; Cell Signaling #9523), phospho-specific Smad3 Ser423/425 (1:1000; Cell Signaling #9520), protein kinase B (Akt; 1:1000; Cell Signaling #9272), phospho-specific Akt-1/protein kinase B-α Ser473 (1:1000; Cell Signaling #4060), glycogen synthase kinase-3β (GSK-3β; 1:1000; Cell Signaling #9832), phospho-specific glycogen synthase kinase -3β Ser9 (1:1000; Cell Signaling #5558), p38 mitogen-activated protein kinase (p38MAPK; 1:1000; Cell Signaling #8690), phospho-specific p38 mitogen-activated protein kinase Thr180/Tyr182 (1:1000; Cell Signaling #4511), c-Jun N-terminal kinase (JNK; 1:1000; Cell Signaling

#9252), phospho-specific c-Jun N-terminal kinase Thr183/Tyr185 (1:1000; Cell Signaling #9255), extracellular signal–regulated kinase (ERK1/2; 1:1000; Cell Signaling #4695), phospho-specific extracellular signal–regulated kinase 1/2 Thr202 (1:1000; Cell Signaling #4370), mitogen-activated protein kinase phosphatase-1 (MKP-1; 1:100; Santa Cruz Biotechnology, sc-373841, optic atrophy 1 (OPA1; 1:1000; Cell Signaling #80471), mitofusin-1 (MFN1; 1:1000; Abcam ab57602), mitofusin-2 (MFN2; 1:1000; Cell Signaling #9482), dynamin-related protein 1 (DRP1; 1:1000; Cell Signaling #8570), phospho-specific DRP1 Ser637 (1:500; Cell Signaling #4867), phospho-specific DRP1 Ser616 (1:500; Cell Signaling #3455), voltage-dependent anion channel (VDAC; 1:1000; Cell Signaling #4661), mitochondrial fission 1 protein (FIS1; 2μg/mL, Abcam, ab71498), peroxisome proliferator-activated receptor gamma coactivator 1-alpha (PGC-1α; 1:1000; Novus Biologicals, NBP1-04676), cAMP response element-binding protein (CREB; 1:1000; Cell Signaling #4820), phospho-specific cAMP response element-binding protein Ser133(1:1000; Cell Signaling #9198), 5' AMP-activated protein kinase (AMPK; 1:1000; Cell Signaling #2532), phospho-specific 5' AMP-activated protein kinase Thr172 (1:1000; Cell Signaling #2535), anti-NADH dehydrogenase Fe-S protein 1 (NDUFs1, Novus Biologicals, NBP1-31142, 1:1000), anti-Ubiquinol-cytochrome c reductase core protein I (UQCRC1, Novus Biologicals, NBP2-03825, 1:1000). Membranes were washed six times for 5 min in Tris-buffered saline (pH 7.5) containing 0.2% Tween (TBST) before the addition of horseradish peroxidase-conjugated secondary antibody (goat anti-rabbit IgG, Sigma Aldrich Co. A0545, 1:3000 dilution; rabbit anti-mouse IgG, Sigma Aldrich Co., A9044, 1:5000 dilution). Membranes were washed six times for 5 min in TBST, and then the antibody-antigen complexes were visualized by enhanced chemiluminescence. The results of Western blots were quantified using the NIH ImageJ program.

### 3.10 Capillary electrophoresis immunoassay

Due to the limited availability of primary neonatal cardiomyocytes and the lower protein concentration of the fractionated samples made from it, the more sensitive capillary immunoassay method with less sample requirements and higher throughput is more suitable for measurement. Simple western analysis (Wes) was performed on a Wes system (ProteinSimple, product number 004–600) according to the manufacturer's instructions using a 12-230 kDa Separation Module (ProteinSimple SM-W004) and either the Anti-Rabbit Detection Module (ProteinSimple DM-001) or the Anti-Mouse Detection

Module (ProteinSimple DM-002), depending on the primary used antibody. Subcellular NRCM samples were mixed with Fluorescent Master Mix and heated at 95˚C for 5 min. The samples, blocking reagent (antibody diluent), primary antibodies (in antibody diluent), HRP-conjugated secondary antibodies and
chemiluminescent substrate were pipetted into the plate (part of Separation Module). Instrument default settings were used: stacking and separation at 475 V for 30 min; blocking reagent for 5 min, primary and secondary antibody both for 30 min; Luminol/peroxide chemiluminescence detection for ~15 min (exposures of 1-2-4-8-16-32-64-128-512 s). The resulting electropherograms were inspected to check whether automatic peak detection required any manual correction.

### 3.11 Evaluation of mitochondrial fragmentation with fluorescent microscopy

NRCM cells were seeded at a density of $10^5$ cells/well in 6 well plates on glass coverslips with 1 % gelatin coating and cultured at least for 2 days before the experiment. On the day of the experiment, cells were washed once in PBS and added fresh medium, then treated with $H_2O_2$ with or without BGP-15. After the appropriate treatment coverslips were rinsed in PBS, and 75 nM MitoTracker Red CMXRos dissolved in serum free DMEM were added and it was incubated for 30 min at 37°C. After the incubation, coverslips were rinsed in PBS and the mitochondrial network was visualized by a Nikon Eclipse Ti-U fluorescent microscope equipped with a Spot RT3 camera using a 60x objective and epifluorescent illumination.

### 3.12 Quantification of mitochondrial DNA (mtDNA) damage by real-time PCR

After the appropriate treatment cells were harvested, and total DNA was isolated using GenElute™ Mammalian Genomic DNA Miniprep Kits (Sigma-Aldrich # G1N350-1KT). Realtime DNA amplification was performed using a CFX96 Touch Real-Time PCR Detection System (Bio-Rad). The following rat primer sequences were used: SRPCR (210 bp) forward: 5’-ATGCACGATAGCTAAGACCCAA-3’; reverse: 5’-CTGAATTAGCGAGAAGGGGTA-3’and LRPCR (14958 bp) forward: 5’-ATTTTCTCCCAGTTACGAAAG-3’, reverse: 5’-CTTGGTAAGTAAATTTCTTTCTCC-3’. Short fragment, cytochrome c oxidase

subunit 1 (COX1), cytochrome c oxidase subunit 3 (COX3) and β-actin were done using a Brilliant II QPCR Master Mix (Agilent Technologies, # 600804). The final SRPCR, COXI, COXIII and β-actin cycling parameters followed hot start of 10 min @95°C followed by; 30sec@95°C, 1min@60°C,30sec@72°C for 40 cycles. LRPCR was done using PfuUltra II Hotstart 2× Master Mix (Agilent Technologies, #600852). The final LRPCR cycling parameters, following the manufacturer's recommendations: hot start of 2min@92°C followed by; 15sec@92°C, 30sec@50°C, 8:00min@68°C for 40 cycles. The relative mitochondrial DNA content was determined by real-time PCR, using COX1 and COX3 primers, normalized to a nuclear-encoded β-actin gene. The following rat primer sequences were used: COX1 (199 bp) forward: 5'- CACAGTAGGGGGCCTAACAG-3', reverse: 5'-CAAAGTGGGCTTTTGCTCAT-3'; COX3 (244 bp) forward 5'-TCAGGAGTCTCAATTACATG-3', reverse: 5'- CGTAGTAGACAGACAATTAGG-3'; β-actin (191 bp) forward 5'-GCGGTGACCATAGCCCTCTTT-3', reverse: 5'-TGCCACTCCCAAAGTAAAGGGTCA-3'. The software automatically generated crossing points and calculation of mtDNA damage was made using the Δ2Ct method. EvaGreen dye was used (Biotium # 31000).

### 3.13 Mitochondrial membrane potential measurement with JC-1 assay

The mitochondrial membrane potential (ΔΨm) was measured using the mitochondrial membrane potential specific fluorescent probe, JC-1 (Enzo Life Sciences, ENZ-52304). NRCM cells were seeded on glass coverslips coated with gelatin and cultured for at least 2 days before the experiment. After the treatment, cells were washed in PBS and incubated for 15 min at 37°C in media containing 5 μg/mL JC-1. When excited at 488 nm, the dye emits red fluorescence (590 nm) at high ΔΨm and green (530 nm) at low ΔΨm. Following incubation, the cells were washed once with PBS and then imaged with a Nikon Eclipse Ti-U fluorescent microscope equipped with a Spot RT3 camera using a 60x objective and epifluorescent illumination. All experiments were repeated three times. Fluorescent signals were quantified by using the ImageJ software (NIH, Bethesda, MD, USA).

## 3.14 Evaluation of the mitochondrial energy metabolism and function

Agilent Seahorse Extracellular Flux (XFp) Analyzer (Agilent Technologies, (Santa Clara, CA, USA)) was used to determine the NRCM cells' oxygen consumption rate (OCR). NRCM cells were seeded in XFp Miniplate at a density of $4x10^4$ cells/well in 80 µL complete growth medium (DMEM for Primary Cell Isolation containing 10% FBS, 100 IU/mL penicillin and 100 µg/mL streptomycin) and incubated at 37 °C, 5% $CO_2$ for 2 days. On the day before the experiment, Sensor cartridges were hydrated in XFp calibrant and maintained at 37°C without $CO_2$ overnight. On the day of the assay, after subjecting cells to the appropriate treatment, DMEM for Primary Cell Isolation medium was replaced by Agilent Seahorse XF Base Medium containing 1 mM pyruvate, 2 mM glutamine and 10 mM glucose (adjusted pH to 7.4 with 0.1 N NaOH). Before measurement, different compounds were loaded into the appropriate ports of a hydrated sensor cartridge (10 µM oligomycin, 10 µM FCCP, and 5 µM rotenone/antimycin) Three measurements were performed after each injection. OCR was used to determine mitochondrial energy metabolism. The parameter values, including basal respiration, maximal respiration, ATP-associated OCR and spare respiratory capacity, were determined according to the Seahorse XFp Cell Mito Stress user guide protocol. Data were analysed using the Seahorse XF test report analysis.

## 3.15 Analysis of citrate synthase activity in NRCM cells

NRCM cells were seeded at a density of $10^6$ cells/well in 6-well plates and cultured. After the appropriate treatment, cells were harvested, the cell pellet was suspended in ice-cold citrate synthase cell lysis buffer, then centrifuged for 5 min at 4°C at 10,000 x g, then the supernatant was collected for further use. Citrate synthase was measured using a kit from Sigma Aldrich (MAK193) following the manufacturer's instruction. The absorbance was recorded at 412 nm every 5 minutes for 50 minutes. The colorimetric product (GSH) was proportional to the enzymatic activity of citrate synthase and normalized to the quantity of cells.

## 3.16 Statistical analysis

Statistical analysis was performed by SPSS for Windows, version 26.0. All of the data were expressed as the mean ± SEM. Normality of distribution was assessed by Shapiro-Wilk test. Baseline comparison between the strains were conducted by Student's t-test before randomization. The homogeneity of the groups was tested by Levene's test. Differences between treatment groups were determined by one-way ANOVA. For post-hoc comparison Tukey HSD or Dunnett T3 test were applied. A value of $p<0.05$ was considered statistically significant.

# 4. RESULTS

## 4.1 In vivo results

### 4.1.1 BGP-15 administration improved gravimetric parameters in SHR animals

At the beginning of the study, the body weight of WKY rats was significantly higher than the SHR rats (WKY: 386.40±4.33 g, SHR-Baseline: 343.21±2.48 g, SHR-C: 346.90±6.65 g, SHR-B: 340.73±6.32 g; $p<0.01$, WKY vs. SHR groups; Table 1). Similar observation can be made at the end of the study (WKY: 401.45±8.94 g, SHR-C: 358.13±5.08 g, SHR-B: 356.85±4.54 g; $p<0.05$ WKY vs. SHR groups). At the end of the study, heart weights (HW) and weight of ventricles (VW) were significantly increased in the SHR groups compared to the WKY group (HW: WKY: 1.12±0.04 g, SHR-Baseline: 1.16±0.02, SHR-C: 1.49±0.05 g, SHR-B: 1.23±0.02 g; $p<0.01$ SHR-B and SHR-C vs. WKY; VW: WKY: 0.95±0.04 g, SHR-Baseline: 1.09±0.02 g, SHR-C: 1.33±0.05 g, SHR-B: 1.23±0.02 g; $p<0.01$ SHR-C vs. WKY, $p<0.01$ SHR-B vs. SHR-C). The ratio of ventricular weight to body weight (VW/BW) was markedly increased in SHR groups compared to WKY animals (VW/BW(mg/g): WKY: 2.28±0.11, SHR-Baseline: 3.19±0.08, SHR-C: 3.73±0.16, SHR-B: 3.21±0.03; $p<0.01$ SHR groups vs. WKY, $p<0.05$ SHR-B vs. WKY, $p<0.01$ WKY vs. SHR-Baseline and SHR-C, $p<0.01$ SHR-C vs. SHR-Baseline, $p<0.01$ SHR-B vs. SHR-C). The ratio of ventricular weight to the length of right tibia (VW/TL) was also significantly increased (VW/TL (mg/mm): WKY: 21.27±0.79, SHR-Baseline: 24.76±0.82, SHR-C: 29.79±0.94, SHR-B: 25.76±0.46; $p<0.05$ WKY vs. SHR-Baseline and SHR-B, $p<0.01$ SHR-C vs. WKY and SHR-Baseline). BGP-15 treatment caused a significant moderation of these ratios ($p<0.01$ SHR-B vs. SHR-C). The ratio of the lung wet weight-to-dry weight was also significantly enhanced in the SHR-C group (Lung wet weight/dry weight(g/g): WKY: 4.42 ± 0.26 g/g, SHR-Baseline: 4.51±0.13, SHR-C: 5.68±0.24, SHR-B: 4.68±0.13; $p<0.01$ SHR-C vs. WKY and SHR-Baseline). BGP-15 caused a significant moderation of this ratio ($p<0.01$ SHR-B vs. SHR-C).

**Table 1. Effect of BGP-15 administration on gravimetric parameters of SHR animals**

| | WKY (n=7) | SHR-Baseline (n=7) | SHR-C (n=7) | SHR-B (n=7) |
|---|---|---|---|---|
| **$BW^{START}$ (g)** | 386.40 ± 4.33 | 343.21 ± 2.48$^{**}$ | 346.90 ± 6.65$^{**}$ | 340.73 ± 6.32$^{**}$ |
| **$BW^{END}$ (g)** | 401.45 ± 8.94 | - | 358.13 ± 5.08$^{**}$ | 356.85 ± 4.54$^{**}$ |
| **$HW^{END}$ (g)** | 1.12 ± 0.04 | 1.16 ± 0.02 | 1.49 ±0.05$^{**,\#\#}$ | 1.23± 0.02$^{\S\S}$ |
| **$VW^{END}$ (g)** | 0.95 ± 0.04 | 1.09± 0.02 | 1.33 ± 0.05$^{**,\#\#}$ | 1.14 ± 0.02$^{\S\S}$ |
| **$VW/BW^{END}$ (mg/g)** | 2.28 ± 0.11 | 3.19 ± 0.08$^{**}$ | 3.73 ± 0.16$^{**,\#\#}$ | 3.21 ± 0.03$^{*,\S}$ |
| **$VW/TL^{END}$ (mg/mm)** | 21.27 ± 0.79 | 24.76 ± 0.82$^{*}$ | 29.79 ± 0.94$^{**,\#\#}$ | 25.76 ± 0.46$^{*,\S\S}$ |
| **Lung wet/dry $weight^{END}$ (g/g)** | 4.42 ± 0.26 | 4.51 ± 0.13 | 5.68 ± 0.24$^{**,\#\#}$ | 4.68 ± 0.13$^{\S\S}$ |

*$BW^{START}$: body weight at the beginning of the treatment; $BW^{END}$: body weight at the end of the treatment; $HW^{END}$: heart weight at the end of the treatment; $VW^{END}$: ventricles weight at the end of the treatment; $TL^{END}$: length of right tibia at the end of the treatment. Values are means±SEM. WKY: age-matched normotensive Wistar-Kyoto rats, n=7; SHR-Baseline: 15-month-old spontaneously hypertensive rats, n=7; SHR-C: non-treated spontaneously hypertensive rats, n=7; SHR-B: spontaneously hypertensive rats receiving BGP-15 for 18 weeks, n=7. $^{*}p<0.05$ vs. WKY, $^{**}p<0.01$ vs. WKY, $^{\#\#}p<0.01$ vs. SHR-Baseline, $^{\S}p<0.05$ vs. SHR-C, $^{\S\S}p<0.01$ vs. SHR-C.*

### 4.1.2 BGP-15 improved left ventricular function and moderated left ventricular hypertrophy

At the beginning of the study there was a significant difference between the systolic arterial blood pressure of the WKY and the SHR group. (WKY: 134.85 ± 1.95 mmHg, SHR-Baseline: 214.28 ± 3.70 mmHg; $p<0.05$; n=7). Systolic arterial blood pressure values did not differ significantly between the SHR groups at the end of the study (SHR-C: 226.14 ± 3.88 mmHg, SHR-B: 216.85 ± 3.90 mmHg; $p>0.05$; n=7). Long-term BGP-15 treatment apparently did not exert any significant effect on systolic blood pressure.

At the beginning of the study, the septum and posterior wall thickness was significantly higher in SHR animals compared to WKY animals ($p<0.01$ SHR-Baseline vs. WKY) (Table 2). By the end of the 18-week-long treatment period, the severity of left ventricular hypertrophy remained unchanged in SHR-C animals. However, wall thicknesses were significantly reduced as a result of BGP-15 treatment ($p<0.05$, SHR-B vs. SHR-C). LV end-diastolic (LVEDV) and LV end-systolic volumes (LVESV) were also significantly

elevated in SHR-C animals ($p<0.01$, SHR-C vs. WKY, SHR-Baseline). BGP-15 treatment, however, was able to moderate this elevation in SHR-B animals ($p<0.05$ vs. SHR-C). LV mass was significantly higher in SHR-Baseline group compared to WKY ($p<0.05$ SHR-Baseline vs. WKY). In SHR-C animals, this parameter increased further compared to the initial value ($p<0.01$, SHR-C vs. WKY; $p<0.05$, SHR-C vs. SHR-Baseline). This parameter was also decreased in the SHR-B group compared to non-treated animals ($p<0.05$, SHR-B vs. SHR-C).

The left ventricular systolic function (EF%) reduced in both SHR groups compared to the initial value, however, this decrease was more pronounced in the SHR-C group than in the treated animals ($p<0.05$ SHR-B vs. SHR-C). The diastolic function marker E/E' ratio was significantly increased in the SHR-C group ($p<0.05$ SHR-C vs. SHR-Baseline), indicating a worsening of diastolic function. However, BGP-15 treatment decreased significantly the E/E' ratio in the treated group, compared to the SHR-C animals ($p<0.01$, SHR-B vs. SHR-C).

**Table 2. Effect of BGP-15 treatment on echocardiographic parameters**

| | **WKY (n=7)** | **SHR-Baseline (n=7)** | **SHR-C (n=7)** | **SHR-B (n=7)** |
|---|---|---|---|---|
| | **Mean ± SEM** | **Mean ± SEM** | **Mean ± SEM** | **Mean ± SEM** |
| **Septum** | 1.93±0.03 | 2.29±0.07** | 2.32 ± 0.07** | 2.09 ± 0.08*,§ |
| **PW** | 1.90±0.04 | 2.06±0.06* | 1.97 ± 0.08* | 1.81 ± 0.07§ |
| **LVIDd (mm)** | 7.61±0.14 | 7.75±0.15 | 8.55 ± 0.23**,## | 8.31 ± 0.18** |
| **LVIDs (mm)** | 4.54±0.13 | 4.60±0.21 | 5.87 ± 0.31**,## | 5.19 ± 0.32§ |
| **LVEDV (µl)** | 310.25±12.85 | 323.07±14.59 | 402.40 ± 24.76**,## | 377.19 ± 17.37** |
| **LVESV (µl)** | 96.01±6.85 | 101.51±12.27 | 175.52 ± 22.46**,## | 137.23 ± 16.46**,§ |
| **LV mass (mg)** | 1029.81±43.84 | 1384.42±40.69** | 1587.38 ± 106.36**,# | 1321.44 ± 75.58*,§ |
| **EF%** | 70.48±1.12 | 69.59±2.41 | 57.21 ± 3.02**,## | 64.30 ± 2.88*,§ |
| **E/A** | 1.37±0.07 | 1.70±0.09** | 2.02 ± 0.06** | 1.27 ± 0.08§§ |
| **E/E'** | 30.45±2.00 | 30.32±2.98 | 40.41± 2.94**,## | 25.71 ± 3.03§§ |
| **BNP (pg/ml)** | 302.76±13.76 | 325.19±10.89 | 755.14±33.34*,# | 352.04±22.50§ |

*Septum: thickness of the septum, PW: thickness of the posterior wall, LVIDd: left ventricular (LV) end-diastolic inner diameter, LVIDs: LV end-systolic inner diameter, LVEDV: LV end-diastolic volume, LVESV: LV end-systolic volume, LV mass: calculated weight of left ventricle, EF: ejection fraction, E: mitral peak velocity of early diastolic filling, A: mitral peak velocity of late diastolic filling, E': early diastolic mitral annular velocity, A': late diastolic mitral annular velocity, BNP: B-type natriuretic peptide. WKY: age-matched normotensive Wistar-Kyoto rats, n=7; SHR-Baseline: 15-month-old spontaneously hypertensive rats, n=7; SHR-C: 19-month-old spontaneously hypertensive rats received placebo for 18 weeks, n=7; SHR-B: 19-month-old*

*spontaneously hypertensive rats received BGP-15 for 18 weeks, n=7. *p<0.05 vs. WKY, **p<0.01 vs. WKY, #p<0.05 vs. SHR-Baseline, ##p<0.01 SHR-Baseline, §p<0.05 vs. SHR-C, §§p<0.01 vs. SHR-C.*

### 4.1.3 BGP-15 decreased the heart-failure-induced elevation of plasma BNP level

By the end of the treatment period the plasma BNP level increased significantly in the SHR-C group compared to the WKY and SHR-Baseline group ($p<0.05$, SHR-C vs. WKY and SHR-Baseline group; Table 2.). BGP-15 treatment, however, caused a significant decrease in the level of this biomarker of heart failure in SHR animals ($p<0.05$, SHR-B vs. SHR-C). The BNP level was only slightly elevated in the SHR-B group.

### 4.1.4 BGP-15 treatment prevented interstitial collagen deposition

Histological staining of the left ventricle of rat hearts was performed with Picrosirius red staining (Fig. 5.a-b) and collagen I immunohistochemistry (Fig. 5.c-d), that were used to monitor the degree of fibrosis. Only a low amount of interstitial collagen could be seen in the WKY group using the Picrosirius red staining (Fig. 5.a). The extent of fibrosis was significantly higher in the SHR groups compared to the WKY group ($p<0.05$, SHR-Baseline vs. WKY; $p<0.01$, SHR-C and SHR-B vs. WKY; Fig. 5.a). Chronic high blood pressure-induced heart failure caused a further elevation of collagen deposition in SHR-C group ($p<0.01$, vs. SHR-Baseline group). BGP-15 treatment, however, resulted in a significant decrease in the amount of interstitial fibrosis in the SHR-B group compared to non-treated hypertensive animals ($p<0.01$, SHR-B vs. SHR-C; Fig. 5.a) (WKY: 11.78±1.00%; SHR-Baseline: 16.59±1.03%; SHR-C: 32.42±1.52%; SHR-B: 22.64±1.09%; Fig. 5.b).

Similar observations could be made in the case of type I collagen immunohistochemistry (Fig. 5.c-d). Only a low amount of interstitial collagen was observed in the WKY group (WKY: 9.15±0.54%; SHR-Baseline: 15.45±0.69%; SHR-C: 31.24±0.77%; SHR-B: 19.92±0.72%; Fig. 5.d), however, in the case of hypertensive groups, even the initial value was higher than in the WKY group ($p<0.01$ vs. SHR-Baseline). This elevation became more pronounced by the end of the treatment period ($p<0.01$ SHR-C vs. WKY, SHR-Baseline groups; Fig. 5.c). Due to BGP-15 treatment the interstitial collagen deposition was significantly decreased in the SHR-B group compared to the SHR-C group

($p<0.01$; Fig. 5.c). It can be concluded that BGP-15 treatment significantly reduced the extent of interstitial fibrosis in the myocardium (Fig. 5.a-d).

### 4.1.5 Effect of BGP-15 administration on the diameter of cardiomyocytes

Histological sections from the left ventricle of the heart stained with Picrosirius red were also used to study the cell diameters (Fig. 5.e-f). The diameter of cardiomyocytes was markedly elevated in SHR groups compared to the WKY group (WKY: 16.02±0.64μm; SHR-Baseline: 22.76±0.70 μm; SHR-C: 33.86±1.82 μm; SHR-B: 28.57±0.57 μm; Fig. 5.f). This difference was the most pronounced in the case of SHR-C ($p<0.01$, SHR-C vs. WKY). BGP-15 treatment resulted in significantly lower cell diameters in the SHR-B group compared to the SHR-C group ($p<0.01$; SHR-B vs. SHR-C; Fig. 5.e).

### 4.1.6 BGP-15 treatment favourably influenced the TGF-β/SMAD signalling pathway

The level of TGF-β was significantly elevated in all hypertensive groups compared to the WKY group ($p<0.05$, SHR-B vs. WKY, $p<0.01$ SHR-Baseline, SHR-C vs. WKY; Fig. 6.). In case of SHR-C group a further increasing tendency could be seen by the end of the treatment period compared to the baseline values (NS). However, BGP-15 treatment caused a significant decrease in the TGF-β level compared to the untreated SHR animals ($p<0.01$, SHR-B vs. SHR-C), moreover TGF-β level in this group was even lower than in the SHR-Baseline group ($p<0.05$, SHR-B vs. SHR-Baseline; Fig. 6.). In the case of Smad2 phosphorylation we observed a mild increase in the SHR-Baseline group compared to the WKY group, however this elevation was not significant. The phosphorylation of $Smad2^{Ser465/467}$ was significantly increased in the SHR-C animals compared to the WKY and Baseline Groups ($p<0.05$). BGP-15 treatment resulted in a significant reduction in the phosphorylation level of $Smad2^{Ser465/467}$ in the treated group ($p<0.01$ SHR-B vs. SHR-C). There were no significant differences regarding the phosphorylation of $Smad3^{Ser423/425}$ between the groups (Fig. 6.).

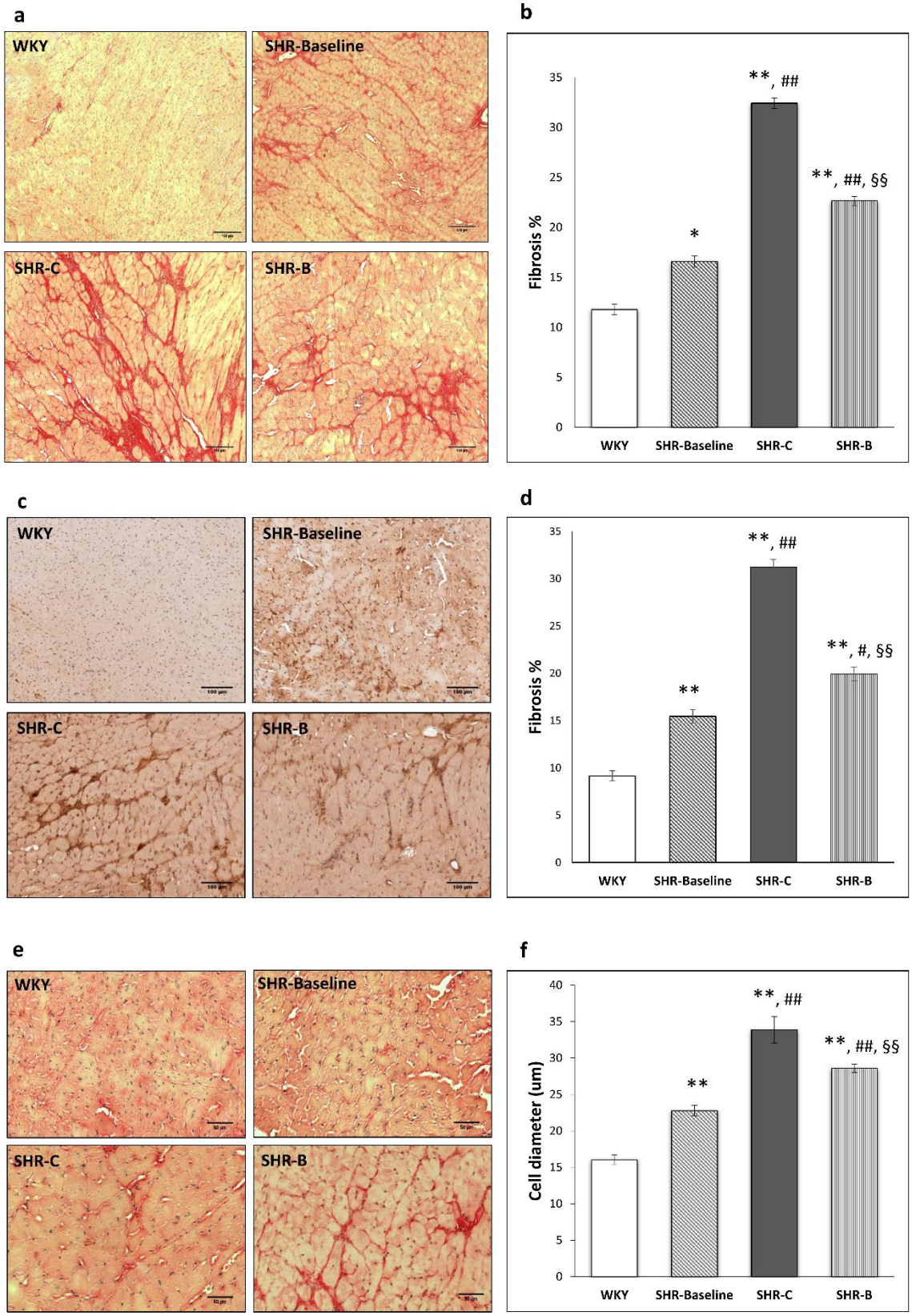


***Figure 5. Effect of BGP-15 treatment on the extent of interstitial fibrosis, on the type I collagen deposition and on the diameter of cardiomyocytes.*** *Representative histological sections stained with Picrosirius red (a) (n=7). Scale bar: 150 µm, magnification: 10-fold. Densitometric*

*evaluation of the sections is shown (b). * p<0.05 vs. WKY, ** p<0.01 vs. WKY, ##p<0.01 vs. SHR-Baseline, §§p<0.01 vs. SHR-C. Representative histological sections detected with type I collagen immunohistochemistry (c) (n=7). Scale bar: 100 µm, magnification: 10-fold. Densitometric evaluation of the sections is shown (d). ** p<0.01 vs. WKY, ## p<0.01 vs. SHR-C, §§ p<0.01 vs. SHR-C. Representative histological sections stained with Picrosirius red (e) (n=7). Scale bar: 50 µm, magnification: 10-fold. Average cellular diameter in the different groups is shown (f). **p<0.01 vs. WKY, #p<0.05 vs. SHR-Baseline, §§ p<0.01 vs. SHR-C. WKY: age-matched normotensive Wistar-Kyoto rats; SHR-Baseline: 15-month-old spontaneously hypertensive rats; SHR-C: 19-month-old spontaneously hypertensive rats received placebo for 18 weeks; SHR-B: 19-month-old spontaneously hypertensive rats received BGP-15 for 18 weeks.*

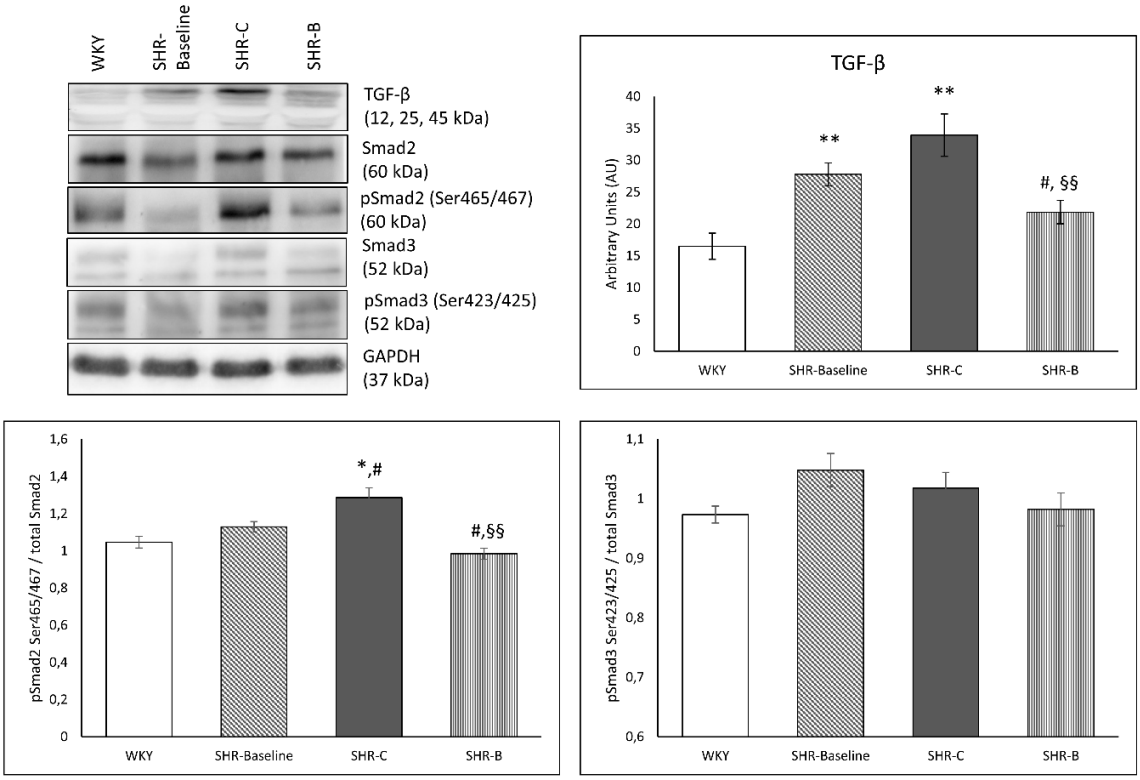


***Figure 6. Effect of BGP-15 treatment on the TGFβ/Smad signalling pathway.*** *Representative Western blot analysis of TGFβ, Smad2, Smad3 and phosphorylation as well as densitometric evaluation are shown. GAPDH was used as a loading control. WKY: age-matched normotensive Wistar-Kyoto rats, n=7; SHR-Baseline: 15-month-old spontaneously hypertensive rats, n=7; SHR-C: non-treated spontaneously hypertensive rats, n=7; SHR-B: spontaneously hypertensive rats receiving BGP-15 for 18 weeks, n=7. Values are mean±SEM. *p<0.05 vs. WKY, **p<0.01 vs. WKY, #p<0.05 vs. SHR-Baseline, §§p<0.01 vs. SHR-C.*

### 4.1.7 BGP-15 favourably affected the phosphorylation of Akt-1$^{Ser473}$ and GSK-3β$^{Ser9}$

The level of Akt-1$^{Ser473}$ phosphorylation was moderate both in the WKY group and in the SHR-Baseline group (Fig. 7.). In the SHR-C group, phosphorylation of Akt-1$^{Ser473}$ was slightly, but significantly increased (p<0.01 SHR-C vs. WKY and SHR-Baseline groups;

Fig 7.). However, BGP-15 treatment caused a marked increase in the Akt-1$^{Ser473}$ phosphorylation in SHR-B animals ($p<0.01$ SHR-B vs. SHR-C group).

The phosphorylation level of GSK-3β$^{Ser9}$ was low in the WKY group similarly to Akt-1$^{Ser473}$ phosphorylation. In the SHR-Baseline and the SHR-C groups, however, slightly but not significantly elevated phosphorylation could be seen. The highest phosphorylation of GSK-3β$^{Ser9}$ was measured in the SHR-B group. This elevation was highly significant comparing to other SHR groups ($p<0.05$ SHR-B vs. SHR-C, $p<0.01$, SHR-B vs. SHR-Baseline group; Fig. 7.).

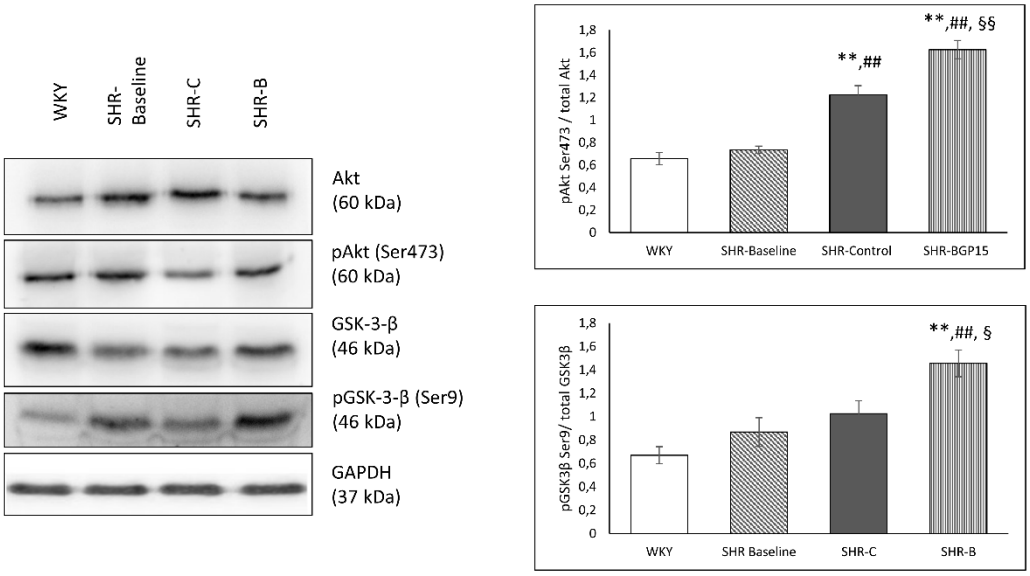


***Figure 7. Effect of BGP-15 treatment on the phosphorylation of Akt-1$^{Ser473}$ and GSK-3β$^{Ser9}$.*** *Representative Western blot analysis of Akt-1 and GSK-3β phosphorylation as well as densitometric evaluation are shown. GAPDH was used as a loading control. WKY: age-matched normotensive Wistar-Kyoto rats, n=7; SHR-Baseline: 15-month-old spontaneously hypertensive rats, n=7; SHR-C: non-treated spontaneously hypertensive rats, n=7; SHR-B: spontaneously hypertensive rats receiving BGP-15 for 18 weeks, n=7. Values are mean±SEM. **p<0.01 vs WKY, ##p<0.01 vs SHR-Baseline, §p<0.05 vs SHR-C, §§ p<0.01 vs. SHR-C.*

### 4.1.8 BGP-15 decreased the activity of MAPKs

The level of MKP-1 protein was low in the WKY and SHR-Baseline groups (Fig. 8.), however, a significant increase was observed in the SHR-C group ($p<0.01$, SHR-C vs. WKY as well as in the SHR-Baseline groups). The amount of MKP-1 protein increased further in the SHR-B group as a result of the BGP-15 treatment ($p<0.01$, SHR-B vs. SHR-C; Fig. 8.). The level of Erk1/2$^{Thr202/Tyr204}$ phosphorylation was less pronounced in the SHR-C group compared to the WKY group and to the baseline level ($p<0.05$, SHR-C vs. WKY, Fig. 8.). BGP-15 treatment, however, caused a significant elevation in the

phosphorylation of Erk1/2$^{Thr202/Tyr204}$ compared to the SHR-C group ($p<0.01$, SHR-B vs. SHR-C; Fig. 8.). The level of p38-MAPK$^{Thr180/Tyr182}$ and JNK$^{Thr183/Tyr185}$ phosphorylation was low in the WKY and in the SHR-Baseline groups (Fig. 8.). The highest phosphorylation level of p38-MAPK$^{Thr180/Tyr182}$ and JNK$^{Thr183/Tyr185}$ could be seen in the SHR-C animals ($p<0.01$, SHR-C vs. WKY and SHR-Baseline). BGP-15 treatment reduced this phosphorylation of p38-MAPK$^{Thr180/Tyr182}$ and JNK$^{Thr183/Tyr185,}$ too and this reduce was significant in the case of JNK$^{Thr183/Tyr185}$ compared to the SHR-C group ($p<0.01$; Fig. 8.).

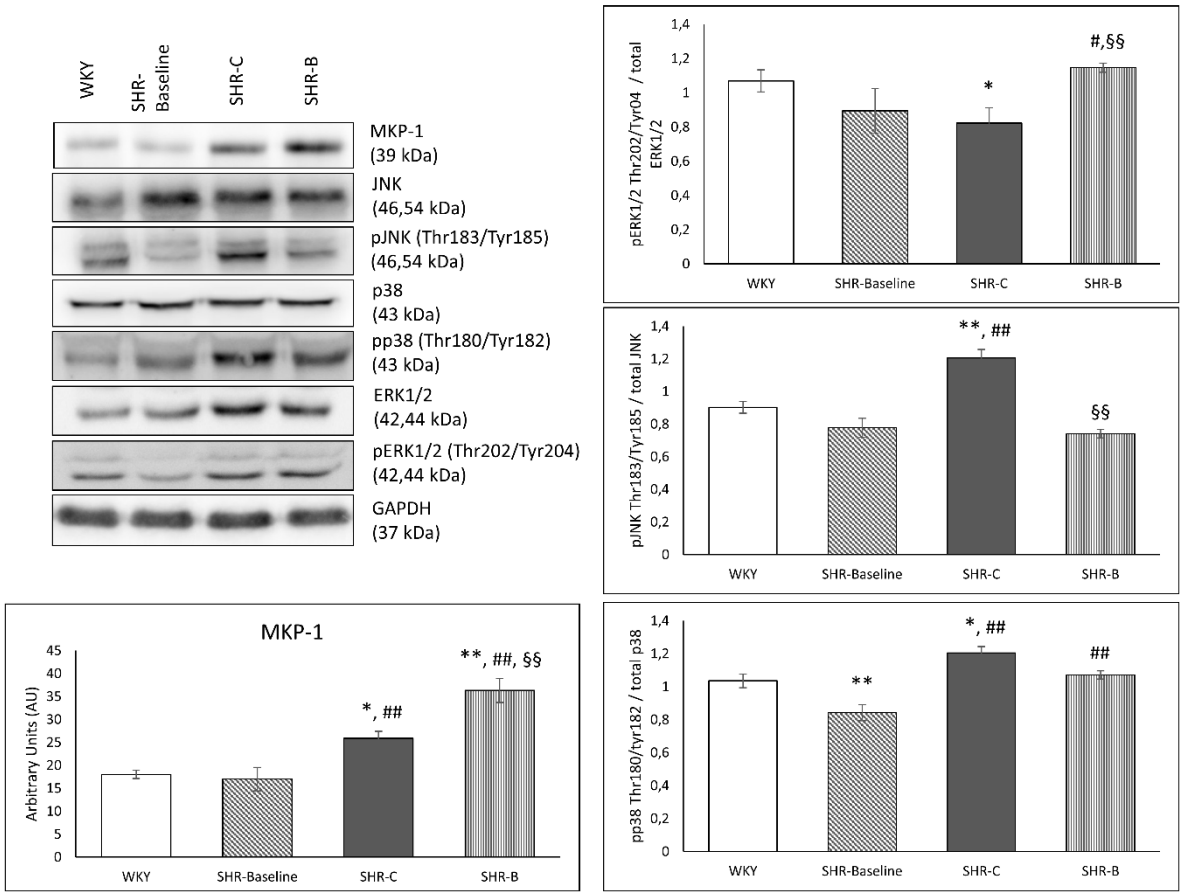


***Figure 8. Effect of BGP-15 treatment on the phosphorylation state of MAP kinases and on the amount of MKP-1.*** *Representative Western blot analyses of MKP-1 as well as ERK1/2, p38 and JNK phosphorylation. Densitometric evaluations are also shown. GAPDH was used as a loading control. WKY: age-matched normotensive Wistar-Kyoto rats, n=7; SHR-Baseline: 15-month-old spontaneously hypertensive rats, n=7; SHR-C: non-treated spontaneously hypertensive rats, n=7; SHR-B: spontaneously hypertensive rats receiving BGP-15 for 18 weeks, n=7. Values are mean±SEM. *p<0.05 vs. WKY, **p<0.01 vs. WKY, ##p<0.01 vs. SHR-Baseline, §§p<0.01 vs. SHR-C.*

### 4.1.9 BGP-15 improved the mitochondrial ultrastructure in a hypertension-induced heart failure animal model

Longitudinal sections of myocardium were evaluated to assess the morphology of interfibrillar mitochondria (IFM) by electron microscopy. The mitochondria of SHR-C rats differ from the normal mitochondria of WKY rats (Fig. 9 a-c), because they are morphologically more heterogeneous (n = 5 from each group, 3–5 block from each animal). In the non-treated hypertensive animals (SHR-C), mitochondria were loosely arranged between the contractile elements (Fig. 10 a, b). Moreover, in the SHR-C group extensive disruption of mitochondrial cristae and enlarged intracristal spaces could be observed (Fig. 10c). Their shape was often elongated, and the mitochondrial matrix was very light. The mitochondrial ultrastructure in the SHR-B group was similar to that of WKY rats (Fig. 10 d,e). In treated SHR animals (SHR-B) normal, large and less elongated mitochondria with tightly packed cristae and electron-dense matrix was seen (Fig. 10 f). The area of IFM was assessed on electron micrographs (~500 mitochondria/group were measured; Fig. 11 b). We assessed relative frequencies of the measured mitochondrial areas in arbitrary intervals of 0.3 $\mu m^2$ (Fig. 11 a). In all the groups, less than 1% of mitochondrial areas were above the 1.81 $\mu m^2$ value. In the SHR-C group, 43.7% of the measured mitochondria belonged to the lowest area range (<0.3 $\mu m^2$). However, in the WKY group the predominant area range of the measured mitochondria was between 0.3-0.6 $\mu m^2$. Due to BGP-15 treatment (SHR-B), the distribution of mitochondria was similar to that of WKY group and the highest number of mitochondria (48%) belonged to the 0.3-0.6 $\mu m^2$ range ($p<0.05$, SHR-B vs. SHR-C). Our results showed a profound decrease in the mean mitochondrial area of SHR-C group compared to the mitochondria of WKY animals ($p<0.05$, SHR-C, vs. WKY). The values of BGP-15 treated SHRs differed from that of the SHR-C group ($p<0.05$), and it was similar to the mitochondria of normotensive animals (WKY).

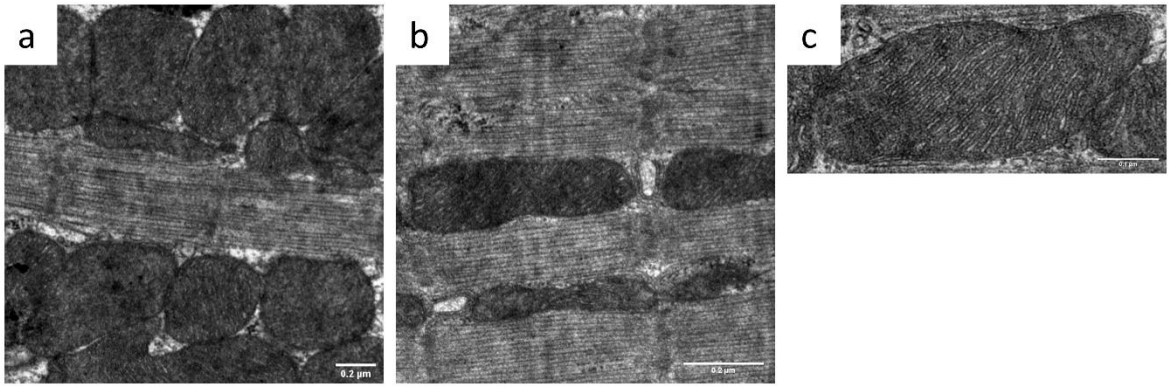


***Figure 9. Ultrastructural analysis of interfibrillar mitochondria in the myocardium of WKY animals.*** *Representative electron micrographs of interfibrillar mitochondria in the myocardium of (a, b) WKY animals (a: magnification: 15k, scale bar: 0.2 µm, b: magnification: 20k, scale bar: 0.2 µm). Ultrastructure of interfibrillar mitochondria in the myocardium of (c) WKY animals (magnification: 40k, scale bar: 0.1 µm (n=4 from each group, 3–5 blocks from each animal). WKY: age-matched normotensive Wistar-Kyoto rats.*

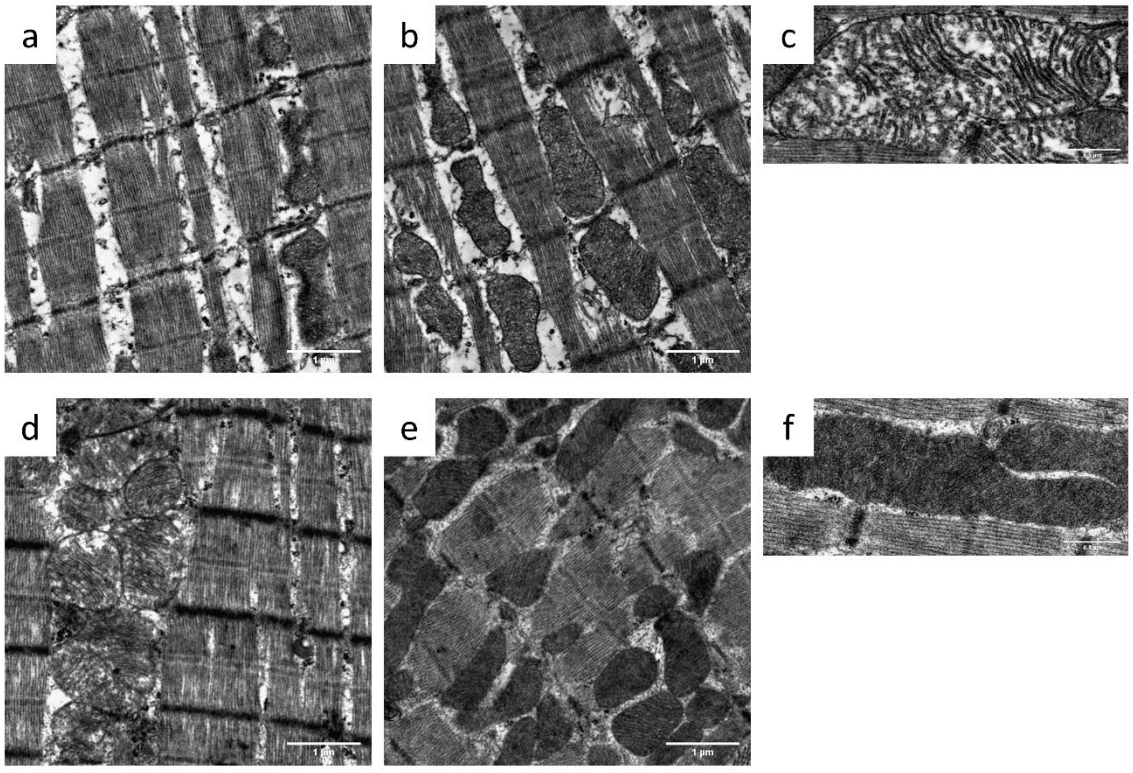


***Figure 10. Ultrastructural analysis of interfibrillar mitochondria in the myocardium of SHR animals.*** *Representative electron micrographs of interfibrillar mitochondria in the myocardium of (a, b) SHR-C and (d, e) SHR-B animals (magnification: 10k, scale bar: 1 µm). Ultrastructure of interfibrillar mitochondria in the myocardium of (c) SHR-C and (f) SHR-B animals (magnification: 25k, scale bar: 0.5 µm). SHR-C: non-treated spontaneously hypertensive rats, SHR-B: spontaneously hypertensive rats receiving BGP-15 for 18 weeks (n=4 from each group, 3–5 blocks from each animal).*

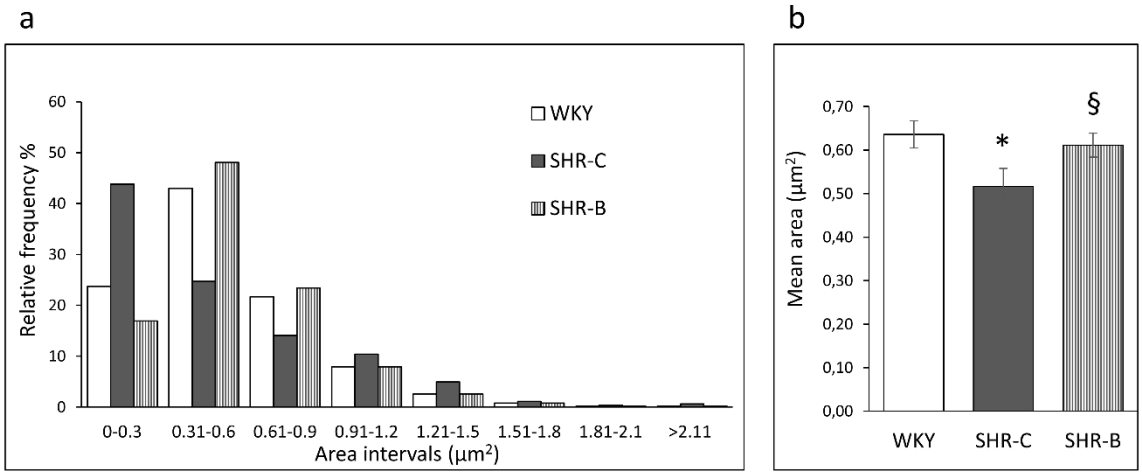


***Figure 11. Heart failure-induced fragmentation of interfibrillar mitochondria in the myocardium.*** *(a) Relative frequencies of measured mitochondrial areas in each arbitrary area interval. (b) Means of area values in the given groups (~500 mitochondria/group). WKY: age-matched normotensive Wistar-Kyoto rats, SHR-C: non-treated spontaneously hypertensive rats, SHR-B: spontaneously hypertensive rats receiving BGP-15 for 18 weeks. Data are expressed as mean±SEM. *p<0.05 vs WKY, §p<0.05 vs SHR-C).*

### 4.1.10 BGP-15 increased the expression level of mitochondrial fusion proteins in SHR animals

Regarding the mitochondrial fusion proteins, we determined the levels of OPA1, MFN1 and MFN2 in the myocardium using Western blot analysis (Fig. 12). We observed that the level of OPA1 was moderately decreased in the SHR-C group compared to the WKY group ($p<0.05$, SHR-C vs. WKY). However, BGP-15 treatment caused a significant elevation of OPA1 level in the SHR-B group ($p<0.01$ SHR-B vs. WKY, $p<0.05$ SHR-B vs. SHR-C). Considering the amount of MFN1 protein level, there was a significant increase in hypertensive animals by the end of the study compared to the baseline levels ($p<0.05$, SHR-C and SHR-B vs. SHR-Baseline), however, there was no difference between the SHR groups. The level of MFN2 protein was moderately lower in the SHR-C group than in the WKY group ($p<0.05$), and very similar changes could be seen in the case of OPA1. In the SHR-B group these parameters significantly increased due to the BGP-15 treatment compared to the other groups ($p<0.01$ SHR-B vs WKY, SHR-C).

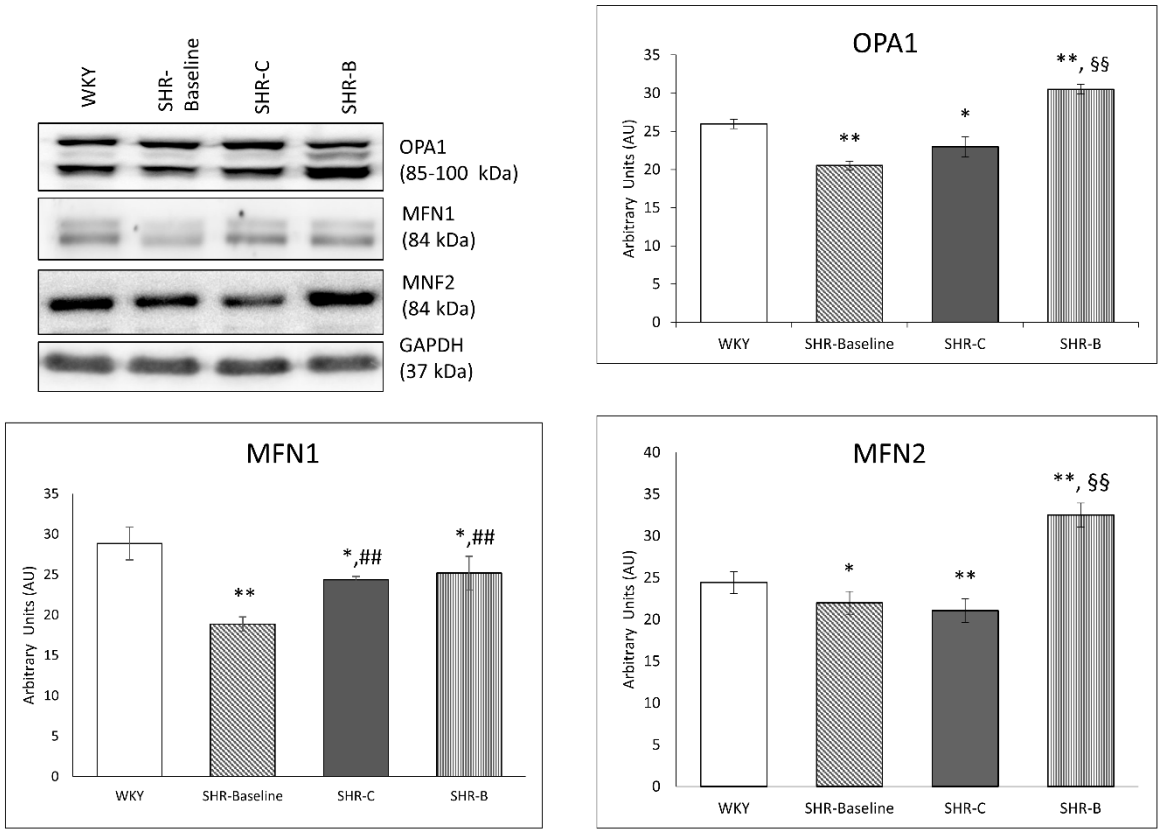


***Figure 12. Effect of BGP-15 treatment on mitochondrial fusion proteins in a hypertension-induced heart failure model.*** *Western blot analysis of OPA1, MFN1 and MFN2 proteins as well as densitometric evaluations are shown. GAPDH was used as a loading control. WKY: age-matched normotensive Wistar-Kyoto rats, SHR-Baseline: 15-month-old spontaneously hypertensive rats, SHR-C: 19-month-old non-treated spontaneously hypertensive rats, SHR-B: 19-month-old spontaneously hypertensive rats receiving BGP-15 for 18 weeks. (n=4). Values are mean±SEM. *p<0.05 vs. WKY, **p<0.01 vs WKY, ##p<0.01 vs. SHR-Baseline, §§p<0.01 vs SHR-C.*

### 4.1.11 BGP-15 decreased the expression level of mitochondrial fission proteins in SHR animals

The myocardial concentration of fission proteins Fis1 and DRP1 were determined in both total and fractionated Western blot samples (Fig. 13). The level of Fis1 increased in the SHR-C group compared to the WKY group ($p<0.05$, SHR-C vs. WKY). This elevation was, however, significantly diminished due to BGP-15 treatment ($p<0.05$ SHR-B vs. SHR-C). In the case of the fission protein DRP1, the total level was significantly decreased due to BGP-15 treatment compared to other groups ($p<0.01$ SHR-B vs. WKY, SHR-C). The phosphorylation level of DRP1 at the Ser616 and Ser637 residues was also measured. The phosphorylation of $DRP1^{Ser616}$ and $DRP1^{Ser637}$ was moderate in the WKY group. In the SHR-C group, however, phosphorylation of $DRP1^{Ser616}$ was significantly

higher (p<0.01 vs. WKY and SHR-Baseline). BGP-15 treatment on the other hand decreased the DRP1$^{Ser616}$ phosphorylation in SHR-B animals (p<0.01 vs. SHR-C group). Regarding the phosphorylation level of DRP1$^{Ser637}$, we observed a significant increase in the SHR-C group (p<0.01 vs WKY, SHR-Baseline). Moreover, BGP-15 treatment caused a further increase in the DRP1$^{Ser637}$ phosphorylation in SHR-B animals (p<0.01 SHR-B vs. SHR-C).

The intracellular distribution of DRP1 was also measured (Fig. 14). We observed that the DRP1 accumulated in the mitochondrial fractions of SHR-C animals compared to normotensive animals (p<0.01, SHR-C vs. WKY). BGP-15 treatment resulted in a significantly reduced translocation of DRP1 into the mitochondria (p<0.01 vs SHR-C), thereby preserving it in a higher concentration in the cytosolic fraction.

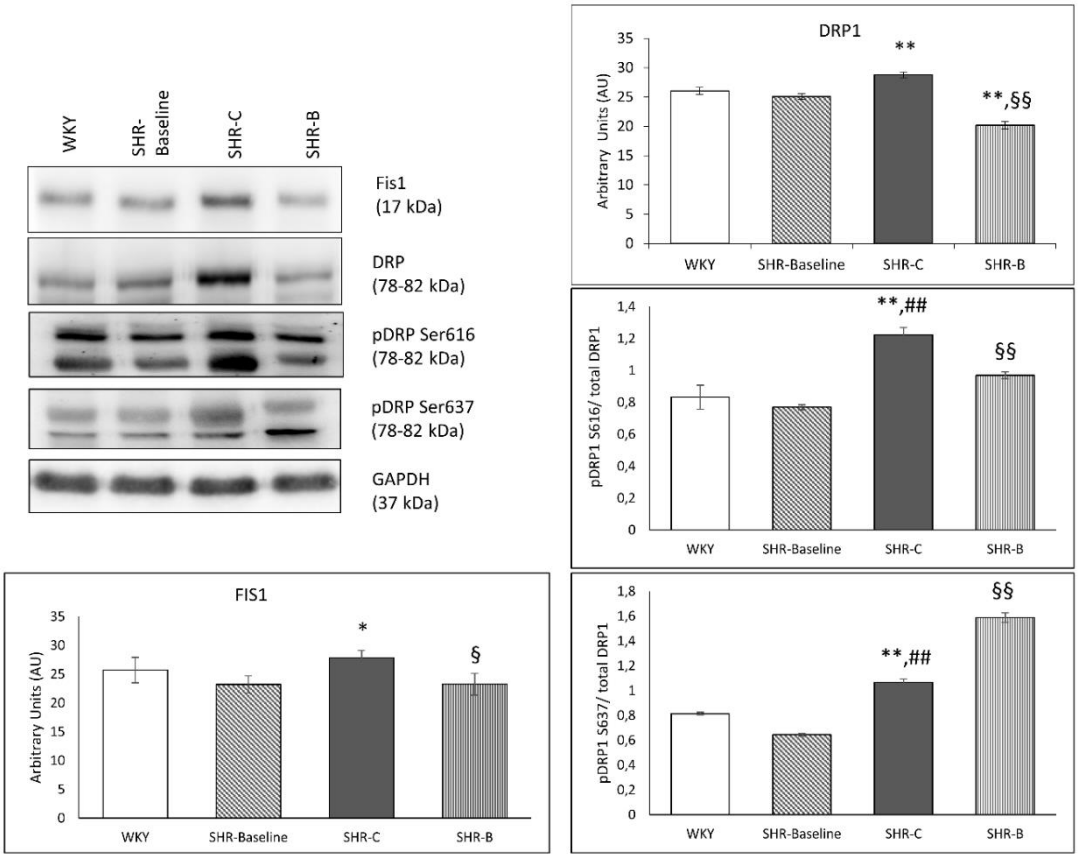


***Figure 13. Effect of BGP-15 treatment on mitochondrial fission proteins in a hypertension induced-heart failure model.*** *Western blot analysis of Fis1 and DRP1 proteins, as well as densitometric evaluations are shown. GAPDH was used as a loading control. WKY: age-matched normotensive Wistar-Kyoto rats, SHR-Baseline: 15-month-old spontaneously hypertensive rats, SHR-C: 19-month-old non-treated spontaneously hypertensive rats, SHR-B: 19-month-old spontaneously hypertensive rats receiving BGP-15 for 18 weeks (n=4). Values are mean±SEM. *p<0.05 vs. WKY, **p<0.01 vs WKY, ##p<0.01 vs. SHR-Baseline, §p<0.05 vs SHR-C, §§p<0.01 vs SHR-C.*

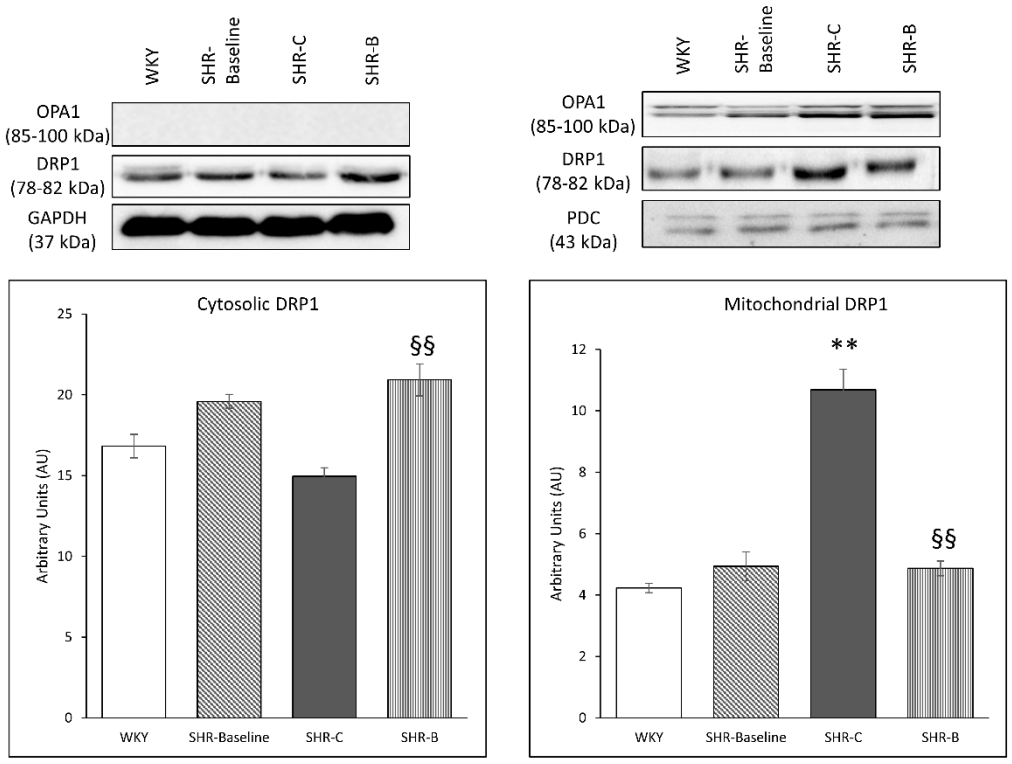


***Figure 14. Effect of BGP-15 treatment on the intracellular distribution of DRP1 protein in a hypertension-induced heart failure model***. *Western blot analysis of the intracellular distribution of DRP1 protein, densitometric evaluation are also shown. GAPDH and PDC were used as a loading control. WKY: age-matched normotensive Wistar-Kyoto rats, SHR-Baseline: 15-month-old spontaneously hypertensive rats, SHR-C: 19-month-old non-treated spontaneously hypertensive rats, SHR-B: 19-month-old spontaneously hypertensive rats receiving BGP-15 for 18 weeks (n=4). Values are mean±SEM. **p<0.01 vs. WKY, §§p<0.01 vs SHR-C.*

### 4.1.12 BGP-15 enhanced the mitochondrial biogenesis in SHR animals

There were no significant differences between the WKY, SHR-Baseline and SHR-C groups regarding the PGC-1α level (Fig. 15). However, BGP-15 treatment caused a significant increase in the amount of PGC-1α compared to the non-treated hypertensive animals ($p<0.01$, SHR-B vs. SHR-Baseline and SHR-C group; Fig. 15). In the case of $AMPK^{Thr172}$ phosphorylation a significant increase was observed in the SHR-C group compared to the SHR-Baseline group ($p<0.01$, SHR-C vs. SHR-Baseline; Fig. 15). BGP-15 treatment significantly reduced the phosphorylation of $AMPK^{Thr172}$ compared to the SHR-C group ($p<0.01$ SHR-B vs. SHR-C). The $CREB^{Ser133}$ phosphorylation was modest in the WKY group similarly to the phosphorylation of $AMPK^{Thr172}$ (Fig. 15). There was

significant increase in the phosphorylation level of CREB$^{Ser133}$ in the SHR-C group compared to the baseline value and to the normotensive animals ($p<0.01$, SHR-C vs. WKY; Fig. 15). Moreover, BGP-15 treatment caused a further increase in the CREB$^{Ser133}$ phosphorylation compared to non-treated SHR animals ($p<0.05$ SHR-B vs. SHR-C group) and to the baseline value ($p<0.01$ SHR-B vs. SHR-Baseline). The highest VDAC protein level was observed in the WKY group. This level was significantly lower in the hypertensive groups ($p<0.01$ WKY vs. SHR- Baseline, SHR-C and SHR-B). By the end of the treatment period VDAC became higher compared to the initial value ($p<0.01$, SHR-C vs. SHR-Baseline). Further significant increase was seen in the SHR-B group ($p<0.05$ SHR-B vs. SHR-C).

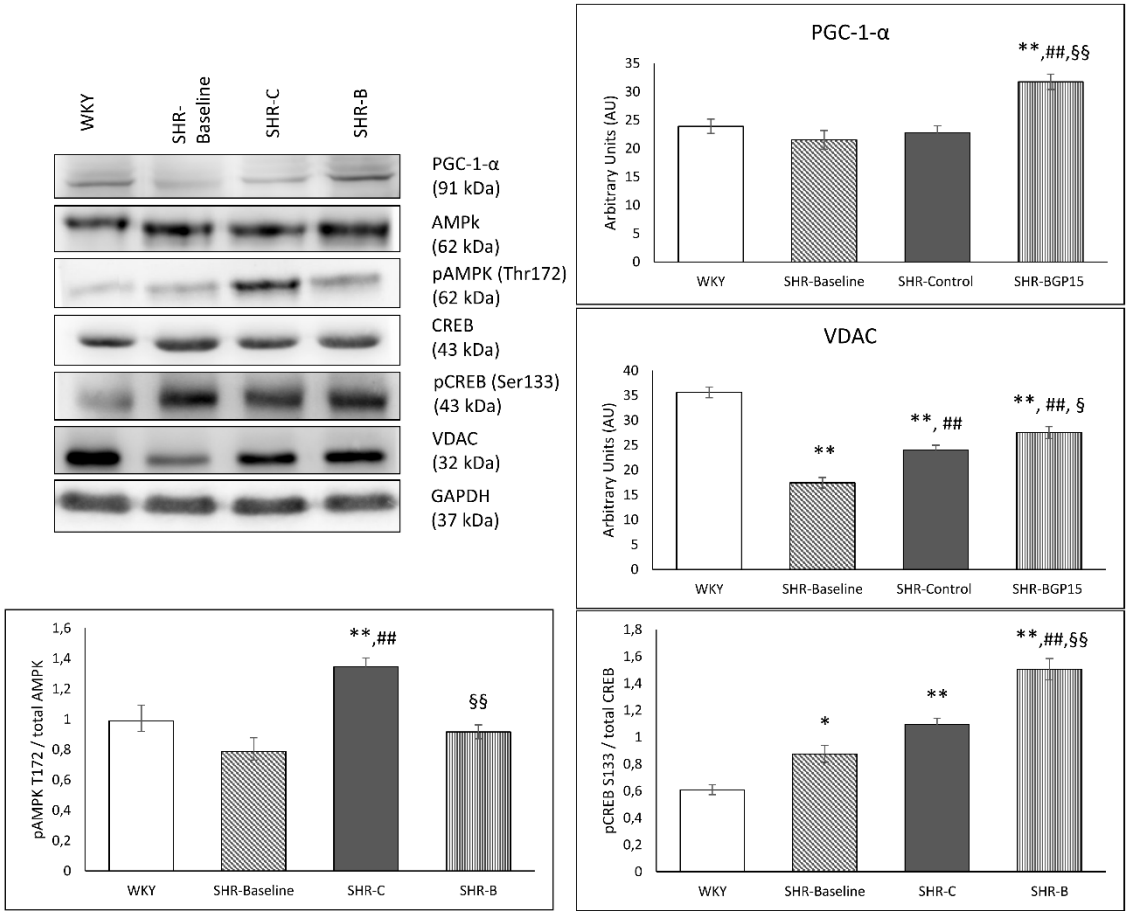


***Figure 15. Effect of BGP-15 treatment on the regulation of mitochondrial biogenesis.*** *Representative Western blot analysis of PGC-1α, VDAC, CREB, AMPK as well as phosphorylation of CREB and AMPK. Densitometric evaluation are also shown. GAPDH was used as a loading control. WKY: age-matched normotensive Wistar-Kyoto rats, n=7; SHR-Baseline: 15-month-old spontaneously hypertensive rats, n=7; SHR-C: non-treated spontaneously hypertensive rats, n=7; SHR-B: spontaneously hypertensive rats receiving BGP-15 for 18 weeks, n=7. Values are mean±SEM. *p<0.05 vs WKY, **p<0.01 vs WKY, ##p<0.01 vs SHR-Baseline, §p<0.05 vs. SHR-C, §§p<0.01 vs. SHR-C.*

## 4.2 In vitro results

### 4.2.1 Effect of BGP-15 administration on mitochondrial morphology of NRCM cells

To examine the changes of the mitochondrial network we used the MitoTracker Red CMXRos staining method (Fig. 16). BGP-15 per se had no effect on the complexity of the mitochondrial network. Filamentous mitochondrial network was observed in the Control group, $H_2O_2$ treatment, however, caused a marked injury to the mitochondrial network. As a result of the $H_2O_2$ induced fission processes, degradation of the mitochondrial network could be observed, which led to mitochondrial fragmentation. BGP-15 treatment prevented the mitochondrial network from the oxidative stress-induced fragmentation and preserved the normal filamentous network of mitochondria.

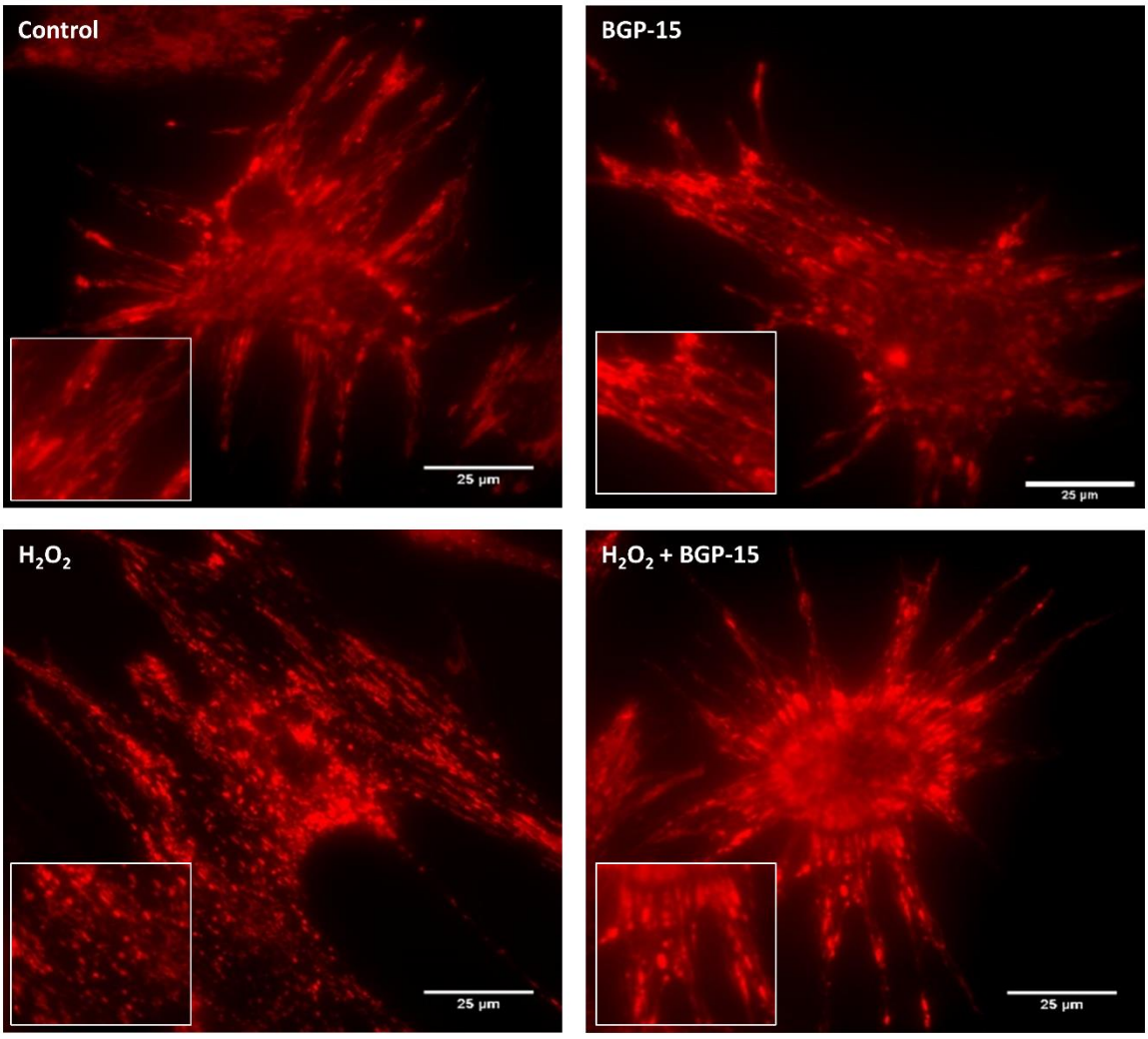


***Figure 16. Effect of BGP-15 administration on the morphology of mitochondrial network in NRCM cells.*** *For methodical details see chapter "Materials and Methods". BGP-15 treatment prevented the mitochondrial network from the oxidative stress induced fragmentation and*

*preserved mitochondria predominantly in the normal filamentous state. The inserts show the filamentous and fragmented states, showing that BGP-15 protected the mitochondrial network. Control group: cells without any treatment, BGP-15 group: cells with only 50 μM BGP-15 for 0.5 hour, $H_2O_2$ group: cells with 150 μM $H_2O_2$ for 0.5 hour, $H_2O_2$+BGP-15 group: cells with 150 μM $H_2O_2$ and 50 μM BGP-15 for 0.5 hour.*

### 4.2.2 BGP-15 treatment increased the level of fusion proteins in NRCMs

We assessed the levels of OPA1, MFN1 and MFN2 proteins in total Western blot samples of NRCM cells (Fig. 17). BGP-15 treatment per se had no effect on the amount of these parameters in the non-stressed cells in compared to the Control group. $H_2O_2$ treatment caused a slight decrease in the level of MFN1 and MFN2 proteins and a slight increase in the level of OPA1, but these changes were not significant. However, BGP-15 treatment caused a significant increase in the amount of OPA1, MFN1 and MFN2 proteins in $H_2O_2$ stressed cells compared to the untreated $H_2O_2$-stressed group ($p<0.05$ $H_2O_2$-BGP15 vs. $H_2O_2$).

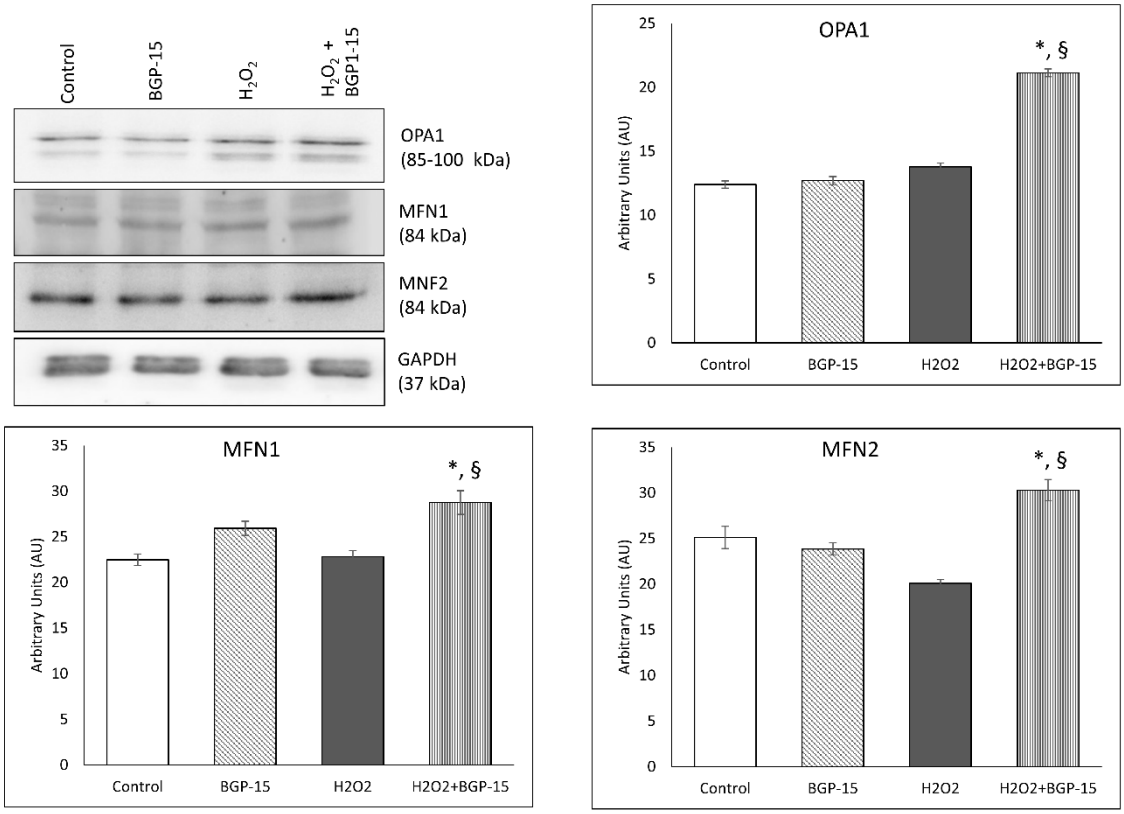


***Figure 17. Effect of BGP-15 treatment on mitochondrial fusion proteins in NRCM cells.*** *Western blot analysis of OPA1, MFN1 and MFN2 as well as densitometric evaluation are shown. GAPDH was used as a loading control. Control group: cells without any treatment, BGP-15 group: cells with only 50 μM BGP-15 for 0.5 hour, $H_2O_2$ group: cells with 150 μM $H_2O_2$ for 0.5*

*hour, $H_2O_2$+BGP-15 group: cells with 150 µM $H_2O_2$ and 50 µM BGP-15 for 0.5 hour. Values are mean±SEM (n=4). *p<0.05 vs. Control, §p<0.05 vs. $H_2O_2$ group.*

### 4.2.3 BGP-15 reduced the mitochondrial fission proteins level in NRCMs

We determined the levels of Fis1 and DRP1 in total and in fractionated Western blot samples in NRCM cells (Fig. 18). No significant difference was found in non-stressed cells due to BGP-15 compared to the Control group. The level of Fis1 increased markedly in the $H_2O_2$ group compared to the Control group ($p<0.01$, $H_2O_2$ vs. Control). BGP-15 treatment blunted this change ($p<0.05$, $H_2O_2$-BGP15 vs. $H_2O_2$ group). In the case of the total level of the fission mediator DRP1 protein, that was a significant elevation in the $H_2O_2$ group due to oxidative stress ($p<0.05$ $H_2O_2$ vs. Control group). However, a control-like value could be seen in the treated group compared to the $H_2O_2$ group ($p<0.05$ $H_2O_2$-BGP15 vs. $H_2O_2$ group). The phosphorylation of DRP1 on Ser616 and Ser637 residues was also evaluated. The phosphorylation of both DRP1 phospho-form was moderate in the Control group. Phosphorylation of $DRP1^{Ser616}$ considerably increased in the $H_2O_2$ group ($p<0.05$ $H_2O_2$ vs. Control group). However, BGP-15 treatment decreased $DRP1^{Ser616}$ phosphorylation compared to non-treated stressed cells ($p<0.05$ $H_2O_2$-BGP-15 vs. $H_2O_2$ group). Measuring the phosphorylation level of $DRP1^{Ser637}$, a significant decrease could be observed in the $H_2O_2$ group compared to the Control group ($p<0.01$ $H_2O_2$ vs. Control group). However, BGP-15 treatment remarkably enhanced the $DRP1^{Ser637}$ phosphorylation ($p<0.01$ $H_2O_2$-BGP15 vs. $H_2O_2$ group).

Finally, the intracellular distribution of the fission mediator DRP1 protein was examined (Fig. 19). Significantly higher portion of DRP1 could be found in the mitochondrial fraction of cells in the $H_2O_2$ group compared to the BGP-15 treated group. The translocation of DRP1 protein from the cytosol to the mitochondria was decreased due to BGP-15 treatment and in this way it resulted in higher levels of DRP1 in the cytosolic fraction and lower concentration in the mitochondrial fraction ($p<0.01$ vs. $H_2O_2$ group).

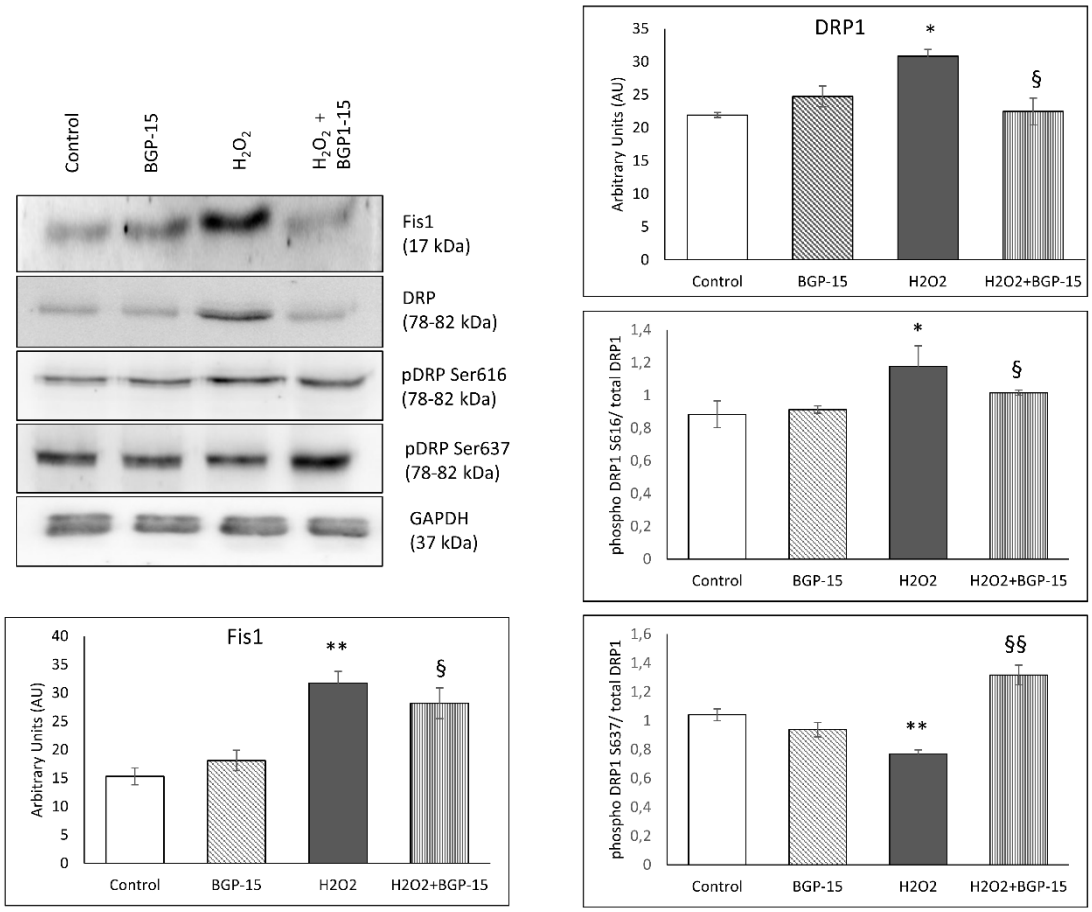


***Figure 18. Effect of BGP-15 treatment on mitochondrial fission proteins in NRCM cells***. *Western blot analysis of Fis1, DRP1 proteins, as well as densitometric evaluations are shown. GAPDH was used as a loading control. Control group: cells without any treatment, BGP-15 group: cells with only 50 μM BGP-15 for 0.5 hour, $H_2O_2$ group: cells with 150 μM $H_2O_2$ for 0.5 hour, $H_2O_2$+BGP-15 group: cells with 150 μM $H_2O_2$ and 50 μM BGP-15 for 0.5 hour. Values are mean±SEM (n=4). *p<0.05 vs. Control, **p<0.01 vs. Control, §p<0.05 vs. $H_2O_2$ group, §§ p<0.01 vs. $H_2O_2$ group.*

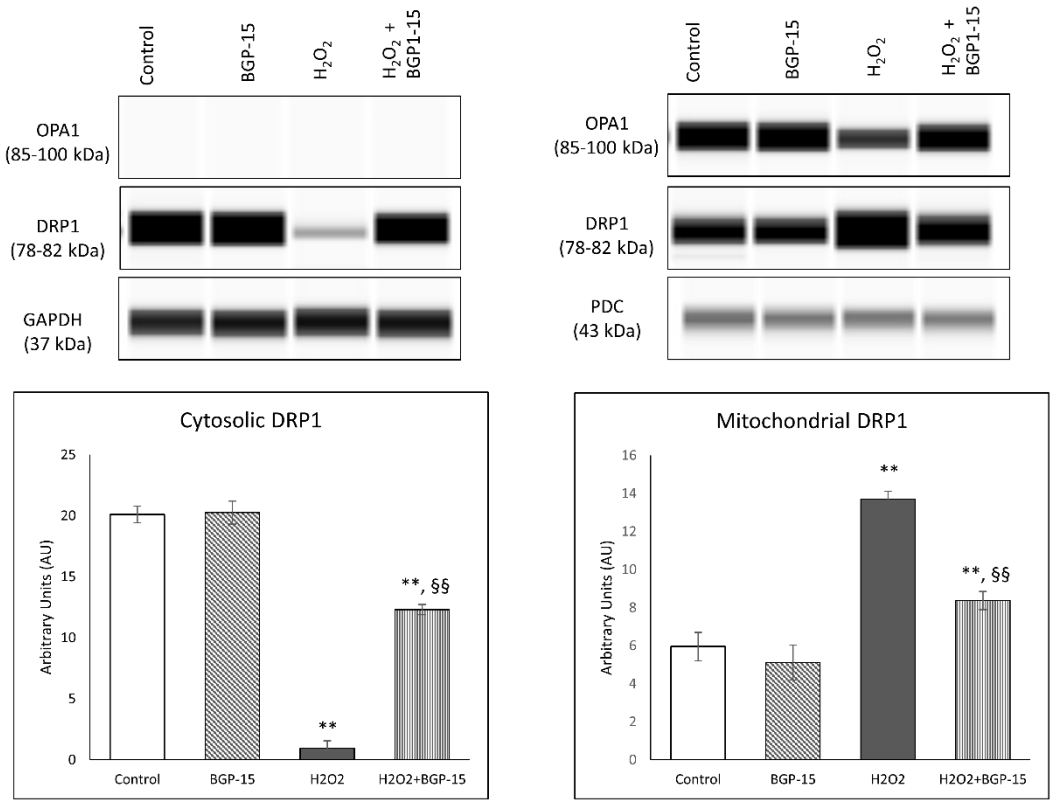


***Figure 19. Effect of BGP-15 treatment on intracellular distribution of DRP1 protein in stressed NRCM cells.*** *Western blot analysis of DRP1 protein regarding its intracellular disruption, as well as densitometric evaluations are shown. GAPDH and PDC were used as a loading control. Control group: cells without any treatment, BGP-15 group: cells with only 50 μM BGP-15 for 0.5 hour, $H_2O_2$ group: cells with 150 μM $H_2O_2$ for 0.5 hour, $H_2O_2$ +BGP-15 group: cells with 150 μM $H_2O_2$ and 50 μM BGP-15 for 0.5 hour. Values are mean±SEM (n=4). **p<0.01 vs. Control, §§p<0.01 vs. $H_2O_2$ group.*

### 4.2.4 BGP-15 favourably influenced the regulation of mitochondrial biogenesis in NRCMs

We determined the levels of PGC-1α, CREB and VDAC in the total Western blot samples of NRCMs. BGP-15 treatment had no effect on these factors in non-stressed cells compared to the Control group. The PGC-1α level was increased in the $H_2O_2$ group compared to the Control group ($p<0.01$ vs. Control; Fig. 20). However, this elevation was much more marked in the treated group ($p<0.01$ $H_2O_2$-BGP15 vs. Control and $H_2O_2$ groups). The phosphorylation level of $CREB^{Ser133}$ was low in the Control group. However, a significant increase was seen in the phosphorylation level of $CREB^{Ser133}$ in the $H_2O_2$ group ($p<0.01$ $H_2O_2$ vs. Control) (Fig. 20). BGP-15 treatment further increased the phosphorylation level of $CREB^{Ser133}$ ($p<0.01$, $H_2O_2$-BGP15 vs. $H_2O_2$ group). The level

of VDAC was slightly decreased in the $H_2O_2$ group compared to the Control group ($p<0.05$ $H_2O_2$ vs. Control). However, it was significantly elevated in the BGP-15 treated group ($p<0.01$ $H_2O_2$-BGP-15 vs. $H_2O_2$ group).

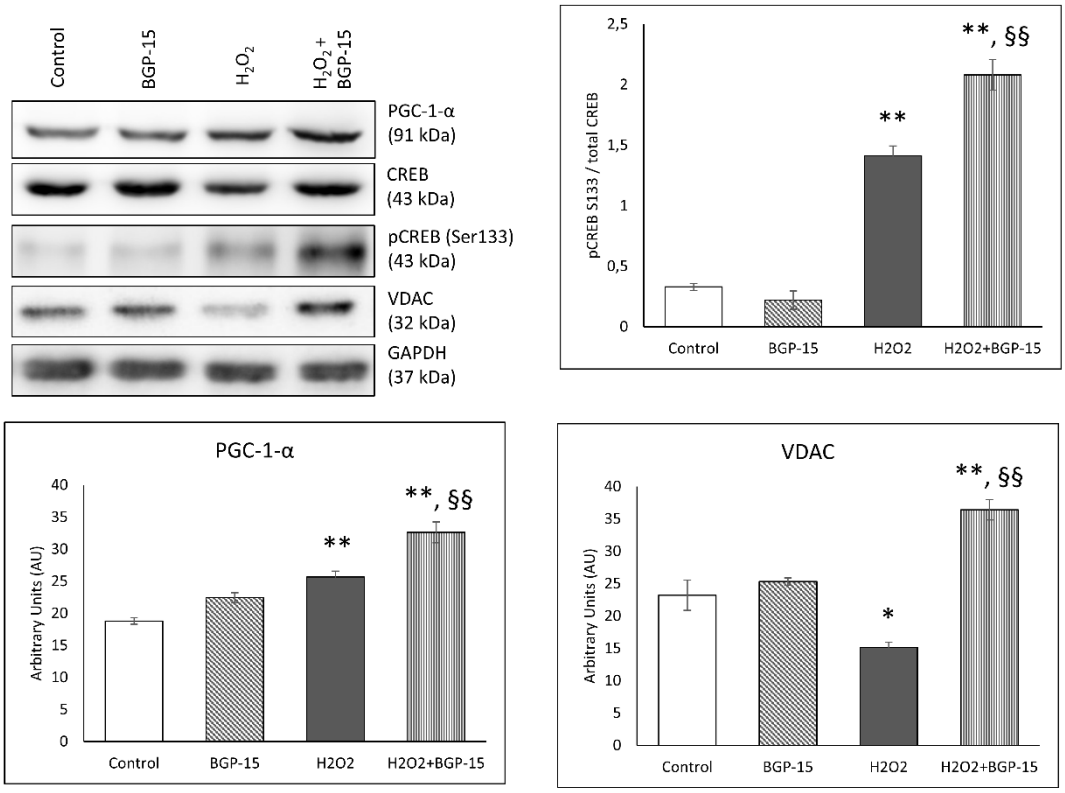


***Figure 20. Effect of BGP-15 treatment on the regulation of mitochondrial biogenesis in NRCM cells.*** *Western blot analysis of PGC-1α, CREB and VDAC proteins as well as densitometric evaluations are shown. GAPDH was used as a loading control. Control group: cells without any treatment, BGP-15 group: cells with only 50 μM BGP-15 for 0.5 hour, $H_2O_2$ group: cells with 150 μM $H_2O_2$ for 0.5 hour, $H_2O_2$ +BGP-15 group: cells with 150 μM $H_2O_2$ and 50 μM BGP-15 for 0.5 hour. Values are mean±SEM (n=4). *p<0.05 vs. Control, **p<0.01 vs. Control, §§p<0.01 vs $H_2O_2$ group.*

Moreover, we investigated mitochondrial DNA content compared to the nuclear DNA. The relative mitochondrial DNA content was determined by "real-time" PCR, using COX1 and COX3 primers, normalized to a nuclear-encoded β-actin gene. We found that BGP-15 treatment increased the relative expression levels of COXI and COXIII genes compared to the $H_2O_2$ group ($p<0.05$ $H_2O_2$-BGP-15 vs. $H_2O_2$ group; Fig. 21).

Furthermore, we also performed a widely used method for studying mitochondrial biogenesis by measuring the activity of citrate synthase (Fig. 21). Citrate synthase activity was reduced in hydrogen-peroxide stressed group compared to control group ($p<0.01$

$H_2O_2$ vs. Control). The citrate synthase activity was increased significantly due to the treatment ($p<0.01$ $H_2O_2$-BGP-15 vs. $H_2O_2$ group; Fig. 21).

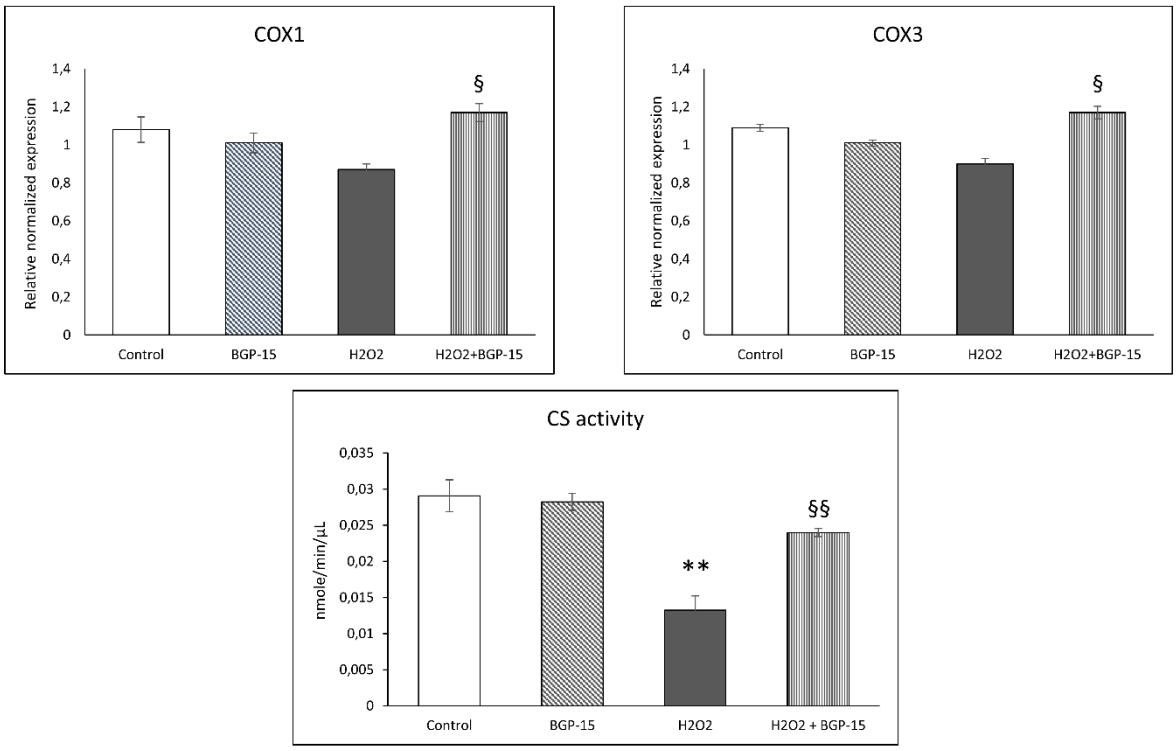


***Figure 21. Effect of BGP-15 treatment on the relative DNA content and citrate synthase activity.*** *Relative expression level of electron transport chain complex IV genes (COX1 and COX3) are presented. Comparison of citrate synthase activity in NRCM cells. Control group: cells without any treatment, BGP-15 group: cells with only 50 µM BGP-15 for 0.5 hour, $H_2O_2$ group: cells with 150 µM $H_2O_2$ for 0.5 hour, $H_2O_2$+BGP-15 group: cells with 150 µM $H_2O_2$ and 50 µM BGP-15 for 0.5 hour. Values are mean±SEM (n=4). **p<0.01 vs. Control, §§p<0.01 vs $H_2O_2$ group.*

Finally, we measured the level of NDUFs1 subunit of NADH-ubiquinone oxidoreductase and UQCRC1 subunit of Ubiquinol Cytochrome c Reductase proteins in order to support our finding regarding the effect of BGP-15 on mitochondrial biogenesis. The expression level of NDUFs1 was significantly decreased in the $H_2O_2$ group ($p<0.01$ $H_2O_2$ vs. Control; Fig. 22). Similar observation was made in the case of UQCRC1 ($p<0.05$ $H_2O_2$ vs. Control). However, BGP-15 treatment not only protected against the decrease but also significantly increased the amount of NDUFs1 and UQCRC1 proteins ($p<0.01$ $H_2O_2$-BGP-15 vs. $H_2O_2$ group).

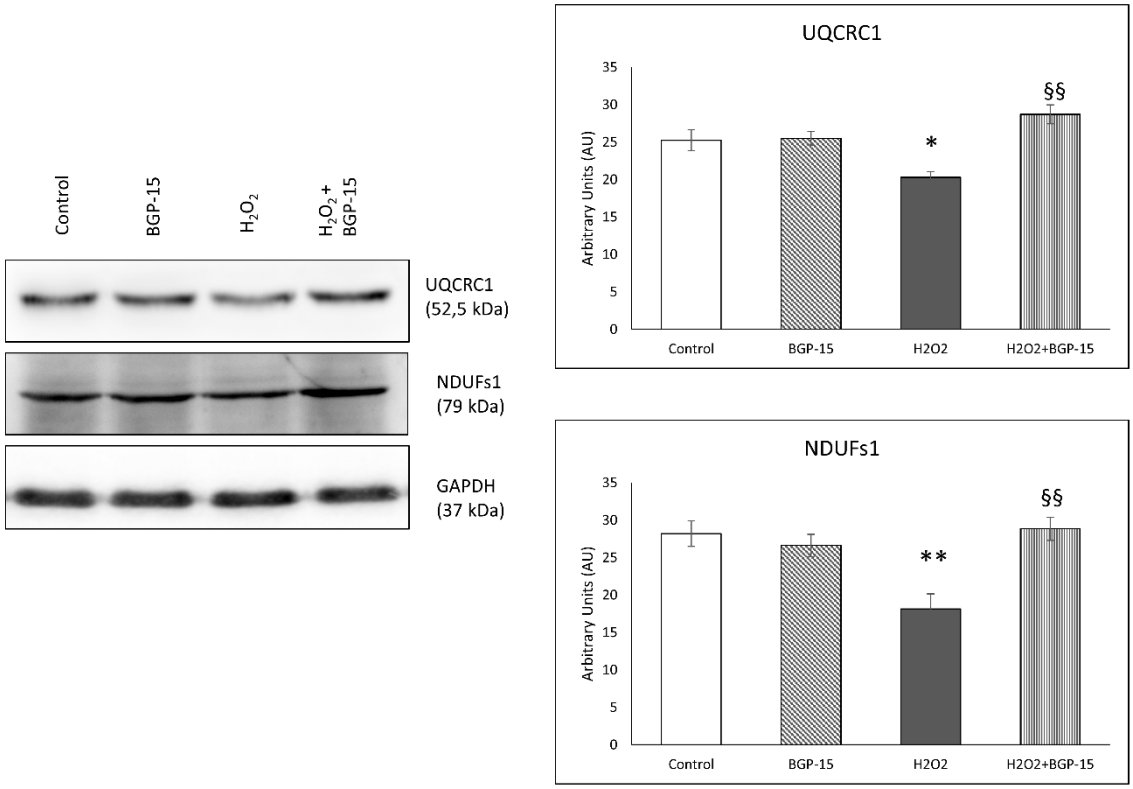


***Figure 22. Effect of BGP-15 treatment on the electron transport chain complex I and III proteins in NRCMs.*** *Western blot analysis of UQCRC1 and NDUFs1 proteins as well as densitometric evaluation are shown. GAPDH was used as a loading control. Control group: cells without any treatment, BGP-15 group: cells with only 50 µM BGP-15 for 0.5 hour, $H_2O_2$ group: cells with 150 µM $H_2O_2$ for 0.5 hour, $H_2O_2$ +BGP-15 group: cells with 150 µM $H_2O_2$ and 50 µM BGP-15 for 0.5 hour. Values are mean±SEM (n=4). *p<0.05 vs. Control, **p<0.01 vs. Control, §§p<0.01 vs $H_2O_2$ group.*

### 4.2.5 BGP-15 treatment protected mitochondrial genome integrity against the ROS-induced damage

Real time detection of long-range polymerase chain reaction (LRPCR) was used to examine the impact of $H_2O_2$-induced oxidative injury on mtDNA (Fig. 23). No significant difference was found with BGP-15 treatment alone compared to the Control group. $H_2O_2$ induced a significant damage of the mtDNA ($p<0.05$, $H_2O_2$ vs Control), the amplification rate of the entire mitochondrial genome was markedly diminished. This unfavourable damage was significantly reduced by BGP-15 treatment ($p<0.01$, $H_2O_2$-BGP15 vs. $H_2O_2$).

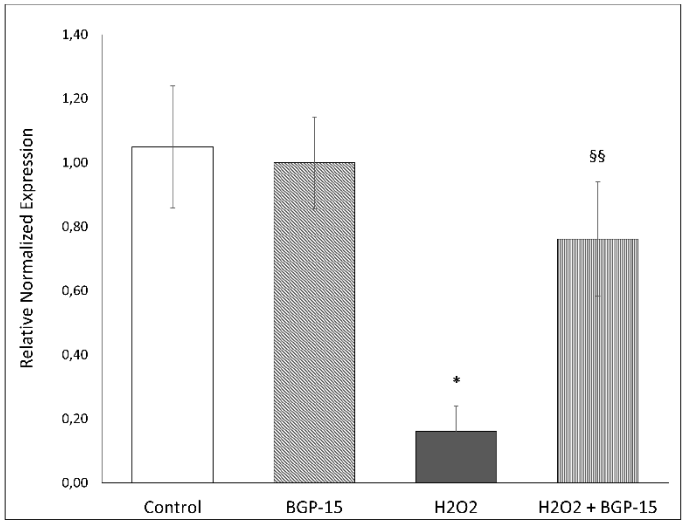


***Figure 23. Effect of BGP-15 treatment on oxidative stress-induced mitochondrial DNA damage.*** *Total DNA was isolated for LRPCR and SRPCR analysis. mtDNA damage was calculated using the Δ2Ct method. Control group: cells without any treatment, BGP-15 group: cells with only 50 μM BGP-15 for 0.5 hour, $H_2O_2$ group: cells with 150 μM $H_2O_2$ for 0.5 hour, $H_2O_2$+BGP-15 group: cells with 150 μM $H_2O_2$ and 50 μM BGP-15 for 0.5 hour. Values are mean±SEM (n=4). *p<0.05 vs. Control, §§p<0.01 vs $H_2O_2$ group.*

### 4.2.6 Effect of BGP-15 on mitochondrial membrane potential (ΔΨ) in NRCM cells

We examined the effect of BGP-15 on mitochondrial membrane potential using JC-1, a cell-permeable voltage-sensitive fluorescent mitochondrial dye (Fig. 24). JC-1 emits red fluorescence if the mitochondrial membrane potential is high (aggregated dye), while depolarized mitochondria emit green fluorescence (monomer dye). In the control cells fluorescence microscopy showed strong red fluorescence and weak green fluorescence, what indicates a high ΔΨm in mitochondria (Fig. 24a). BGP-15 per se had no effect on mitochondrial membrane potential. The addition of $H_2O_2$ to cells facilitates the depolarization of mitochondria, resulting in weaker red fluorescence and stronger green fluorescence ($p<0.01$ $H_2O_2$ vs. Control; Fig. 24b). If BGP-15 was also administered in peroxide-stressed NRCM cells, the intensity of red fluorescence increased and green fluorescence decreased compared to the $H_2O_2$ treated cells ($p<0.01$, $H_2O_2$-BGP15 vs. $H_2O_2$; Fig. 24b). Therefore, the quantitative assessment revealed that BGP-15 treatment

reduced the $H_2O_2$-induced depolarization of the mitochondrial membrane, the ΔΨm was similar to that of the Control cells.

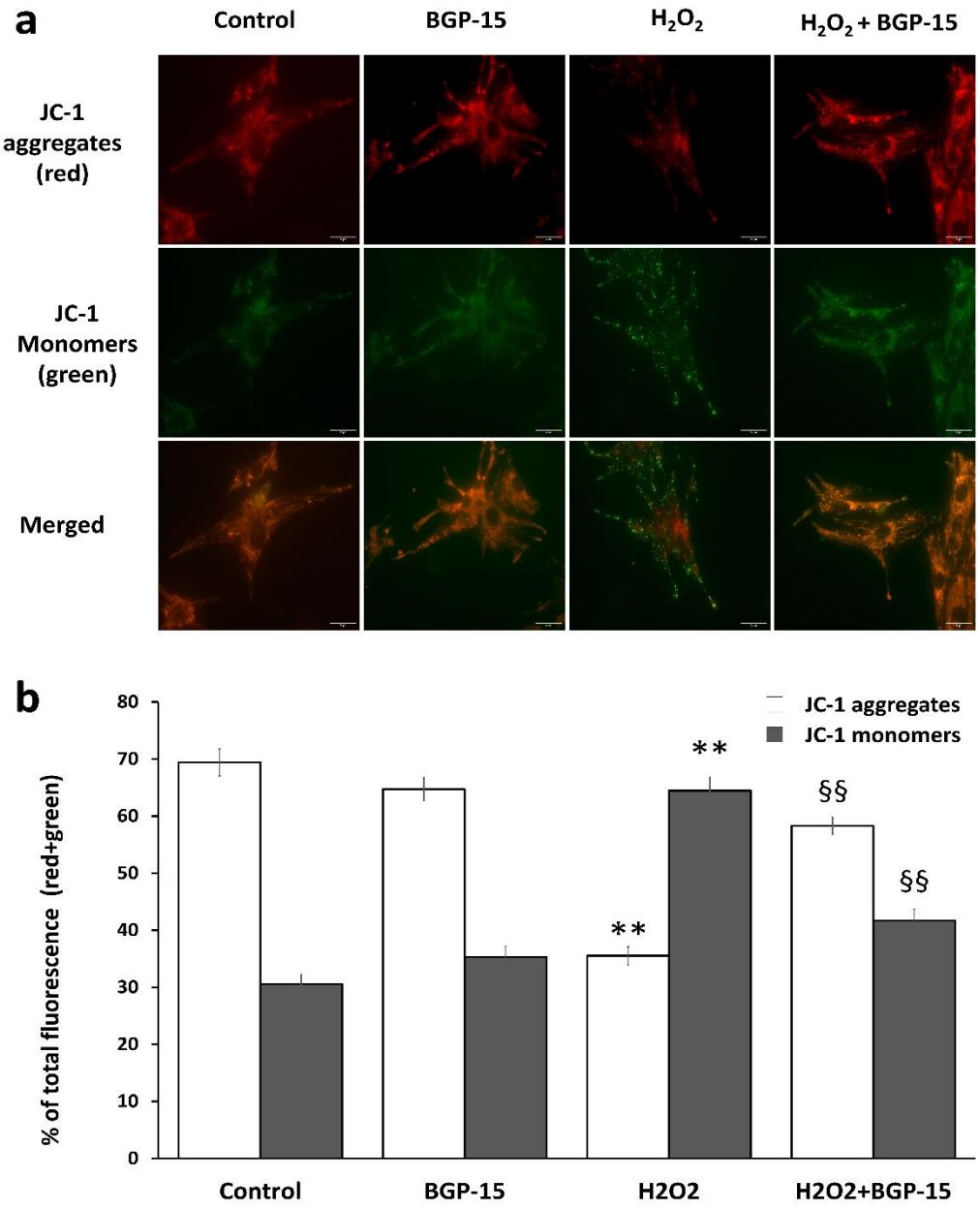


***Figure 24. Effect of BGP-15 on the mitochondrial membrane potential in NRCMs, as determined by JC-1.*** *(A) Effect of BGP-15 on $H_2O_2$-induced mitochondrial membrane depolarization in NRCM cells. Cells were exposed to 150 μm $H_2O_2$ in the absence or presence of 50 μm BGP-15 for 0.5 hours, after that stained with 100ng/ml of JC-1. The dye was loaded, and after a 15-minute-long incubation fluorescent microscopic images were taken using both the red and green channels. Representative merged images are presented. (B) Quantitative analysis of mitochondrial depolarization induced by $H_2O_2$ (150 μM) and its reduction by BGP-15 (50 μM) in NRCM cells. Control group: cells without any treatment, BGP-15 group: cells with only 50 μM BGP-15 for 0.5 hour, $H_2O_2$ group: cells with 150 μM $H_2O_2$ for 0.5 hour, $H_2O_2$+BGP-15 group:*

*cells with 150 μM $H_2O_2$ and 50 μM BGP-15 for 0.5 hour. Data are presented as the mean ± SEM. **p<0.01 vs. Control cells; §§ p<0.01 vs $H_2O_2$-treated cells.*

### 4.2.7 BGP-15 improved mitochondrial oxygen consumption and energy metabolism in NRCM cells under oxidative stress

To determine the mitochondrial energy metabolism and respiratory function, we used the Agilent Seahorse XFp Analyzer system and the Agilent Seahorse XFp Cell Mito Stress Test (Fig. 25). BGP-15 itself had no effect on the rate of mitochondrial respiration. Oxygen consumption rate of NRMC cells was decreased in the presence of $H_2O_2$ to cells compared to Control cells (Fig. 25a). $H_2O_2$ treatment decreased the basal respiration although this difference was not significant (Fig. 25b). However, the maximal respiration, the spare respiratory capacity and the ATP production were markedly decreased as a result of $H_2O_2$-induced oxidative damage compared to the Control group ($p<0.05$, $H_2O_2$ vs. Control) (Fig. 25c-e). In the presence of both $H_2O_2$ and BGP-15, the maximal respiration, spare respiratory capacity and the ATP production were significantly higher compared to the $H_2O_2$ group ($p<0.05$, $H_2O_2$ – BGP15 vs. $H_2O_2$).

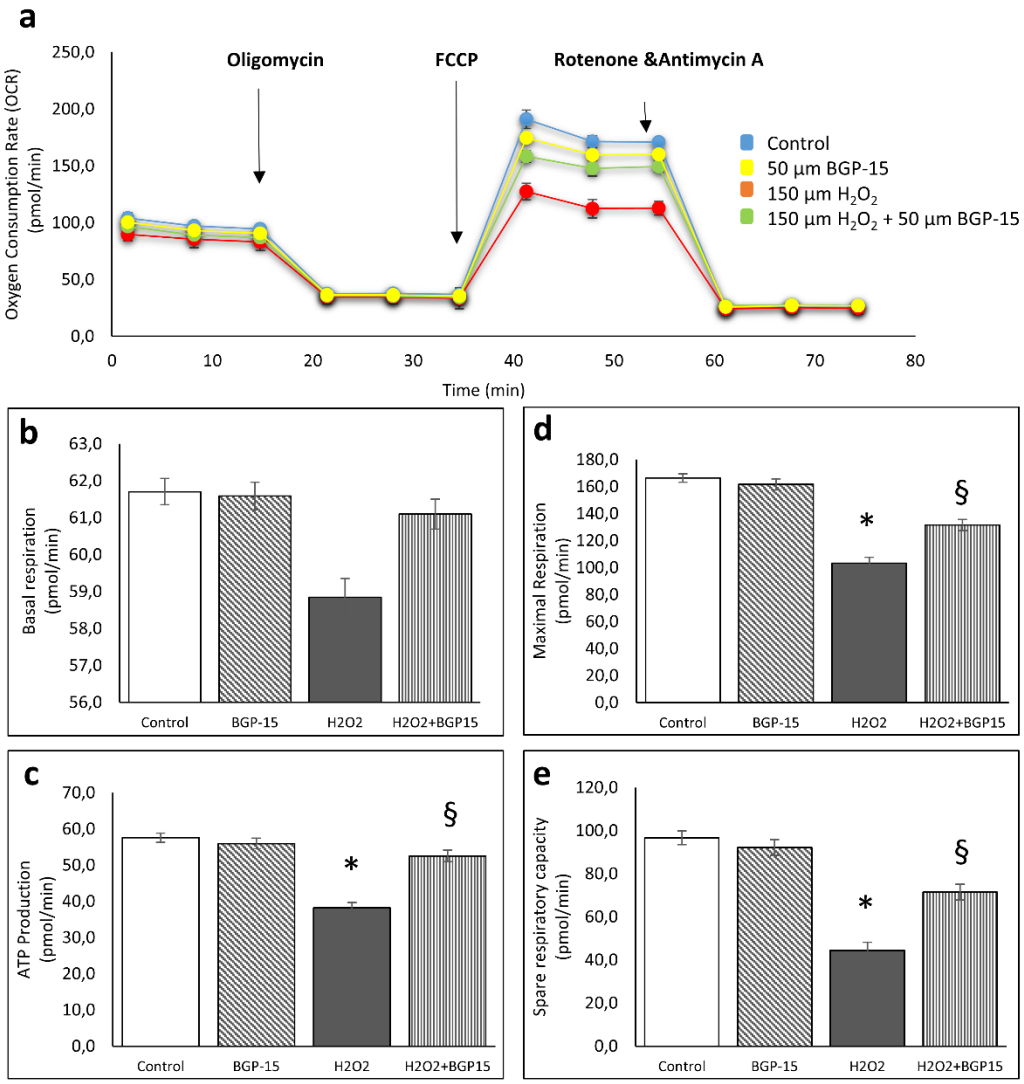


***Figure 25. Effect of BGP-15 on mitochondrial oxygen consumption and energy metabolism in NRCM cells, as determined by Agilent Seahorse XFp.*** *Mitochondrial energy metabolism was measured using a Seahorse XFp analyser. During testing, NRCMs cells were treated with 10 µM oligomycin, 10 µM FCCP, and 5 µM rotenone/antimycin A. Data were automatically calculated according to the Agilent Seahorse XF Cell Mito Stress Test Report Generator. (A) Oxygen consumption rate (OCR). (B) basal respiration. (C) ATP production. (D) maximal respiration. (E) spare respiratory capacity. Control group: cells without any treatment, BGP-15 group: cells with only 50 µM BGP-15 for 0.5 hour, $H_2O_2$ group: cells with 150 µM $H_2O_2$ for 0.5 hour, $H_2O_2$+BGP-15 group: cells with 150 µM $H_2O_2$ and 50 µM BGP-15 for 0.5 hour. Values are mean±SEM (n=4). *p<0.05 vs. Control, §p<0.05 vs. $H_2O_2$ group.*

# 5. DISCUSSION

In this work we aimed to examine the cardio protective effect of BGP-15 in chronic hypertension induced heart failure. Furthermore, we aimed to clarify the effect of BGP-15 on various processes of mitochondrial quality control in a hypertension-induced heart failure model and in vitro using hydrogen peroxide-induced oxidative stress.

The major findings of this study are that BGP-15 has positive effects on cardiac function and structure by inhibiting profibrotic signalling factors and therefore the remodelling itself in an animal model of hypertension-induced heart failure. This cardio protective effect can also be attributable to the mitochondrial effects of BGP-15. BGP-15, besides its mitochondrial fusion promoting effect, also inhibits factors playing part in the mitochondrial fission and enhances their de novo biogenesis under stress situations. As a result of these effects, BGP-15 preserves mitochondrial structure and energy production during hydrogen peroxide-induced oxidative stress as well as in an in vivo heart failure model.

In our recent work, spontaneously hypertensive rats (SHR) were used, which is a widely used model in experimental cardiology for the examination of hypertension-induced cardiovascular remodelling and heart failure because it resembles the human essential hypertension [19, 21, 114]. In SHRs by the age of 15 months a severe left ventricular hypertrophy with mild signs of heart failure has already been developed. In our work, BGP-15 exerted a positive effect on cardiac remodelling and on cardiac function [115]. BGP-15 treatment decreased slightly the severity of cardiac hypertrophy, which was proved by several gravimetric ratios (weight of ventricles/body weight and weight of ventricles/tibia length) as well as by echocardiography.

Left ventricular wall thicknesses and LV mass were already markedly increased in the SHR animals compared to normotensives (Table 2.). However, systolic left ventricular function was still normal in both normotensive and hypertensive animals. This is in accordance with the results of other workgroups and with our former results [23, 116]. The signs of left ventricular hypertrophy remained marked also by the end of the study in SHR animals. However, systolic (EF%) as well as diastolic left ventricular function (E/E') worsened significantly by that time and animals showed the signs of heart failure. The worsening of these parameters were considerably lower due to BGP-15 treatment of hypertensive animals (Table 2.). This result supports and complements the results of Sapra et al., that BGP-15 has beneficial effects on cardiac function in murine heart failure

[108]. Moreover, left ventricular hypertrophy as well as the severity of left ventricular diastolic dysfunction were not only moderated due to BGP-15 treatment but also improved slightly, showing a so-called “reverse remodelling” phenomenon.

BNP plasma level is a biomarker of heart failure. There is a direct proportionality between the severity of heart failure and the BNP level [117]. The marked increase of BNP that was seen in non-treated hypertensive animals (SHR-C) was also positively affected by BGP-15, because it decreased the BNP level to the level of normotensive animals (Table 2.).

Hypertensive heart disease including heart failure is characterized by cardiomyocyte hypertrophy and cardiac fibrosis. Extracellular matrix (ECM) accumulation can be observed during cardiac remodelling, which is characterized by abnormalities in matrix composition and quality and it can decrease the heart function [8, 118]. Heart failure and the remodelling are characterized by increased type I collagen deposition. Thus type I collagen is a marker of cardiac fibrosis. Type I collagen is the major interstitial component of the adult human cardiac tissue (approximately 85%) while type III collagen is the other important component (11%) [72]. Both phenomena could be seen in our hypertensive animals. BGP-15, however, prevented against hypertension-induced cardiac interstitial fibrosis and cardiomyocyte hypertrophy (Fig. 5).

Transforming growth factor-β (TGFβ)/Smad signalling route has a major role in the regulation of cardiac fibrosis [74, 75]. Activation of TGF-β/Smad signalling promotes myofibroblast formation and extracellular matrix (ECM) production, that are leading to cardiac fibrosis[76]. In our recent work, hypertension induced a marked cardiac fibrosis by the activation of the TGF-β/Smad pathway (Fig. 6). Both the level of TGF-β and the phosphorylation state of $Smad2^{Ser465/467}$ were significantly reduced due to BGP-15 treatment; therefore, it can be a mechanism of the decreased fibrosis, which could be observed in the SHR-B group. The BGP-15-induced inhibition of fibrosis and cardiomyocyte hypertrophy are on the other hand the main causes of the improved cardiac function and structure compared to non-treated SHRs (Table 1., 2.).

It is well known, that MAPK signalling pathway also plays an important role in the pathogenesis of hypertension-induced cardiac remodelling and heart failure [11, 67, 68]. MAP kinases, predominantly p38 MAPK and JNK are other important regulators of myocardial fibrosis [24, 69, 70] . The activity of MAP kinases are regulated by dual-specificity phosphatases (DUSPs) or MAPK phosphatases (MKPs) that can dephosphorylate MAPKs and in this way they can regulate – actually inhibit – their

activity [67, 71]. In our recent work, the expression of MKP-1 increased significantly due to BGP-15 treatment compared to SHR-C animals (Fig. 8) As a consequence of the increased amount of MKP-1, the p38 MAPK and JNK phosphorylation decreased in the treated animals, in accordance with several previous studies that also confirmed the beneficial effect of BGP-15 on the phosphorylation state of p38 MAPK and JNK (Fig. 8) [103, 110]. In the case of ERK phosphorylation, an opposite change could be seen in our work, namely BGP-15 increased the ERK1/2 phosphorylation (Fig. 8). Regarding this effect of BGP-15, there are studies that are in accordance with our results. Szabo et al. demonstrated that BGP-15 treatment increased the phosphorylation of ERK1/2 in WRL-68 cells[103]. However, in another work, BGP-15 decreased the phosphorylation of ERK1/2 in imatinib-induced cardiotoxicity [110]. Because ERK1/2 is a member of pro-survival signalling factors, its activation is beneficial in the failed myocardium[23, 63].

Akt-1 also belongs to the prosurvival signalling factors and it can promote the so-called "physiological" hypertrophy, however, it inhibits the pathological hypertrophy that is mainly characterized by cardiac collagen accumulation [58–60]. GSK-3β is a downstream target of Akt-1 and Akt-1 via the phosphorylation of GSK-3β can promote the survival of chronically stressed cardiomyocytes in heart failure as demonstrated by previous works [23]. The cytoprotective effect due to increased phosphorylation of Akt-1 and GSK-3β is mediated via their protective effect on the structure and function of mitochondria[61]. In our recent study, BGP-15 increased significantly the phosphorylation of Akt-1 and GSK-3β compared to non-treated SHR animals (Fig. 7), therefore BGP-15 treatment activates the pro-survival signalling pathways.

Mitochondria are dynamic organelles constantly undergoing fusion and fission processes. Hypertension-induced heart failure is characterized by the fragmentation of mitochondria and by compromised energy production leading to decreased contractile force of myofilaments [119, 120]. In our work, mitochondria were structurally damaged in non-treated hypertensive animals (SHR-C). They were loosely arranged between the contractile elements (Fig. 10a-c). The average size of mitochondria was markedly reduced in the SHR-C group, approximately 40% of mitochondria were smaller than 0.3 μm2 as a result of heart failure-induced mitochondrial fragmentation (Fig. 11). Ultrastructurally extensive disruption of mitochondrial cristae and enlarged intracristal spaces were observed. However, BGP-15 treatment resulted in structurally markedly healthier mitochondria that were similar to that of normotensive animals. Mitochondria in the SHR-B group were tightly packed between the myofibrils. Most of mitochondria

belonged to the normal size range (0.3-0.6 μm2), which can be – at least partially – the consequence of increased mitochondrial biogenesis. On the ultrastructural level large mitochondria with tightly packed cristae and electron-dense matrix were seen in the treated group (Figure 10d-f).

Oxidative stress induces an imbalance in processes of mitochondrial dynamics, potentially leading to cell death. Proper mitochondrial functions regulated by the quality control processes are fundamental for cardiac work. The deterioration of mitochondrial quality control greatly contributes to the hypertension-induced cardiac remodelling and its progression to heart failure [121–123]. In our recent study, the expression level of proteins promoting the mitochondrial fusion, particularly OPA1 and MFN2 were increased significantly in the BGP-15 treated animals compared to the SHR-C group (Fig. 12). Our results are in accordance with the results of Szabo et al., who published earlier that BGP-15 has promoted mitochondrial fusion in both in vitro and in vivo [103].

Regarding mitochondrial fission, a marked decrease could be seen in the expression levels of DRP1 and Fis1 in hypertensive animals due to BGP-15 treatment (Fig. 13). DRP1 is regulated by several posttranslational modifications [87, 90, 124]. DRP1$^{Ser637}$ phosphorylation suppresses its translocation to mitochondria and thus inhibits its activity, while DRP1$^{Ser616}$ phosphorylation promotes DRP1 translocation and therefore the mitochondrial fission. BGP-15 treatment increased markedly the DRP1$^{Ser637}$ phosphorylation and decreased the DRP1$^{Ser616}$ phosphorylation in SHR-B animals compared to non-treated hypertensive animals (Fig. 13). The subcellular distribution of DRP1 showed changes consistent with the phosphorylation pattern of DRP1. In non-treated hypertensive animals (SHR-C) a high portion of DRP1 could be found in the mitochondrial fraction (Fig. 14). BGP-15 treatment resulted in a significantly reduced translocation to mitochondria of DRP1, retaining it in the cytosolic fraction. This can be a consequence of increased DRP1$^{Ser637}$ phosphorylation in SHR-B animals. Altogether BGP-15 prevented mitochondria against hypertension-induced fragmentation.

Contractile function of cardiomyocytes is in strong correlation with the energy producing capacity of the mitochondrial network [125]. Numerous studies have demonstrated that mitochondrial biogenesis is an essential step in mitochondrial quality control and is a highly vulnerable process in heart failure [126, 127]. PGC-1α is the master signalling factor of biogenesis, and it is regulated by different ways, among others by AMPK and CREB [94, 128, 129]. We found that the expression level of PCG-1α increased due to BGP-15 treatment compared to SHR-C animals (Fig. 15). Phosphorylation of AMPK

was, however, reduced as a result of the treatment (Fig. 15). AMPK activation is a consequence of increased AMP:ATP ratio, which is a sign of energy depletion. Therefore this reduction of AMPK phosphorylation indicates a favourable change in the energy production of cardiomyocytes [130, 131]. Phosphorylation of CREB was on the other hand increased in BGP-15 treated SHR animals compared to non-treated ones (Fig. 15). BGP-15 via the activation of CREB increased the expression level of PGC-1α, which in turn can yield in enhanced mitochondrial biogenesis and in increased high energy phosphate production. CREB transcription factor can also increase the production of MKP-1 and thereby can decrease the activity of MAPKs signal pathway, too [132, 133], which could be seen in our study. We determined the amount of VDAC, an outer mitochondrial membrane protein to characterize the number of mitochondria in cardiomyocytes. The elevation of VDAC in BGP-15 treated animals proved that there is an increased mitochondrial biogenesis and mitochondrial mass in cardiomyocytes.

In our in vitro experiments hydrogen-peroxide was used to induce oxidative injury of NRCM cells. Degradation of the filamentous mitochondrial network by mitochondrial fragmentation could be observed in $H_2O_2$-stressed NRCM cells similarly to heart failure. BGP-15 treatment prevented the mitochondrial network from the oxidative stress-induced fragmentation and preserved mitochondria predominantly in the filamentous state.

Similar changes were seen in the case of fusion and fission processes in NRCM cell culture compared to in vivo model. BGP-15 treatment increased the expression level of fusion proteins (OPA1, MFN1, MFN2) and thus it can promote mitochondrial fusion during oxidative stress (Fig. 17). On the other hand, the level of fission mediators (DRP1, Fis1) was decreased due to BGP-15 treatment (Fig. 18). BGP-15 also moderated the mitochondrial translocation of DRP1 protein from the cytosol as a result of enhanced $DRP1^{Ser637}$ phosphorylation and decreased phosphorylation of $DRP1^{Ser616}$ (Fig. 19). Therefore, BGP-15 treatment has beneficial effects on mitochondrial dynamics by promoting the fusion and moderating the fission processes.

Several studies have demonstrated that mitochondrial biogenesis is compromised in cardiac remodelling and heart failure [126, 127, 134]. PGC-1α is the key regulator of mitochondrial biogenesis, which in turn is regulated by CREB [94, 128, 129]. In accordance with these data, we also found that oxidative stress had negative effect on mitochondrial morphology and function via impaired mitochondrial biogenesis. We observed that the expression level of PCG-1α increased significantly due to BGP-15 treatment (Fig. 20). Moreover, BGP-15 treatment further enhanced the phosphorylation

of CREB compared to $H_2O_2$ group, too (Fig. 20). CREB increased the expression level of PGC-1α and therefore can enhance mitochondrial biogenesis. VDAC is located in the outer mitochondrial membrane and can be used for mitochondrial loading protein. We found that VDAC was significantly elevated in BGP-15 treated cells that can support our previous results regarding enhanced biogenesis.

Furthermore, we examined the level of NDUFs1 subunit of NADH-ubiquinone oxidoreductase and UQCRC1 subunit of Ubiquinol Cytochrome c Reductase proteins. These proteins are the part of the mitochondrial electron transport chain (ETC Complex I and III) and in this way they are essentially important in the maintaining of proper mitochondrial function [80, 135]. The amount of ETC Complex I and Complex III proteins levels were increased significantly due to BGP-15 treatment, which is consistent with our previous results (Fig. 22).

In order to support our finding more adequately regarding the effect of BGP-15 on mitochondrial biogenesis, the relative content of ETC Complex IV was determined. We found that BGP-15 treatment increased the relative expression levels of both tested genes (COXI and COXIII; Fig. 21). Since both genes are encoded by mitochondrial DNA, this suggests that mitochondrial DNA content were increased in NRCMs cells treated with BGP-15.

Moreover, we also performed a well-accepted and frequently used method for studying mitochondrial biogenesis by measuring the activity of citrate synthase (CS) [136–138]. Citrate synthase is localized within the mitochondrial matrix and it catalyses the synthesis of citrate from oxaloacetate in the Krebs tricarboxylic acid cycle [137]. Maximal activity of citrate synthase indicates the mitochondrial content of heart muscle. Citrate synthase activity was reduced in hydrogen-peroxide stressed group compared to control group. The citrate synthase activity was increased significantly due to the treatment (Fig. 21). Summarizing these results, we can conclude that mitochondrial biogenesis was increased under oxidative stress in treated NRCMs cells as a result of BGP-15 treatment and in this way, it was able to enhance the proper mitochondrial function.

Oxidative stress can damage the mtDNA, which is extremely sensitive to it[30, 98]. In our recent work, PCR results showed extensive damage of mtDNA caused by hydrogen peroxide. Thus, the amplification of the entire mitochondrial genome was restrained. BGP-15 treatment, however, preserved mitochondrial genome integrity markedly decreasing the breakage of mtDNA (Fig. 23). The protection of mtDNA is extremely important, because the mitochondrial respiratory chain (ETC) complexes are encoded on

mtDNA [83, 139]. Complex I-III are critical for ROS production by the respiratory chain[81]. It can generate significant amounts of ROS under several conditions including hypoxia, mitochondrial hyperpolarization and inhibition of respiratory complexes. BGP-15 is able to reduce the mitochondrial ROS production at complex I [103, 107]. Along these lines, BGP-15 can protect against ROS induced mitochondrial DNA damage and maintain the appropriate mitochondrial function.

The preservation of mitochondrial membrane potential is also important to maintain the metabolic capacity of mitochondria. Well-functioning mitochondrial oxidative phosphorylation and ATP production are essential for the proper function of cardiomyocytes [140, 141]. BGP-15 is able to prevent oxidative stress-induced mitochondrial membrane potential loss and therefore improved mitochondrial function (Fig. 24). We observed that oxidative stress lead to mitochondrial respiration damage (Fig. 25). However, BGP-15 treatment preserved the mitochondrial function characterized by ATP production and spare respiratory capacity thereby ensuring the ability of cells to respond to increased energy demand under stress scenario.

BGP-15 also supports the maintenance of mitochondrial function partially via the preservation of the mitochondrial structure.

In conclusion, BGP-15 treatment exerted a marked protective effect against the development of hypertension-induced heart failure via the inhibition of fibrotic remodelling of the heart (Fig. 26). This effect could be explained by its beneficial effect on signal transduction factors and on mitochondrial dynamics as well as on mitochondrial biogenesis.

Moreover, our study is the first to demonstrate that BGP-15 preserved the mitochondrial ultrastructure by increased mitochondrial fusion and decreased fission processes and positively affected the translocation processes in chronic hypertension-induced heart failure animal model. Very similar observation could be made in another oxidative stress, in a primary rat cardiomyocytes cell culture stressed by hydrogen-peroxide. Similar changes were seen in the case of fusion and fission processes in NRCM cell culture compared to in vivo model. Moreover, BGP-15 treatment preserved the mitochondrial membrane potential and improved the mitochondrial function. BGP-15 protected the integrity of the mitochondrial genome and enhanced the de novo biogenesis of mitochondria during hydrogen peroxide-induced oxidative stress. Nevertheless, the exact molecular mechanism of the effects is still unknown, but there are clear evidences regarding the specific mechanism how to BGP-15 acts at important integrator points of

signal transduction in certain pathological processes. In order to elucidate the potential underlying molecular mechanisms, further targeted studies should be performed in the future.

Our results revealed that pharmacological modulation of the mitochondrial dynamics under cellular stress could be a novel therapeutic approach in various cardiac diseases characterized by oxidative stress-induced mitochondrial damage.

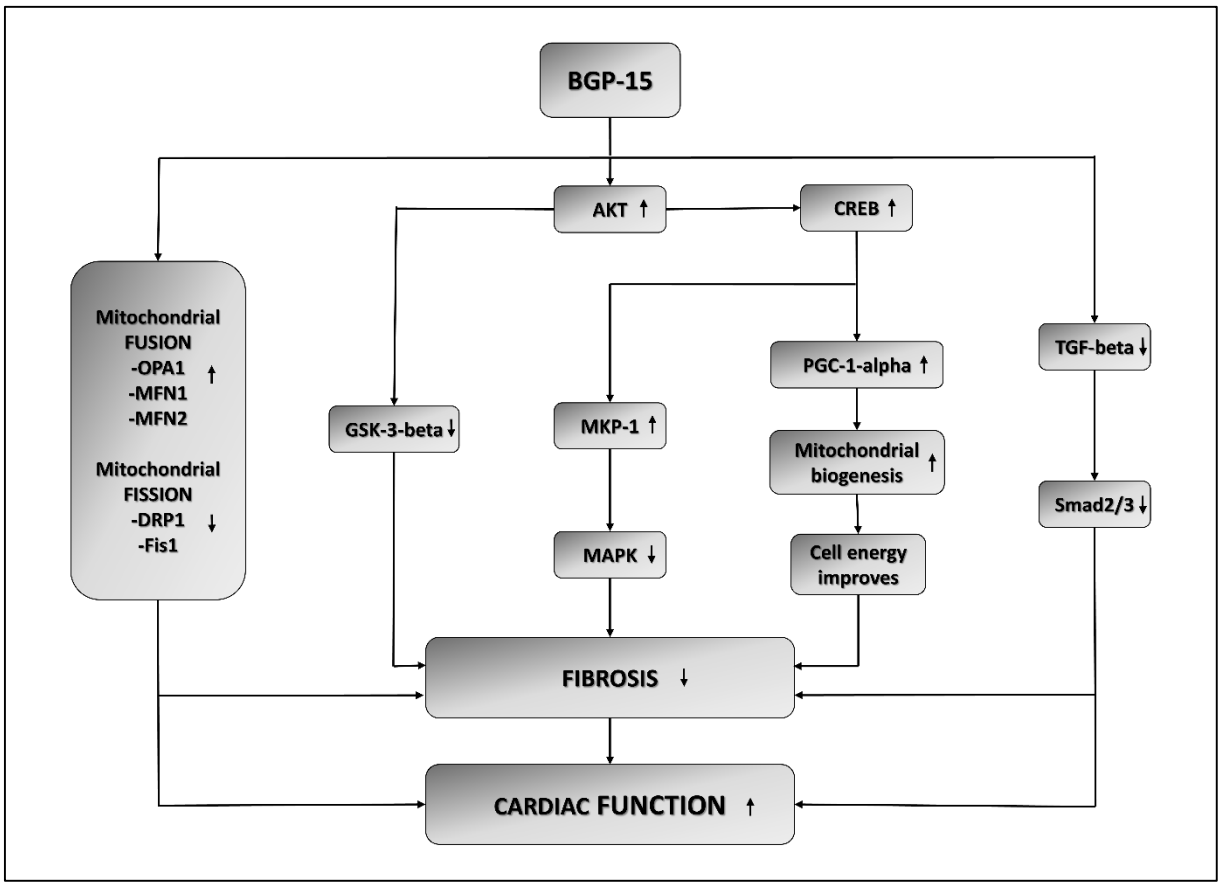


***Figure 26. The suspected mechanism of BGP-15 treatment in a hypertension-induced heart failure model.*** *BGP-15 has beneficial effect against hypertension induced cardiac remodelling and cardiac fibrosis. BGP-15 treatment decreases the activity of TGFβ/Smad and MAPKs signalling factors and in this way it prevents against hypertension induced interstitial collagen deposition. BGP-15 favourably influences the pro-survival signalling pathways. Moreover, the mitochondrial biogenesis is activated due to BGP-15 administration, thereby resulting in an increase in mitochondrial mass. BGP-15 increases the expression level of fusion mediators OPA1 and MFN1/2, moreover decreases the expression level of fission mediators DRP1 and Fis1.*

# 6. SUMMARY OF THE NEW FINDINGS

1. **The effect of BGP-15 on structure and function of heart.**
   Our research group verified the first time that BGP-15 treatment has beneficial effects on cardiac function in hypertension-induced heart failure.
2. **The effects of BGP-15 on signal transduction pathways taking part in the development of cardiac remodelling and heart failure.**
   BGP-15 treatment beneficially influences the activity of signalling pathways involved in remodelling (Akt/GSK-3β, ERK1/2, JNK, p38 MAPK).
3. **The effect of BGP-15 on the myocardial fibrotic processes.**
   BGP-15 protects against the interstitial collagen deposition via favourable effect on TGF-β/Smad pathway.
4. **The effects of BGP-15 on mitochondrial fusion and fission processes as well as on mitochondrial biogenesis.**
   - BGP-15 prevents mitochondrial ultrastructure against ROS-induced mitochondrial fragmentation.
   - BGP-15 increases the expression level of fusion mediators OPA1 and MFN1/2, moreover decreases the expression level of fission mediators DRP1 and Fis1 in the animal model of heart failure.
   - Mitochondrial biogenesis is enhanced due to BGP-15 treatment in heart failure.
   - BGP-15 preserves the mitochondrial network against oxidative stress-induced mitochondrial fragmentation.
   - BGP-15 increases the expression level of fusion mediators OPA1 and MFN1/2, moreover decreases the expression level of fission mediators DRP1 and Fis1 in NRCMs cell culture in oxidative stress scenarios.
   - Mitochondrial biogenesis increases under hydrogen-peroxide-induced oxidative stress in treated NRCMs cells as a result of BGP-15 treatment.
   - BGP-15 protects against oxidative stress-induced mitochondrial DNA damage.
5. **The role of BGP-15 on mitochondrial function under stress situations.**
   BGP-15 treatment preserves the mitochondrial membrane potential and improves mitochondrial function.

# 6. REFERENCES


1. Kemp CD, Conte JV (2012) The pathophysiology of heart failure. Cardiovascular Pathology 21:365–371. https://doi.org/10.1016/j.carpath.2011.11.007

2. Groenewegen A, Rutten FH, Mosterd A, Hoes AW (2020) Epidemiology of heart failure. European Journal of Heart Failure 22:1342–1356. https://doi.org/10.1002/ejhf.1858

3. Benjamin Emelia J., Muntner Paul, Alonso Alvaro, et al (2019) Heart Disease and Stroke Statistics—2019 Update: A Report From the American Heart Association. Circulation 139:e56–e528. https://doi.org/10.1161/CIR.0000000000000659

4. Ponikowski P, Voors AA, Anker SD, et al (2016) 2016 ESC Guidelines for the diagnosis and treatment of acute and chronic heart failure: The Task Force for the diagnosis and treatment of acute and chronic heart failure of the European Society of Cardiology (ESC)Developed with the special contribution of the Heart Failure Association (HFA) of the ESC. European Heart Journal 37:2129–2200. https://doi.org/10.1093/eurheartj/ehw128

5. Ziaeian B, Fonarow GC (2016) Epidemiology and aetiology of heart failure. Nat Rev Cardiol 13:368–378. https://doi.org/10.1038/nrcardio.2016.25

6. Lip GYH, Gibbs CR, Beevers DG (2000) Aetiology. BMJ 320:104–107

7. Jarraya F (2017) Treatment of Hypertension: Which Goal for Which Patient? Adv Exp Med Biol 956:117–127. https://doi.org/10.1007/5584_2016_97

8. Kong P, Christia P, Frangogiannis NG (2014) The pathogenesis of cardiac fibrosis. Cell Mol Life Sci 71:549–574. https://doi.org/10.1007/s00018-013-1349-6

9. Travers JG, Kamal FA, Robbins J, et al (2016) Cardiac Fibrosis: The Fibroblast Awakens.Circ.Res.118:1021–1040. https://doi.org/10.1161/CIRCRESAHA.115.306565

10. Rababa'h AM, Guillory AN, Mustafa R, Hijjawi T (2018) Oxidative Stress and Cardiac Remodeling: An Updated Edge. Curr Cardiol Rev 14:53–59. https://doi.org/10.2174/1573403X14666180111145207

11. Muslin AJ (2008) MAPK signalling in cardiovascular health and disease: molecular mechanisms and therapeutic targets. Clin Sci 115:203–218. https://doi.org/10.1042/CS20070430

12. Zhang W, Elimban V, Nijjar MS, et al (2003) Role of mitogen-activated protein kinase in cardiac hypertrophy and heart failure. Exp Clin Cardiol 8:173–183

13. Dorn GW, Vega RB, Kelly DP (2015) Mitochondrial biogenesis and dynamics in the developing and diseased heart. Genes Dev 29:1981–1991. https://doi.org/10.1101/gad.269894.115

14. Zhou B, Tian R (2018) Mitochondrial dysfunction in pathophysiology of heart failure. J Clin Invest 128:3716–3726. https://doi.org/10.1172/JCI120849

15. Zorov DB, Juhaszova M, Sollott SJ (2006) Mitochondrial ROS-induced ROS release: an update and review. Biochim Biophys Acta 1757:509–517. https://doi.org/10.1016/j.bbabio.2006.04.029

16. Tham YK, Bernardo BC, Ooi JYY, et al (2015) Pathophysiology of cardiac hypertrophy and heart failure: signaling pathways and novel therapeutic targets. Arch Toxicol 89:1401–1438. https://doi.org/10.1007/s00204-015-1477-x

17. Di Palo KE, Barone NJ (2020) Hypertension and Heart Failure: Prevention, Targets, and Treatment. Heart Failure Clinics 16:99–106. https://doi.org/10.1016/j.hfc.2019.09.001

18. Okamoto K, Aoki K (1963) Development of a Strain of Spontaneously Hypertensive Rats. Japanese Circulation Journal 27:282–293. https://doi.org/10.1253/jcj.27.282

19. Doggrell SA, Brown L (1998) Rat models of hypertension, cardiac hypertrophy and failure. Cardiovasc Res 39:89–105. https://doi.org/10.1016/S0008-6363(98)00076-5

20. Pfeffer JM, Pfeffer MA, Fishbein MC, Frohlich ED (1979) Cardiac function and morphology with aging in the spontaneously hypertensive rat. American Journal of Physiology-Heart and Circulatory Physiology. https://doi.org/10.1152/ajpheart.1979.237.4.H461

21. Kokubo M, Uemura A, Matsubara T, Murohara T (2005) Noninvasive evaluation of the time course of change in cardiac function in spontaneously hypertensive rats by echocardiography. Hypertens Res 28:601–609. https://doi.org/10.1291/hypres.28.601

22. Adams M A, Bobik A, Korner P I (1989) Differential development of vascular and cardiac hypertrophy in genetic hypertension. Relation to sympathetic function. Hypertension 14:191–202. https://doi.org/10.1161/01.HYP.14.2.191

23. Bartha E, Solti I, Kereskai L, et al (2009) PARP inhibition delays transition of hypertensive cardiopathy to heart failure in spontaneously hypertensive rats. Cardiovasc Res 83:501–510. https://doi.org/10.1093/cvr/cvp144

24. Deres L, Eros K, Horvath O, et al (2019) The Effects of Bradykinin B1 Receptor Antagonism on the Myocardial and Vascular Consequences of Hypertension in SHR Rats. Front Physiol 10:. https://doi.org/10.3389/fphys.2019.00624

25. Bing OH, Brooks WW, Robinson KG, et al (1995) The spontaneously hypertensive rat as a model of the transition from compensated left ventricular hypertrophy to failure. J Mol Cell Cardiol 27:383–396. https://doi.org/10.1016/s0022-2828(08)80035-1

26. Conrad Chester H., Brooks Wesley W., Hayes John A., et al (1995) Myocardial Fibrosis and Stiffness With Hypertrophy and Heart Failure in the Spontaneously

Hypertensive Rat. Circulation 91:161–170. https: //doi.org/10.1161/01. CIR.91.1. 161

27. Tsutsui H, Kinugawa S, Matsushima S (2011) Oxidative stress and heart failure. Am J Physiol Heart Circ Physiol 301:H2181-2190. https://doi.org/10.1152/ajpheart.00554.2011

28. Phaniendra A, Jestadi DB, Periyasamy L (2015) Free Radicals: Properties, Sources, Targets, and Their Implication in Various Diseases. Indian J Clin Biochem 30:11–26. https://doi.org/10.1007/s12291-014-0446-0

29. Lobo V, Patil A, Phatak A, Chandra N (2010) Free radicals, antioxidants and functional foods: Impact on human health. Pharmacogn Rev 4:118–126. https://doi.org/10.4103/0973-7847.70902

30. Peoples JN, Saraf A, Ghazal N, et al (2019) Mitochondrial dysfunction and oxidative stress in heart disease. Experimental & Molecular Medicine 51:1–13. https://doi.org/10.1038/s12276-019-0355-7

31. Dubois-Deruy E, Peugnet V, Turkieh A, Pinet F (2020) Oxidative Stress in Cardiovascular Diseases. Antioxidants 9:864. https:// doi.org/ 10.3390/ antiox9090864

32. Peng J-R, Lu T-T, Chang H-T, et al (2016) Elevated Levels of Plasma Superoxide Dismutases 1 and 2 in Patients with Coronary Artery Disease. Biomed Res Int 2016:. https://doi.org/10.1155/2016/3708905

33. Fukai T, Ushio-Fukai M (2011) Superoxide Dismutases: Role in Redox Signaling, Vascular Function, and Diseases. Antioxid Redox Signal 15:1583–1606. https://doi.org/10.1089/ars.2011.3999

34. Fukai T, Folz RJ, Landmesser U, Harrison DG (2002) Extracellular superoxide dismutase and cardiovascular disease. Cardiovascular Research 55:239–249. https://doi.org/10.1016/S0008-6363(02)00328-0

35. Birben E, Sahiner UM, Sackesen C, et al (2012) Oxidative Stress and Antioxidant Defense. World Allergy Organ J 5:9–19. https:// doi.org /10. 1097 / WOX.0b013e3182439613

36. Pham-Huy LA, He H, Pham-Huy C (2008) Free Radicals, Antioxidants in Disease and Health. Int J Biomed Sci 4:89–96

37. Moussa Z, Judeh ZMA, Ahmed SA (2019) Nonenzymatic Exogenous and Endogenous Antioxidants. Free Radical Medicine and Biology. https://doi.org/10.5772/intechopen.87778

38. Nimse SB, Pal D (2015) Free radicals, natural antioxidants, and their reaction mechanisms. RSC Adv 5:27986–28006. https://doi.org/10.1039/C4RA13315C

39. Mirończuk-Chodakowska I, Witkowska AM, Zujko ME (2018) Endogenous non-enzymatic antioxidants in the human body. Advances in Medical Sciences 63:68–78. https://doi.org/10.1016/j.advms.2017.05.005

40. Belch JJ, Bridges AB, Scott N, Chopra M (1991) Oxygen free radicals and congestive heart failure. Br Heart J 65:245–248. https://doi.org/10.1136/hrt.65.5.245

41. Hill MF, Singal PK (1996) Antioxidant and oxidative stress changes during heart failure subsequent to myocardial infarction in rats. Am J Pathol 148:291–300

42. van der Pol A, van Gilst WH, Voors AA, van der Meer P (2019) Treating oxidative stress in heart failure: past, present and future. Eur J Heart Fail 21:425–435. https://doi.org/10.1002/ejhf.1320

43. Tsutsui H, Kinugawa S, Matsushima S (2009) Mitochondrial oxidative stress and dysfunction in myocardial remodelling. Cardiovasc Res 81:449–456. https://doi.org/10.1093/cvr/cvn280

44. Panday A, Sahoo MK, Osorio D, Batra S (2015) NADPH oxidases: an overview from structure to innate immunity-associated pathologies. Cellular & Molecular Immunology 12:5–23. https://doi.org/10.1038/cmi.2014.89

45. Gál R, Halmosi R (2015) Az oxidatív stressz szerepe szívelégtelenségben. Orvosi Hetilap 156:1916–1920. https://doi.org/10.1556/650.2015.30301

46. Lambeth JD (2004) NOX enzymes and the biology of reactive oxygen. Nature Reviews Immunology 4:181–189. https://doi.org/10.1038/nri1312

47. Kuroda J, Ago T, Matsushima S, et al (2010) NADPH oxidase 4 (Nox4) is a major source of oxidative stress in the failing heart. Proc Natl Acad Sci U S A 107:15565–15570. https://doi.org/10.1073/pnas.1002178107

48. Carnicer R, Crabtree MJ, Sivakumaran V, et al (2013) Nitric Oxide Synthases in Heart Failure. Antioxid Redox Signal 18:1078–1099. https://doi.org/10.1089/ars.2012.4824

49. D'Oria R, Schipani R, Leonardini A, et al (2020) The Role of Oxidative Stress in Cardiac Disease: From Physiological Response to Injury Factor. In: Oxidative Medicine and Cellular Longevity. https://www.hindawi.com/journals/omcl/2020/5732956/. Accessed 25 Feb 2021

50. Bendall JK, Cave AC, Heymes C, et al (2002) Pivotal role of a gp91(phox)-containing NADPH oxidase in angiotensin II-induced cardiac hypertrophy in mice. Circulation 105:293–296. https://doi.org/10.1161/hc0302.103712

51. Ko HL, Ren EC (2012) Functional Aspects of PARP1 in DNA Repair and Transcription. Biomolecules 2:524–548. https://doi.org/10.3390/biom2040524

52. D'Amours D, Desnoyers S, D'Silva I, Poirier GG (1999) Poly(ADP-ribosyl)ation reactions in the regulation of nuclear functions. Biochem J 342 ( Pt 2):249–268

53. DeLeon-Pennell KY, Meschiari CA, Jung M, Lindsey ML (2017) Matrix Metalloproteinases in Myocardial Infarction and Heart Failure. Prog Mol Biol Transl Sci 147:75–100. https://doi.org/10.1016/bs.pmbts.2017.02.001

54. Hilfiker-Kleiner D, Landmesser U, Drexler H (2006) Molecular Mechanisms in Heart Failure: Focus on Cardiac Hypertrophy, Inflammation, Angiogenesis, and Apoptosis. Journal of the American College of Cardiology 48:A56–A66. https://doi.org/10.1016/j.jacc.2006.07.007

55. Azevedo PS, Polegato BF, Minicucci MF, et al (2016) Cardiac Remodeling: Concepts, Clinical Impact, Pathophysiological Mechanisms and Pharmacologic Treatment. Arq Bras Cardiol 106:62–69. https://doi.org/10.5935/abc.20160005

56. Ferrari R, Ceconi C, Campo G, et al (2009) Mechanisms of remodelling: a question of life (stem cell production) and death (myocyte apoptosis). Circ J 73:1973–1982. https://doi.org/10.1253/circj.cj-09-0573

57. Selvetella G, Hirsch E, Notte A, et al (2004) Adaptive and maladaptive hypertrophic pathways: points of convergence and divergence. Cardiovascular Research 63:373–380. https://doi.org/10.1016/j.cardiores.2004.04.031

58. Rossello X, Yellon DM (2018) The RISK pathway and beyond. Basic Res Cardiol 113:. https://doi.org/10.1007/s00395-017-0662-x

59. Chaanine AH, Hajjar RJ (2011) AKT signalling in the failing heart. Eur J Heart Fail 13:825–829. https://doi.org/10.1093/eurjhf/hfr080

60. Heineke J, Molkentin JD (2006) Regulation of cardiac hypertrophy by intracellular signalling pathways. Nat Rev Mol Cell Biol 7:589–600. https://doi.org/10.1038/nrm1983

61. Miyamoto S, Murphy AN, Brown JH (2009) Akt mediated mitochondrial protection in the heart. J Bioenerg Biomembr 41:169–180. https://doi.org/10.1007/s10863-009-9205-y

62. Hunter JJ, Chien KR (1999) Signaling pathways for cardiac hypertrophy and failure. N Engl J Med 341:1276–1283. https://doi.org/10.1056/NEJM199910213411706

63. Zhu L, Fang N, Gao P, et al (2015) Differential ERK1/2 Signaling and Hypertrophic Response to Endothelin-1 in Cardiomyocytes from SHR and Wistar-Kyoto Rats: A Potential Target for Combination Therapy of Hypertension. Curr Vasc. Pharmacol. 13:467–474. https:// doi.org/ 10. 2174 / 157016111266614101415 0007

64. Wheeler-Jones CPD (2005) Cell signalling in the cardiovascular system: an overview. Heart 91:1366–1374. https://doi.org/10.1136/hrt.2005.072280

65. Sadoshima J, Izumo S (1993) Molecular characterization of angiotensin II--induced hypertrophy of cardiac myocytes and hyperplasia of cardiac fibroblasts. Critical role of the AT1 receptor subtype. Circ Res 73:413–423. https://doi.org/10.1161/01.res.73.3.413

66. Cohn JN, Ferrari R, Sharpe N (2000) Cardiac remodeling--concepts and clinical implications: a consensus paper from an international forum on cardiac

remodeling. Behalf of an International Forum on Cardiac Remodeling. J Am Coll Cardiol 35:569–582. https://doi.org/10.1016/s0735-1097(99)00630-0

67. Liu R, Molkentin JD (2016) Regulation of cardiac hypertrophy and remodeling through the dual-specificity MAPK phosphatases (DUSPs). Journal of Molecular and Cellular Cardiology 101:44–49. https://doi.org/10.1016/j.yjmcc.2016.08.018

68. Rose BA, Force T, Wang Y (2010) Mitogen-activated protein kinase signaling in the heart: angels versus demons in a heart-breaking tale. Physiol Rev 90:1507–1546. https://doi.org/10.1152/physrev.00054.2009

69. Turner NA, Blythe NM (2019) Cardiac Fibroblast p38 MAPK: A Critical Regulator of Myocardial Remodeling. J Cardiovasc Dev Dis 6:. https://doi.org/10.3390/jcdd6030027

70. Craige SM, Chen K, Blanton RM, et al (2019) JNK and cardiometabolic dysfunction. Biosci Rep 39:. https://doi.org/10.1042/BSR20190267

71. Magyar K, Deres L, Eros K, et al (2014) A quinazoline-derivative compound with PARP inhibitory effect suppresses hypertension-induced vascular alterations in spontaneously hypertensive rats. Biochim Biophys Acta 1842:935–944. https://doi.org/10.1016/j.bbadis.2014.03.008

72. Hinderer S, Schenke-Layland K (2019) Cardiac fibrosis – A short review of causes and therapeutic strategies. Advanced Drug Delivery Reviews 146:77–82. https://doi.org/10.1016/j.addr.2019.05.011

73. Cowling RT, Kupsky D, Kahn AM, et al (2019) Mechanisms of cardiac collagen deposition in experimental models and human disease. Transl Res 209:138–155. https://doi.org/10.1016/j.trsl.2019.03.004

74. Zi Z, Chapnick DA, Liu X (2012) Dynamics of TGF-β/Smad Signaling. FEBS Lett 586:1921–1928. https://doi.org/10.1016/j.febslet.2012.03.063

75. Khalil H, Kanisicak O, Prasad V, et al (2017) Fibroblast-specific TGF-β-Smad2/3 signaling underlies cardiac fibrosis. J Clin Invest 127:3770–3783. https://doi.org/10.1172/JCI94753

76. Biernacka A, Dobaczewski M, Frangogiannis NG (2011) TGF-β signaling in fibrosis. Growth Factors 29:196–202. https:// doi.org/ 10.3109/08977194.2011.595714

77. Khurana Rohit, Simons Michael, Martin John F., Zachary Ian C. (2005) Role of Angiogenesis in Cardiovascular Disease. Circulation 112:1813–1824. https://doi.org/10.1161/CIRCULATIONAHA.105.535294

78. Sabbah HN (2020) Targeting the Mitochondria in Heart Failure. JACC Basic Transl Sci 5:88–106. https://doi.org/10.1016/j.jacbts.2019.07.009

79. Guo R, Gu J, Zong S, et al (2018) Structure and mechanism of mitochondrial electron transport chain. Biomed J 41:9–20. https://doi.org/10.1016/j.bj.2017.12.001

80. Nolfi-Donegan D, Braganza A, Shiva S (2020) Mitochondrial electron transport chain: Oxidative phosphorylation, oxidant production, and methods of measurement. Redox Biol 37:. https://doi.org/10.1016/j.redox.2020.101674

81. Hebert SL, Lanza IR, Nair KS (2010) Mitochondrial DNA Alterations and Reduced Mitochondrial Function in Aging. Mech Ageing Dev 131:451–462. https://doi.org/10.1016/j.mad.2010.03.007

82. Birk AV, Chao WM, Bracken C, et al (2014) Targeting mitochondrial cardiolipin and the cytochrome c/cardiolipin complex to promote electron transport and optimize mitochondrial ATP synthesis. Br J Pharmacol 171:2017–2028. https://doi.org/10.1111/bph.12468

83. Taanman J-W (1999) The mitochondrial genome: structure, transcription, translation and replication. Biochimica et Biophysica Acta (BBA) - Bioenergetics 1410:103–123. https://doi.org/10.1016/S0005-2728(98)00161-3

84. Barshad G, Marom S, Cohen T, Mishmar D (2018) Mitochondrial DNA Transcription and Its Regulation: An Evolutionary Perspective. Trends in Genetics 34:682–692. https://doi.org/10.1016/j.tig.2018.05.009

85. Shokolenko I, Venediktova N, Bochkareva A, et al (2009) Oxidative stress induces degradation of mitochondrial DNA. Nucleic Acids Res 37:2539–2548. https://doi.org/10.1093/nar/gkp100

86. Boland ML, Chourasia AH, Macleod KF (2013) Mitochondrial Dysfunction in Cancer. Front Oncol 3:. https://doi.org/10.3389/fonc.2013.00292

87. Chang C-R, Blackstone C (2010) Dynamic regulation of mitochondrial fission through modification of the dynamin-related protein Drp1. Ann N Y Acad Sci 1201:34–39. https://doi.org/10.1111/j.1749-6632.2010.05629.x

88. Tilokani L, Nagashima S, Paupe V, Prudent J (2018) Mitochondrial dynamics: overview of molecular mechanisms. Essays Biochem 62:341–360. https://doi.org/ 10.1042/ EBC20170104

89. Serasinghe MN, Chipuk JE (2017) Mitochondrial Fission in Human Diseases. Handb Exp Pharmacol 240:159–188. https://doi.org/10.1007/164_2016_38

90. Kanamaru Y, Sekine S, Ichijo H, Takeda K (2012) The Phosphorylation-Dependent Regulation of Mitochondrial Proteins in Stress Responses. In: Journal of Signal Transduction. https://www.hindawi.com/journals/jst/2012/931215/. Accessed 7 Apr 2020

91. Chang C-R, Blackstone C (2007) Drp1 phosphorylation and mitochondrial regulation. EMBO Rep 8:1088–1089. https://doi.org/10.1038/sj.embor.7401118

92. Chang C-R, Blackstone C (2007) Cyclic AMP-dependent Protein Kinase Phosphorylation of Drp1 Regulates Its GTPase Activity and Mitochondrial Morphology. J Biol Chem 282:21583–21587. https://doi.org/10.1074/jbc.C700083200

93. Jornayvaz FR, Shulman GI (2010) Regulation of mitochondrial biogenesis. Essays Biochem 47:. https://doi.org/10.1042/bse0470069

94. Fernandez-Marcos PJ, Auwerx J (2011) Regulation of PGC-1α, a nodal regulator of mitochondrial biogenesis. Am J Clin Nutr 93:884S–90. https://doi.org/10.3945/ajcn.110.001917

95. Popov L (2020) Mitochondrial biogenesis: An update. J Cell Mol Med 24:4892–4899. https://doi.org/10.1111/jcmm.15194

96. Hollander JM, Thapa D, Shepherd DL (2014) Physiological and structural differences in spatially distinct subpopulations of cardiac mitochondria: influence of cardiac pathologies. Am J Physiol Heart Circ Physiol 307:H1–H14. https://doi.org/10.1152/ajpheart.00747.2013

97. Papanicolaou KN, Khairallah RJ, Ngoh GA, et al (2011) Mitofusin-2 Maintains Mitochondrial Structure and Contributes to Stress-Induced Permeability Transition in Cardiac Myocytes. Mol Cell Biol 31:1309–1328. https://doi.org/10.1128/MCB.00911-10

98. Tsutsui H, Kinugawa S, Matsushima S (2008) Oxidative stress and mitochondrial DNA damage in heart failure. Circ J 72 Suppl A:A31-37. https://doi.org/10.1253/circj.cj-08-0014

99. Ide T, Tsutsui H, Hayashidani S, et al (2001) Mitochondrial DNA damage and dysfunction associated with oxidative stress in failing hearts after myocardial infarction. Circ Res 88:529–535. https://doi.org/10.1161/01.res.88.5.529

100. Hall AR, Burke N, Dongworth RK, Hausenloy DJ (2014) Mitochondrial fusion and fission proteins: novel therapeutic targets for combating cardiovascular disease. Br J Pharmacol 171:1890–1906. https://doi.org/10.1111/bph.12516

101. Rosdah AA, Bond ST, Sivakumaran P, et al (2017) Mdivi-1 Protects Human W8B2+ Cardiac Stem Cells from Oxidative Stress and Simulated Ischemia-Reperfusion Injury. Stem Cells Dev 26:1771–1780. https://doi.org/10.1089/scd.2017. 0157

102. Smith G, Gallo G (2017) To mdivi-1 or not to mdivi-1: Is that the question? Dev Neurobiol 77:1260–1268. https://doi.org/10.1002/dneu.22519

103. Szabo A, Sumegi K, Fekete K, et al (2018) Activation of mitochondrial fusion provides a new treatment for mitochondria-related diseases. Biochem Pharmacol 150:86–96. https://doi.org/10.1016/j.bcp.2018.01.038

104. Literati-Nagy Z, Tory K, Literáti-Nagy B, et al (2013) Synergic insulin sensitizing effect of rimonabant and BGP-15 in Zucker-obese rats. Pathol Oncol Res 19:571–575. https://doi.org/10.1007/s12253-013-9620-6

105. Literáti-Nagy B, Kulcsár E, Literáti-Nagy Z, et al (2009) Improvement of insulin sensitivity by a novel drug, BGP-15, in insulin-resistant patients: a proof of concept randomized double-blind clinical trial. Horm Metab Res 41:374–380. https://doi.org/10.1055/s-0028-1128142

106. Halmosi R, Berente Z, Osz E, et al (2001) Effect of poly(ADP-ribose) polymerase inhibitors on the ischemia-reperfusion-induced oxidative cell damage and mitochondrial metabolism in Langendorff heart perfusion system. Mol Pharmacol 59:1497–1505. https://doi.org/10.1124/mol.59.6.1497

107. Szabados E, Literati-Nagy P, Farkas B, Sumegi B (2000) BGP-15, a nicotinic amidoxime derivate protecting heart from ischemia reperfusion injury through modulation of poly(ADP-ribose) polymerase. Biochem Pharmacol 59:937–945. https://doi.org/10.1016/s0006-2952(99)00418-9

108. Sapra G, Tham YK, Cemerlang N, et al (2014) The small-molecule BGP-15 protects against heart failure and atrial fibrillation in mice. Nat Commun 5:5705. https://doi.org/10.1038/ncomms6705

109. Bombicz M, Priksz D, Gesztelyi R, et al (2019) The Drug Candidate BGP-15 Delays the Onset of Diastolic Dysfunction in the Goto-Kakizaki Rat Model of Diabetic Cardiomyopathy. Molecules 24:. https://doi.org/10.3390/molecules 24030586

110. Sarszegi Z, Bognar E, Gaszner B, et al (2012) BGP-15, a PARP-inhibitor, prevents imatinib-induced cardiotoxicity by activating Akt and suppressing JNK and p38 MAP kinases. Mol Cell Biochem 365:129–137. https://doi.org/10.1007/s11010-012-1252-8

111. Sumegi K, Fekete K, Antus C, et al (2017) BGP-15 Protects against Oxidative Stress- or Lipopolysaccharide-Induced Mitochondrial Destabilization and Reduces Mitochondrial Production of Reactive Oxygen Species. PLoS ONE 12:e0169372. https://doi.org/10.1371/journal.pone.0169372

112. Nagy G, Szarka A, Lotz G, et al (2010) BGP-15 inhibits caspase-independent programmed cell death in acetaminophen-induced liver injury. Toxicol Appl Pharmacol 243:96–103. https://doi.org/10.1016/j.taap.2009.11.017

113. Kubota Y, Umegaki K, Kagota S, et al (2006) Evaluation of Blood Pressure Measured by Tail-Cuff Methods (without Heating) in Spontaneously Hypertensive Rats. Biological and Pharmaceutical Bulletin 29:1756–1758. https://doi.org/10.1248/bpb.29.1756

114. Itter G, Jung W, Juretschke P, et al (2004) A model of chronic heart failure in spontaneous hypertensive rats (SHR). Lab Anim 38:138–148. https://doi.org/10.1258/002367704322968812

115. Horvath, O., Ordog, K., Bruszt, K., et al (2019) Role of BGP-15 treatment in hypertensive heart failure progression and mitochondrial protection. European Heart Journal 40:

116. Loch D, Chan V, Hoey A, Brown L (2009) Rosuvastatin Attenuates Heart Failure and Cardiac Remodelling in the Ageing Spontaneously Hypertensive Rat. Basic & Clinical Pharmacology & Toxicology 105:262–270. https://doi.org/10.1111/j.1742-7843.2009.00440.x

117. Magnussen C, Blankenberg S (2018) Biomarkers for heart failure: small molecules with high clinical relevance. Journal of Internal Medicine 283:530–543. https://doi.org/10.1111/joim.12756

118. Frangogiannis NG (2019) Cardiac fibrosis: Cell biological mechanisms, molecular pathways and therapeutic opportunities. Molecular Aspects of Medicine 65:70–99. https://doi.org/10.1016/j.mam.2018.07.001

119. Ong S-B, Hausenloy DJ (2010) Mitochondrial morphology and cardiovascular disease. Cardiovasc Res 88:16–29. https://doi.org/10.1093/cvr/cvq237

120. Scheuermann DW (1993) The ultrastructure of Cardiac muscle in health and disease. Micron 24:47–73. https://doi.org/10.1016/0968-4328(93)90015-S

121. Knowlton AA, Chen L, Malik ZA (2014) Heart failure and mitochondrial dysfunction: the role of mitochondrial fission/fusion abnormalities and new therapeutic strategies. J Cardiovasc Pharmacol63:196–206. https://doi.org/10.1097/01.fjc.0000432861.55968.a6

122. Nan J, Zhu W, Rahman MS, et al (2017) Molecular regulation of mitochondrial dynamics in cardiac disease. Biochim Biophys Acta Mol Cell Res 1864:1260–1273. https://doi.org/10.1016/j.bbamcr.2017.03.006

123. Vásquez-Trincado C, García-Carvajal I, Pennanen C, et al (2016) Mitochondrial dynamics, mitophagy and cardiovascular disease. J Physiol (Lond) 594:509–525. https://doi.org/10.1113/JP271301

124. Lee H, Yoon Y (2014) Mitochondrial Fission: Regulation and ER Connection. Mol Cells 37:89–94. https://doi.org/10.14348/molcells.2014.2329

125. Energetic metabolism in cardiomyocytes: molecular basis of heart ischemia and arrhythmogenesis. https://vpjournal.net/article/view/2339. Accessed 30 Apr 2020

126. Pisano A, Cerbelli B, Perli E, et al (2016) Impaired mitochondrial biogenesis is a common feature to myocardial hypertrophy and end-stage ischemic heart failure. Cardiovasc Pathol 25:103–112. https://doi.org/10.1016/j.carpath.2015.09.009

127. Garnier A, Fortin D, Deloménie C, et al (2003) Depressed mitochondrial transcription factors and oxidative capacity in rat failing cardiac and skeletal muscles. J Physiol 551:491–501. https://doi.org/10.1113/jphysiol.2003.045104

128. Cantó C, Auwerx J (2009) PGC-1alpha, SIRT1 and AMPK, an energy sensing network that controls energy expenditure. Curr Opin Lipidol 20:98–105. https://doi.org/10.1097/MOL.0b013e328328d0a4

129. Jornayvaz FR, Shulman GI (2010) Regulation of mitochondrial biogenesis. Essays Biochem 47:. https://doi.org/10.1042/bse0470069

130. Beauloye C, Bertrand L, Horman S, Hue L (2011) AMPK activation, a preventive therapeutic target in the transition from cardiac injury to heart failure. Cardiovasc Res 90:224–233. https://doi.org/10.1093/cvr/cvr034

131. Li X, Liu J, Lu Q, et al (2019) AMPK: a therapeutic target of heart failure—not only metabolism regulation. Biosci Rep 39:. https://doi.org/10.1042/BSR20181767

132. Huang C-Y, Tan T-H (2012) DUSPs, to MAP kinases and beyond. Cell Biosci 2:24. https://doi.org/10.1186/2045-3701-2-24

133. Casals-Casas C, Álvarez E, Serra M, et al (2009) CREB and AP-1 activation regulates MKP-1 induction by LPS or M-CSF and their kinetics correlate with macrophage activation versus proliferation. European Journal of Immunology 39:1902–1913. https://doi.org/10.1002/eji.200839037

134. Riehle C, Abel ED (2012) PGC-1 Proteins and Heart Failure. Trends Cardiovasc Med 22:98–105. https://doi.org/10.1016/j.tcm.2012.07.003

135. Zhao R-Z, Jiang S, Zhang L, Yu Z-B (2019) Mitochondrial electron transport chain, ROS generation and uncoupling (Review). International Journal of Molecular Medicine 44:3–15. https://doi.org/10.3892/ijmm.2019.4188

136. Larsen S, Nielsen J, Hansen CN, et al (2012) Biomarkers of mitochondrial content in skeletal muscle of healthy young human subjects. J Physiol 590:3349–3360. https://doi.org/10.1113/jphysiol.2012.230185

137. Wiegand G, Remington SJ (1986) Citrate synthase: structure, control, and mechanism. Annu Rev Biophys Biophys Chem 15:97–117. https://doi.org/10.1146/annurev.bb.15.060186.000525

138. Molina AJA, Bharadwaj MS, Van Horn C, et al (2016) Skeletal Muscle Mitochondrial Content, Oxidative Capacity, and Mfn2 Expression are Reduced in Older Patients with Heart Failure and Preserved Ejection Fraction and are Related to Exercise Intolerance. JACC Heart Fail 4:636–645. https://doi.org/10.1016/j.jchf.2016.03.011

139. Gustafsson CM, Falkenberg M, Larsson N-G (2016) Maintenance and Expression of Mammalian Mitochondrial DNA. Annual Review of Biochemistry 85:133–160. https://doi.org/10.1146/annurev-biochem-060815-014402

140. Ingwall JS (2009) Energy metabolism in heart failure and remodelling. Cardiovasc Res 81:412–419. https://doi.org/10.1093/cvr/cvn301

141. Doenst T, Nguyen TD, Abel ED (2013) Cardiac Metabolism in Heart Failure - Implications beyond ATP production. Circ Res 113:709–724. https://doi.org/10.1161/CIRCRESAHA.113.300376

# 7. ACKNOWLEDGEMENT

These studies were carried out at the 1st Department of Medicine and Department of Biochemistry and Medical Chemistry, Medical School of the University of Pecs between 2017 and 2021.

I would like to express my thanks to my program leader, Professor Kálmán Tóth, who gave me support and useful advice during my work.

I would like to express my deepest appreciation to my project leaders Professor Róbert Halmosi and Dr. László Deres for guiding my studies throughout the field of cardiovascular sciences and providing the possibility of the current work. Without their fundamental guidance and persistent help this dissertation would not have been possible.

I am extremely grateful to Professor Balázs Sümegi (†), who was an extraordinary mentor and taught me a biochemical way of thinking.

My colleagues, Dr. Krisztián Erős, Katalin Ördög and Dr. Kitti Bruszt gave also a hand with the experiments.

I am grateful to Tímea Dózsa, József Nyirádi and Heléna Halász, who provided considerable assistance in the laboratory work throughout my studies.

I express my special thanks to my close friends for their encouraging support and their immense patience during my work.

It is my privilege to thank to my family for their love, caring and sacrifices for educating and preparing me for my future life. I am grateful to them for trusting me in the most difficult times and for encouraging me despite all the difficulties.

# 8. PUBLICATIONS OF THE AUTHOR

## RELEVANT PUBLICATIONS

HORVATH O, ORDOG K, BRUSZT K, KALMAN N, KOVACS D, RADNAI B, GALLYAS F, TOTH K, HALMOSI R, DERES L. Modulation of mitochondrial quality control processes by BGP-15 in oxidative stress scenarios: from cell culture to heart failure.
Oxidative Medicine and Cellular Longevity 2021 Paper: 6643871, 22 p. (2021)
**IF: 6,543**

HORVATH O, ORDOG K, BRUSZT K, DERES L, GALLYAS F, SUMEGI B, TOTH K, HALMOSI R. BGP-15 protects against heart failure by enhanced mitochondrial biogenesis and decreased fibrotic remodelling in spontaneously hypertensive rats.
Oxidative Medicine and Cellular Longevity 2021 Paper: 1250858, 13 p. (2021)
**IF: 6,543**

## ADDITIONAL PUBLICATIONS

ORDOG K, HORVATH O, EROS K, BRUSZT K, TOTH SZ, KOVACS D, KALMAN N, RADNAI B, DERES L, GALLYAS F, TOTH K, HALMOSI R. Mitochondrial protective effects of PARP-inhibition in hypertension-induced myocardial remodeling and in stressed cardiomyocytes.
Life Sciences 268 Paper: 118936, 15 p. (2021)
**IF: 5,037**

GAL R, DERES L, HORVATH O, EROS K, SANDOR B, URBAN P, SOOS SZ, MARTON ZS, SUMEGI B, TOTH K, HABON T, HALMOSI R. Resveratrol improves heart function by moderating inflammatory processes in patients with systolic heart failure.
Antioxidants 9: 11 Paper: 1108, 19 p. (2020)
**IF: 6,312**

DERES L, EROS K, HORVATH O, BENCZE N, CSEKO CS, FARKAS S, SERESS L, TOTH K, HALMOSI R. The effects of bradykinin B1 Receptor antagonism on the myocardial and vascular consequences of hypertension in SHR rats.
FRONTIERS IN PHYSIOLOGY 10 Paper: 624, 14 p. (2019)
**IF: 3,201**

VARADI O, HORVATH O, MARCSIK A, MOLNAR E, PALFI GY, BERECZKI ZS. Különleges formájú jelképes trepanációk a Dél-Alföldről.
Anthropologiai Közlemények 56 pp. 91-104, 14 p. (2015)

## PUBLISHED ABSTRACTS

HORVATH O, DERES L, ORDOG K, BRUSZT K, SUMEGI B, TOTH K, HALMOSI R.
Role of BGP-15 treatment in hypertensive heart failure Progression and mitochondrial protection.
EUROPEAN HEART JOURNAL 40: Suppl. 1 Paper: P5994 (2019)

HALMOSI R, GAL R, DERES L, HORVATH O, MARTON ZS, SUMEGI B, TOTH K, HABON T. Resveratrol improves cardiac function and exerts an anti-inflammatory effect in systolic heart failure patients.
EUROPEAN HEART JOURNAL 40: Suppl. 1 Paper: P781 (2019)

HORVATH O, ORDOG K, BRUSZT K, DERES L, SUMEGI B, TOTH K, HALMOSI R.
A BGP-15 kezelés hatása a mitokondriális dinamikára és funkcióra élő állat modellen és sejtkultúrában.
CARDIOLOGIA HUNGARICA 49: Suppl. B Paper: B23 (2019)

ORDOG K, HORVATH O, BRUSZT K, HALMOSI R, TOTH K, SUMEGI B, DERES L.
Az L-2286 kezelés hatása oxidatív stresszben a mitokondriális dinamikára és funkcióra in vitro kardiomioblaszt modellben.
CARDIOLOGIA HUNGARICA 49: Suppl. B Paper: B14 (2019)

HORVATH O, DERES L, EROS K, ORDOG K, HABON T, SUMEGI B, TOTH K, HALMOSI R.
Oxidatív stressz indukálta változások a szívizomsejtek mitokondriális dinamikájára sejtes modellekben.
CARDIOLOGIA HUNGARICA 48: Suppl. C Paper: C38 (2018)

ORDOG K, DERES L, EROS K, HORVATH O, HABON T, SUMEGI B, TOTH K, HALMOSI R.
A BGP-15 kezelés hatása a hipertenzió indukált kardiális remodellingrein vivo SHR modellben.
CARDIOLOGIA HUNGARICA 48: Suppl. C Paper: C34 (2018)

GAL R, DERES L, HORVATH O, PRAKSCH D, MARTON ZS, SUMEGI B, TOTH K, HABON T, HALMOSI R.
A rezveratrol hatása a non-invazív klinikai kardiológiai és laboratóriumi paraméterekre szisztolés típusú szívelégtelenségben.
CARDIOLOGIA HUNGARICA 48: Suppl. C Paper: C65 (2018)

HORVATH O, DERES L, EROS K, ORDOG K, HABON T, SUMEGI B, TOTH K, HALMOSI R.
Oxidative stress-induced changes in mitochondrial dynamics of cardiomyocytes in cell culture.
EUROPEAN JOURNAL OF HEART FAILURE 20: Suppl. 1 pp. 616-616. Paper: P2281, 1 p. (2018)

ORDOG K, DERES L, EROS K, HORVATH O, HABON T, SUMEGI B, TOTH K, HALMOSI R.
Effect of BGP-15 treatment on hypertension induced cardiac remodeling in an in vivo SHR model.
EUROPEAN JOURNAL OF HEART FAILURE 20: Suppl. 1 pp. 515-515. Paper: P1975, 1 p. (2018)

HALMOSI R, GAL R, DERES L, HORVATH O, PRAKSCH D, MARTON ZS, SUMEGI B, TOTH K, HABON T.
The effect of resveratrol on non-invasive cardiologic and laboratory parameters in systolic heart failure.
EUROPEAN JOURNAL OF HEART FAILURE 20: Suppl. 1 pp. 565-565. Paper: P2133, 1 p. (2018)

HORVATH O.
A paraoxonáz aktivitás, a totál oxidáns státusz és a lipid profil alakulása különböző kardiovaszkuláris rizikócsoportba tartozó egyénekben.
Érbetegségek, XXIII. évfolyam 2. szám, 2016/2

BERECZKI ZS, VARADI O, HORVATH O, MARCSIK A, MOLNÁR E, PALFI GY.
Healing and Sexual Symbolism - Avar Trephinations in the 7-9th Century AD Carpathian Basin.
In: McGlynn, George; Kirchengast, Sylvia; Zink, Albert; Grosskopf, Birgit (szerk.) 11th Meeting of the Society for Anthropology (GfA). Evolutionary and Modern Challenges to Homo sapiens – An Anthropological Inquiry. Abstract and Program Booklet
München, Németország (2015) 105 p. pp. 15-15, 1 p.

VARADI O, TIHANYI B, HORVATH O, MARCSIK A, MOLNAR E, PALFI GY, BERECZKI ZS.
Symbolic trephinations of extraordinary shape in the Carpathian Basin.
In: Gál, Szilárd Sándor (szerk.) 1st Conference of the Anthropological Association "Aurél Török"
Târgu-Mureş, Románia (2015) pp. 6-6, 1 p.

VARADI O, HORVATH O, BERECZKI ZS.
Szilvamag alakú jelképes trepanációk a Kárpát-medencében.
In: Mesterházy, B (szerk.) XIII. Természet-, Műszaki és Gazdaságtudományok Alkalmazása Nemzetközi Konferencia: Előadások: 13th International Conference on Applications of Natural, Technological and Economic Sciences: Proceedings from Conference
Szombathely, Magyarország: Nyugat-magyarországi Egyetem, Természettudományi és Műszaki Kar, Természetföldrajzi Tanszék, (2014) pp. 25-25, 1 p.

Hindawi
Oxidative Medicine and Cellular Longevity
Volume 2021, Article ID 1250858, 13 pages
https://doi.org/10.1155/2021/1250858

*Research Article*

# BGP-15 Protects against Heart Failure by Enhanced Mitochondrial Biogenesis and Decreased Fibrotic Remodelling in Spontaneously Hypertensive Rats

**Orsolya Horvath**,[1,2] **Katalin Ordog**,[1,2] **Kitti Bruszt**,[1,2] **Laszlo Deres**,[1,2,3] **Ferenc Gallyas**,[2,3,4] **Balazs Sumegi**,[2,3,4] **Kalman Toth**,[1,2] **and Robert Halmosi**[1,2]

[1]*1st Department of Medicine, University of Pecs, Medical School, Hungary*
[2]*Szentágothai Research Centre, University of Pecs, Hungary*
[3]*HAS-UP Nuclear-Mitochondrial Interactions Research Group, 1245 Budapest, Hungary*
[4]*Department of Biochemistry and Medical Chemistry, University of Pecs, Medical School, Hungary*

Correspondence should be addressed to Robert Halmosi; halmosi.robert@pte.hu

Received 5 August 2020; Revised 18 December 2020; Accepted 15 January 2021; Published 30 January 2021

Academic Editor: Paula Felippe Martinez



Heart failure (HF) is a complex clinical syndrome with poor clinical outcomes despite the growing number of therapeutic approaches. It is characterized by interstitial fibrosis, cardiomyocyte hypertrophy, activation of various intracellular signalling pathways, and damage of the mitochondrial network. Mitochondria are responsible for supplying the energy demand of cardiomyocytes; therefore, the damage of the mitochondrial network causes cellular dysfunction and finally leads to cell death. BGP-15, a hydroxylamine derivative, is an insulin-sensitizer molecule and has a wide range of cytoprotective effects in animal as well as in human studies. Our recent work was aimed at examining the effects of BGP-15 in a chronic hypertension-induced heart failure model. 15-month-old male SHRs were used in our experiment. The SHR-Baseline group represented the starting point ($n = 7$). Animals received BGP-15 (SHR-B, $n = 7$) or placebo (SHR-C, $n = 7$) for 18 weeks. WKY rats were used as age-matched normotensive controls ($n = 7$). The heart function was monitored by echocardiography. Histological preparations were made from cardiac tissue. The levels of signalling proteins were determined by Western blot. At the end of the study, systolic and diastolic cardiac function was preserved in the BGP-treated animals. BGP-15 decreased the interstitial collagen deposition via decreasing the activity of TGF$\beta$/Smad signalling factors and prevented the cardiomyocyte hypertrophy in hypertensive animals. BGP-15 enhanced the prosurvival signalling pathways (Akt/Gsk3$\beta$). The treatment increased the activity of MKP1 and decreased the activity of p38 and JNK signalling routes. The mitochondrial mass of cardiomyocytes was also increased in BGP-15-treated SHR animals due to the activation of mitochondrial biogenesis. The mitigation of remodelling processes and the preserved systolic cardiac function in hypertension-induced heart failure can be a result—at least partly—of the enhanced mitochondrial biogenesis caused by BGP-15.

## 1. Introduction

Heart failure remained a leading cause of death despite the broadening of therapeutic possibilities [1]. The most important risk factors of heart failure are ischemic heart disease and hypertension [2]. The treatment of hypertension is challenging; there is a high portion of patients who cannot reach the goal blood pressure level having a high risk for the development of heart failure [3]. Sustained elevation of blood pressure induces myocardial remodelling, which is characterized by interstitial fibrosis and cardiomyocyte hypertrophy [4, 5]. These cellular alterations are promoted by oxidative stress [6] and by the activation of various intracellular signal transduction pathways [7, 8]. Numerous

studies have demonstrated that mitochondria which are responsible for the cellular energy supply are also damaged in hypertension-induced cardiac remodelling and heart failure [9, 10]. ROS-induced mtDNA damage can be found in the background of these injuries, and mitochondria themselves become the main sources of endogenous ROS production [11]. The long-term presence of these pathophysiological factors finally can lead to heart failure [12]. Spontaneously hypertensive rat (SHR) has become one of the most intensively studied murine strain in experimental cardiology with pathologies resembling human essential hypertension [13, 14]. Therefore, SHR was used in our work as a hypertension-induced heart failure animal model.

BGP-15 (O-[3-piperidino-2-hydroxy-1-propyl]-nicotinic acid amidoxime dihydrochloride) is an insulin sensitizer molecule, with a protective effect in a wide range of experimental models. BGP-15 protects against oxidative stress in ischemia-reperfusion-induced injury in the Langendorff heart perfusion system [15, 16]. Furthermore, it prevents against atrial fibrillation in a transgenic mouse model of heart failure [17]. BGP-15 has beneficial effects on diastolic dysfunction in diabetic cardiomyopathy on Goto–Kakizaki rats [18]. BGP-15 prevented against the imatinib-induced cardiotoxic effects via decreasing the oxidative damages [19]. BGP-15 protects against the ROS-induced mitochondrial ROS production and preserved the mitochondrial membrane potential in the WRL-68 cell line [20]. Nagy et al. demonstrated that BGP-15 protects against the acetaminophen-provoked hepatocellular injury [21]. Moreover, BGP-15 protects lung structure and activates mitochondrial fusion processes in a model of pulmonary arterial hypertension [22].

Fibrotic remodelling, increased ROS production, activation of MAPK signalling pathways, and mitochondrial damage play a significant role in the abovementioned diseases as well as in the pathomechanism of heart failure. Furthermore, it appears that very little information is available or nothing at all on the effect of BGP-15 in the development of hypertensive cardiomyopathy. Therefore, the aim of our study was to investigate the role of BGP-15 in hypertension-induced heart failure.

We focused predominantly on factors that regulate the remodelling processes, myocardial fibrosis, the pattern of related signalling pathways, and the regulation of mitochondrial biogenesis as well.

## 2. Materials and Methods

*2.1. Ethics Statement.* Animals received care according to the Guide for the Care and Use of Laboratory Animals published by the US National Institute of Health (NIH Publication No. 85–23, revised 1996), and the experiment was approved by the Animal Welfare Committee of the University of Pecs, Medical School (permit number: BA02/2000-54/2017).

*2.2. Experimental Protocol.* 15-month-old male Wistar Kyoto (WKY) and spontaneously hypertensive rats (Charles River Laboratories, Budapest, Hungary) were used in the experiments. One or two animals were housed per cage under standardized conditions throughout the experiment, with 12 h dark-light cycle in solid-bottomed polypropylene cages, and received commercial rat chew and water ad libitum. Seven SHRs were sacrificed at the beginning of the experiment, as a baseline group (SHR-Baseline). SHRs were randomly divided into two groups: SHR-B and SHR-C. The SHR-B group was treated with BGP-15, a water-soluble compound (25 mg/b.w. in kg/day, $n = 7$), while the SHR-C group received only placebo ($n = 7$, SHR-C) per os for 18 weeks. BGP-15 was a gift from N-Gene Inc. (New York, NY, USA). The dosage of BGP-15 administered in the drinking water was based on preliminary data regarding the volume of daily fluid consumption. WKY rats were used as age-matched normotensive controls ($n = 7$). Noninvasive blood pressure measurements were performed on each animal on three occasions at weeks 0, 9, and 18 of the treatment period. Blood pressure measurements were performed by a noninvasive tail-cuff method as described earlier [23, 24]. Blood pressure was measured by the Non-Invasive Blood Pressure System with rat species platform (Panlab, Harvard Apparatus; LE5002). At the beginning and at the end of the 18-week-long period, echocardiographic measurements were performed. At the end of the 18 weeks, the animals were sacrificed, blood was collected to determine the concentration of plasma brain-derived natriuretic peptide (BNP), then hearts were removed. Atria and great vessels were trimmed from the ventricles, and the weight of the ventricles was measured. Hearts were fixed in 10% formalin for histology or freeze-clamped for Western blot analysis. In order to detect the extent of fibrotic areas, histologic samples were stained with Picrosirius red, and collagen type I immunohistochemistry was made. The phosphorylation state of TGF$\beta$, Smad2 and 3, Akt-1, GSK-3$\beta$, and MAPK signalling molecules were monitored by Western blotting. In our research, the following group notations were used according to the applied treatment: WKY: age-matched normotensive Wistar-Kyoto rats; SHR-Baseline: 15-month-old spontaneously hypertensive rats before the treatment period; SHR-C: 19-month-old spontaneously hypertensive rats after the 18-week-long placebo treatment; and SHR-B: 19-month-old spontaneously hypertensive rats after the 18-week-long treatment period with BGP-15.

*2.3. Echocardiographic Measurements.* Transthoracic echocardiography was performed under inhalation anaesthesia at the beginning of the experiment and on the day of sacrifice. The rats were lightly anesthetized with a mixture of 1.5% isoflurane and 98.5% oxygen. The chest of the animals was shaved, and acoustic coupling gel was applied. The animals were imaged in the left lateral position, and a warming pad was used to maintain normothermia. Heart rate did not differ considerably during anaesthesia among the groups. Ventricular dimensions, wall thicknesses, and systolic functions were measured from parasternal short and long-axis views at the midpapillary level. Parameters (E, A, and E') required for the evaluation of diastolic function were measured from the apical 4 chamber view. For the imaging of rats, VEVO 770 high-resolution ultrasound imaging system (VisualSonics, Toronto, Canada) was used, which was equipped with a 25 MHz transducer. The investigators were blinded to the treatment protocol. LV inner dimensions (LVIDd and LVIDs), the thickness

of septum and posterior wall (PW), LV end-diastolic volume (LVEDV), LV end-systolic volume (LVESV), E/A, and E/E' ratio were determined. EF (percentage) was calculated by 100 × [(LVEDV − LVESV)/LVEDV].

*2.4. Determination of Plasma B Type Natriuretic Peptide Level.* Blood samples were collected into vacutainer tubes containing EDTA and aprotinin (0.6 IU/ml) and centrifuged at 1600 g for 15 minutes at 4°C to separate plasma, which was collected and kept at −70°C. Plasma B type natriuretic peptide-32 levels (BNP-32) were determined by Enzyme-Linked Immunosorbent Assay method (BNP-32, Rat BNP 32 ELISA Kit, Abcam, ab108815CA, USA) as the datasheet recommends.

*2.5. Histology.* For histological examination, hearts were removed at the end of the study after euthanasia was performed by overdosing isoflurane. Ventricles were fixed in 6% formalin and sliced and embedded in paraffin. Five-micrometer-thick sections were cut serially from the base to the apex by a microtome. Seven animals from each group and 3 sections from each animal were used to determine the degree of cardiac fibrosis. Three images (magnification 10x) were randomly taken from the middle region of the LV wall on each section. The fibrotic area was determined on each image, and the mean value of nine images represents each animal. LV sections were stained with Picrosirius red to detect interstitial fibrosis. Slices were also processed for type I collagen (Bios rabbit polyclonal 1 : 500) immunohistochemistry. The binding was visualized with biotinylated/HRP-conjugated secondary antibody followed by the avidin-biotin-peroxidase detection system (PK-6200 Universal Vectastain ABC Elite Kit, Vector Laboratories, Burlingame, CA) using 3,3′-diaminobenzidine (DAB) as a chromogen. Progress of the immunoreaction was monitored using a light microscope, and the reaction was stopped by the removal of excess DAB with a gentle buffer wash. Animals from each group were used. The degree of fibrosis was quantified by the NIH ImageJ image processing program via its colour deconvolution plug-in.

Picrosirius red staining was performed to measure cardiomyocyte diameter (CD) as a cellular marker of myocardial hypertrophy. Seven animals from each group and 3 sections from each animal were used to determine the cell diameter. Three images (magnification 10x) were randomly taken from the free LV wall on each section. The fitted polygon technique was used to determine the area of the cells. Then, the calculated diameter was used for statistical analysis. In order to evaluate the cardiomyocyte diameter, 250 cardiomyocytes were measured from each animal. The mean value of cell diameter of an animal derived from 250 measurements and each group contained 7 animals.

*2.6. Western Blot Analysis.* Fifty milligrams of heart samples were homogenized in ice-cold Tris buffer (50 mmol/l, pH 8.0) containing protease inhibitor (1 : 100; Sigma-Aldrich Co., #P8340) and phosphatase inhibitor (1 : 100; Sigma-Aldrich Co., #P5726) as well as 50 mM sodium vanadate. The supernatant was harvested in 2x concentrated SDS-polyacrylamide gel electrophoresis sample buffer. Protein levels were measured with NanoDrop. Glyceraldehyde 3-phosphate dehydrogenase (GAPDH; 1 : 1000; Cell Signaling #2118) was used as a loading control. Proteins were separated on 12% SDS-polyacrylamide gel and transferred to nitrocellulose membranes. After blocking (2 h with 5% BSA in Tris-buffered saline contained with 1% Tween-20), membranes were probed overnight at 4°C with primary antibodies recognizing the following antigens: transforming growth factor-$\beta$ (TGF-$\beta$; 1 : 1000; Cell Signaling #3711), Smad2 (1 : 1000; Invitrogen, 436500), phospho-specific Smad2 Ser465/467 (1 : 1000; Invitrogen, MA5-15122), Smad3 (1 : 1000; Cell Signaling #9523), phospho-specific Smad3 Ser423/425 (1 : 1000; Cell Signaling #9520), protein kinase B (Akt; 1 : 1000; Cell Signaling #9272), phospho-specific Akt-1/protein kinase B-$\alpha$ Ser473 (1 : 1000; Cell Signaling #4060), glycogen synthase kinase-3$\beta$ (GSK-3$\beta$; 1 : 1000; Cell Signaling #9832), phospho-specific glycogen synthase kinase-3$\beta$ Ser9 (1 : 1000; Cell Signaling #5558), p38 mitogen-activated protein kinase (p38MAPK; 1 : 1000; Cell Signaling #8690), phospho-specific p38 mitogen-activated protein kinase Thr180/Tyr182 (1 : 1000; Cell Signaling #4511), c-Jun N-terminal kinase (JNK; 1 : 1000; Cell Signaling #9252), phospho-specific c-Jun N-terminal kinase Thr183/Tyr185 (1 : 1000; Cell Signaling #9255), extracellular signal-regulated kinase (ERK1/2; 1 : 1000; Cell Signaling #4695), phospho-specific extracellular signal-regulated kinase 1/2 Thr202 (1 : 1000; Cell Signaling #4370), mitogen-activated protein kinase phosphatase-1 (MKP-1; 1 : 100; Santa Cruz Biotechnology, sc-373841), peroxisome proliferator-activated receptor gamma coactivator 1-alpha (PGC-1$\alpha$; 1 : 1000; Novus Biologicals, NBP1-04676), cAMP response element-binding protein (CREB; 1 : 1000; Cell Signaling #4820), phospho-specific cAMP response element-binding protein Ser133(1 : 1000; Cell Signaling #9198), 5′ AMP-activated protein kinase (AMPK; 1 : 1000; Cell Signaling #2532), phospho-specific 5′ AMP-activated protein kinase Thr172 (1 : 1000; Cell Signaling #2535), and voltage-dependent anion channel (VDAC; 1 : 1000; Cell Signaling #4661). Membranes were washed six times for 5 min in Tris-buffered saline (pH 7.5) containing 1% Tween-20 (TBST) before the addition of horseradish peroxidase-conjugated secondary antibody (goat antirabbit IgG, Sigma Aldrich Co. A0545, 1 : 3000 dilution; rabbit antimouse IgG, Sigma Aldrich Co., A9044, 1 : 5000 dilution). Membranes were washed six times for 5 min in TBST, and the antibody-antigen complexes were visualized by means of enhanced chemiluminescence. The results of Western blots were quantified using the NIH ImageJ program.

*2.7. Statistical Analysis.* Statistical analysis was performed by SPSS for Windows, version 26.0. All of the data were expressed as the mean ± SEM. The normality of distribution was assessed by the Shapiro-Wilk test. The baseline comparison between the strains was conducted by Student's $t$-test before randomization. The homogeneity of the groups was tested by Levene's test. Differences between treatment groups were determined by one-way ANOVA. For post hoc comparison, Tukey HSD or Dunnett T3 test was applied. A value of $p < 0.05$ was considered statistically significant.

## 3. Results

*3.1. Effect of BGP-15 Administration on Gravimetric Parameters.* At the beginning of the study, the body weight of WKY rats was significantly higher than the SHR rats (WKY: 386.40 ± 4.33 g, SHR-Baseline: 343.21 ± 2.48 g, SHR-C: 346.90 ± 6.65 g, SHR-B: 340.73 ± 6.32 g; $p < 0.01$, WKY vs. SHR groups; Table 1). A similar observation can be made at the end of the study (WKY: 401.45 ± 8.94 g, SHR-C: 358.13 ± 5.08 g, SHR-B: 356.85 ± 4.54 g; $p < 0.05$ WKY vs. SHR groups). At the end of the study, the heart weights (HW) and ventricles weight (VW) were significantly increased in the SHR groups compared to the WKY group (HW: WKY: 1.12 ± 0.04 g, SHR-Baseline: 1.16 ± 0.02, SHR-C: 1.49 ± 0.05 g, SHR-B: 1.23 ± 0.02 g; $p < 0.01$ SHR-B and SHR-C vs. WKY; VW: WKY: 0.95 ± 0.04 g, SHR-Baseline: 1.09 ± 0.02 g , SHR-C: 1.33 ± 0.05 g, SHR-B: 1.23 ± 0.02 g; $p < 0.01$ SHR-C vs. WKY, $p < 0.01$ SHR-B vs. SHR-C). The ratio of ventricular weight to body weight (VW/BW) was increased markedly in the SHR groups compared to WKY animals (VW/BW(mg/g): WKY: 2.28 ± 0.11, SHR-Baseline: 3.19 ± 0.08, SHR-C: 3.73 ± 0.16, SHR-B: 3.21 ± 0.03; $p < 0.01$ SHR groups vs. WKY, $p < 0.05$ SHR-B vs. WKY, $p < 0.01$ WKY vs. SHR-Baseline and SHR-C, $p < 0.01$ SHR-C vs. SHR-Baseline, $p < 0.01$ SHR-B vs. SHR-C). Ventricular weight to the length of right tibia ratio (VW/TL) was also significantly increased (VW/TL (mg/mm): WKY: 21.27 ± 0.79, SHR-Baseline: 24.76 ± 0.82, SHR-C: 29.79 ± 0.94, SHR-B: 25.76 ± 0.46; $p < 0.05$ WKY vs. SHR-Baseline and SHR-B, $p < 0.01$ SHR-C vs. WKY and SHR-Baseline). BGP-15 treatment caused a significant moderation of these ratios ($p < 0.01$ SHR-B vs. SHR-C). The ratio of the lung wet weight-to-dry weight was enhanced in the SHR-C group significantly (lung wet weight/-dry weight(g/g): WKY: 4.42 ± 0.26 g/g, SHR-Baseline: 4.51 ± 0.13, SHR-C: 5.68 ± 0.24, SHR-B: 4.68 ± 0.13; $p < 0.01$ SHR-C vs. WKY and SHR-Baseline). BGP-15 caused a significant moderation of this ratio ($p < 0.01$ SHR-B vs. SHR-C).

*3.2. Effect of BGP-15 Administration on Systolic Blood Pressure and Echocardiographic Parameters.* At the beginning of the study, there was a significant difference between the systolic arterial blood pressure of the WKY and the SHR-Baseline group (WKY: 134.85 ± 1.95 mmHg, SHR-Baseline: 214.28 ± 3.70 mmHg; $p < 0.05$; $n = 7$). Systolic arterial blood pressure values did not differ significantly between the SHR groups at the end of the study (SHR-C: 226.14 ± 3.88 mmHg, SHR-B: 216.85 ± 3.90 mmHg; $p > 0.05$; $n = 7$). Long-term BGP-15 treatment apparently did not exert any significant effect on systolic blood pressure.

At the beginning of the study, the septum and posterior wall thickness was significantly higher in SHR animals compared to WKY animals ($p < 0.01$ SHR-Baseline vs. WKY) (Table 1). By the end of the 18-week treatment period, the severity of left ventricular hypertrophy remained unchanged in SHR-C animals. However, wall thicknesses were significantly reduced as a result of BGP-15 treatment ($p < 0.05$, SHR-B vs. SHR-C). LV end-diastolic (LVEDV) and LV end-systolic volumes (LVESV) were also significantly elevated in SHR-C animals ($p < 0.01$, SHR-C vs. WKY, SHR-Baseline). BGP-15 treatment was however able to moderate this elevation in SHR-B animals ($p < 0.05$ vs. SHR-C). LV mass was significantly higher in the SHR-Baseline group compared to WKY ($p < 0.05$ SHR-Baseline vs. WKY). In SHR-C animals, this parameter increased further compared to the initial value ($p < 0.01$, SHR-C vs. WKY; $p < 0.05$, SHR-C vs. SHR-Baseline). This parameter was also decreased in the SHR-B group compared to the nontreated animals ($p < 0.05$, SHR-B vs. SHR-C).

The left ventricular systolic function (EF%) reduced in both the SHR groups compared to the initial value; however, this decrease was more pronounced in the SHR-C group than in the treated animals ($p < 0.05$ SHR-B vs. SHR-C). The diastolic function marker E/E' ratio was significantly increased in the SHR-C group ($p < 0.05$ SHR-C vs. SHR-Baseline), indicating a decrease a diastolic dysfunction.

Meanwhile, the BGP-15 treatment decreased significantly the E/E' ratio in the treated group, compared to the SHR-C animals ($p < 0.01$, SHR-B vs. SHR-C).

*3.3. Effect of BGP-15 Administration on Plasma BNP Level.* By the end of the treatment period, the plasma BNP level increased significantly in the SHR-C group compared to the WKY and SHR-Baseline group ($p < 0.05$, SHR-C vs. WKY and SHR-Baseline group; Table 2). The BGP-15 treatment, however, caused a significant decrease in the level of the biomarker of heart failure in SHR animals ($p < 0.05$, SHR-B vs. SHR-C). The BNP level was only slightly elevated in the SHR-B group.

*3.4. Effect of the BGP-15 Administration on Interstitial Collagen Deposition.* Histological staining of the left ventricle of the heart was performed with Picrosirius red staining (Figures 1(a) and (b)) and collagen I immunohistochemistry (Figures 1(c) and (d)), which was used to monitor the degree of fibrosis. Only a low amount of interstitial collagen could be seen in the WKY group with Picrosirius red staining (Figure 1(a)). The extent of fibrosis was significantly higher in the SHR groups compared to the WKY group ($p < 0.05$, SHR-Baseline vs. WKY; $p < 0.01$, SHR-C and SHR-B vs. WKY; Figure 1(a)). Chronic high blood pressure-induced heart failure caused a further elevation of collagen deposition in the SHR-C group ($p < 0.01$, vs. SHR-Baseline group). The BGP-15 treatment however resulted in a significant decrease in the amount of interstitial fibrosis in the SHR-B group compared to nontreated hypertensive animals ($p < 0.01$, SHR-B vs. SHR-C; Figure 1(a)) (WKY: 11.78 ± 1.00%; SHR-Baseline: 16.59 ± 1.03%; $\mathrm{SHR-C}: 32.42 \pm 1.52\%$; $\mathrm{SHR-B}: 22.64 \pm 1.09\%$; Figure 2(b)).

Similar observations were made in the case of type I collagen immunohistochemistry (Figures 1(c) and (d)). Moderate interstitial collagen deposition was observed in the WKY group (WKY: 9.15 ± 0.54%; SHR-Baseline: 15.45 ± 0.69%; SHR-C: 31.24 ± 0.77%; SHR-B: 19.92 ± 0.72%; Figure 1(d)), in the case of hypertensive groups, even the initial value was higher than the in the WKY group ($p < 0.01$ vs. SHR-Baseline). This elevation became more pronounced by the end of the treatment period ($p < 0.01$ SHR-C vs. WKY, SHR-Baseline groups; Figure 1(c)). Due to the treatment, the interstitial collagen deposition was significantly decreased in the

Table 1: Effect of BGP-15 administration on gravimetric parameters of SHR animals.

| | WKY ($n = 7$) | SHR-baseline ($n = 7$) | SHR-C ($n = 7$) | SHR-B ($n = 7$) |
|---|---|---|---|---|
| $BW^{START}$ (g) | $386.40 \pm 4.33$ | $343.21 \pm 2.48^{**}$ | $346.90 \pm 6.65^{**}$ | $340.73 \pm 6.32^{**}$ |
| $BW^{END}$ (g) | $401.45 \pm 8.94$ | — | $358.13 \pm 5.08^{**}$ | $356.85 \pm 4.54^{**}$ |
| $HW^{END}$ (g) | $1.12 \pm 0.04$ | $1.16 \pm 0.02$ | $1.49 \pm 0.05^{**,\#\#}$ | $1.23 \pm 0.02^{\S\S}$ |
| $VW^{END}$ (g) | $0.95 \pm 0.04$ | $1.09 \pm 0.02$ | $1.33 \pm 0.05^{**,\#\#}$ | $1.14 \pm 0.02^{\S\S}$ |
| $VW/BW^{END}$ (mg/g) | $2.28 \pm 0.11$ | $3.19 \pm 0.08^{**}$ | $3.73 \pm 0.16^{**,\#\#}$ | $3.21 \pm 0.03^{*,\S}$ |
| $VW/TL^{END}$ (mg/mm) | $21.27 \pm 0.79$ | $24.76 \pm 0.82^{*}$ | $29.79 \pm 0.94^{**,\#\#}$ | $25.76 \pm 0.46^{*,\S\S}$ |
| Lung wet weight/$weight^{END}$ (g/g) | $4.42 \pm 0.26$ | $4.51 \pm 0.13$ | $5.68 \pm 0.24^{**,\#\#}$ | $4.68 \pm 0.13^{\S\S}$ |

$BW^{START}$: body weight at the beginning of the treatment; $BW^{END}$: body weight at the end of the treatment; $HW^{END}$: heart weight at the end of the treatment; $VW^{END}$: ventricles weight at the end of the treatment; $TL^{END}$: length of the right tibia at the end of the treatment. Values are means + SEM. WKY: age-matched normotensive Wistar-Kyoto rats, $n = 7$; SHR-Baseline: 15-month-old spontaneously hypertensive rats, $n = 7$; SHR-C: nontreated spontaneously hypertensive rats, $n = 7$; SHR-B: spontaneously hypertensive rats receiving BGP-15 for 18 weeks, $n = 7$. $^{*}p < 0.05$ vs. WKY, $^{**}p < 0.01$ vs. WKY, $^{\#\#}p < 0.01$ vs. SHR-Baseline, $^{\S}p < 0.05$ vs. SHR-C, $^{\S\S}p < 0.01$ vs. SHR-C.

Table 2: Effect of BGP-15 treatment on echocardiographic parameters.

| | WKY ($n = 7$) Mean ± SEM | SHR-Baseline ($n = 7$) Mean ± SEM | SHR-C ($n = 7$) Mean ± SEM | SHR-B ($n = 7$) Mean ± SEM |
|---|---|---|---|---|
| Septum | $1.93 \pm 0.03$ | $2.29 \pm 0.07^{**}$ | $2.32 \pm 0.07^{**}$ | $2.09 \pm 0.08^{*,\S}$ |
| PW | $1.90 \pm 0.04$ | $2.06 \pm 0.06^{*}$ | $1.97 \pm 0.08^{*}$ | $1.81 \pm 0.07^{\S}$ |
| LVIDd (mm) | $7.61 \pm 0.14$ | $7.75 \pm 0.15$ | $8.55 \pm 0.23^{**,\#\#}$ | $8.31 \pm 0.18^{**}$ |
| LVIDs (mm) | $4.54 \pm 0.13$ | $4.60 \pm 0.21$ | $5.87 \pm 0.31^{**,\#\#}$ | $5.19 \pm 0.32^{\S}$ |
| LVEDV ($\mu$l) | $310.25 \pm 12.85$ | $323.07 \pm 14.59$ | $402.40 \pm 24.76^{**,\#\#}$ | $377.19 \pm 17.37^{**}$ |
| LVESV ($\mu$l) | $96.01 \pm 6.85$ | $101.51 \pm 12.27$ | $175.52 \pm 22.46^{**,\#\#}$ | $137.23 \pm 16.46^{**,\S}$ |
| LV mass (mg) | $1029.81 \pm 43.84$ | $1384.42 \pm 40.69^{**}$ | $1587.38 \pm 106.36^{**,\#}$ | $1321.44 \pm 75.58^{*,\S}$ |
| EF% | $70.48 \pm 1.12$ | $69.59 \pm 2.41$ | $57.21 \pm 3.02^{**,\#\#}$ | $64.30 \pm 2.88^{*,\S}$ |
| E/A | $1.37 \pm 0.07$ | $1.70 \pm 0.09^{**}$ | $2.02 \pm 0.06^{**}$ | $1.27 \pm 0.08^{\S\S}$ |
| E/E' | $30.45 \pm 2.00$ | $30.32 \pm 2.98$ | $40.41 \pm 2.94^{**,\#\#}$ | $25.71 \pm 3.03^{\S\S}$ |
| BNP (pg/ml) | $302.76 \pm 13.76$ | $325.19 \pm 10.89$ | $755.14 \pm 33.34^{*,\#}$ | $352.04 \pm 22.50^{\S}$ |

Septum: thickness of the septum; PW: thickness of the posterior wall; LVIDd: left ventricular (LV) inner diameter end-diastolic; LVIDs: LV inner diameter end-systolic; LVEDV: LV end-diastolic volume; LVESV: LV end-systolic volume; LV mass: calculated weight of left ventricle; EF: ejection fraction; E: mitral peak velocity of early filling; A: mitral peak velocity of late filling; E': early diastolic mitral annular velocity; A': late diastolic mitral annular velocity; BNP: B type natriuretic peptide. WKY: age-matched normotensive Wistar-Kyoto rats, $n = 7$; SHR-Baseline: 15-month-old spontaneously hypertensive rats, $n = 7$; SHR-C: 19-month-old spontaneously hypertensive rats received placebo for 18 weeks, $n = 7$; SHR-B: 19-month-old spontaneously hypertensive rats received BGP-15 for 18 weeks, $n = 7$. $^{*}p < 0.05$ vs. WKY, $^{**}p < 0.01$ vs. WKY, $^{\#}p < 0.05$ vs. SHR-Baseline, $^{\#\#}p < 0.01$ SHR-Baseline, $^{\S}p < 0.05$ vs. SHR-C, $^{\S\S}p < 0.01$ vs. SHR-C.

SHR-B group compared to the SHR-C group ($p < 0.01$; Figure 1(c)). It can be concluded that BGP-15 treatment significantly reduced the formation of fibrotic deposits in the myocardium (Figures 1(a)–(d)).

*3.5. Effect of BGP-15 Administration on the Diameter of Cardiomyocytes.* Histological sections from the left ventricle of the heart stained with Picrosirius red were also used to study the cell diameters (Figures 1(e) and (f)). The diameter of cardiomyocytes was markedly elevated in SHR groups compared to the WKY group (WKY: $16.02 \pm 0.64\,\mu$m; SHR-Baseline: $22.76 \pm 0.70\,\mu$m; SHR-C: $33.86 \pm 1.82\,\mu$m; SHR-B: $28.57 \pm 0.57\,\mu$m; Figure 1(f)). This difference was the most pronounced in the case of SHR-C ($p < 0.01$, SHR-C vs. WKY). The BGP-15 treatment resulted in significantly lower cell diameters in the SHR-B group compared to the SHR-C group ($p < 0.01$; SHR-B vs. SHR-C; Figure 1(e)).

*3.6. Effect of BGP-15 Administration on the TGF-β/SMAD Signalling Pathway.* The level of TGF-$\beta$ was significantly elevated in all hypertensive groups compared to the WKY group ($p < 0.05$, SHR-B vs. WKY, $p < 0.01$ SHR-Baseline, SHR-C vs. WKY; Figure 2). In the case of the SHR-C group, a further increasing tendency could be seen by the end of the treatment period compared to the baseline values (NS). However, the BGP-15 treatment caused a significant decrease in the TGF-$\beta$ level compared to the untreated SHR animals ($p < 0.01$, SHR-B vs. SHR-C); moreover, the TGF-$\beta$ level in this group was even lower than in the SHR-Baseline group ($p < 0.05$, SHR-B vs. SHR-Baseline; Figure 2). In the case of

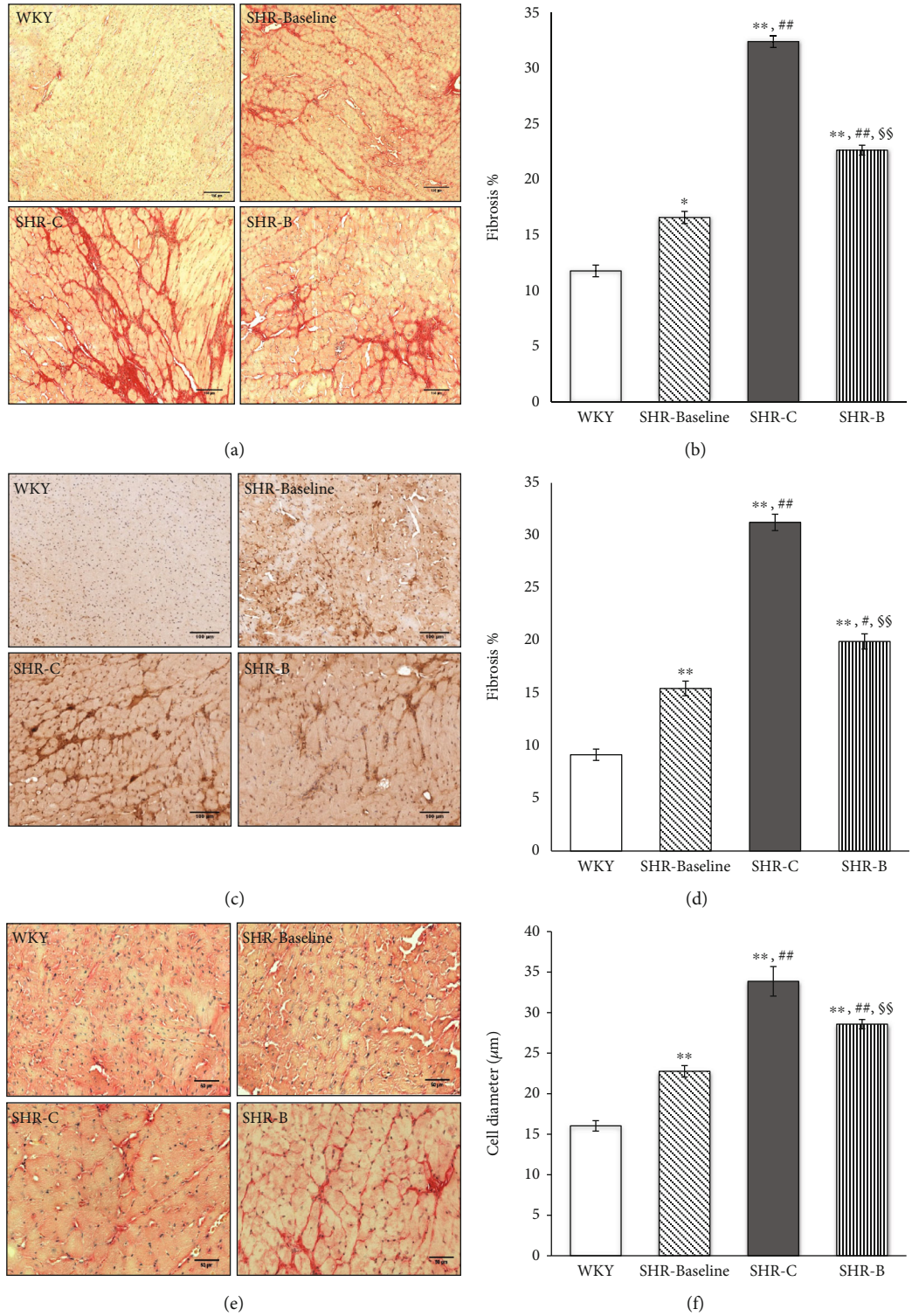


Figure 1: Effect of BGP-15 treatment on the extent of interstitial fibrosis, collagen type I deposition, and on the diameter of cardiomyocytes. Representative histological sections stained with Picrosirius red (a) ($n = 7$). Scale bar: 150 $\mu$m, magnification: 10-fold. Densitometric evaluation of the sections is shown (b). $^{*}p < 0.05$ vs. WKY, $^{**}p < 0.01$ vs. WKY, $^{\#\#}p < 0.01$ vs. SHR-Baseline, $^{\S\S}p < 0.01$ vs. SHR-C. Representative histological sections detected with collagen type I immunohistochemistry (c) ($n = 7$). Scale bar: 100 $\mu$m, magnification: 10-fold. Densitometric evaluation of the sections is shown (d). $^{**}p < 0.01$ vs. WKY, $^{\#\#}p < 0.01$ vs. SHR-C, $^{\S\S}p < 0.01$ vs. SHR-C. Representative histological sections stained with Picrosirius red (e) ($n = 7$). Scale bar: 50 $\mu$m, magnification: 10-fold. The average cellular diameter in the different groups is shown (f). $^{**}p < 0.01$ vs. WKY, $^{\#}p < 0.05$ vs. SHR-Baseline, $^{\S\S}p < 0.01$ vs. SHR-C. WKY: age-matched normotensive Wistar-Kyoto rats; SHR-Baseline: 15-month-old spontaneously hypertensive rats; SHR-C: 19-month-old spontaneously hypertensive rats received placebo for 18 weeks; SHR-B: 19-month-old spontaneously hypertensive rats received BGP-15 for 18 weeks.

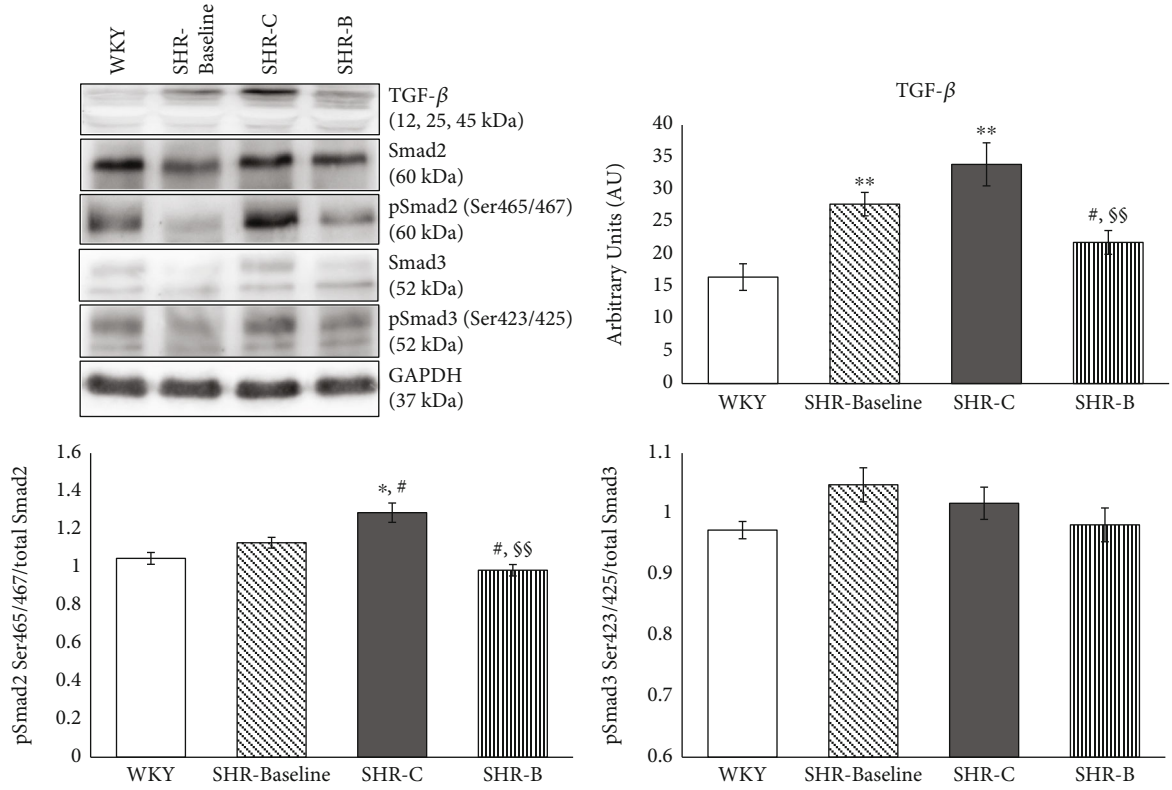


Figure 2: Effect of BGP-15 treatment on the TGF$\beta$/Smad signalling pathway. Representative Western blot analysis of TGF$\beta$, Smad2, Smad3, and phosphorylation and densitometric evaluation are shown. GAPDH was used as a loading control. WKY: age-matched normotensive Wistar-Kyoto rats, $n = 7$; SHR-Baseline: 15-month-old spontaneously hypertensive rats, $n = 7$; SHR-C: nontreated spontaneously hypertensive rats, $n = 7$; SHR-B: spontaneously hypertensive rats receiving BGP-15 for 18 weeks, $n = 7$. Values are mean ± SEM. $^{*}p < 0.05$ vs. WKY, $^{**}p < 0.01$ vs. WKY, $^{\#}p < 0.05$ vs. SHR-Baseline, $^{\S\S}p < 0.01$ vs. SHR-C.

Smad2 phosphorylation, we observed a mild increase in the SHR-Baseline compared to the WKY; however, this elevation was not significant. The phosphorylation of Smad2$^{Ser465/467}$ was significantly increased in the SHR-C compared to the WKY and Baseline groups ($p < 0.05$). BGP-15 treatment resulted in a significant reduction in the phosphorylation level of Smad2$^{Ser465/467}$ in the treated group ($p < 0.01$ SHR-B vs. SHR-C). There were no significant differences regarding the phosphorylation of Smad3$^{Ser423/425}$ between the groups (Figure 2). GAPDH was used as a loading control.

*3.7. Effect of BGP-15 Administration on the Phosphorylation Level of Akt-1 and GSK-3β.* The level of Akt-1$^{Ser473}$ phosphorylation was moderate in the WKY group as well as in the SHR-Baseline group (Figure 3.). In the SHR-C group, the phosphorylation of Akt-1$^{Ser473}$ was increased slightly, but significantly ($p < 0.01$ SHR-C vs. WKY and SHR-Baseline groups; Figure 3). However, BGP-15 treatment increased a marked increase in the Akt-1$^{Ser473}$ phosphorylation in SHR-B animals ($p < 0.01$ SHR-B vs. SHR-C group).

The phosphorylation level of GSK-3$\beta^{Ser9}$ was low in the WKY group similar to the Akt-1$^{Ser473}$ phosphorylation. In the SHR-Baseline and the SHR-C groups, however, slightly but not significantly elevated phosphorylation could be seen. The highest phosphorylation of GSK-3$\beta^{Ser9}$ was measured in the SHR-B group. This elevation was highly significant to other SHR groups ($p < 0.05$ SHR-B vs. SHR-C; $p < 0.01$, SHR-B vs. SHR-Baseline group; Figure 3). GAPDH was used as a loading control.

*3.8. Effect of BGP-15 Administration on the Activity of MAPKs.* The level of MKP-1 protein was low in the WKY and SHR-Baseline groups (Figure 4). A significant increase was however observed in the SHR-C group ($p < 0.01$, SHR-C vs. WKY as well as SHR-Baseline groups). The amount of MKP-1 protein increased further in the SHR-B group as a result of the BGP-15 treatment ($p < 0.01$, SHR-B vs. SHR-C; Figure 4). The level of Erk1/2$^{Thr202/Tyr204}$ phosphorylation was less pronounced in the SHR-C group compared to the WKY group and to baseline level ($p < 0.05$, SHR-C vs. WKY, Figure 4). BGP-15 treatment however caused a significant elevation in the phosphorylation of Erk1/2$^{Thr202/Tyr204}$ compared to the SHR-C group ($p < 0.01$, SHR-B vs. SHR-C; Figure 4). The level of p38-MAPK$^{Thr180/Tyr182}$ and JNK$^{Thr183/Tyr185}$ phosphorylation was low in the WKY and in the SHR-Baseline groups (Figure 4). The highest phosphorylation level of p38-MAPK$^{Thr180/Tyr182}$ and JNK$^{Thr183/Tyr185}$ could be seen in the SHR-C animals ($p < 0.01$, SHR-C vs. WKY and SHR-Baseline). The BGP-15 treatment reduced this phosphorylation of p38-MAPK$^{Thr180/Tyr182}$ and JNK$^{Thr183/Tyr185}$ too, and

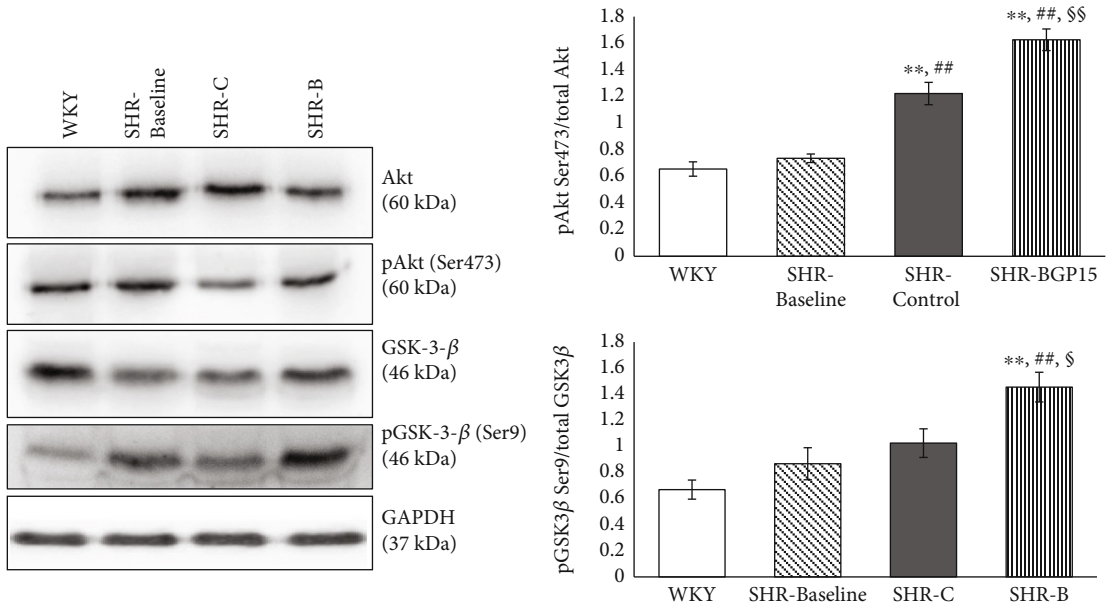


Figure 3: Effect of BGP-15 treatment on the phosphorylation of Akt-1$^{Ser473}$ and GSK-3$\beta^{Ser9}$. Representative Western blot analysis of Akt-1 and GSK-3$\beta$ phosphorylation and densitometric evaluation are shown. GAPDH was used as a loading control. WKY: age-matched normotensive Wistar-Kyoto rats, $n = 7$; SHR-Baseline: 15-month-old spontaneously hypertensive rats, $n = 7$; SHR-C: nontreated spontaneously hypertensive rats, $n = 7$; SHR-B: spontaneously hypertensive rats receiving BGP-15 for 18 weeks, $n = 7$. Values are mean ± SEM. $^{**}p < 0.01$ vs. WKY, $^{\#\#}p < 0.01$ vs. SHR-Baseline, $^{\S}p < 0.05$ vs. SHR-C, $^{\S\S}p < 0.01$ vs. SHR-C.

this reduction was significant in the case of JNK$^{Thr183/Tyr185}$ compared to the SHR-C group ($p < 0.01$; Figure 4). GAPDH was used as a loading control.

*3.9. Effect of BGP-15 Administration on the Regulation of Mitochondrial Biogenesis.* There were no significant differences between the WKY, SHR-Baseline, and SHR-C groups regarding the PGC-1$\alpha$ level (Figure 5). However, the BGP-15 treatment caused a significant increase in the amount of PGC-1$\alpha$ compared to the nontreated hypertensive animals ($p < 0.01$, SHR-B vs. SHR-Baseline and SHR-C group; Figure 5). In the case of AMPK$^{Thr172}$ phosphorylation, a significant increase was observed in the SHR-C group compared to the SHR-Baseline group ($p < 0.01$, SHR-C vs. SHR-Baseline; Figure 5). The BGP-15 treatment significantly reduced the phosphorylation of AMPK$^{Thr172}$ compared to the SHR-C group ($p < 0.01$ SHR-B vs. SHR-C). The CREB-$^{Ser133}$ phosphorylation was modest in the WKY group similar to the phosphorylation of AMPK$^{Thr172}$ (Figure 5). There was a significant increase in the phosphorylation level of CREB-$^{Ser133}$ in the SHR-C group compared to the baseline value and to the normotensive animals ($p < 0.01$, SHR-C vs. WKY; Figure 5). However, the BGP-15 treatment caused a further increase in the CREB$^{Ser133}$ phosphorylation compared to nontreated SHR animals ($p < 0.05$ SHR-B vs. SHR-C group) and to the baseline value ($p < 0.01$ SHR-B vs. SHR-Baseline). The highest VDAC protein level was observed in the WKY group. This level was significantly lower in the hypertensive groups ($p < 0.01$ WKY vs. SHR-Baseline, SHR-C, and SHR-B). By the end of the treatment period, VDAC became higher compared to the initial value ($p < 0.01$, SHR-C vs. SHR-Baseline). A further significant increase was seen in the SHR-B group ($p < 0.05$ SHR-B vs. SHR-C). GAPDH was used as a loading control.

## 4. Discussion

In this work, we aimed to examine the cardioprotective effect of BGP-15 in chronic hypertension-induced heart failure. The major findings of this study are that BGP-15 has a positive effect on cardiac function and on remodelling processes by inhibiting profibrotic signalling factors and by promoting mitochondrial biogenesis in an animal model of hypertension-induced heart failure.

SHR was used to provoke hypertension-induced heart failure. SHR is a widely used animal model in experimental cardiology because it resembles the human essential hypertension [13]. 15-months-old SHRs already showed the unquestionable signs of hypertensive heart disease at the start of the experiments. Left ventricular wall thicknesses and the LV mass were markedly increased in the SHR animals compared to normotensives (Table 2). However systolic left ventricular function was still normal in both normotensive and hypertensive animals. This is in accordance with the results of other workgroups and with our former results [25, 26]. The signs of left ventricular hypertrophy remained marked also by the end of the study in SHR animals. However, systolic (EF%) as well as diastolic left ventricular function (E/E') worsened significantly by that time, and animals showed the signs of heart failure. The worsening of these parameters was considerably lower due to the BGP-15 treatment of hypertensive animals (Table 2). This result

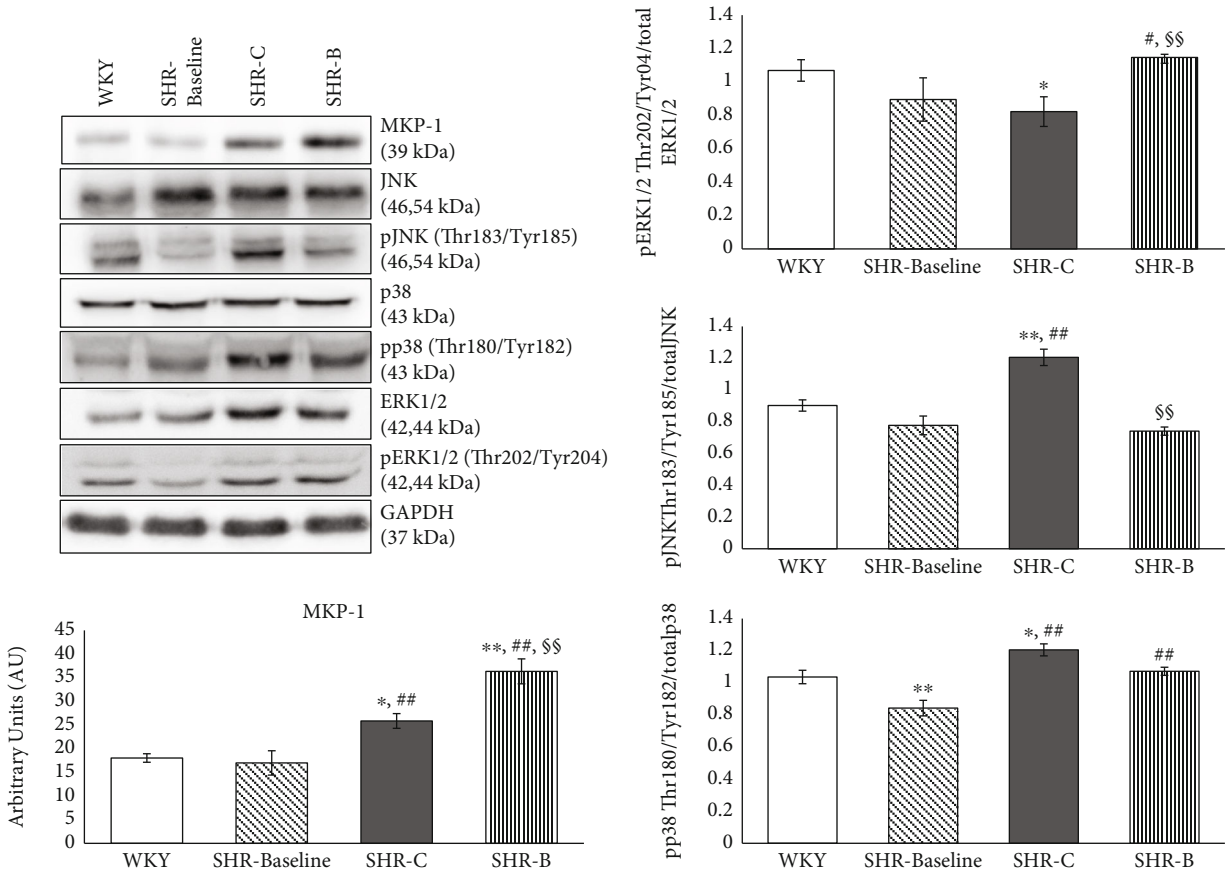


Figure 4: Effect of the BGP-15 treatment on the phosphorylation state of MAP kinases and on MKP-1. Representative Western blot analysis of MKP-1 as well as ERK1/2, p38, and JNK phosphorylation. Densitometric evaluation is also shown. GAPDH was used as a loading control. WKY: age-matched normotensive Wistar-Kyoto rats, $n = 7$; SHR-Baseline: 15-month-old spontaneously hypertensive rats, $n = 7$; SHR-C: nontreated spontaneously hypertensive rats, $n = 7$; SHR-B: spontaneously hypertensive rats receiving BGP-15 for 18 weeks, $n = 7$. Values are mean ± SEM. $^{*}p < 0.05$ vs. WKY, $^{**}p < 0.01$ vs. WKY, $^{\#\#}p < 0.01$ vs. SHR-Baseline, $^{\S\S}p < 0.01$ vs. SHR-C.

supports and complements the results of Sapra et al. that BGP-15 has beneficial effects on cardiac function in murine heart failure [17]. Moreover, left ventricular hypertrophy as well as the severity of left ventricular diastolic dysfunction was not only moderated due to BGP-15 treatment but also improved slightly, showing a so-called reverse remodelling phenomenon.

The BNP plasma level is a biomarker of heart failure. There is a direct proportionality between the severity of heart failure and the BNP level [27]. The marked increase of BNP that was seen in nontreated hypertensive animals (SHR-C) was also positively affected by BGP-15, because it decreased the BNP level to the level of normotensive animals (Table 2).

Hypertensive heart disease including heart failure is characterised by cardiac fibrosis. Extracellular matrix (ECM) remodelling can be observed during cardiac fibrosis, which leads to abnormalities in matrix composition and quality, as well as to decrease heart function [4, 28]. Heart failure is characterized by an increased collagen type I deposition. Thus, collagen type I is a marker of cardiac fibrosis. Collagen type I is one of the major components of the adult human cardiac tissue (approximately 85%) while collagen type III is the other important component (11%) [29]. Ventricular remodelling was characterized by cardiomyocyte hypertrophy and an extensive myocardial collagen deposition [30]. Both phenomena could be seen in hypertensive animals. BGP-15, however, prevented against hypertension-induced cardiac interstitial fibrosis and cardiomyocyte hypertrophy (Figure 1). The transforming growth factor-$\beta$ (TGF$\beta$)/Smad signalling route has a major role in the regulation of cardiac fibrosis [31, 32]. Activation of TGF-$\beta$/Smad signalling promotes myofibroblast formation and extracellular matrix (ECM) production that are leading to cardiac fibrosis [33]. In our recent work, hypertension induced a marked cardiac fibrosis by the activation of the TGF-$\beta$/Smad pathway (Figure 2). Both the level of TGF-$\beta$ and the phosphorylation of Smad2$^{\text{Ser465/467}}$ were significantly reduced due to BGP-15 treatment; therefore, it can be a mechanism in the background of decreased fibrosis, observed in the SHR-B group. The BGP-15-induced inhibition of fibrosis and cardiomyocyte hypertrophy are on the other hand the main causes of the improved cardiac function and structure compared to nontreated SHRs (Tables 1 and 2).

It is well known that the MAPK signalling pathway also plays an important role in the pathogenesis of hypertension-induced cardiac remodelling and heart failure [7, 34, 35].

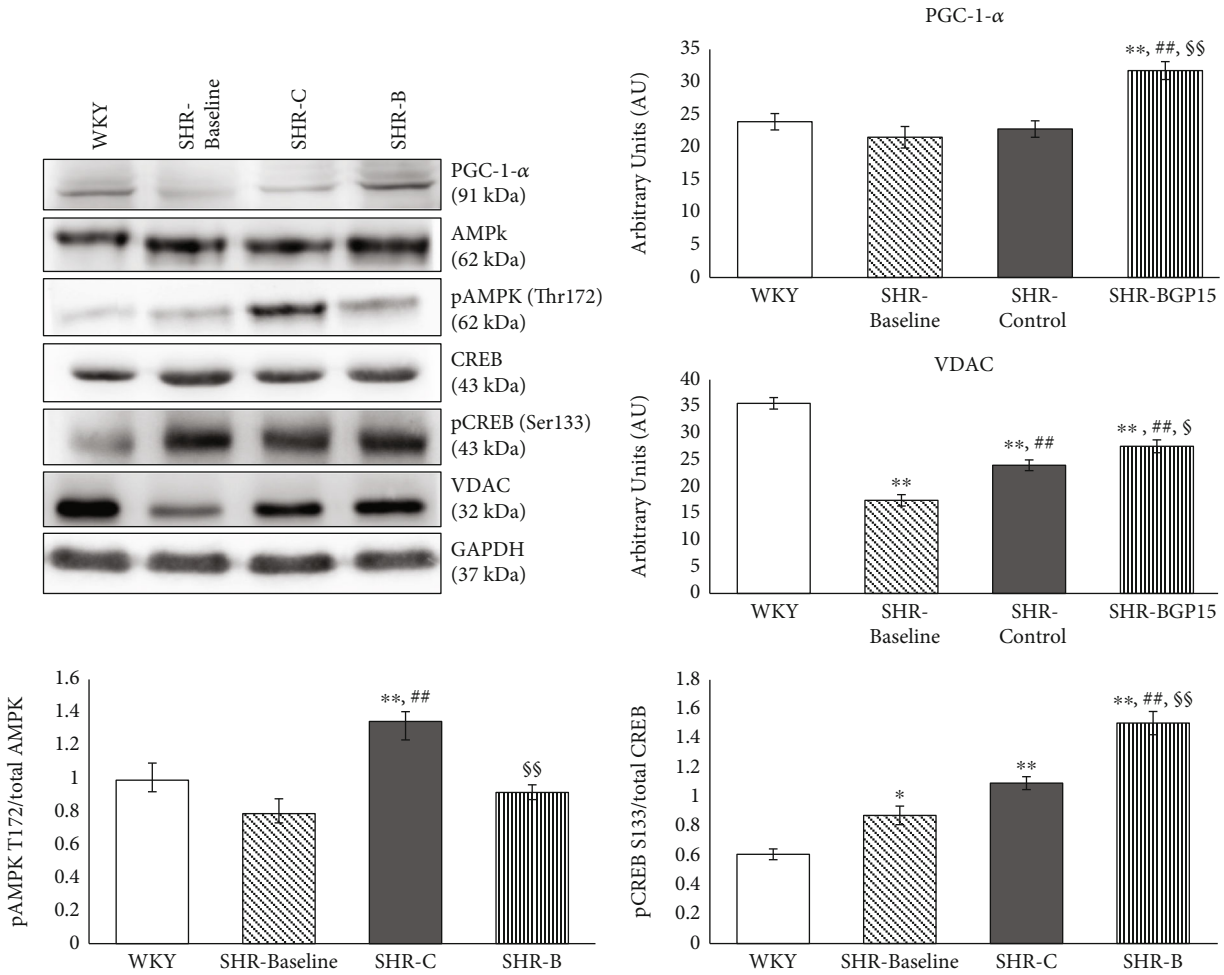


Figure 5: Effect of the BGP-15 treatment on the regulation of mitochondrial biogenesis. Representative Western blot analysis of PGC-1$\alpha$, VDAC, CREB, AMPK, and phosphorylation of CREB and AMPK. Densitometric evaluation is also shown. GAPDH was used as a loading control. WKY: age-matched normotensive Wistar-Kyoto rats, $n = 7$; SHR-Baseline: 15-month-old spontaneously hypertensive rats, $n = 7$; SHR-C: nontreated spontaneously hypertensive rats, $n = 7$; SHR-B: spontaneously hypertensive rats receiving BGP-15 for 18 weeks, $n = 7$. Values are mean ± SEM. $^{*}p < 0.05$ vs. WKY, $^{**}p < 0.01$ vs. WKY, $^{\#\#}p < 0.01$ vs. SHR-Baseline, $^{\S}p < 0.05$ vs. SHR-C, $^{\S\S}p < 0.01$ vs. SHR-C.

MAP kinases, predominantly p38 MAPK and JNK, are other important regulators of myocardial fibrosis [24, 36, 37]. The activity of MAP kinases are regulated by dual-specificity phosphatases (DUSPs) or MAPK phosphatases (MKPs) that can dephosphorylate MAPKs and in this way regulate—actually inhibit—their activity [34, 38]. In our recent work, the expression of MKP-1 increased significantly due to BGP-15 treatment in comparison with the SHR-C animals (Figure 4) As a consequence of the increased amount of MKP-1, the p38 MAPK and JNK phosphorylation decreased in the treated animals, in accordance with several previous studies that also confirmed the beneficial effect of BGP-15 on the phosphorylation state of p38 MAPK and JNK (Figure 4) [19, 22]. In the case of ERK phosphorylation, an opposite change could be seen in our work, because BGP-15 increased the ERK1/2 phosphorylation (Figure 4). Regarding BGP-15, there are studies that are in accordance with our results. Szabo et al. demonstrated that BGP-15 treatment increased the phosphorylation of ERK1/2 in WRL-68 cells [22]. However, in another work, BGP-15 decreased the phosphorylation of ERK1/2 in imatinib-induced cardiotoxicity [19]. Because ERK1/2 is a member of prosurvival signalling factors, its activation is beneficial in the failed myocardium [25, 39].

Akt-1 also belongs to prosurvival signalling factors, and it can promote "physiological" hypertrophy; however, it inhibits the pathological hypertrophy that is mainly characterised by cardiac collagen accumulation [40–42]. GSK-3$\beta$ is a downstream target of Akt-1 and Akt-1 which via the phosphorylation of GSK-3$\beta$ can promote the survival of chronically stressed cardiomyocytes in heart failure as demonstrated by previous works [25]. The cytoprotective effect due to increased phosphorylation of Akt-1 and GSK-3$\beta$ is mediated via their protective effect on the structure and function of mitochondria [43]. In our recent study, BGP-15 increased significantly the phosphorylation of Akt-1 and GSK-3$\beta$ compared to the nontreated SHR animals (Figure 3); therefore, the BGP-15 treatment activates the prosurvival signalling pathways.

The contractile function of cardiomyocytes is in strong correlation with the energy-producing capacity of the mitochondrial network [44]. Numerous studies have demonstrated

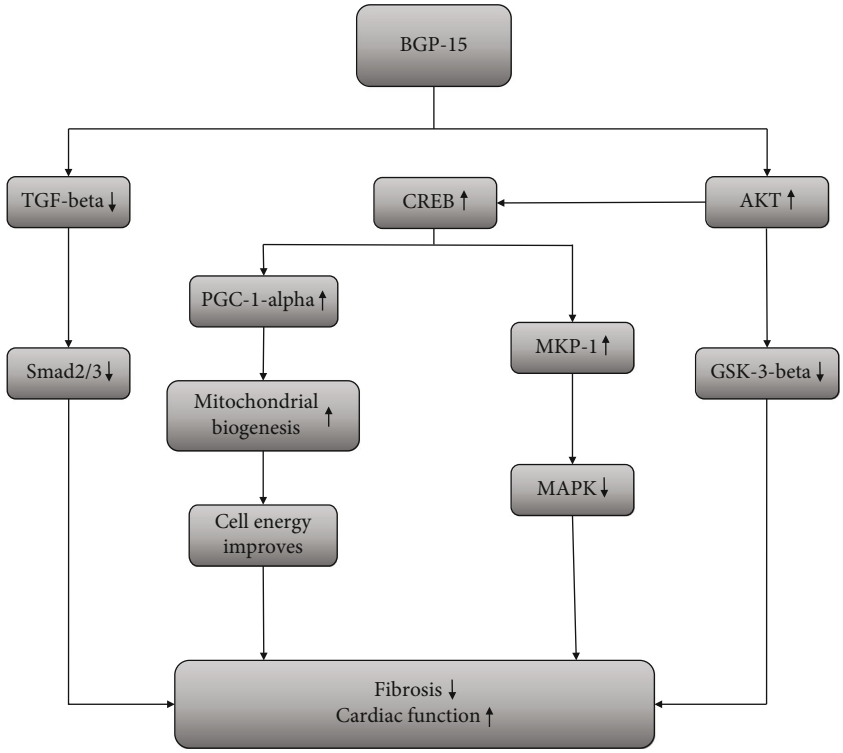


Figure 6: The suspected mechanism of BGP-15 treatment in a hypertension-induced heart failure model. BGP-15 has a beneficial effect against hypertension-induced cardiac remodelling and cardiac fibrosis. The BGP-15 treatment decreases the activity of TGF$\beta$/Smad and MAPK signalling factors and in this way prevents against hypertension-induced interstitial collagen deposition. BGP-15 favourably influences the prosurvival signalling pathways. Moreover, the mitochondrial biogenesis is activated due to BGP-15 administration, thereby resulting in an increase in mitochondrial mass.

that mitochondrial biogenesis is an essential step in mitochondrial quality control and is a highly vulnerable process in heart failure [45, 46]. PGC-1$\alpha$ is the master signalling factor of biogenesis, and it is regulated in different ways, among others by AMPK and CREB [47–49]. We found that the expression level of PCG-1$\alpha$ increased due to BGP-15 treatment compared to SHR-C animals (Figure 5). Phosphorylation of AMPK was however reduced as a result of the treatment (Figure 5). AMPK activation is a consequence of increased AMP to ATP ratio, which is a sign of energy depletion. Therefore, this reduction of AMPK phosphorylation indicates a favourable change in the energy production of cardiomyocytes [50, 51]. Phosphorylation of CREB was on the other hand increased in BGP-15-treated SHR animals compared to nontreated ones (Figure 5). BGP-15 via the activation of CREB increased the expression level of PGC-1$\alpha$, which in turn can yield in enhanced mitochondrial biogenesis and in increased high energy phosphate production. CREB transcription factor can also increase the production of MKP-1 and thereby can decrease the activity of the MAPK signal pathway, too [52, 53], which could be seen in our study. We determined the amount of VDAC, an outer mitochondrial membrane protein to characterize the number of mitochondria in cardiomyocytes. The elevation of VDAC in BGP-15-treated animals proved that there is an increased mitochondrial biogenesis and mitochondrial mass in cardiomyocytes.

In conclusion, BGP-15 treatment exerted a marked protective effect against the development of hypertension-induced heart failure via the inhibition of the fibrotic remodelling of the heart. This effect could be explained by its beneficial effect on signal transduction factors and by the increased mitochondrial biogenesis (Figure 6).

## Data Availability

The authors confirm that all data is fully available without restriction. All relevant data is described within the paper.

## Ethical Approval

Animals received care according to the Guide for the Care and Use of Laboratory Animals published by the US National Institute of Health, and the experiment was approved by the Animal Research Review Committee of the University of Pecs, Medical School (permit number: BA02/2000-54/2017). The manuscript does not contain clinical studies or patient data.

## Conflicts of Interest

On behalf of all authors, the corresponding author states that there is no conflict of interest.

## Authors' Contributions

All authors contributed to the study conception and design. Material preparation, data collection, and analysis were performed by Orsolya Horvath, Katalin Ordog, Kitti Bruszt, Laszlo Deres, Ferenc Gallyas, Balazs Sumegi, Kalman Toth, and Robert Halmosi. The first draft of the manuscript was written by Orsolya Horvath, and all authors commented on the previous versions of the manuscript. All authors read and approved the final manuscript. Prof. Balazs Sumegi has unexpectedly passed away during the course of this study. This paper is dedicated to his memory.

## Acknowledgments

This study was supported by the Hungarian National Research Foundations Grant (GINOP-2.3.2-15-2016-00048, GINOP 2.3.2-15-2016-00049) and NKFIH in Hungary, within the framework of the 2020-4.1.1-TKP2020 1st thematic programme of the University of Pécs. (2020-4.1.1-TKP2020).

## References

[1] E. J. Benjamin, P. Muntner, A. Alonso et al., "Heart Disease and Stroke Statistics—2019 update: a report from the American Heart Association," *Circulation*, vol. 139, pp. e56–e528, 2019.

[2] C. D. Kemp and J. V. Conte, "The pathophysiology of heart failure," *Cardiovascular Pathology*, vol. 21, no. 5, pp. 365–371, 2012.

[3] F. Jarraya, "Treatment of hypertension: which goal for which patient?," *Advances in Experimental Medicine and Biology*, vol. 956, pp. 117–127, 2016.

[4] P. Kong, P. Christia, and N. G. Frangogiannis, "The pathogenesis of cardiac fibrosis," *Cellular and Molecular Life Sciences*, vol. 71, no. 4, pp. 549–574, 2014.

[5] J. G. Travers, F. A. Kamal, J. Robbins, K. E. Yutzey, and B. C. Blaxall, "Cardiac fibrosis: the fibroblast awakens," *Circulation Research*, vol. 118, no. 6, pp. 1021–1040, 2016.

[6] A. M. Rababa'h, A. N. Guillory, R. Mustafa, and T. Hijjawi, "Oxidative stress and cardiac remodeling: an updated edge," *Current Cardiology Reviews*, vol. 14, no. 1, pp. 53–59, 2018.

[7] A. J. Muslin, "MAPK signalling in cardiovascular health and disease: molecular mechanisms and therapeutic targets," *Clinical Science*, vol. 115, no. 7, pp. 203–218, 2008.

[8] W. Zhang, V. Elimban, M. S. Nijjar, S. K. Gupta, and N. S. Dhalla, "Role of mitogen-activated protein kinase in cardiac hypertrophy and heart failure," *Experimental and Clinical Cardiology*, vol. 8, no. 4, pp. 173–183, 2003.

[9] G. W. Dorn, R. B. Vega, and D. P. Kelly, "Mitochondrial biogenesis and dynamics in the developing and diseased heart," *Genes & Development*, vol. 29, no. 19, pp. 1981–1991, 2015.

[10] B. Zhou and R. Tian, "Mitochondrial dysfunction in pathophysiology of heart failure," *The Journal of Clinical Investigation*, vol. 128, no. 9, pp. 3716–3726, 2018.

[11] D. B. Zorov, M. Juhaszova, and S. J. Sollott, "Mitochondrial ROS-induced ROS release: an update and review," *Biochimica et Biophysica Acta*, vol. 1757, no. 5-6, pp. 509–517, 2006.

[12] Y. K. Tham, B. C. Bernardo, J. Y. Y. Ooi, K. L. Weeks, and J. R. McMullen, "Pathophysiology of cardiac hypertrophy and heart failure: signaling pathways and novel therapeutic targets," *Archives of Toxicology*, vol. 89, no. 9, pp. 1401–1438, 2015.

[13] G. Itter, W. Jung, P. Juretschke, B. A. Schoelkens, and W. Linz, "A model of chronic heart failure in spontaneous hypertensive rats (SHR)," *Laboratory Animals*, vol. 38, no. 2, pp. 138–148, 2016.

[14] M. Kokubo, A. Uemura, T. Matsubara, and T. Murohara, "Noninvasive evaluation of the time course of change in cardiac function in spontaneously hypertensive rats by echocardiography," *Hypertension Research*, vol. 28, no. 7, pp. 601–609, 2005.

[15] R. Halmosi, Z. Berente, E. Osz, K. Toth, P. Literati-Nagy, and B. Sumegi, "Effect of poly(ADP-ribose) polymerase inhibitors on the ischemia-reperfusion-induced oxidative cell damage and mitochondrial metabolism in Langendorff heart perfusion system," *Molecular Pharmacology*, vol. 59, no. 6, pp. 1497–1505, 2001.

[16] E. Szabados, P. Literati-Nagy, B. Farkas, and B. Sumegi, "BGP-15, a nicotinic amidoxime derivate protecting heart from ischemia reperfusion injury through modulation of poly(-ADP-ribose) polymerase," *Biochemical Pharmacology*, vol. 59, no. 8, pp. 937–945, 2000.

[17] G. Sapra, Y. K. Tham, N. Cemerlang et al., "The small-molecule BGP-15 protects against heart failure and atrial fibrillation in mice," *Nature Communications*, vol. 5, no. 1, p. 5705, 2014.

[18] M. Bombicz, D. Priksz, R. Gesztelyi et al., "The drug candidate BGP-15 delays the onset of diastolic dysfunction in the Goto-Kakizaki rat model of diabetic cardiomyopathy," *Molecules*, vol. 24, no. 3, p. 586, 2019.

[19] Z. Sarszegi, E. Bognar, B. Gaszner et al., "BGP-15, a PARP-inhibitor, prevents imatinib-induced cardiotoxicity by activating Akt and suppressing JNK and p38 MAP kinases," *Molecular and Cellular Biochemistry*, vol. 365, no. 1-2, pp. 129–137, 2012.

[20] K. Sumegi, K. Fekete, C. Antus et al., "BGP-15 protects against oxidative stress- or lipopolysaccharide-induced mitochondrial destabilization and reduces mitochondrial production of reactive oxygen species," *PLoS One*, vol. 12, no. 1, p. e0169372, 2017.

[21] G. Nagy, A. Szarka, G. Lotz et al., "BGP-15 inhibits caspase-independent programmed cell death in acetaminophen-induced liver injury," *Toxicology and Applied Pharmacology*, vol. 243, no. 1, pp. 96–103, 2010.

[22] A. Szabo, K. Sumegi, K. Fekete et al., "Activation of mitochondrial fusion provides a new treatment for mitochondria-related diseases," *Biochemical Pharmacology*, vol. 150, pp. 86–96, 2018.

[23] Y. Kubota, K. Umegaki, S. Kagota et al., "Evaluation of blood pressure measured by tail-cuff methods (without heating) in spontaneously hypertensive rats," *Biological & Pharmaceutical Bulletin*, vol. 29, no. 8, pp. 1756–1758, 2006.

[24] L. Deres, K. Eros, O. Horvath et al., "The effects of bradykinin B1 receptor antagonism on the myocardial and vascular consequences of hypertension in SHR rats," *Front Physiol*, vol. 10, 2019.

[25] E. Bartha, I. Solti, L. Kereskai et al., "PARP inhibition delays transition of hypertensive cardiopathy to heart failure in spontaneously hypertensive rats," *Cardiovascular Research*, vol. 83, no. 3, pp. 501–510, 2009.

[26] D. Loch, V. Chan, A. Hoey, and L. Brown, "Rosuvastatin attenuates heart failure and cardiac remodelling in the ageing spontaneously hypertensive rat," *Basic & Clinical Pharmacology & Toxicology*, vol. 105, no. 4, pp. 262–270, 2009.

[27] C. Magnussen and S. Blankenberg, "Biomarkers for heart failure: small molecules with high clinical relevance," *Journal of Internal Medicine*, vol. 283, no. 6, pp. 530–543, 2018.

[28] N. G. Frangogiannis, "Cardiac fibrosis: cell biological mechanisms, molecular pathways and therapeutic opportunities," *Molecular Aspects of Medicine*, vol. 65, pp. 70–99, 2019.

[29] S. Hinderer and K. Schenke-Layland, "Cardiac fibrosis - a short review of causes and therapeutic strategies," *Advanced Drug Delivery Reviews*, vol. 146, pp. 77–82, 2019.

[30] R. T. Cowling, D. Kupsky, A. M. Kahn, L. B. Daniels, and B. H. Greenberg, "Mechanisms of cardiac collagen deposition in experimental models and human disease," *Translational Research*, vol. 209, pp. 138–155, 2019.

[31] Z. Zi, D. A. Chapnick, and X. Liu, "Dynamics of TGF-$\beta$/Smad signaling," *FEBS Letters*, vol. 586, no. 14, pp. 1921–1928, 2012.

[32] H. Khalil, O. Kanisicak, V. Prasad et al., "Fibroblast-specific TGF-$\beta$-Smad2/3 signaling underlies cardiac fibrosis," *The Journal of Clinical Investigation*, vol. 127, no. 10, pp. 3770–3783, 2017.

[33] A. Biernacka, M. Dobaczewski, and N. G. Frangogiannis, "TGF-$\beta$ signaling in fibrosis," *Growth Factors*, vol. 29, no. 5, pp. 196–202, 2011.

[34] R. Liu and J. D. Molkentin, "Regulation of cardiac hypertrophy and remodeling through the dual-specificity MAPK phosphatases (DUSPs)," *Journal of Molecular and Cellular Cardiology*, vol. 101, pp. 44–49, 2016.

[35] B. A. Rose, T. Force, and Y. Wang, "Mitogen-activated protein kinase signaling in the heart: angels versus demons in a heart-breaking tale," *Physiological Reviews*, vol. 90, no. 4, pp. 1507–1546, 2010.

[36] N. A. Turner and N. M. Blythe, "Cardiac fibroblast p38 MAPK: a critical regulator of myocardial remodeling," *Journal of Cardiovascular Development and Disease*, vol. 6, no. 3, p. 27, 2019.

[37] S. M. Craige, K. Chen, R. M. Blanton, J. F. Keaney Jr., and S. Kant, "JNK and cardiometabolic dysfunction," *Bioscience Reports*, vol. 39, no. 7, 2019.

[38] K. Magyar, L. Deres, K. Eros et al., "A quinazoline-derivative compound with PARP inhibitory effect suppresses hypertension-induced vascular alterations in spontaneously hypertensive rats," *Biochimica et Biophysica Acta*, vol. 1842, no. 7, pp. 935–944, 2014.

[39] L. Zhu, N. Fang, P. Gao, X. Jin, H. Wang, and Z. Liu, "Differential ERK1/2 signaling and hypertrophic response to endothelin-1 in cardiomyocytes from SHR and Wistar-Kyoto rats: a potential target for combination therapy of hypertension," *Current Vascular Pharmacology*, vol. 13, no. 4, pp. 467–474, 2015.

[40] X. Rossello and D. M. Yellon, "The RISK pathway and beyond," *Basic Research in Cardiology*, vol. 113, no. 1, 2018.

[41] A. H. Chaanine and R. J. Hajjar, "AKT signalling in the failing heart," *European Journal of Heart Failure*, vol. 13, no. 8, pp. 825–829, 2011.

[42] J. Heineke and J. D. Molkentin, "Regulation of cardiac hypertrophy by intracellular signalling pathways," *Nature Reviews. Molecular Cell Biology*, vol. 7, no. 8, pp. 589–600, 2006.

[43] S. Miyamoto, A. N. Murphy, and J. H. Brown, "Akt mediated mitochondrial protection in the heart: metabolic and survival pathways to the rescue," *Journal of Bioenergetics and Biomembranes*, vol. 41, no. 2, pp. 169–180, 2009.

[44] M. S. Martínez, A. García, E. Luzardo et al., "Energetic metabolism in cardiomyocytes: molecular basis of heart ischemia and arrhythmogenesis," *Vessel Plus*, vol. 1, pp. 130–141, 2017.

[45] A. Pisano, B. Cerbelli, E. Perli et al., "Impaired mitochondrial biogenesis is a common feature to myocardial hypertrophy and end-stage ischemic heart failure," *Cardiovascular Pathology*, vol. 25, no. 2, pp. 103–112, 2016.

[46] A. Garnier, D. Fortin, C. Deloménie, I. Momken, V. Veksler, and R. Ventura-Clapier, "Depressed mitochondrial transcription factors and oxidative capacity in rat failing cardiac and skeletal muscles," *The Journal of Physiology*, vol. 551, no. 2, pp. 491–501, 2003.

[47] P. J. Fernandez-Marcos and J. Auwerx, "Regulation of PGC-1$\alpha$, a nodal regulator of mitochondrial biogenesis," *The American Journal of Clinical Nutrition*, vol. 93, no. 4, pp. 884S–890S, 2011.

[48] C. Cantó and J. Auwerx, "PGC-1alpha, SIRT1 and AMPK, an energy sensing network that controls energy expenditure," *Current Opinion in Lipidology*, vol. 20, no. 2, pp. 98–105, 2009.

[49] F. R. Jornayvaz and G. I. Shulman, "Regulation of mitochondrial biogenesis," *Essays Biochem*, vol. 47, pp. 69–84, 2010.

[50] C. Beauloye, L. Bertrand, S. Horman, and L. Hue, "AMPK activation, a preventive therapeutic target in the transition from cardiac injury to heart failure," *Cardiovascular Research*, vol. 90, no. 2, pp. 224–233, 2011.

[51] X. Li, J. Liu, Q. Lu et al., "AMPK: a therapeutic target of heart failure—not only metabolism regulation," *Bioscience Reports*, vol. 39, no. 1, 2019.

[52] C.-Y. Huang and T.-H. Tan, "DUSPs, to MAP kinases and beyond," *Cell & Bioscience*, vol. 2, no. 1, p. 24, 2012.

[53] C. Casals-Casas, E. Álvarez, M. Serra et al., "CREB and AP-1 activation regulates MKP-1 induction by LPS or M-CSF and their kinetics correlate with macrophage activation versus proliferation," *European Journal of Immunology*, vol. 39, no. 7, pp. 1902–1913, 2009.

Hindawi
Oxidative Medicine and Cellular Longevity
Volume 2021, Article ID 6643871, 22 pages
https://doi.org/10.1155/2021/6643871

*Research Article*

# Modulation of Mitochondrial Quality Control Processes by BGP-15 in Oxidative Stress Scenarios: From Cell Culture to Heart Failure

**Orsolya Horvath**[1,2] **Katalin Ordog**[1,2] **Kitti Bruszt**[1,2] **Nikoletta Kalman**[3] **Dominika Kovacs**[3] **Balazs Radnai**[3] **Ferenc Gallyas**[2,3,4] **Kalman Toth**[1,2] **Robert Halmosi**[1,2] **and Laszlo Deres**[1,2,4]

[1]*1st Department of Medicine, University of Pecs, Medical School, Pecs, Hungary*
[2]*Szentágothai Research Centre, University of Pecs, Pecs, Hungary*
[3]*Department of Biochemistry and Medical Chemistry, University of Pecs, Medical School, Pecs, Hungary*
[4]*HAS-UP Nuclear-Mitochondrial Interactions Research Group, 1245 Budapest, Hungary*

Correspondence should be addressed to Laszlo Deres; deres.laszlo@pte.hu

Received 4 November 2020; Revised 15 January 2021; Accepted 9 February 2021; Published 28 February 2021

Academic Editor: Hao Zhou



Heart failure (HF) is a complex chronic clinical disease characterized by among others the damage of the mitochondrial network. The disruption of the mitochondrial quality control and the imbalance in fusion-fission processes lead to a lack of energy supply and, finally, to cell death. BGP-15 (O-[3-piperidino-2-hydroxy-1-propyl]-nicotinic acid amidoxime dihydrochloride) is an insulin sensitizer molecule and has a cytoprotective effect in a wide variety of experimental models. In our recent work, we aimed to clarify the mitochondrial protective effects of BGP-15 in a hypertension-induced heart failure model and "in vitro." Spontaneously hypertensive rats (SHRs) received BGP-15 or placebo for 18 weeks. BGP-15 treatment preserved the normal mitochondrial ultrastructure and enhanced the mitochondrial fusion. Neonatal rat cardiomyocytes (NRCMs) were stressed by hydrogen-peroxide. BGP-15 treatment inhibited the mitochondrial fission processes, promoted mitochondrial fusion, maintained the integrity of the mitochondrial genome, and moreover enhanced the de novo biogenesis of the mitochondria. As a result of these effects, BGP-15 treatment also supports the maintenance of mitochondrial function through the preservation of the mitochondrial structure during hydrogen peroxide-induced oxidative stress as well as in an "in vivo" heart failure model. It offers the possibility, which pharmacological modulation of mitochondrial quality control under oxidative stress could be a novel therapeutic approach in heart failure.

## 1. Introduction

Several studies have demonstrated that mitochondria, the powerhouse of cells are damaged in heart failure as well as in hypertension-induced cardiac remodelling [1–3]. The balance of fusion and fission processes that regulate mitochondrial dynamics is essential for maintaining energy production [4, 5]. The most important fusion proteins in the regulation of mitochondrial dynamics are the optic atrophy 1 (OPA1) and the mitofusin 1 and 2 (MFN1, MFN2) proteins, while the fission processes of mitochondria are controlled by dynamin-related protein 1 (DRP1) [6–8].

In heart failure due to the increased ROS production, fission processes become predominant, resulting in fragmented mitochondrial network, which is unable to perform its function of providing energy to the cell; thereby, mitochondrial fragmentation can induce cell death [2, 4, 9, 10]. The subject of numerous researches is the regulation of mitochondrial dynamics as a new therapeutic target in cardiovascular diseases [6, 11–14].

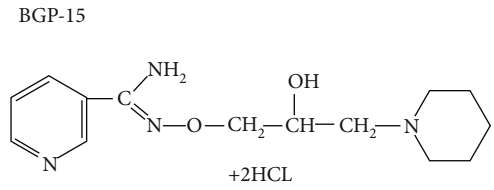


Figure 1: Chemical structure of BGP-15 (O-[3-piperidino-2-hydroxy-1-propyl]-nicotinic acid amidoxime dihydrochloride) [24].

BGP-15 (O-[3-piperidino-2-hydroxy-1-propyl]-nicotinic acid amidoxime dihydrochloride) is an insulin sensitizer molecule and has a cytoprotective effect in a wide variety of experimental models (Figure 1). BGP-15 protects against oxidative stress [15–17], promotes mitochondrial fusion [18], inhibits the mitogen-activated protein kinase (MAPK) activation [19–22], and improves cardiac function [21–23], but its specific intracellular target is still unknown.

This study was aimed to further characterize the mitochondrial effects of BGP-15 in a chronic hypertension-induced heart failure animal model and "in vitro" using primer neonatal rat cardiomyocytes (NRCM). We studied the effect of BGP-15 on the processes of mitochondrial quality control, particularly on fusion-fission processes, on mitochondrial biogenesis as well as on mitochondrial function.

## 2. Materials and Methods

*2.1. Ethics Statement.* Animals received care according to the Guide for the Care and Use of Laboratory Animals published by the US National Institute of Health and the experiment was approved by the Animal Research Review Committee of the University of Pecs, Medical School (Permit number: BA02/2000-54/2017).

*2.2. Animal Model.* 15-month-old male Wistar Kyoto (WKY) and spontaneously hypertensive rats (SHR) (Charles River Laboratories, Budapest, Hungary) were used. Two animals were housed per cage under standardized conditions throughout the experiment, with 12 hours of dark-light cycle in solid-bottomed polypropylene cages and received commercial rat chew and water ad libitum. 8 of the 24 animals were sacrificed at the beginning of the experiment, as a baseline (SHR-Baseline). The surviving 16 SHRs were randomly divided into two groups: SHR-B and SHR-C. SHR-B group was treated with the water-soluble BGP-15 (25 mg/b.w. in kg/day, $n = 8$), while SHR-C group received only placebo ($n = 8$, SHR-C) per os for 18 weeks. BGP-15 was a gift from N-Gene Inc. (New York, NY, USA). The dosage of BGP-15 administered in the drinking water was based on preliminary data about the volume of daily water consumption. WKY rats were used as age-matched controls ($n = 8$). At the end of the 18-week long treatment period, animals were sacrificed, and blood was collected to determine the concentration of plasma brain-derived natriuretic peptide (BNP). Hearts were removed, atria and great vessels were trimmed from the ventricles, and the weight of the ventricles was measured; then, it was normalized to the body mass and to the length of the right tibia (indices of cardiac hypertrophy). Hearts were fixed in modified Kranovsky fixative for transmission electron microscopy or freeze-clamped for Western blot analysis. The levels of proteins which are involved in the processes of mitochondrial dynamics and biogenesis were monitored by Western blot analysis. In our research, the following group notations were used according to the applied treatment: WKY: age-matched normotensive Wistar Kyoto rats; SHR-Baseline: 15-month-old spontaneously hypertensive rats; SHR-C: 19-month-old spontaneously hypertensive rats received placebo for 18 weeks; SHR-B: 19-month-old spontaneously hypertensive rats received BGP-15 for 18 weeks.

*2.3. Neonatal Rat Cardiomyocyte (NRCM) Cell Culture.* Cardiomyocytes were isolated using the Pierce™ Primary Cardiomyocyte Isolation Kit (Life Technologies, Carlsbad, CA, USA #88281) from 1-3-day-old neonatal Wistar rats. The animals were sacrificed, and then, their hearts were removed and minced into 1-3 $mm^3$ pieces. The pieces were digested with an enzyme complex (Cardiomyocyte Isolation Enzyme 1 (with papain) and Cardiomyocyte Isolation Enzyme 2 (with thermolysin)). After the tissue became primarily a single-cell suspension, the cells had been plated in 6-well plates with a density of $2.5 \times 10^6$ cell/well with specific Dulbecco's Modified Eagle Medium (DMEM) for Primary Cell Isolation containing 10% fetal bovine serum (FBS), 100 IU/mL penicillin and 100 $\mu$g/mL streptomycin. The medium was replaced 24 hours later with fresh Complete DMEM for Primary Cell Isolation containing Cardiomyocyte Growth Supplement, which inhibited the division of fibroblasts and therefore maintained the cardiomyocyte suspension in high purity during the culture period. NRCMs were cultivated in normal culture conditions, 37°C, saturated humidity atmosphere of 95% air and 5% CO2. Fresh medium was added every 2-3 days.

*2.4. Treatments of Neonatal Rat Cardiomyocytes.* On the day of the experiments, cells were washed once in PBS and added fresh medium and, then, treated with 150 $\mu$M $H_2O_2$ with or without 50 $\mu$M BGP-15 for 0.5 hours. The following groups were created according to the applied treatment: Control group: cells without any treatment; BGP-15 group: cells with only 50 $\mu$M BGP-15 for 0.5 hours; $H_2O_2$ group: cells with 150 $\mu$M $H_2O_2$ for 0.5 hours; $H_2O_2$+BGP-15 group: cells with 150 $\mu$M $H_2O_2$ and 50 $\mu$M BGP-15 for 0.5 hours.

*2.5. Determination of Plasma B-Type Natriuretic Peptide Level.* Blood samples were collected into Vacutainer tubes containing EDTA and aprotinin (0.6 IU/ml) and centrifuged at 1600 g for 15 minutes at 4°C to separate plasma, which was collected and kept at −70°C. Plasma B-type natriuretic peptide-32 levels (BNP-32) were determined by Enzyme-Linked Immunosorbent Assay method (BNP-32, Rat BNP 32 ELISA Kit, Abcam, ab108815CA, USA) as the datasheet recommends.

*2.6. Transmission Electron Microscopy.* For electron microscopy analysis, hearts were perfused retrogradely through the aortic root with ice-cold PBS to wash out the blood and then with modified Kranovsky fixative (2% paraformaldehyde,

Table 1: Effect of BGP-15 administration on gravimetric parameters and on BNP level of SHR animals.

| | WKY | SHR-C | SHR-B |
|---|---|---|---|
| $BW^{START}$ (g) | 391.51 ± 8.64 | 340.66 ± 6.74* | 347.4 ± 10.38* |
| $BW^{END}$ (g) | 403.22 ± 10.35 | 352.13 ± 6.86* | 365.29 ± 6.82* |
| $HW^{END}$ (g) | 1.11 ± 0.03 | 1.41 ± 0.03** | 1.28 ± 0.02**,# |
| $VW^{END}$ (g) | 0.98 ± 0.03 | 1.27 ± 0.02* | 1.12 ± 0.02* |
| $VW/BW^{END}$ (mg/g) | 2.43 ± 0.07 | 3.60 ± 0.04* | 3.07 ± 0.09*,# |
| $VW/TL^{END}$ (mg/mm) | 21.43 ± 0.71 | 29.14 ± 0.39* | 24.81 ± 0.53*,# |
| p-BNP (pg/ml) | 302.76 ± 13.77 | 755.15 ± 33.34* | 352.05 ± 22.50# |

$BW^{START}$: body weight at the beginning of the treatment; $BW^{END}$: body weight at the end of the treatment; $HW^{END}$: heart weight at the end of the treatment; $VW^{END}$: ventricles weight at the end of the treatment; $TL^{END}$: length of right tibia at the end of the treatment; p-BNP: plasma brain-type natriuretic peptide. Values are means + SEM. WKY: age-matched normotensive Wistar-Kyoto rats, $n = 8$, SHR-C: nontreated spontaneously hypertensive rats, $n = 8$, SHR-B: spontaneously hypertensive rats receiving BGP-15 for 18 weeks, $n = 8$. *$p < 0.05$ vs. WKY, **$p < 0.01$ vs. WKY, #$p < 0.05$ vs. SHR-C.

2.5% glutaraldehyde, 0.1 M Na-cacodylate buffer, pH 7.4, and 3 mM $CaCl_2$). 1 mm thick sections were cut from the free wall of the left ventricle. Dehydrated blocks were embedded in Durcupan resin. From the embedded blocks, semithin sections of 500 nm and ultrathin sections of 50 nm were cut with a Leica ultramicrotome and mounted either on mesh or on Collodion-coated (Parlodion, Electron Microscopy Sciences, Fort Washington, PA) single-slot, copper grids. Additional contrast was provided to these sections with uranyl acetate and lead citrate solutions, and the preparations were examined with a JEOL 1200EX-II electron microscope. 4 animals from each group, 3–5 blocks from each animal were used. The area of the interfibrillar mitochondria (IFM) was measured by freehand polygon selection (n~500/group) using the ImageJ software.

### 2.7. Western-Blot Analysis

*2.7.1. Total Western Blot Sample Preparation from Cardiac Tissue.* 50 milligrams of heart samples were homogenized in ice-cold Tris buffer (50 mmol/l, pH 8.0) containing protease inhibitor (1 : 100; Sigma-Aldrich Co., #P8340) and phosphatase inhibitor (1 : 100; Sigma-Aldrich Co., #P5726) and 50 mM sodium vanadate. The supernatants were harvested in 2x concentrated sodium dodecyl sulfate- (SDS-) polyacrylamide gel electrophoresis sample buffer.

*2.7.2. Fractionated Western Blot Sample Preparation from Cardiac Tissue.* 100 milligrams of heart tissues were minced in ice-cold isolation solution (150 mM NaCl, 50 mM TRIS, and 1 mM EDTA), protease inhibitor (1 : 100; Sigma-Aldrich Co., #P8340), and phosphatase inhibitor (1 : 100; Sigma-Aldrich Co., #P5726)). Samples were disrupted on ice with gently Turrax and, then, processed in a Potter-Elvehjem tissue homogenizer. Samples were centrifuged for 12 minutes at 750 g. Supernatants containing the cytosolic and mitochondrial fractions were aspirated and the precipitated nuclear fractions were harvested in 2x SDS–polyacrylamide gel electrophoresis sample buffer and denatured at 95°C for 5 minutes. Supernatants were then centrifuged for 12 minutes at 11.000 g to gain cytosolic fraction in the supernatant and mitochondrial fraction in the precipitate. Samples were harvested separately in 2x SDS–polyacrylamide gel electrophoresis sample buffer and denatured at 95°C for 5 minutes.

*2.7.3. Total Western-Blot Sample Preparation from NRCM Cell Culture.* After the appropriate treatment, cells were harvested. The cell pellet was suspended in ice-cold PBS buffer and, then, centrifuged for 5 min at 1,200 rpm at room temperature. The pellets were suspended in 300 $\mu$L NP-40 lysis buffer (Amresco, J619) containing protease inhibitor (1 : 100; Sigma-Aldrich Co., #P8340) and phosphatase inhibitor (1 : 100; Sigma-Aldrich Co., #P5726). The samples were shaken for 30 min at 4°C; then, they were centrifuged for 20 min (4°C 12,000 rpm). 4x concentrated SDS-polyacrylamide gel electrophoresis sample buffer was added to each sample.

*2.7.4. Fractionated Western Blot Sample Preparation from NRCM Cell Culture.* The cell pellet was suspended in an ice-cold isolation solution (0.5 mM TRIS, 1 M EGTA, and 0.4 M sucrose) containing 0.5 mM sodium metavanadate, 0.05 M EDTA, and protease inhibitor (1 : 100; Sigma-Aldrich Co., #P8340). Samples were disrupted on ice by Turrax and, then, processed by a Potter-Elvehjem tissue homogenizer. Centrifugation was carried out for 15 minutes at 750 g. The nuclear fraction in the precipitate was harvested in 72% trichloroacetic acid. Subsequently, supernatants were aspirated and centrifuged for 15 minutes at 10.000 g to gain cytosolic fraction in the supernatant and mitochondrial in the precipitate. Samples were harvested separately in 72% trichloroacetic acid. The precipitated fractions were centrifuged for 10 minutes at 15.000 g. Each precipitate was harvested separately in a 50 mM TRIS and SDS-polyacrylamide gel electrophoresis sample buffer. The samples were shaken for overnight at 4°C and denatured at 95°C for 5 minutes. After that, they were centrifuged for 10 minutes at 15.000 g, and the supernatants were collected as the mitochondrial fraction.

*2.7.5. Electrophoresis and Transfer of Proteins.* After the preparation, the tissue and cell culture samples were processed in the same manner. Protein levels were measured with

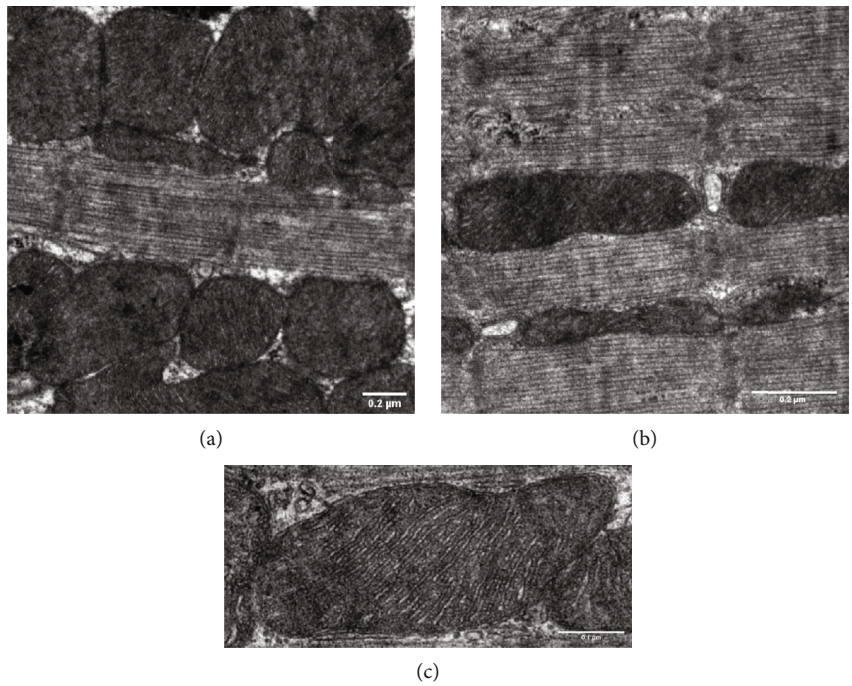


Figure 2: Ultrastructural analysis of interfibrillar mitochondria in the myocardium of WKY animals. Representative electron micrographs of interfibrillar mitochondria in the myocardium of (a, b) WKY animals ((a) magnification: 15 k, scale bar: 0.2 $\mu$m; (b) magnification: 20 k, scale bar: 0.2 $\mu$m). Ultrastructure of interfibrillar mitochondria in the myocardium of (c) WKY animals (magnification: 40 k, scale bar: 0.1 $\mu$m ($n = 4$ from each group, 3–5 blocks from each animal). WKY: age-matched normotensive Wistar-Kyoto rats.

Nanodrop. Glyceraldehyde 3-phosphate dehydrogenase (GAPDH; 1 : 1000; Cell Signaling #2118) and pyruvate dehydrogenase (PDC; 1 : 1000; Cell Signaling #3205) were used as a representative loading control. Proteins were separated on 12% SDS-polyacrylamide gel and transferred to nitrocellulose membranes. After blocking (2 h with 5% BSA in Tris-buffered saline contained with 1% Tween-20), membranes were probed overnight at 4°C with primary antibodies recognizing the following antigens: optic atrophy 1 (OPA1; 1 : 1000; Cell Signaling #80471), mitofusin-1 (MFN1; 1 : 1000; Abcam ab57602), mitofusin-2 (MFN2; 1 : 1000; Cell Signaling #9482), dynamin-related protein 1 (DRP1; 1 : 1000; Cell Signaling #8570), phosphor-specific DRP1 Ser637 (1 : 500; Cell Signaling #4867), phosphor-specific DRP1 Ser616 (1 : 500; Cell Signaling #3455), voltage-dependent anion channel (VDAC; 1 : 1000; Cell Signaling #4661), mitochondrial fission 1 protein (FIS1; 2 $\mu$g/mL, Abcam, ab71498), peroxisome proliferator-activated receptor gamma coactivator 1-alpha (PGC-1$\alpha$; 1 : 1000; Novus Biologicals, NBP1-04676), cAMP response element-binding protein (CREB; 1 : 1000; Cell Signaling #4820), phosphor-specific cAMP response element-binding protein Ser133 (1 : 1000; Cell Signaling #9198), anti-NADH dehydrogenase Fe-S protein 1 (NDUFs1, Novus Biologicals, NBP1-31142, 1 : 1000), and anti-Ubiquinol-cytochrome c reductase core protein I (UQCRC1, Novus Biologicals, NBP2-03825, 1 : 1000). Membranes were washed six times for 5 min in Tris-buffered saline (pH 7.5) containing 0.2% Tween (TBST) before the addition of horseradish peroxidase-conjugated secondary antibody (goat anti-rabbit IgG, Sigma Aldrich Co. A0545, 1 : 3000 dilution; rabbit anti-mouse IgG, Sigma Aldrich Co., A9044, 1 : 5000 dilution). Membranes were washed six times for 5 min in TBST, and then, the antibody-antigen complexes were visualized by enhanced chemiluminescence. The results of Western blots were quantified using the NIH ImageJ program.

*2.8. Capillary Electrophoresis Immunoassay.* Due to the limited availability of primary neonatal cardiomyocytes and the lower protein concentration of the fractionated samples made from it, the more sensitive capillary immunoassay method with less sample requirements and higher throughput is more suitable for measurement. Simple western analysis (Wes) was performed on a Wes system (ProteinSimple, product number 004–600) according to the manufacturer's instructions using a 12-230 kDa Separation Module (ProteinSimple SM-W004) and either the Anti-Rabbit Detection Module (ProteinSimple DM-001) or the Anti-Mouse Detection Module (ProteinSimple DM-002), depending on the primary used antibody. Subcellular NRCM samples were mixed with Fluorescent Master Mix and heated at 95°C for 5 min. The samples, blocking reagent (antibody diluent), primary antibodies (in antibody diluent), HRP-conjugated secondary antibodies, and chemiluminescent substrate, were pipetted into the plate (part of Separation Module). Instrument default settings were used: stacking and separation at 475 V for 30 min; blocking reagent for 5 min, primary and secondary antibody both for 30 min; Luminol/peroxide chemiluminescence detection for ~15 min (exposures of 1-2-4-8-16-32-64-128-512 s). The resulting electropherograms were inspected to check whether automatic peak detection required any manual correction.

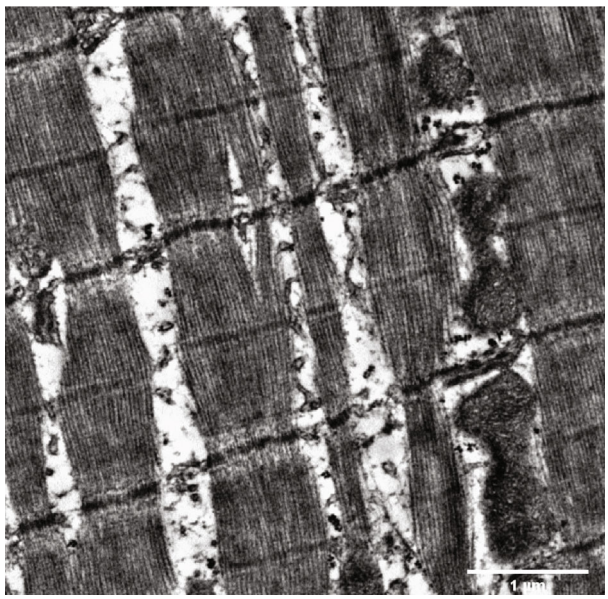


(a)

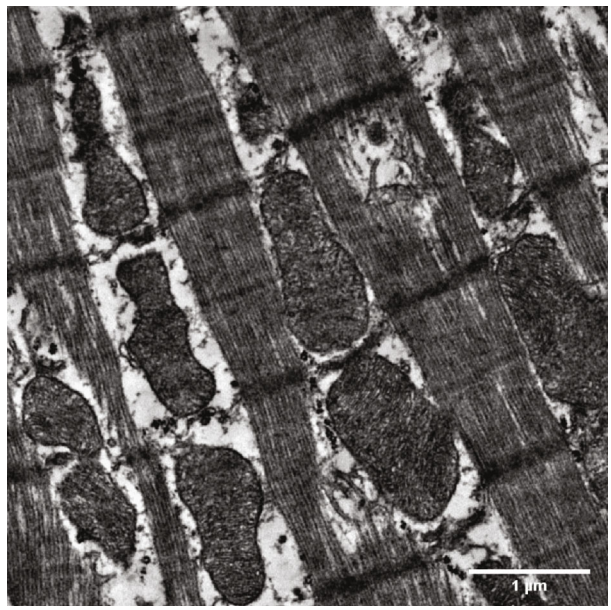


(b)

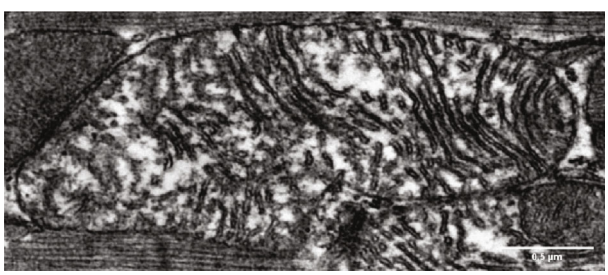

(c)

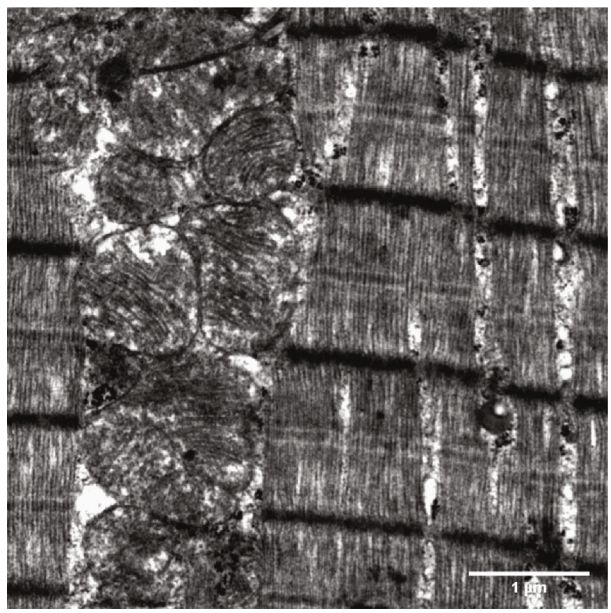


(d)

Figure 3: Continued.

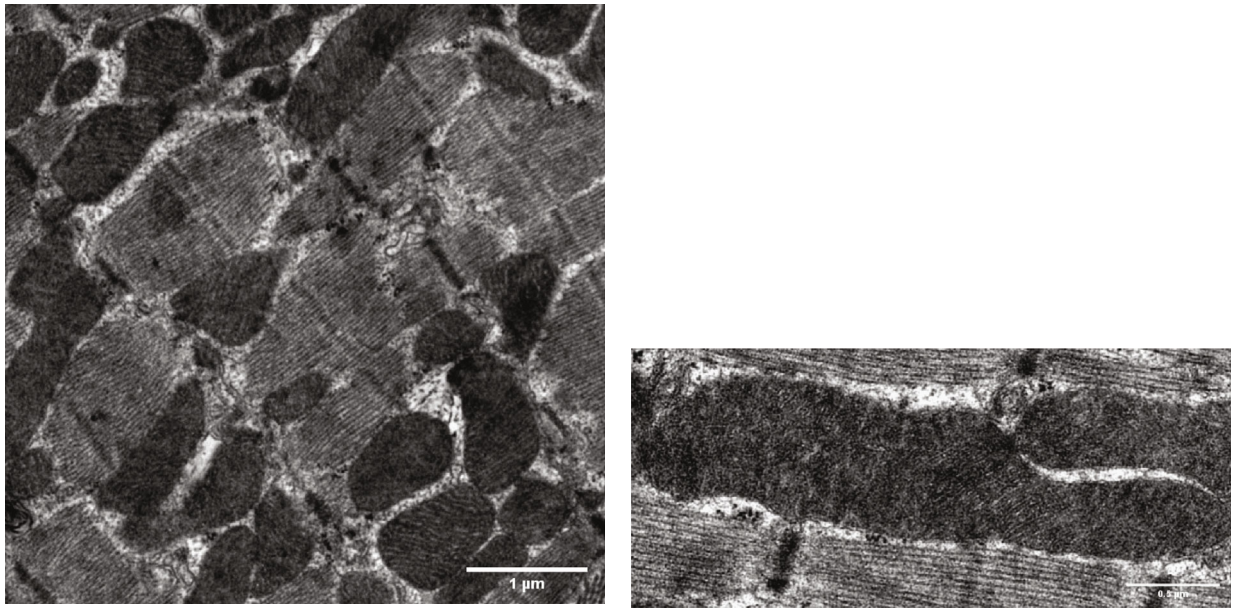


(e) (f)

Figure 3: Ultrastructural analysis of interfibrillar mitochondria in the myocardium of SHR animals. Representative electron micrographs of interfibrillar mitochondria in the myocardium of (a, b) SHR-C and (d, e) SHR-B animals (magnification: 10 k, scale bar: 1 $\mu$m). Ultrastructure of interfibrillar mitochondria in the myocardium of (c) SHR-C and (f) SHR-B animals (magnification: 25 k, scale bar: 0.5 $\mu$m). SHR-C: nontreated spontaneously hypertensive rats; SHR-B: spontaneously hypertensive rats receiving BGP-15 for 18 weeks ($n = 4$ from each group, 3–5 blocks from each animal).

*2.9. Evaluation of Mitochondrial Fragmentation with Fluorescent Microscopy.* NRCM cells were seeded at a density of $10^5$ cells/well in 6 well plates on glass coverslips with 1% gelatin coating and cultured at least for 2 days before the experiment. On the day of the experiment, cells were washed once in PBS and added fresh medium and, then, treated with $H_2O_2$ with or without BGP-15. After the appropriate treatment, coverslips were rinsed in PBS and were added 75 nM MitoTracker Red CMXRos dissolved in serum-free DMEM and incubated for 30 min at 37°C. After the incubation, coverslips were rinsed in PBS, and the mitochondrial network was visualized by a Nikon Eclipse Ti-U fluorescent microscope equipped with a Spot RT3 camera using a 60x objective and epifluorescent illumination.

*2.10. Quantification of Mitochondrial DNA (mtDNA) Damage by Real-Time PCR.* After the appropriate treatment, cells were harvested, and total DNA was isolated using GenElute™ Mammalian Genomic DNA Miniprep Kits (Sigma-Aldrich # G1N350-1KT). Real-time DNA amplification was performed using a CFX96 Touch Real-Time PCR Detection System (Bio-Rad) as we performed earlier [25]. The following rat primer sequences were used: SRPCR (210 bp) forward: 5′-ATGCACGATAGCTAAGACCCAA-3′; reverse: 5′-CTGAATTAGCGAGAAGGGGTA-3′ and LRPCR (14958 bp) forward: 5′-ATTTTCTCCCAGTTACGAAAG-3′, reverse: 5′-CTTGGTAAGTAAATTTCTTTCTCC-3′. Short fragment, cytochrome c oxidase subunit 1 (COX1), cytochrome c oxidase subunit 3 (COX3), and $\beta$-actin were done using a Brilliant II QPCR Master Mix (Agilent Technologies, # 600804). The final SRPCR, COXI, COXIII, and $\beta$-actin cycling parameters followed hot start of 10 min at 95°C, followed by 30 sec at 95°C, 1 min at 60°C, and 30 sec at 72°C for 40 cycles. LRPCR was done using PfuUltra II Hotstart 2x Master Mix (Agilent Technologies, #600852). The final LRPCR cycling parameters followed manufacturer's recommendations: hot start of 2 min at 92°C, followed by 15 sec at 92°C, 30 sec at 50°C, and 8 : 00 min at 68°C for 40 cycles. The relative mitochondrial DNA content was determined by real-time PCR, using COX1 and COX3 primers, normalized to a nuclear-encoded $\beta$-actin gene. The following rat primer sequences were used: COX1 (199 bp) forward: 5′-CACAGTAGGGGGCCTAACAG-3′, reverse: 5′-CAAAGTGGGCTTTTGCTCAT-3′; COX3 (244 bp) forward 5′-TCAGGAGTCTCAATTACATG-3′, reverse: 5′-CGTAGTAGACAGACAATTAGG-3′; $\beta$-actin (191 bp) forward 5′-GCGGTGACCATAGCCCTCTTT-3′, reverse: 5′-TGCCACTCCCAAAGTAAAGGGTCA-3′. The software automatically generated crossing points and calculation of mtDNA damage was made using the $\Delta 2^{Ct}$ method. EvaGreen dye was used (Biotium # 31000).

*2.11. Mitochondrial Membrane Potential Measurement with JC-1 Assay.* The mitochondrial membrane potential ($\Delta\Psi$m) was measured using the mitochondrial membrane potential specific fluorescent probe, JC-1 (Enzo Life Sciences, ENZ-52304) as we performed it earlier [25]. NRCM cells were seeded on glass coverslips coated with gelatin and cultured for at least 2 days before the experiment. After the treatment, cells were washed in PBS and incubated for 15 min at 37°C in

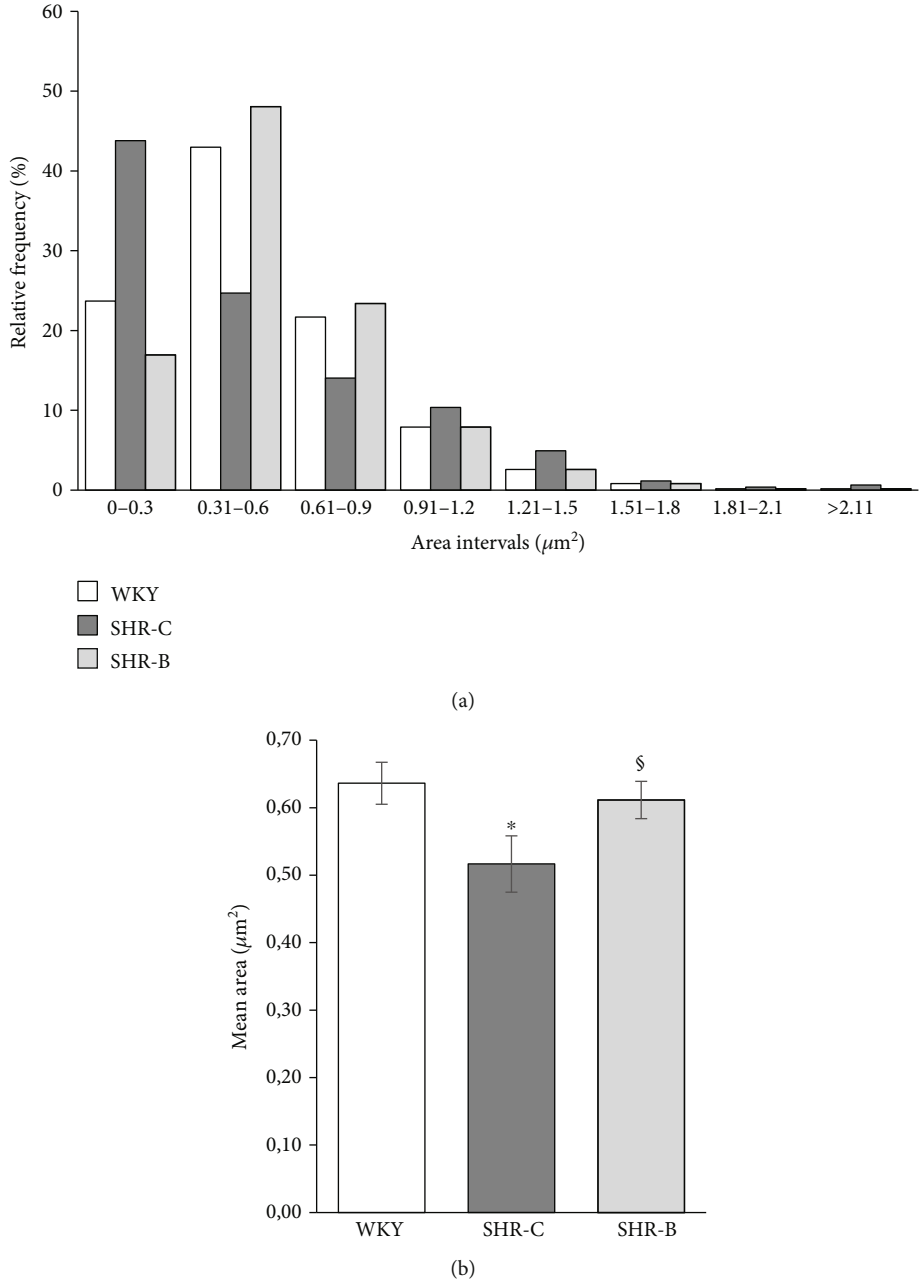


Figure 4: Heart failure-induced fragmentation of interfibrillar mitochondria in the myocardium. (a) Relative frequencies of measured mitochondrial areas in each arbitrary area interval. (b) Means of area values in given groups (~500 mitochondria/group). WKY: age-matched normotensive Wistar-Kyoto rats; SHR-C: nontreated spontaneously hypertensive rats; SHR-B: spontaneously hypertensive rats receiving BGP-15 for 18 weeks. Data are expressed as mean ± SEM. $^*p < 0.05$ vs. WKY, $^§p < 0.05$ vs. SHR-C.

media containing 5 $\mu$g/mL JC-1. When excited at 488 nm, the dye emits red fluorescence (590 nm) at high $\Delta\Psi$m and green (530 nm) at low $\Delta\Psi$m. Following incubation, the cells were washed once with PBS and then imaged with a Nikon Eclipse Ti-U fluorescent microscope equipped with a Spot RT3 camera using a 60x objective and epifluorescent illumination. All experiments were repeated three times. Fluorescent signals were quantified by using the ImageJ software (NIH, Bethesda, MD, USA).

*2.12. Evaluation of the Mitochondrial Energy Metabolism and Function.* As we described earlier, Agilent Seahorse Extracellular Flux (XFp) Analyzer (Agilent Technologies, (Santa Clara, CA, USA)) was used to determine the NRCM cells' oxygen consumption rate (OCR) [25]. NRCM cells were seeded in XFp Miniplate at a density of $4 \times 10^4$ cells/well in 80 $\mu$L complete growth medium (DMEM for Primary Cell Isolation containing 10% FBS, 100 IU/mL penicillin and 100 $\mu$g/mL streptomycin) and incubated at 37°C, 5% $CO_2$

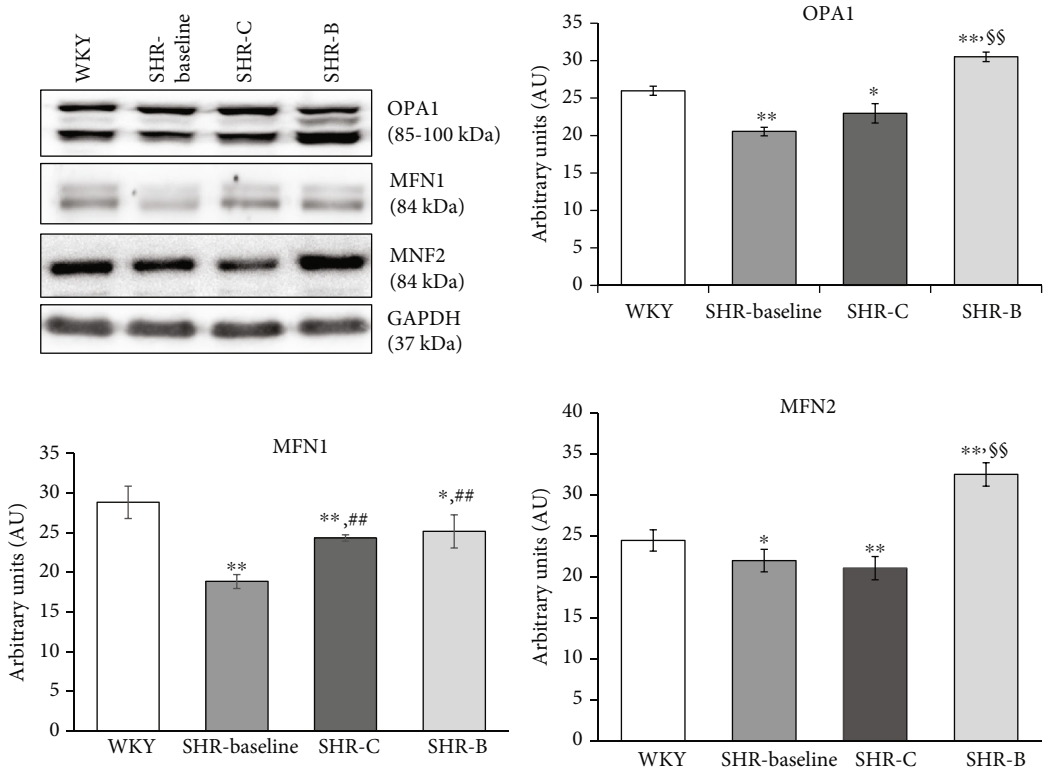


Figure 5: Effect of BGP-15 treatment on mitochondrial fusion proteins in a hypertension-induced heart failure model. Western blot analysis of OPA1, MFN1, and MFN2 proteins as well as densitometric evaluations is shown. GAPDH was used as a loading control. WKY: age-matched normotensive Wistar-Kyoto rats; SHR-Baseline: 15-month-old spontaneously hypertensive rats; SHR-C: 19-month-old nontreated spontaneously hypertensive rats; SHR-B: 19-month-old spontaneously hypertensive rats receiving BGP-15 for 18 weeks ($n = 4$). Values are mean ± SEM. $^{*}p < 0.05$ vs. WKY, $^{**}p < 0.01$ vs. WKY, $^{\#\#}p < 0.01$ vs. SHR-Baseline, $^{\S\S}p < 0.01$ vs SHR-C.

for 2 days. On the day before the experiment, sensor cartridges were hydrated in XFp calibrant and maintained at 37°C without $CO_2$ overnight. On the day of the assay, after subjecting cells to the appropriate treatment, DMEM for Primary Cell Isolation medium was replaced by Agilent Seahorse XF Base Medium containing 1 mM pyruvate, 2 mM glutamine, and 10 mM glucose (adjusted pH to 7.4 with 0.1 N NaOH). Before measurement, different compounds were loaded into the appropriate ports of a hydrated sensor cartridge (10 $\mu$M oligomycin, 10 $\mu$M FCCP, and 5 $\mu$M rotenone/antimycin). Three measurements were performed after each injection. OCR was used to determine mitochondrial energy metabolism. The parameter values, including basal respiration, maximal respiration, ATP-associated OCR, and spare respiratory capacity, were determined according to the Seahorse XFp Cell Mito Stress user guide protocol. Data were analyzed using the Seahorse XF test report analysis.

*2.13. Analysis of Citrate Synthase Activity in NRCM Cells.* NRCM cells were seeded at a density of $10^6$ cells/well in 6-well plates and cultured. After the appropriate treatment, cells were harvested; the cell pellet was suspended in ice-cold citrate synthase cell lysis buffer and, then, centrifuged for 5 min at 4°C at 10,000 x g; then, the supernatant was collected for further use. Citrate synthase was measured using a kit from Sigma Aldrich (MAK193) following the manufacturer's instruction. The absorbance was recorded at 412 nm every 5 minutes for 50 minutes. The colorimetric product (GSH) was proportional to the enzymatic activity of citrate synthase and normalized to the quantity of cells.

*2.14. Statistical Analysis.* Statistical analysis was performed by analysis of variance, and all of the data were expressed as the mean ± SEM. The homogeneity of the groups was tested by F-test (Levene's test). There were no significant differences among the groups. Comparisons among groups were made by one-way ANOVA with a post hoc correction (SPSS for Windows, version 21.0). The Student's $t$-test was used to compare the mean values of two groups. A value of $p < 0.05$ was considered statistically significant.

## 3. Results

### 3.1. In Vivo Results

*3.1.1. Effect of BGP-15 Administration on Gravimetric Parameters and on BNP Level.* At the beginning of the study, the body weight of WKY rats was significantly higher than the SHR rats (WKY: 391.51 ± 8.64 g, SHR-C: 340.66 ± 6.74 g, SHR-B: 347.4 ± 10.38 g; $p < 0.05$, WKY vs. SHR groups; Table 1). Similar observation can be made at the end of the study (WKY: 403.22 ± 10.35 g, SHR-C: 352.13 ± 6.86 g, SHR-B: 365.29 ± 6.82 g; $p < 0.05$ WKY vs. SHR groups). At the end of the study, heart weights (HW) and ventricles

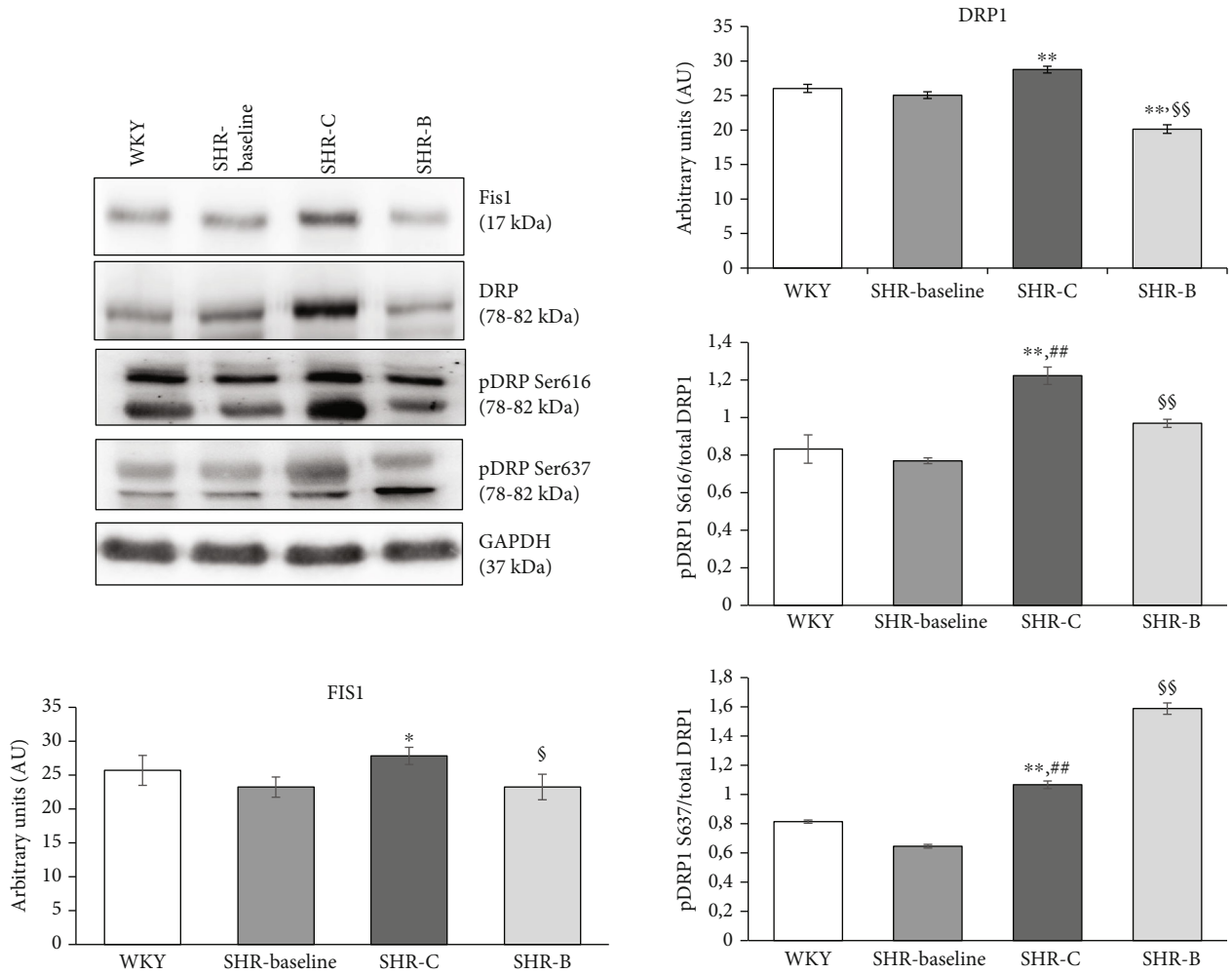


Figure 6: Effect of BGP-15 treatment on mitochondrial fission proteins in a hypertension induced-heart failure model. Western blot analysis of Fis1 and DRP1 proteins, as well as densitometric evaluation, is shown. GAPDH was used as a loading control. WKY: age-matched normotensive Wistar-Kyoto rats; SHR-Baseline: 15-month-old spontaneously hypertensive rats; SHR-C: 19-month-old nontreated spontaneously hypertensive rats; SHR-B: 19-month-old spontaneously hypertensive rats receiving BGP-15 for 18 weeks ($n = 4$). Values are mean ± SEM. $^{*}p < 0.05$ vs. WKY, $^{**}p < 0.01$ vs. WKY, $^{\#\#}p < 0.01$ vs. SHR-Baseline, $^{\S}p < 0.05$ vs. SHR-C, $^{\S\S}p < 0.01$ vs. SHR-C.

weight (VW) were significantly increased in the SHR groups compared to the WKY group (HW: WKY: 1.11 ± 0.03 g, SHR-C: 1.41 ± 0.03 g, SHR-B: 1.28 ± 0.02 g; $p < 0.01$ SHR-B and SHR-C vs.WKY, $p < 0.05$ SHR-B vs. SHR-C; VW: WKY: 0.98 ± 0.03 g, SHR-C: 1.27 ± 0.02 g, SHR-B: 1.12 ± 0.02 g; $p < 0.05$ SHR-groups vs. WKY). The ratio of ventricular weight to body weight (VW/BW) was increased markedly in SHR groups compared to WKY animals (VW/BW (mg/g): WKY: 2.43 ± 0.07, SHR-C: 3.60 ± 0.04, SHR-B: 3.07 ± 0.09; $p < 0.01$ SHR groups vs. WKY, $p < 0.05$ SHR-B vs. SHR-C). Ventricular weight to the length of right tibia ratio (VW/TL) was also significantly increased (VW/TL (mg/mm): WKY: 21.43 ± 0.71, SHR-C: 29.14 ± 0.14, SHR-B: 24.81 ± 0.53; $p < 0.05$ SHR-groups vs. WKY). BGP-15 treatment caused a significant moderation of these ratios ($p < 0.05$ SHR-B vs. SHR-C).

By the end of the treatment, the plasma BNP level increased significantly in the SHR-C group compared to the WKY group (BNP (pg/ml): WKY: 302.76 ± 13.7684; SHR-C: 755.14 ± 33.34; SHR-B: 352.04 ± 22.50; $p < 0.05$ vs. WKY group; Table 1). However, BGP-15 treatment caused a marked reduction of the BNP level in hypertensive animals ($p < 0.05$, SHR-B vs. SHR-C).

*3.1.2. Effect of BGP-15 Administration on Mitochondrial Ultrastructure.* Longitudinal sections of the myocardium were evaluated to assess the status of interfibrillar mitochondria (IFM) by electron microscopy. The mitochondria of SHR-C rats differ from the normal mitochondria of WKY rats (Figures 2(a)–2(c)), because they are morphologically more heterogeneous ($n = 5$ from each group, 3–5 block from each animal). In the nontreated hypertensive animals (SHR-C), mitochondria were loosely arranged between the contractile elements (Figures 3(a) and 3(b)). Moreover, in the SHR-C group, extensive disruption of mitochondrial cristae and enlarged intracristal spaces could be observed (Figure 3(c)). Their shape was often elongated, and the mitochondrial matrix was very light. The mitochondrial ultrastructure in the SHR-B group was

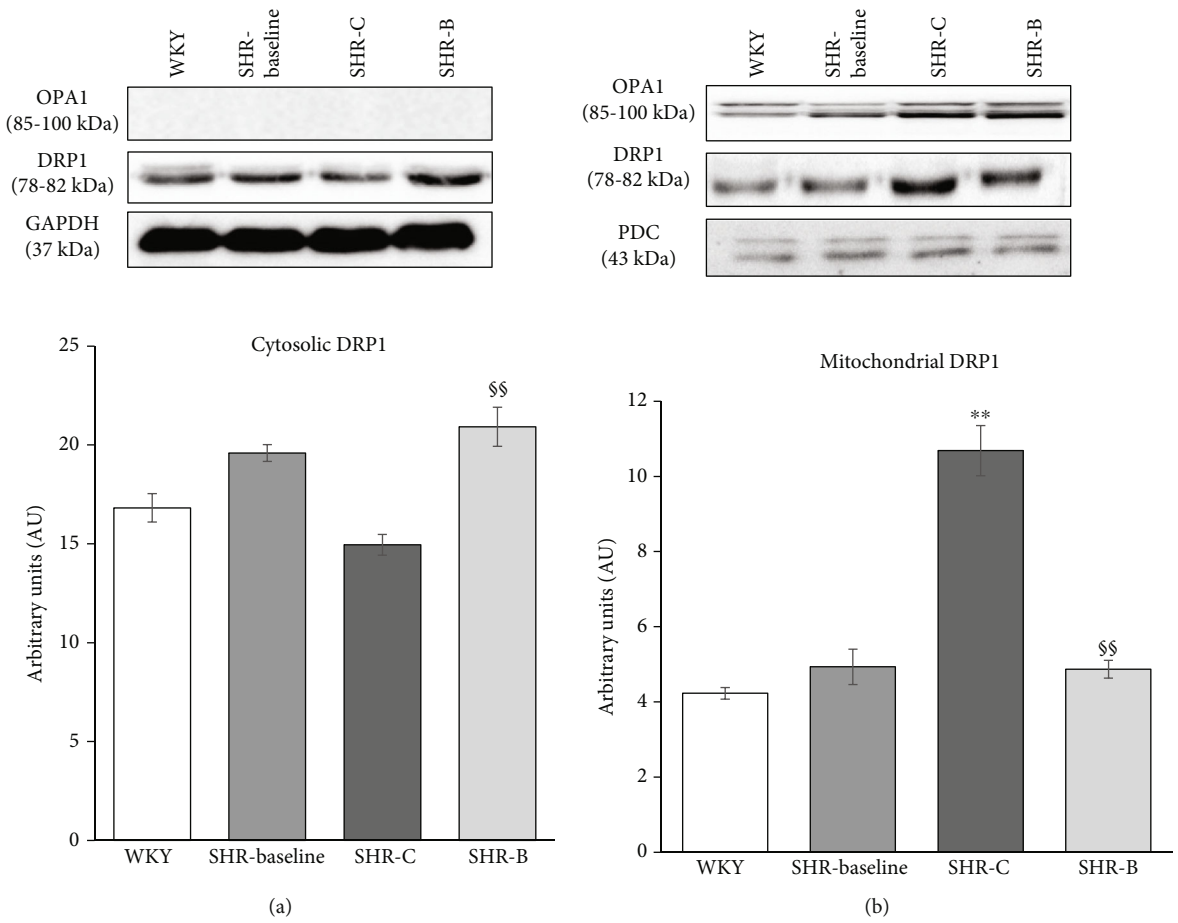


Figure 7: Effect of BGP-15 treatment on DRP1 protein intracellular distribution in a hypertension-induced heart failure model. Western blot analysis regarding the intracellular distribution of DRP1 protein and densitometric evaluation are also shown. GAPDH and PDC were used as a loading control. WKY: age-matched normotensive Wistar-Kyoto rats; SHR-Baseline: 15-month-old spontaneously hypertensive rats; SHR-C: 19-month-old nontreated spontaneously hypertensive rats; SHR-B: 19-month-old spontaneously hypertensive rats receiving BGP-15 for 18 weeks ($n = 4$). Values are mean ± SEM. $^{**}p < 0.01$ vs. WKY, $^{§§}p < 0.01$ vs SHR-C.

similar to that of WKY rats (Figures 3(d) and 3(e)). In treated SHR animals (SHR-B), normal, large, and less elongated mitochondria with tightly packed cristae and electron-dense matrix were seen (Figure 3(f)). The area of IFM was assessed on electron micrographs (~500 mitochondria/group were measured; Figure 4(b)). We assessed relative frequencies of the measured mitochondrial areas in arbitrary intervals of $0.3\,\mu m^2$ (Figure 4(a)). In all the groups, less than 1% of mitochondrial areas were above the $1.81\,\mu m^2$ value. In the SHR-C group, 43.7% of the measured mitochondria belonged to the lowest area range ($<0.3\,\mu m^2$). However, in the WKY group, the predominant area range of the measured mitochondria was between 0.3 and $0.6\,\mu m^2$. Due to BGP-15 treatment (SHR-B), the distribution of mitochondria was similar to that of the WKY group and the highest number of mitochondria (48%) belonged to the 0.3-0.6 $\mu m^2$ range ($p < 0.05$, SHR-B vs. SHR-C). Our results showed a profound decrease in the mean mitochondrial area of SHR-C group compared to the mitochondria of WKY animals ($p < 0.05$, SHR-C, vs. WKY). The values of BGP-15-treated SHRs differed from that of the SHR-C group ($p < 0.05$), and it was similar to the mitochondria of normotensive animals (WKY).

*3.1.3. Effect of BGP-15 Treatment on Mitochondrial Fusion Proteins in SHR Animals.* Regarding the mitochondrial fusion proteins, we determined the levels of OPA1, MFN1, and MFN2 in the myocardium using Western blot analysis (Figure 5). We observed that the level of OPA1 was moderately decreased in the SHR-C group compared to the WKY group ($p < 0.05$, SHR-C vs. WKY). However, BGP-15 treatment caused a significant elevation of OPA1 level in the SHR-B group ($p < 0.01$ SHR-B vs. WKY, $p < 0.05$ SHR-B vs. SHR-C). Considering the amount of MFN1 protein level, there was a significant increase in hypertensive animals by the end of the study compared to the baseline levels ($p < 0.05$, SHR-C and SHR-B vs. SHR-Baseline); however, there was no difference between the SHR groups. The level of MFN2 protein was moderately lower in the SHR-C group than in the WKY group ($p < 0.05$), as observed in the case of OPA1. In the SHR-B group, this parameter increased significantly due to the treatment compared to the other groups ($p < 0.01$ SHR-B vs WKY, SHR-C).

*3.1.4. Effect of BGP-15 Administration on Mitochondrial Fission Proteins in SHR Animals.* The levels of fission

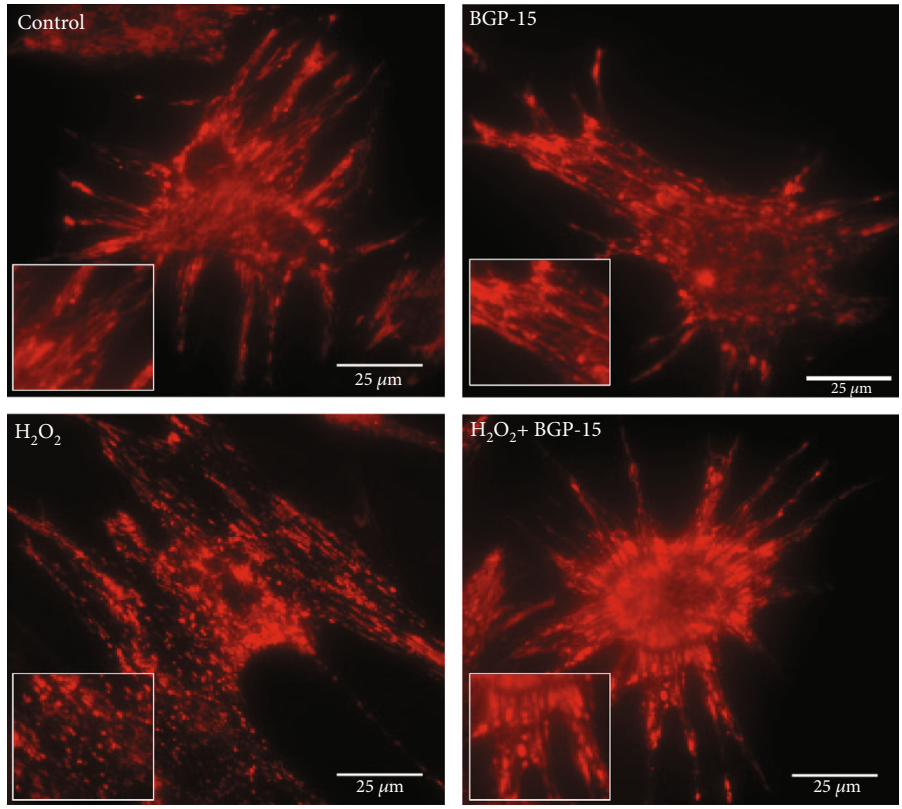


Figure 8: Effect of BGP-15 administration on the morphology of mitochondrial network in NRCM cells. For methodical details, see chapter "Materials and Methods." BGP-15 treatment prevented the mitochondrial network from the oxidative stress-induced fragmentation and preserved mitochondria predominantly in the normal filamentous state. The inserts show the filamentous and fragmented states, showing that BGP-15 protected the mitochondrial network. Control group: cells without any treatment; BGP-15 group: cells with only 50 $\mu$M BGP-15 for 0.5 hours; $H_2O_2$ group: cells with 150 $\mu$M $H_2O_2$ for 0.5 hours; $H_2O_2$+BGP-15 group: cells with 150 $\mu$M $H_2O_2$ and 50 $\mu$M BGP-15 for 0.5 hours.

proteins Fis1 and DRP1 were determined in the myocardium in total and in fractionated Western blot samples (Figure 6). The level of Fis1 increased in the SHR-C group compared to the WKY group ($p < 0.05$, SHR-C vs. WKY). This elevation was, however, diminished significantly due to BGP-15 treatment ($p < 0.05$ SHR-B vs. SHR-C). In the case of the fission protein DRP1, the total level was significantly decreased due to BGP-15 treatment compared to other groups ($p < 0.01$ SHR-B vs. WKY, SHR-C). The phosphorylation level of DRP1 at the Ser616 and Ser637 residues was also measured. The phosphorylation of $DRP1^{Ser616}$ and $DRP1^{Ser637}$ was moderate in the WKY group. In the SHR-C group, however, phosphorylation of $DRP1^{Ser616}$ was increased significantly ($p < 0.01$ vs. WKY and SHR-Baseline). BGP-15 treatment decreased $DRP1^{Ser616}$ phosphorylation in SHR-B animals ($p < 0.01$ vs. SHR-C group). Regarding the phosphorylation level of $DRP1^{Ser637}$, we observed a significant increase in the SHR-C group ($p < 0.01$ vs. WKY, SHR-Baseline). Moreover, BGP-15 treatment caused a further increase in the $DRP1^{Ser637}$ phosphorylation in SHR-B animals ($p < 0.01$ SHR-B vs. SHR-C).

The intracellular distribution of DRP1 was also measured (Figure 7). We observed that the Drp1 accumulated in the mitochondrial fractions of SHR-C animals compared to normotensive animals ($p < 0.01$, SHR-C vs. WKY). BGP-15 treatment resulted in a significantly reduced translocation of Drp1 into the mitochondria ($p < 0.01$ vs. SHR-C), thereby preserving it in a higher concentration in the cytosolic fraction.

### 3.2. In Vitro Results

*3.2.1. Effect of BGP-15 Administration on Mitochondrial Morphology of NRCM Cells.* To examine the changes of the mitochondrial network, we used the MitoTracker Red CMXRos staining method (Figure 8). BGP-15 per se had no effect on the complexity of the mitochondrial network. Filamentous mitochondrial network was observed in the Control group; $H_2O_2$ treatment, however, caused a marked injury to the mitochondrial network. As a result of the $H_2O_2$-induced fission processes, degradation of the mitochondrial network could be observed which led to mitochondrial fragmentation. BGP-15 treatment prevented the mitochondrial network from the oxidative stress-induced fragmentation and preserved the normal filamentous network of mitochondria.

*3.2.2. Effect of BGP-15 Treatment on Mitochondrial Fusion Proteins in NRCMs.* We assessed the levels of OPA1, MFN1 and MFN2 proteins in total Western blot samples of NRCM cells (Figure 9). BGP-15 treatment per se had no effect in the

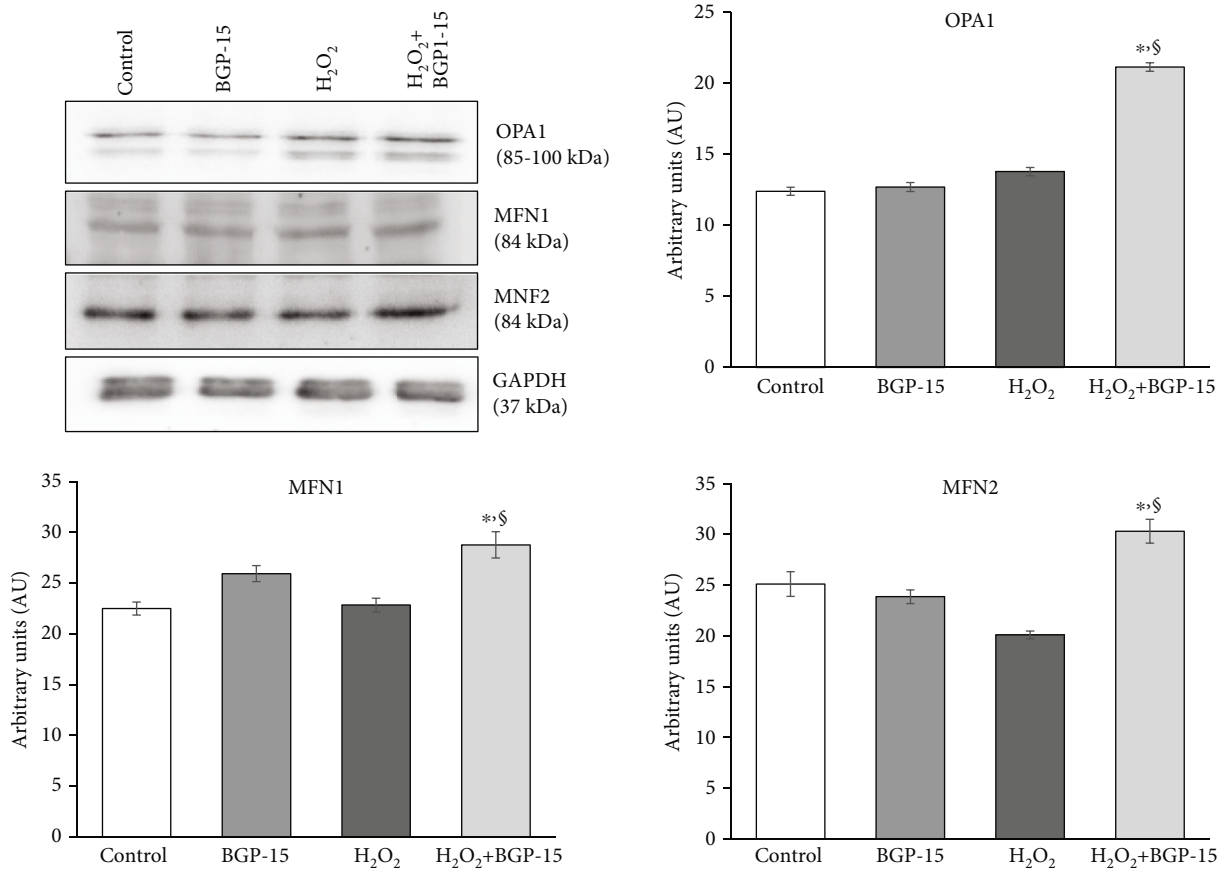


Figure 9: Effect of BGP-15 treatment on mitochondrial fusion proteins in NRCM cells. Western blot analysis of OPA1, MFN1, and MFN2 as well as densitometric evaluation is shown. GAPDH was used as a loading control. Control group: cells without any treatment; BGP-15 group: cells with only 50 $\mu$M BGP-15 for 0.5 hours; $H_2O_2$ group: cells with 150 $\mu$M $H_2O_2$ for 0.5 hours; $H_2O_2$+BGP-15 group: cells with 150 $\mu$M $H_2O_2$ and 50 $\mu$M BGP-15 for 0.5 hours. Values are mean ± SEM ($n = 4$). $^*p < 0.05$ vs. Control, $^§p < 0.05$ vs. $H_2O_2$ group.

nonstressed cells in comparison to the Control group. $H_2O_2$ treatment caused a slight decrease in the level of MFN1 and MFN2 proteins and a slight increase in the level of OPA1, but these changes were not significant. BGP-15 treatment caused a significant increase of OPA1, MFN1, and MFN2 proteins in $H_2O_2$ stressed cells compared to the $H_2O_2$-stressed group ($p < 0.05$ $H_2O_2$-BGP15 vs. $H_2O_2$).

*3.2.3. Effect of BGP-15 Administration on Mitochondrial Fission Proteins in NRCMs.* We determined the levels of Fis1 and DRP1 in total and in fractionated Western blot samples in NRCM cells (Figure 10). No significant difference was found with BGP-15 treatment in nonstressed cells compared to the Control group. The level of Fis1 increased markedly in the $H_2O_2$ group compared to the Control group ($p < 0.01$, $H_2O_2$ vs. Control). Due to BGP-15 treatment, this change was blunted ($p < 0.05$, $H_2O_2$-BGP15 vs. $H_2O_2$ group). The case of the fission mediator DRP1 protein total level was a significant elevation in the $H_2O_2$ group due to oxidative stress ($p < 0.05H_2O_2$ vs. Control group). However, a control-like value could be seen in the treated group compared to the $H_2O_2$ group ($p < 0.05$ $H_2O_2$-BGP15 vs. $H_2O_2$ group). The phosphorylation of DRP1 on Ser616 and Ser637 residues was also evaluated. The phosphorylation of both DRP1 phospho-form was moderate in the Control group. Phosphorylation of DRP1$^{Ser616}$ increased considerably in the $H_2O_2$ group ($p < 0.05$ $H_2O_2$ vs. Control group). However, BGP-15 treatment decreased DRP1$^{Ser616}$ phosphorylation compared to nontreated stressed cells ($p < 0.05$ $H_2O_2$-BGP-15 vs. $H_2O_2$ group). Measuring the phosphorylation level of DRP1$^{Ser637}$, a significant decrease could be observed in the $H_2O_2$ group compared to the Control group ($p < 0.01$ $H_2O_2$ vs. Control group). However, BGP-15 treatment enhanced remarkably the DRP1$^{Ser637}$ phosphorylation ($p < 0.01$ $H_2O_2$-BGP15 vs. $H_2O_2$ group).

Finally, the intracellular distribution of fission mediator DRP1 protein was examined (Figure 11). A significantly higher portion of DRP1 could be found in the mitochondrial fraction of cells in the $H_2O_2$ group compared to the BGP-15-treated group. The translocation of DRP1 protein from the cytosol to the mitochondria was moderated as a result of the BGP-15 treatment and in this way resulted in higher levels of DRP1 in the cytosolic fraction and lower concentration in the mitochondrial fraction ($p < 0.01$ vs. $H_2O_2$ group).

*3.2.4. Effect of BGP-15 Treatment on the Regulatory Factors of Mitochondrial Biogenesis in NRCMs.* We determined the levels of PGC-1$\alpha$, CREB and VDAC in the total Western blot

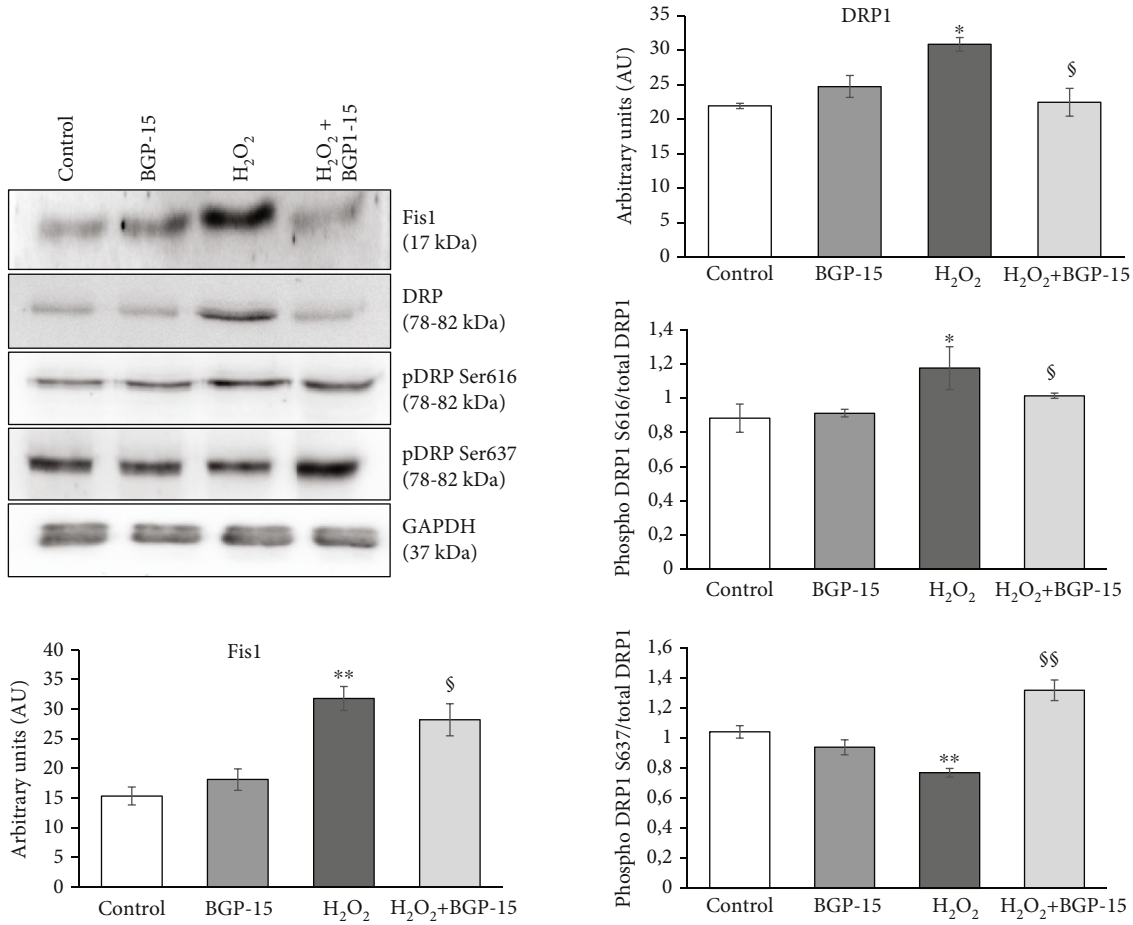


Figure 10: Effect of BGP-15 treatment on mitochondrial fission proteins in NRCM cells. Western blot analysis of Fis1 and DRP1 proteins, as well as densitometric evaluation, is shown. GAPDH was used as a loading control. Control group: cells without any treatment, BGP-15 group: cells with only 50 $\mu$M BGP-15 for 0.5 hours; $H_2O_2$ group: cells with 150 $\mu$M $H_2O_2$ for 0.5 hours; $H_2O_2$+BGP-15 group: cells with 150 $\mu$M $H_2O_2$ and 50 $\mu$M BGP-15 for 0.5 hours. Values are mean ± SEM ($n = 4$). $^{*}p < 0.05$ vs. Control, $^{**}p < 0.01$ vs. Control, $^{\S}p < 0.05$ vs. $H_2O_2$ group, $^{\S\S}p < 0.01$ vs. $H_2O_2$ group.

samples of NRCMs. BGP-15 treatment had no effect on these factors in nonstressed cells compared to the Control group. The PGC-1$\alpha$ level was increased in the $H_2O_2$ group compared to the Control group ($p < 0.01$ vs. Control; Figure 12). However, this elevation was much more marked in the treated group ($p < 0.01$ $H_2O_2$-BGP15 vs. Control and $H_2O_2$ groups). The phosphorylation level of $CREB^{Ser133}$ was low in the Control group. However, a significant increase was seen in the phosphorylation level of $CREB^{Ser133}$ in the $H_2O_2$ group ($p < 0.01$ $H_2O_2$ vs. Control) (Figure 12). BGP-15 treatment increased further the phosphorylation level of $CREB^{Ser133}$ ($p < 0.01$, $H_2O_2$-BGP15 vs. $H_2O_2$ group). The level of VDAC was slightly decreased in the $H_2O_2$ group compared to the Control group ($p < 0.05$ $H_2O_2$ vs. Control). The level of the VDAC, however, was significantly elevated in the BGP-15 treated group ($p < 0.01$ $H_2O_2$-BGP-15 vs. $H_2O_2$ group).

Moreover, we investigated mitochondrial DNA content compared to the nuclear DNA. The relative mitochondrial DNA content was determined by "real-time" PCR, using COX1 and COX3 primers, normalized to a nuclear-encoded $\beta$-actin gene. We found that BGP-15 treatment increased the relative expression levels of COXI and COXIII genes compared to the $H_2O_2$ group ($p < 0.05$ $H_2O_2$-BGP-15 vs. $H_2O_2$ group; Figure 13).

Furthermore, we also performed a well-accepted method for studying mitochondrial biogenesis by measuring the activity of citrate synthase (Figure 13). Citrate synthase activity was reduced in hydrogen-peroxide stressed group compared to the control group ($p < 0.01$ $H_2O_2$ vs. Control). The citrate synthase activity was increased significantly due to the treatment ($p < 0.01$ $H_2O_2$-BGP-15 vs. $H_2O_2$ group; Figure 13).

Finally, we measured the level of NDUFs1 subunit of NADH-ubiquinone oxidoreductase and UQCRC1 subunit of Ubiquinol Cytochrome c Reductase proteins in order to support our finding regarding the effect of BGP-15 on mitochondrial biogenesis. The expression level of NDUFs1 was significantly decreased in the H2O2 group ($p < 0.01$ $H_2O_2$ vs. Control; Figure 14). A similar observation was made in the case of UQCRC1 ($p < 0.05$ $H_2O_2$ vs. Control). However, BGP-15 treatment not only protected against the decrease but also significantly increased the amount of NDUFs1 and UQCRC1 proteins ($p < 0.01$ $H_2O_2$-BGP-15 vs. $H_2O_2$ group).

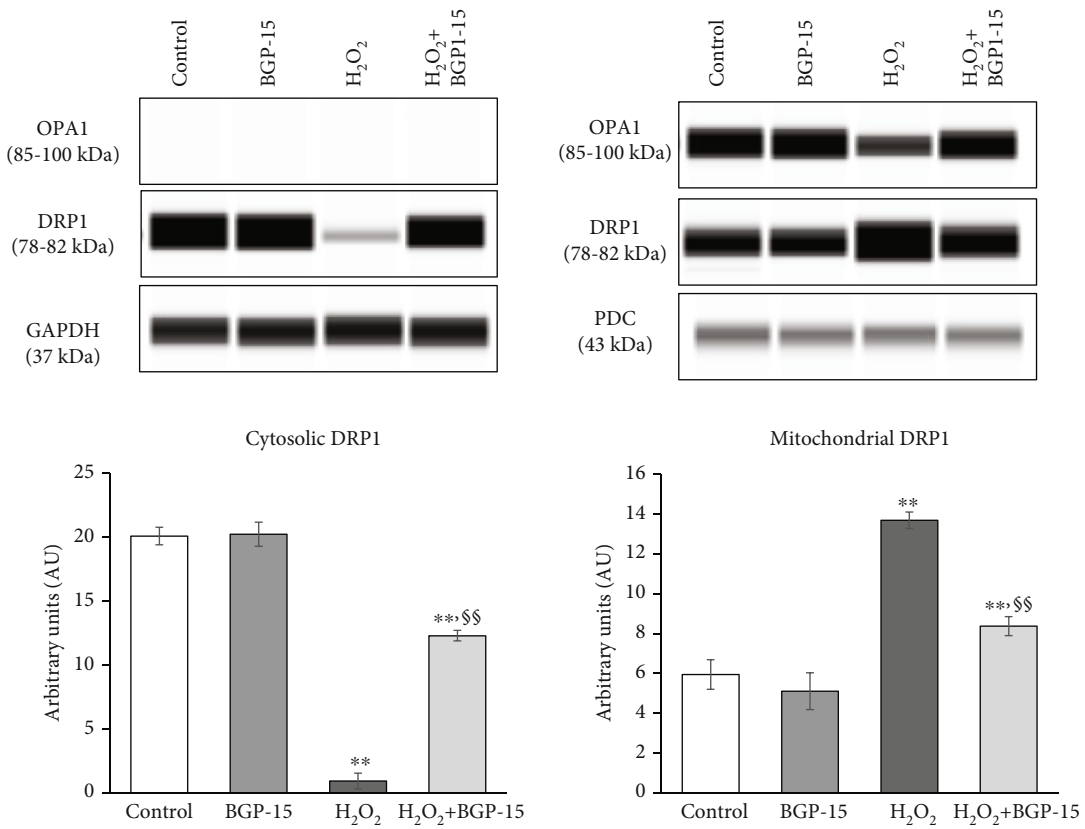


Figure 11: Effect of BGP-15 treatment on intracellular distribution of DRP1 protein in stressed NRCM cells. Western blot analysis of DRP1 protein regarding its intracellular disruption, as well as densitometric evaluation, is shown. GAPDH and PDC were used as a loading control. Control group: cells without any treatment; BGP-15 group: cells with only 50 $\mu$M BGP-15 for 0.5 hours; $H_2O_2$ group: cells with 150 $\mu$M $H_2O_2$ for 0.5 hours; $H_2O_2$+BGP-15 group: cells with 150 $\mu$M $H_2O_2$ and 50 $\mu$M BGP-15 for 0.5 hours. Values are mean ± SEM ($n = 4$). $^{**}p < 0.01$ vs. Control, $^{\S\S}p < 0.01$ vs. $H_2O_2$ group.

*3.2.5. Effect of BGP-15 Administration on Mitochondrial Genome Integrity.* Real-time detection of long-range polymerase chain reaction (LRPCR) was used to examine the impact of $H_2O_2$-induced oxidative injury on mtDNA (Figure 15). No significant difference was found with BGP-15 treatment alone compared to the Control group. $H_2O_2$ induced a significant damage of the mtDNA ($p < 0.05$, $H_2O_2$ vs. Control); the amplification rate of the entire mitochondrial genome was markedly diminished. This unfavourable damage was significantly reduced by BGP-15 treatment ($p < 0.01$, $H_2O_2$-BGP15 vs. $H_2O_2$).

*3.2.6. Effect of BGP-15 on Mitochondrial Membrane Potential ($\Delta\Psi$) in NRCM Cells.* We examined the effect of BGP-15 on mitochondrial membrane potential using JC-1, a cell-permeable voltage-sensitive fluorescent mitochondrial dye (Figure 16). JC-1 emits red fluorescence if the mitochondrial membrane potential is high (aggregated dye), while depolarized mitochondria emit green fluorescence (monomer dye). In the control cells, fluorescence microscopy showed strong red fluorescence and weak green fluorescence, which indicates a high $\Delta\Psi$m in mitochondria (Figure 16(a)). BGP-15 per se had no effect on mitochondrial membrane potential. The addition of $H_2O_2$ to cells facilitates the depolarization of mitochondria, resulting in weaker red fluorescence and stronger green fluorescence ($p < 0.01$ $H_2O_2$ vs. Control; Figure 16(b)). If BGP-15 was also administered in peroxide-stressed NRCM cells, red fluorescence increased and green fluorescence decreased compared to the $H_2O_2$-treated cells ($p < 0.01$, $H_2O_2$-BGP15 vs. $H_2O_2$) (Figure 16(b)). Therefore, the quantitative assessment revealed that BGP-15 treatment reduced the $H_2O_2$-induced depolarization of the mitochondrial membrane; the $\Delta\Psi$m was similar to that of the Control cells.

*3.2.7. Effect of BGP-15 on Mitochondrial Oxygen Consumption and Energy Metabolism in NRCM Cells.* To determine the mitochondrial energy metabolism and respiratory function, we used the Agilent Seahorse XFp Analyzer system and the Agilent Seahorse XFp Cell Mito Stress Test (Figure 17). BGP-15 itself had no effect on the rate of mitochondrial respiration. The oxygen consumption rate of NRMC cells was decreased in the presence of $H_2O_2$ to cells compared to Control cells (Figure 17(a)). $H_2O_2$ treatment decreased the basal respiration although this difference was not significant (Figure 17(b)). However, the maximal respiration, the spare respiratory capacity, and the ATP production were markedly decreased as a result of $H_2O_2$-induced oxidative damage compared to the Control group ($p < 0.05$, $H_2O_2$ vs. Control) (Figures 17(c)–17(e)). In the presence of both

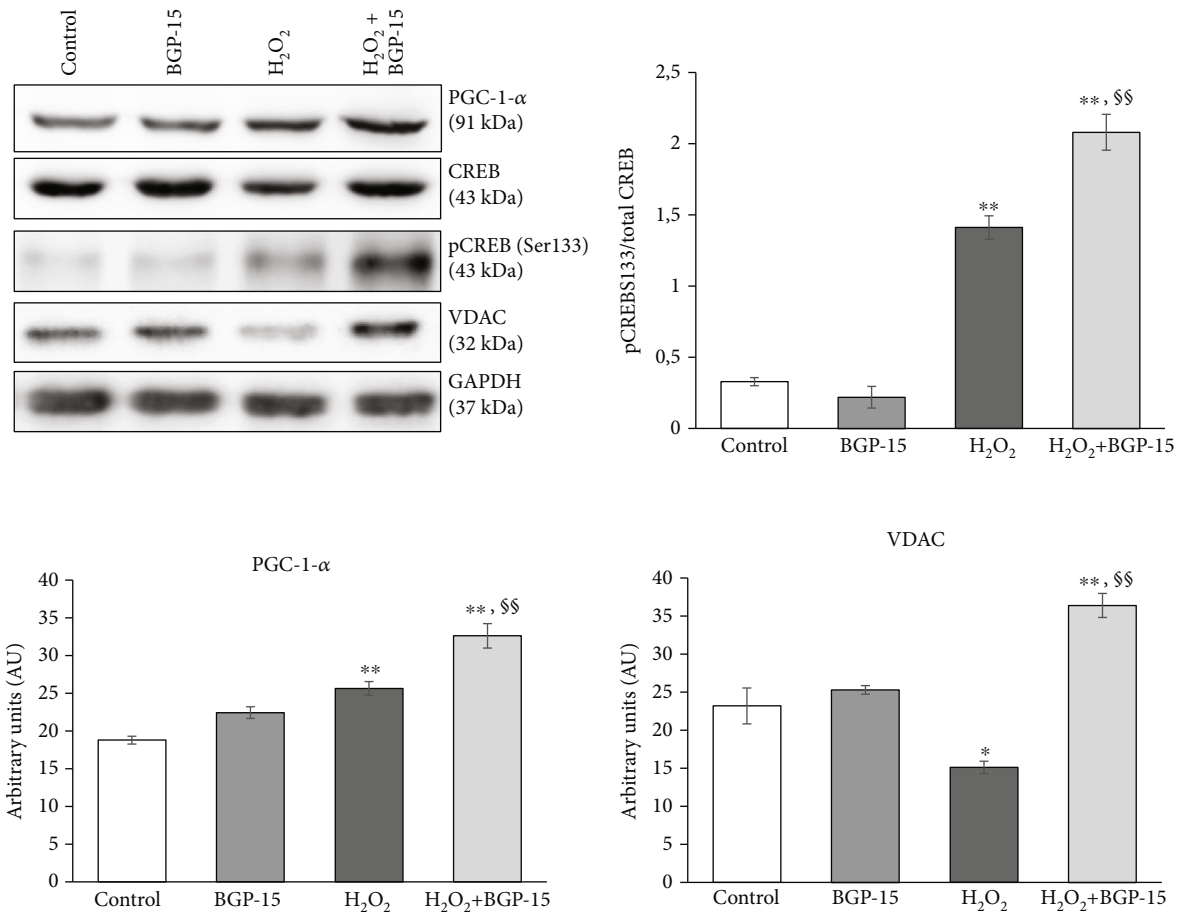


Figure 12: Effect of BGP-15 treatment on the regulation of mitochondrial biogenesis in NRCM cells. Western blot analysis of PGC-1-α, CREB, and VDAC proteins as well as densitometric evaluation is shown. GAPDH was used as a loading control. Control group: cells without any treatment; BGP-15 group: cells with only 50 μM BGP-15 for 0.5 hours; $H_2O_2$ group: cells with 150 μM $H_2O_2$ for 0.5 hours; $H_2O_2$+BGP-15 group: cells with 150 μM $H_2O_2$ and 50 μM BGP-15 for 0.5 hours. Values are mean ± SEM ($n = 4$). $^{*}p < 0.05$ vs. Control, $^{**}p < 0.01$ vs. Control, $^{§§}p < 0.01$ vs $H_2O_2$ group.

$H_2O_2$ and BGP-15, the maximal respiration, spare respiratory capacity, and the ATP production were significantly higher compared to the $H_2O_2$ group ($p < 0.05$, $H_2O_2$–BGP15 vs. $H_2O_2$).

## 4. Discussion

We aimed to study the effect of BGP-15 on various processes of mitochondrial quality control in a hypertension-induced heart failure model and in vitro using hydrogen peroxide-induced oxidative stress. The major findings of this study are that BGP-15, besides its promoting effect on mitochondrial fusion, also inhibits factors playing part in the mitochondrial fission and enhances their de novo biogenesis under stress situations. As a result of these effects, BGP-15 preserves mitochondrial structure and energy production during hydrogen peroxide-induced oxidative stress as well as in an in vivo heart failure model.

In our recent work, spontaneously hypertensive rats (SHR) were used, which is a widely used model in experimental cardiology for the examination of hypertension-induced cardiovascular remodelling and heart failure [26–28]. 15-month-old SHRs showed already severe left ventricular hypertrophy with mild signs of heart failure. BGP-15 has a positive effect on remodelling processes and cardiac function [29]. In our work, BGP-15 treatment decreased slightly the severity of cardiac hypertrophy, which was proved by gravimetric parameters (weight of ventricles/body weight, weight of ventricles/tibia length) and decreased the severity of heart failure characterized by BNP level (Table 1). In the background of these favourable changes, the mitochondrial structural and functional alterations were assumed.

Mitochondria are dynamic organelles constantly undergoing fusion and fission processes. Hypertension-induced heart failure is characterized by the fragmentation of mitochondria and by compromised energy production leading to decreased contractile force of myofilaments [30, 31]. In our work, mitochondria were structurally damaged in non-treated hypertensive animals (SHR-C). They were loosely arranged between the contractile elements (Figures 3(a)–3(c)). The average size of mitochondria was markedly reduced in the SHR-C group; approximately 40% of mitochondria were smaller than 0.3 μm2 as a result of heart failure-induced mitochondrial fragmentation (Figures 4(a)–

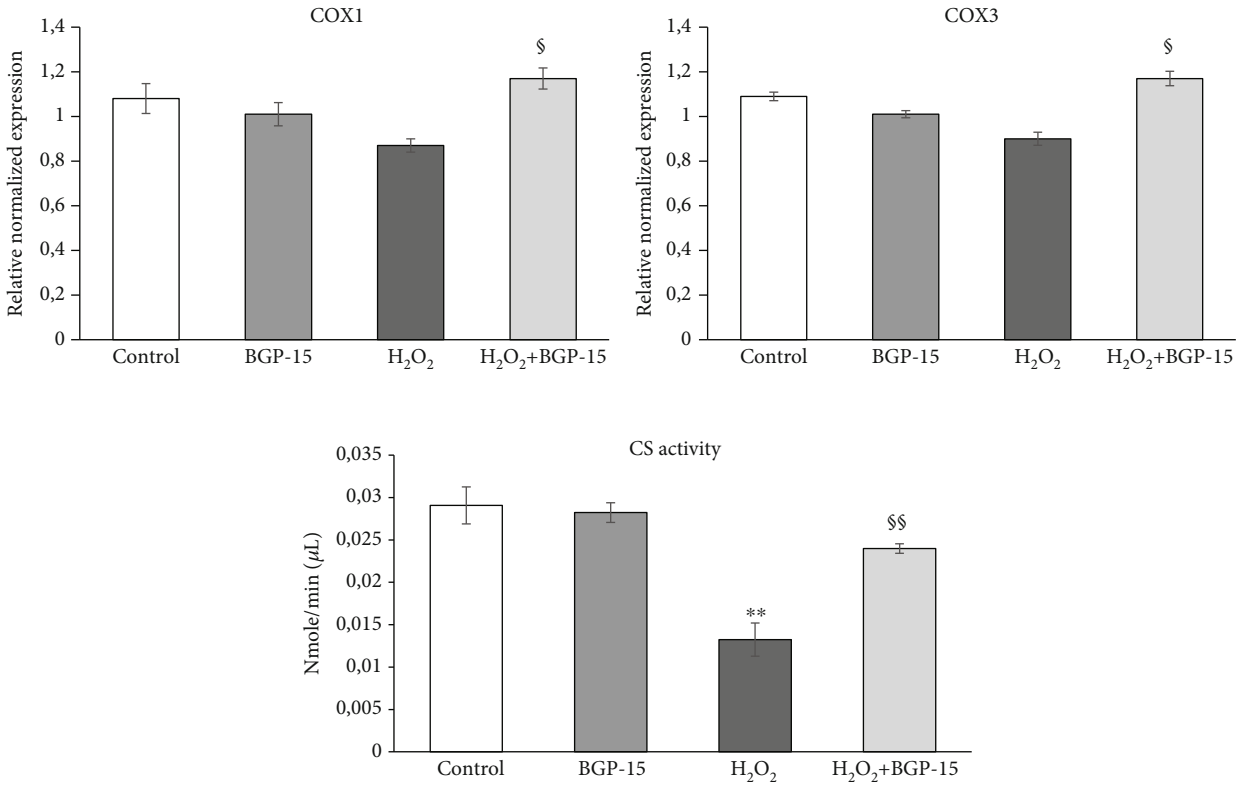


Figure 13: Effect of BGP-15 treatment on the relative DNA content and citrate synthase activity. Relative expression level of electron transport chain complex IV genes (COX1 and COX3 are presented. Comparison of citrate synthase activity in NRCM cells. Control group: cells without any treatment; BGP-15 group: cells with only 50 $\mu$M BGP-15 for 0.5 hours, $H_2O_2$ group: cells with 150 $\mu$M H2O2 for 0.5 hours, H2O2+BGP-15 group: cells with 150 $\mu$M $H_2O_2$ and 50 $\mu$M BGP-15 for 0.5 hours. Values are mean ± SEM ($n = 4$). $^{**}p < 0.01$ vs. Control, $^{\S\S}p < 0.01$ vs. $H_2O_2$ group.

4(c)). Ultrastructurally, extensive disruption of mitochondrial cristae and enlarged intracristal spaces was observed. However, BGP-15 treatment resulted in structurally markedly healthier mitochondria that were similar to that of normotensive animals. Mitochondria in the SHR-B group were tightly packed between the myofibrils. Most of mitochondria belonged to the normal size range (0.3-0.6 $\mu$m2), which can be—at least partially—the consequence of increased mitochondrial biogenesis. On the ultrastructural level, large mitochondria with tightly packed cristae and electron-dense matrix were seen in the treated group (Figures 3(d)–3(f)).

Oxidative stress induces an imbalance in processes of mitochondrial dynamics, potentially leading to cell death. Proper mitochondrial functions regulated by the quality control processes are fundamental for cardiac work. The deterioration of mitochondrial quality control greatly contributes to the hypertension-induced cardiac remodelling and its progression to heart failure [4, 7, 8]. In our recent study, the expression level of proteins promoting the mitochondrial fusion, particularly OPA1 and MFN2, was increased significantly in the BGP-15-treated animals compared to the SHR-C group (Figure 5). Our results are in accordance with the results of Szabo et al., who published earlier that BGP-15 has promoted mitochondrial fusion in both in vitro and in vivo [18].

Regarding mitochondrial fission, a marked decrease could be seen in the expression levels of DRP1 and Fis1 in hypertensive animals due to BGP-15 treatment (Figure 6). DRP1 is regulated by several posttranslational modifications [32–34]. $DRP1^{Ser637}$ phosphorylation suppresses its translocation to mitochondria and thus inhibits its activity, while $DRP1^{Ser616}$ phosphorylation promotes DRP1 translocation and therefore the mitochondrial fission. BGP-15 treatment increased markedly the $DRP1^{Ser637}$ phosphorylation and decreased the $DRP1^{Ser616}$ phosphorylation in SHR-B animals compared to nontreated hypertensive animals (Figure 6). The subcellular distribution of DRP1 showed changes consistent with the phosphorylation pattern of DRP1. In nontreated hypertensive animals (SHR-C), a high portion of DRP1 could be observed in the mitochondrial fraction (Figure 7). BGP-15 treatment resulted in a significantly reduced translocation to mitochondria of DRP1, retaining it in the cytosolic fraction. This can be a consequence of increased $DRP1^{Ser637}$ phosphorylation in SHR-B animals. Altogether, BGP-15 prevented mitochondria against hypertension-induced fragmentation.

In our in vitro experiments, hydrogen-peroxide was used to induce oxidative injury of NRCM cells. Degradation of the filamentous mitochondrial network by mitochondrial fragmentation could be observed in $H_2O_2$-stressed NRCM cells. BGP-15 treatment prevented the mitochondrial network

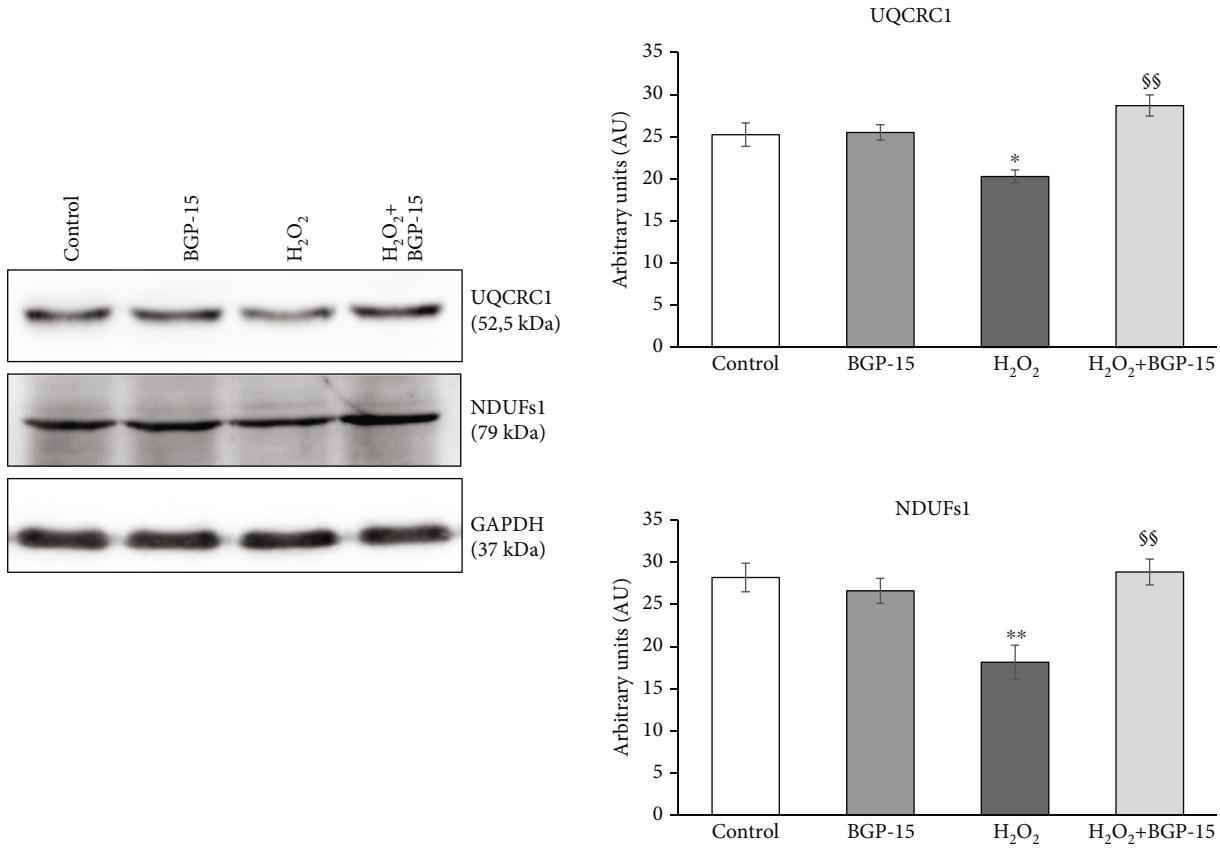


Figure 14: Effect of BGP-15 treatment on the electron transport chain complex I and III proteins in NRCMs. Western blot analysis of UQCRC1 and NDUFs1 proteins as well as densitometric evaluation is shown. GAPDH was used as a loading control. Control group: cells without any treatment; BGP-15 group: cells with only 50 $\mu$M BGP-15 for 0.5 hours; $H_2O_2$ group: cells with 150 $\mu$M $H_2O_2$ for 0.5 hours; $H_2O_2$+BGP-15 group: cells with 150 $\mu$M $H_2O_2$ and 50 $\mu$M BGP-15 for 0.5 hours. Values are mean ± SEM ($n = 4$). $^{*}p < 0.05$ vs. Control, $^{**}p < 0.01$ vs. Control, $^{§§}p < 0.01$ vs $H_2O_2$ group.

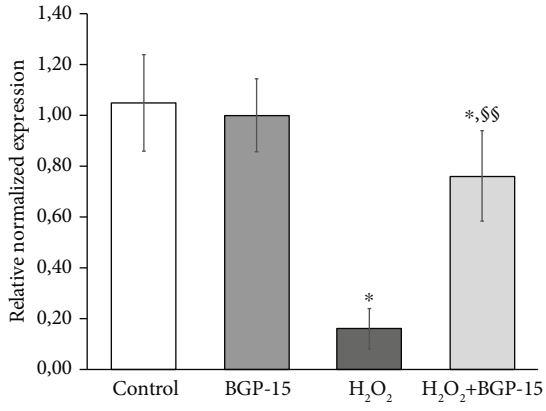


Figure 15: Effect of BGP-15 treatment on oxidative stress-induced mitochondrial DNA damage. Total DNA was isolated for LRPCR and SRPCR analysis. mtDNA damage was calculated using the $\Delta 2^{Ct}$ method. Control group: cells without any treatment; BGP-15 group: cells with only 50 $\mu$M BGP-15 for 0.5 hours; $H_2O_2$ group: cells with 150 $\mu$M $H_2O_2$ for 0.5 hours; $H_2O_2$+BGP-15 group: cells with 150 $\mu$M $H_2O_2$ and 50 $\mu$M BGP-15 for 0.5 hours. Values are mean ± SEM ($n = 4$). $^{*}p < 0.05$ vs. Control, $^{§§}p < 0.01$ vs $H_2O_2$ group.

from the oxidative stress-induced fragmentation and preserved mitochondria predominantly in the filamentous state.

Similar changes were seen in the case of fusion and fission processes in NRCM cell culture compared to in vivo model. BGP-15 treatment increased the expression level of fusion proteins (OPA1, MFN1, and MFN2), and thus, it can promote mitochondrial fusion during oxidative stress (Figure 9). On the other hand, the level of fission mediators (DRP1 and Fis1) was decreased due to BGP-15 treatment (Figure 10). BGP-15 also moderated the mitochondrial translocation of DRP1 protein from the cytosol as a result of enhanced $DRP1^{Ser637}$ phosphorylation and decreased phosphorylation of $DRP1^{Ser616}$ (Figure 11). Therefore, BGP-15 treatment has beneficial effects on mitochondrial dynamics by promoting the fusion and blocking the fission processes.

Several studies have demonstrated that mitochondrial biogenesis is compromised in cardiac remodelling and heart failure [35–37]. PGC-1-$\alpha$ is the key regulator of biogenesis, which in turn is regulated by CREB [38–40]. We found that the expression level of PCG-1$\alpha$ increased significantly due to BGP-15 treatment (Figure 12). Moreover, BGP-15 treatment further enhanced the phosphorylation of CREB compared to $H_2O_2$ group, too (Figure 12). CREB increased the expression level of PGC-1$\alpha$ and therefore

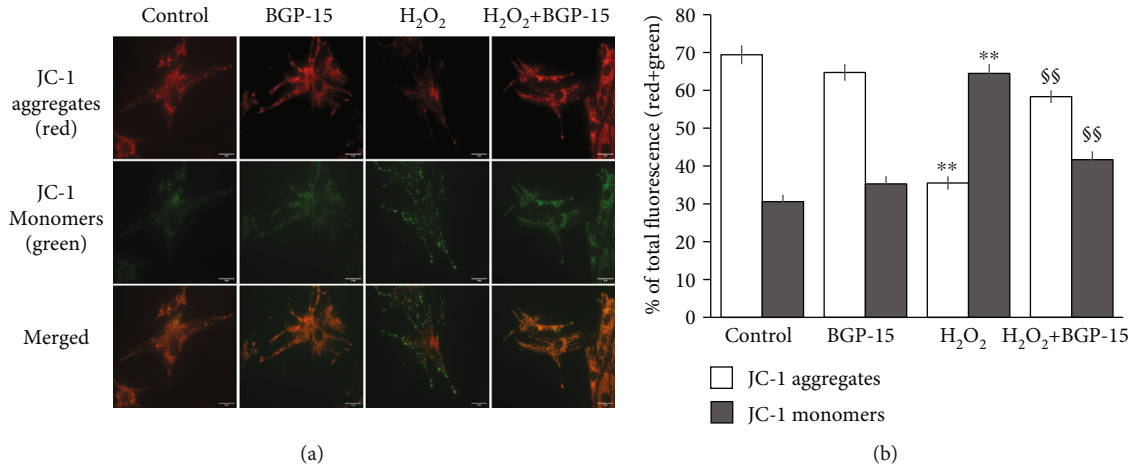


FIGURE 16: Effect of BGP-15 on the mitochondrial membrane potential in NRCMs, as determined by JC-1. (a) Effect of BGP-15 on $H_2O_2$-induced mitochondrial membrane depolarization in NRCM cells. Cells were exposed to 150 $\mu$m $H_2O_2$ in the absence or presence of 50 $\mu$m BGP-15 for 0.5 hours, after that stained with 100 ng/ml of JC-1. The dye was loaded, and after a 15-minute-long incubation, fluorescent microscopic images were taken using both the red and green channels. Representative merged images are presented. (b) Quantitative analysis of mitochondrial depolarization induced by $H_2O_2$ (150 $\mu$M) and its reduction by BGP-15 (50 $\mu$M) in NRCM cells. Control group: cells without any treatment; BGP-15 group: cells with only 50 $\mu$M BGP-15 for 0.5 hours; $H_2O_2$ group: cells with 150 $\mu$M $H_2O_2$ for 0.5 hours; $H_2O_2$+BGP-15 group: cells with 150 $\mu$M $H_2O_2$ and 50 $\mu$M BGP-15 for 0.5 hours. Data are presented as the mean ± SEM. $^{**}p < 0.01$ vs. Control cells; $^{§§}p < 0.01$ vs $H_2O_2$-treated cells.

can enhance mitochondrial biogenesis. VDAC is located in the outer mitochondrial membrane and can be used for mitochondrial loading protein. We found that VDAC was significantly elevated in BGP-15-treated cells that can support our previous results regarding enhanced biogenesis.

Moreover, we examined the level of NDUFs1 subunit of NADH-ubiquinone oxidoreductase and UQCRC1 subunit of Ubiquinol Cytochrome c Reductase proteins. These proteins are part of the mitochondrial electron transport chain (ETC Complex I and III), and in this way, they are essentially important in the maintaining of proper mitochondrial function [41, 42]. The amount of ETC Complex I and Complex III proteins levels was increased significantly due to BGP-15 treatment, which is consistent with our previous results (Figure 14).

In order to support our finding more adequately regarding the effect of BGP-15 on mitochondrial biogenesis, the relative DNA content of ETC Complex IV was determined. We found that BGP-15 treatment increased the relative expression levels of both tested genes (COXI and COXIII; Figure 13). Since both genes are encoded by mitochondrial DNA, this suggests that mitochondrial DNA content was increased in NRCMs cells treated with BGP-15.

Moreover, we also performed a well-accepted and frequently used method for studying mitochondrial biogenesis by measuring the activity of citrate synthase (CS) [43–45]. Citrate synthase is localized within the mitochondrial matrix, and it catalyses the synthesis of citrate from oxaloacetate in the Krebs tricarboxylic acid cycle [44]. Maximal activity of citrate synthase indicates the mitochondrial content of heart muscle. Citrate synthase activity was reduced in hydrogen-peroxide stressed group compared to control group. The citrate synthase activity was increased significantly due to the treatment (Figure 13). Summarizing these results, we can conclude that mitochondrial biogenesis was increased under oxidative stress in treated NRCMs cells as a result of BGP-15 treatment, and in this way, it was able to enhance the proper mitochondrial function.

Oxidative stress can damage the mtDNA, which is extremely sensitive to it [46, 47]. In our recent work, PCR results showed extensive damage of mtDNA caused by hydrogen peroxide. Thus, the amplification of the entire mitochondrial genome was restrained. BGP-15 treatment, however, preserved mitochondrial genome integrity markedly decreasing the breakage of mtDNA (Figure 15). The protection of mtDNA is extremely important, because the mitochondrial respiratory chain (ETC) complexes are encoded on mtDNA [48, 49]. Complex I-III are critical for ROS production by the respiratory chain [50]. It can generate significant amounts of ROS under several conditions including hypoxia, mitochondrial hyperpolarization, and inhibition of respiratory complexes. BGP-15 is able to reduce the mitochondrial ROS production at complex I [18, 24]. Along these lines, BGP-15 can protect against ROS induced mitochondrial DNA damage and maintain the appropriate mitochondrial function.

The preservation of mitochondrial membrane potential is also important to maintain the metabolic capacity of mitochondria. Well-functioning mitochondrial oxidative phosphorylation and ATP production are essential for the proper function of cardiomyocytes [51, 52]. BGP-15 is able to prevent oxidative stress-induced mitochondrial membrane potential loss and therefore improved mitochondrial function (Figure 16). We observed that oxidative stress leads to mitochondrial respiration damage (Figure 17). However, BGP-15 treatment preserved the mitochondrial function characterized by ATP production

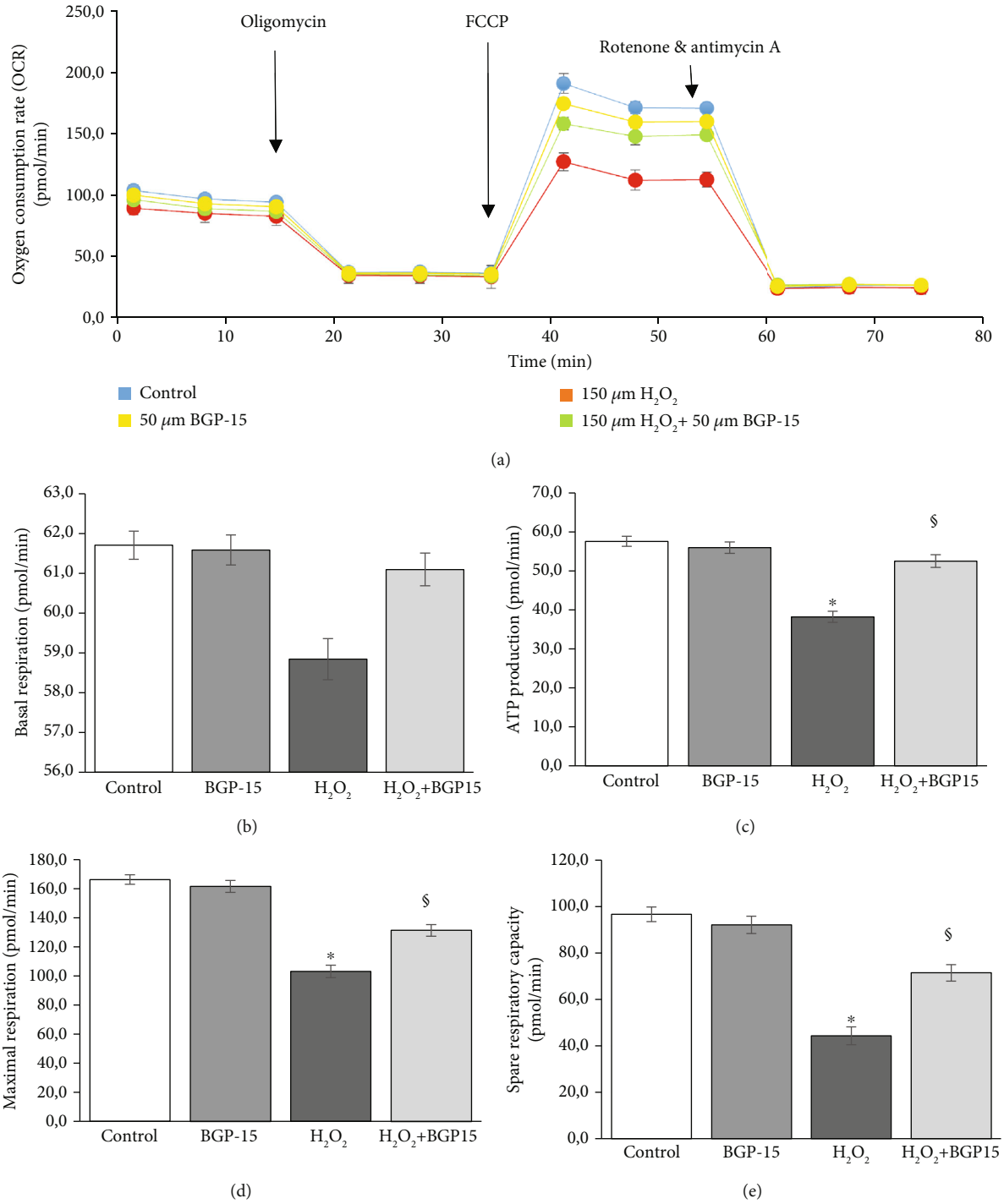


Figure 17: Effect of BGP-15 on mitochondrial oxygen consumption and energy metabolism in NRCM cells, as determined by Agilent Seahorse Xfp. Mitochondrial energy metabolism was measured using a Seahorse XFp analyzer. During testing, H9c2 cells were treated with 10 $\mu$M oligomycin, 10 $\mu$M FCCP, and 5 $\mu$M rotenone/antimycin A. Data were automatically calculated according to the Agilent Seahorse XF Cell Mito Stress Test Report Generator. (a) Oxygen consumption rate (OCR). (b) Basal respiration. (c) ATP production. (d) Maximal respiration. (e) Spare respiratory capacity. Control group: cells without any treatment; BGP-15 group: cells with only 50 $\mu$M BGP-15 for 0.5 hours; $H_2O_2$ group: cells with 150 $\mu$M $H_2O_2$ for 0.5 hours; $H_2O_2$+BGP-15 group: cells with 150 $\mu$M $H_2O_2$ and 50 $\mu$M BGP-15 for 0.5 hours. Values are mean ± SEM ($n = 4$). $^*p < 0.05$ vs. Control, $^\$p < 0.05$ vs. $H_2O_2$ group.

and spare respiratory capacity thereby ensuring the ability of cells to respond to increased energy demand under stress scenario.

BGP-15 also supports the maintenance of mitochondrial function partially via the preservation of the mitochondrial structure.

Our study is the first to demonstrate that BGP-15 preserved the mitochondrial ultrastructure by increased mitochondrial fusion and decreased fission processes as well as positively affected the translocation processes in chronic hypertension-induced heart failure animal model. Furthermore, we can make a similar observation in the case of primer rat cardiomyocytes cell culture experiment during hydrogen-peroxide induced oxidative stress. Comparable changes were seen in the case of fusion and fission processes in NRCM cell culture compared to in vivo model. Moreover, BGP-15 treatment preserved the mitochondrial membrane potential and improved the mitochondrial function. BGP-15 protected the integrity of the mitochondrial genome and enhanced the de novo biogenesis of mitochondria during hydrogen peroxide-induced oxidative stress. Nevertheless, the exact molecular mechanism of the effects is still unknown, but there are clear evidences regarding the specific mechanism of how BGP-15 acts at important integrator points of signal transduction in certain pathological processes. In order to elucidate the potential underlying molecular mechanisms, further targeted studies should be performed in the future.

Our results reveal that pharmacological modulation of the mitochondrial dynamics under cellular stress could be a novel therapeutic approach in various cardiac diseases characterized by oxidative stress-induced mitochondrial damage.

## Data Availability

The authors confirm that all data is fully available without restriction. All relevant data is described within the paper.

## Ethical Approval

Animals received care according to the Guide for the Care and Use of Laboratory Animals published by the US National Institute of Health and the experiment was approved by the Animal Research Review Committee of the University of Pecs, Medical School (Permit number: BA02/2000-54/2017). The manuscript does not contain clinical studies or patient data.

## Conflicts of Interest

On behalf of all authors, the corresponding author states that there is no conflict of interest.

## Authors' Contributions

All authors contributed to the study conception and design. Material preparation, data collection, and analysis were performed by Orsolya Horvath, Katalin Ordog, Kitti Bruszt, Nikoletta Kalman, Dominika Kovacs, Balazs Radnai, Ferenc Gallyas, Balazs Sumegi, Kalman Toth, Robert Halmosi, Laszlo Deres. The first draft of the manuscript was written by Orsolya Horvath, and all authors commented on previous versions of the manuscript. All authors read and approved the final manuscript. Prof. Balazs Sumegi has unexpectedly passed away during the course of this study. This paper is dedicated to his memory.

## Acknowledgments

This study was supported by the Hungarian National Research Foundations Grant (GINOP-2.3.2-15-2016-00048, GINOP 2.3.2-15-2016-00049) and NKFIH in Hungary, within the framework of the 2020-4.1.1-TKP2020 1st thematic programme of the University of Pécs (2020-4.1.1-TKP2020).

## References

[1] M. G. Rosca and C. L. Hoppel, "Mitochondrial dysfunction in heart failure," *Heart Failure Reviews*, vol. 18, no. 5, pp. 607–622, 2013.

[2] B. Zhou and R. Tian, "Mitochondrial dysfunction in pathophysiology of heart failure," *The Journal of Clinical Investigation*, vol. 128, no. 9, pp. 3716–3726, 2018.

[3] A. A. Kumar, D. P. Kelly, and J. A. Chirinos, "Mitochondrial dysfunction in heart failure with preserved ejection fraction," *Circulation*, vol. 139, no. 11, pp. 1435–1450, 2019.

[4] A. A. Knowlton, L. Chen, and Z. A. Malik, "Heart failure and mitochondrial dysfunction: the role of mitochondrial fission/-fusion abnormalities and new therapeutic strategies," *Journal of Cardiovascular Pharmacology*, vol. 63, no. 3, pp. 196–206, 2014.

[5] M. T. Breitzig, M. D. Alleyn, R. F. Lockey, and N. Kolliputi, "A mitochondrial delicacy: dynamin-related protein 1 and mitochondrial dynamics," *American Journal of Physiology-Cell Physiology*, vol. 315, pp. C80–C90, 2018.

[6] A. R. Hall, N. Burke, R. K. Dongworth, and D. J. Hausenloy, "Mitochondrial fusion and fission proteins: novel therapeutic targets for combating cardiovascular disease," *British Journal of Pharmacology*, vol. 171, no. 8, pp. 1890–1906, 2014.

[7] J. Nan, W. Zhu, M. S. Rahman et al., "Molecular regulation of mitochondrial dynamics in cardiac disease," *Biochimica et Biophysica Acta (BBA) - Molecular Cell Research*, vol. 1864, pp. 1260–1273, 2017.

[8] C. Vásquez-Trincado, I. García-Carvajal, C. Pennanen et al., "Mitochondrial dynamics, mitophagy and cardiovascular disease," *The Journal of Physiology*, vol. 594, pp. 509–525, 2016.

[9] H. Tsutsui, S. Kinugawa, and S. Matsushima, "Oxidative stress and heart failure," *American Journal of Physiology Heart and Circulatory Physiology*, vol. 301, no. 6, pp. H2181–H2190, 2011.

[10] E. Takimoto and D. A. Kass, "Role of oxidative stress in cardiac hypertrophy and remodeling," *Hypertension*, vol. 49, pp. 241–248, 2007.

[11] D. A. Brown, J. B. Perry, M. E. Allen et al., "Mitochondrial function as a therapeutic target in heart failure," *Nature Reviews Cardiology*, vol. 14, pp. 238–250, 2017.

[12] G. Siasos, V. Tsigkou, M. Kosmopoulos et al., "Mitochondria and cardiovascular diseases—from pathophysiology to treatment," *Annals of Translational Medicine*, vol. 6, 2018.

[13] M. Bonora, M. R. Wieckowski, D. A. Sinclair, G. Kroemer, P. Pinton, and L. Galluzzi, "Targeting mitochondria for cardiovascular disorders: therapeutic potential and obstacles," *Nature Reviews Cardiology*, vol. 16, pp. 33–55, 2019.

[14] J. Kuzmicic, A. del Campo, C. López-Crisosto et al., "Mitochondrial dynamics: a potential new therapeutic target for heart failure," *Revista Española de Cardiología*, vol. 64, pp. 916–923, 2011.

[15] R. Halmosi, Z. Berente, E. Osz, K. Toth, P. Literati-Nagy, and B. Sumegi, "Effect of poly(ADP-ribose) polymerase inhibitors on the ischemia-reperfusion-induced oxidative cell damage and mitochondrial metabolism in Langendorff heart perfusion system," *Molecular Pharmacology*, vol. 59, pp. 1497–1505, 2001.

[16] G. Nagy, A. Szarka, G. Lotz et al., "BGP-15 inhibits caspase-independent programmed cell death in acetaminophen-induced liver injury," *Toxicology and Applied Pharmacology*, vol. 243, pp. 96–103, 2010.

[17] K. Sumegi, K. Fekete, C. Antus et al., "BGP-15 protects against oxidative stress- or lipopolysaccharide-induced mitochondrial destabilization and reduces mitochondrial production of reactive oxygen species," *PLoS One*, vol. 12, article e0169372, 2017.

[18] A. Szabo, K. Sumegi, K. Fekete et al., "Activation of mitochondrial fusion provides a new treatment for mitochondria-related diseases," *Biochemical Pharmacology*, vol. 150, pp. 86–96, 2018.

[19] Z. Sarszegi, E. Bognar, B. Gaszner et al., "BGP-15, a PARP-inhibitor, prevents imatinib-induced cardiotoxicity by activating Akt and suppressing JNK and p38 MAP kinases," *Molecular and Cellular Biochemistry*, vol. 365, pp. 129–137, 2012.

[20] J. Chung, A.-K. Nguyen, D. C. Henstridge et al., "HSP72 protects against obesity-induced insulin resistance," *Proceedings of the National Academy of Sciences of the United States of America*, vol. 105, pp. 1739–1744, 2008.

[21] G. Sapra, Y. K. Tham, N. Cemerlang et al., "The small-molecule BGP-15 protects against heart failure and atrial fibrillation in mice," *Nature Communications*, vol. 5, article 5705, 2014.

[22] O. Horvath, K. Ordog, K. Bruszt et al., "BGP-15 protects against heart failure by enhanced mitochondrial biogenesis and decreased fibrotic remodelling in spontaneously hypertensive rats," *Oxidative Medicine and Cellular Longevity*, vol. 2021, Article ID 1250858, 13 pages, 2021.

[23] M. Bombicz, D. Priksz, R. Gesztelyi et al., "The drug candidate BGP-15 delays the onset of diastolic dysfunction in the Goto-Kakizaki rat model of diabetic cardiomyopathy," *Molecules*, vol. 24, no. 3, p. 586, 2019.

[24] E. Szabados, P. Literati-Nagy, B. Farkas, and B. Sumegi, "BGP-15, a nicsotinic amidoxime derivate protecting heart from ischemia reperfusion injury through modulation of poly(-ADP-ribose) polymerase," *Biochemical Pharmacology*, vol. 59, pp. 937–945, 2000.

[25] K. Ordog, O. Horvath, K. Eros et al., "Mitochondrial protective effects of PARP-inhibition in hypertension-induced myocardial remodeling and in stressed cardiomyocytes," *Life Sciences*, vol. 268, p. 118936, 2021.

[26] G. Itter, W. Jung, and P. Juretschke, "A model of chronic heart failure in spontaneous hypertensive rats (SHR)," *Laboratory Animals*, vol. 38, pp. 138–148, 2016.

[27] M. Kokubo, A. Uemura, T. Matsubara, and T. Murohara, "Noninvasive evaluation of the time course of change in cardiac function in spontaneously hypertensive rats by echocardiography," *Hypertension Research*, vol. 28, pp. 601–609, 2005.

[28] S. A. Doggrell and L. Brown, "Rat models of hypertension, cardiac hypertrophy and failure," *Cardiovascular Research*, vol. 39, pp. 89–105, 1998.

[29] O. Horvath, K. Ordog, K. Bruszt, B. Sumegi, K. Toth, and R. Halmosi, "Role of BGP-15 treatment in hypertensive heart failure progression and mitochondrial protection," *European Heart Journal*, vol. 40, 2019.

[30] S.-B. Ong and D. J. Hausenloy, "Mitochondrial morphology and cardiovascular disease," *Cardiovascular Research*, vol. 88, pp. 16–29, 2010.

[31] D. W. Scheuermann, "The ultrastructure of cardiac muscle in health and disease," *Micron*, vol. 24, pp. 47–73, 1993.

[32] C.-R. Chang and C. Blackstone, "Dynamic regulation of mitochondrial fission through modification of the dynamin-related protein Drp 1," *Annals of the New York Academy of Sciences*, vol. 1201, pp. 34–39, 2010.

[33] Y. Kanamaru, S. Sekine, H. Ichijo, and K. Takeda, "The phosphorylation-dependent regulation of mitochondrial proteins in stress responses," *Journal of Signal Transduction*, vol. 2012, Article ID 931215, 12 pages, 2012.

[34] H. Lee and Y. Yoon, "Mitochondrial fission: regulation and ER connection," *Molecules and Cells*, vol. 37, pp. 89–94, 2014.

[35] A. Pisano, B. Cerbelli, E. Perli et al., "Impaired mitochondrial biogenesis is a common feature to myocardial hypertrophy and end-stage ischemic heart failure," *Cardiovascular Pathology*, vol. 25, no. 2, pp. 103–112, 2016.

[36] A. Garnier, D. Fortin, C. Deloménie, I. Momken, V. Veksler, and R. Ventura-Clapier, "Depressed mitochondrial transcription factors and oxidative capacity in rat failing cardiac and skeletal muscles," *The Journal of Physiology*, vol. 551, no. 2, pp. 491–501, 2003.

[37] C. Riehle and E. D. Abel, "PGC-1 proteins and heart failure," *Trends in Cardiovascular Medicine*, vol. 22, no. 4, pp. 98–105, 2012.

[38] P. J. Fernandez-Marcos and J. Auwerx, "Regulation of PGC-1$\alpha$, a nodal regulator of mitochondrial biogenesis," *The American Journal of Clinical Nutrition*, vol. 93, no. 4, pp. 884S–890S, 2011.

[39] C. Cantó and J. Auwerx, "PGC-1alpha, SIRT1 and AMPK, an energy sensing network that controls energy expenditure," *Current Opinion in Lipidology*, vol. 20, no. 2, pp. 98–105, 2009.

[40] F. R. Jornayvaz and G. I. Shulman, "Regulation of mitochondrial biogenesis," *Essays in Biochemistry*, vol. 47, pp. 69–84, 2010.

[41] R.-Z. Zhao, S. Jiang, L. Zhang, and Z.-B. Yu, "Mitochondrial electron transport chain, ROS generation and uncoupling (review)," *International Journal of Molecular Medicine*, vol. 44, pp. 3–15, 2019.

[42] D. Nolfi-Donegan, A. Braganza, and S. Shiva, "Mitochondrial electron transport chain: oxidative phosphorylation, oxidant production, and methods of measurement," *Redox Biology*, vol. 37, 2020.

[43] S. Larsen, J. Nielsen, C. N. Hansen et al., "Biomarkers of mitochondrial content in skeletal muscle of healthy young human subjects," *The Journal of Physiology*, vol. 590, no. 14, pp. 3349–3360, 2012.

[44] G. Wiegand and S. J. Remington, "Citrate synthase: structure, control, and mechanism," *Annual Review of Biophysics and Biophysical Chemistry*, vol. 15, pp. 97–117, 1986.

[45] A. J. A. Molina, M. S. Bharadwaj, C. Van Horn et al., "Skeletal muscle mitochondrial content, oxidative capacity, and Mfn2 expression are reduced in older patients with heart failure and preserved ejection fraction and are related to exercise intolerance," *JACC: Heart Failure*, vol. 4, pp. 636–645, 2016.

[46] J. N. Peoples, A. Saraf, N. Ghazal, T. T. Pham, and J. Q. Kwong, "Mitochondrial dysfunction and oxidative stress in heart disease," *Experimental & Molecular Medicine*, vol. 51, no. 12, pp. 1–13, 2019.

[47] H. Tsutsui, S. Kinugawa, and S. Matsushima, "Oxidative stress and mitochondrial DNA damage in heart failure," *Circulation Journal*, vol. 72, Supplement A, pp. A31–A37, 2008.

[48] J.-W. Taanman, "The mitochondrial genome: structure, transcription, translation and replication," *Biochimica et Biophysica Acta (BBA) - Bioenergetics*, vol. 1410, pp. 103–123, 1999.

[49] C. M. Gustafsson, M. Falkenberg, and N.-G. Larsson, "Maintenance and expression of mammalian mitochondrial DNA," *Annual Review of Biochemistry*, vol. 85, no. 1, pp. 133–160, 2016.

[50] S. L. Hebert, I. R. Lanza, and K. S. Nair, "Mitochondrial DNA alterations and reduced mitochondrial function in aging," *Mechanisms of Ageing and Development*, vol. 131, no. 7-8, pp. 451–462, 2010.

[51] J. S. Ingwall, "Energy metabolism in heart failure and remodelling," *Cardiovascular Research*, vol. 81, pp. 412–419, 2008.

[52] T. Doenst, T. D. Nguyen, and E. D. Abel, "Cardiac metabolism in heart failure - implications beyond ATP production," *Circulation Research*, vol. 113, no. 6, pp. 709–724, 2013.